Understanding and Modulating Vessel Formation in Human Rotator Cuff Tendon Disease

A dissertation submitted to the University of Oxford in partial fulfilment of the requirements for the degree of

Doctor of Philosophy

Mathew James Baldwin

Jesus College

Nuffield Department of Orthopaedics, Rheumatology and Musculoskeletal Science

University of Oxford

Trinity Term 2019

Supervisors: Professor Andrew Carr, Associate Professor Sarah Snelling, Associate Professor Stephanie Dakin

Declaration

I certify that this thesis is a true and honest account of my own research, which was conducted ethically, and the results obtained are genuine. Where I have drawn on the work, ideas, and results of others, this has been appropriately acknowledged in the thesis.

Mathew James Baldwin

Abstract

Tears of the rotator cuff tendons are common and often debilitating causing pain and loss of upper limb function. Their prevalence continues to increase as populations age. Although the pathobiology of tendon disease is incompletely understood, it is increasingly evident that inflammation plays a critical role. Persistent immune cell infiltration, fibroblast activation and angiogenesis are cardinal features of rotator cuff tendon disease.

Unfortunately, the surgical repair of rotator cuff tears fails in almost half of cases, often resulting in long-term pain and disability. To this end, the biomaterial augmentation of surgical repairs has gained in popularity. Current augments provide structural support to repairs but do not address the aberrant biology of torn tendons resulting in a compromised repair process. However, a new generation of biomaterials are currently under development. Produced by electrospinning these scaffolds and can alter cellular phenotypes through the provision of topographical cues. The successful tailoring of such biomaterials demands a detailed understanding of tendon disease pathobiology and cell-material interactions, yet the role of the endothelium in tendon disease remains hitherto unexplored.

This thesis aimed to establish a clear need for a new generation of bioactive materials for rotator cuff repair. It then explored an entirely novel area of tendon pathobiology – the role of the endothelium, before attempting to modulate vessel growth through modifying the microscale architecture of electrospun scaffolds.

Firstly, an a priori registered systematic review of all available clinical data for patch augmented repair found a similar complication rate between augmented (2.3%) and standard repair (2.1%). A meta-analysis confirmed an improvement in re-tear rate, and a subsequent subgroup analysis identified a moderate reduction in re-tear rate for synthetic (RR 0.4, 95% CI 0.25-0.64) and decellularised human allograft (RR 0.34, 95% CI 0.18-0.64) patches, but not for xenografts (RR 0.97, 95% CI 0.72-1.30) or human autografts (RR 0.69, 95% CI 0.40-1.18). This corresponded to a small improvement in pain and PROMS for synthetic patches, that was statistically significant but not clinically meaningful.

Secondly, an *in vitro* co-culture model of tenocytes and endothelial cells, with or without the addition of peripheral blood leukocytes, was undertaken. During extended co-culture of healthy tenocytes, EC-tenocyte crosstalk increased mRNA expression of fibroblast activation markers including *CD248*, *PDPN* and *VCAM-1*, pro-inflammatory cytokines, extracellular matrix proteins and matrix proteases. This effect was not observed during EC co-cultures with diseased tenocytes. Cross-talk was bi-directional, tenocytes from healthy, but not diseased tendons, inhibited adhesion of lymphocytes and monocytes to the endothelium.

Thirdly, the effect of electrospun scaffold micro-architecture, specifically fibre diameter and alignment, on the transcriptome of healthy and diseased tenocytes was characterised using bulk RNA sequencing. Aligned electrospun scaffolds with fibre diameters above 1000nm resulted in a downregulation of gene-sets related to fibroblast activation. Conversely, all randomly oriented scaffold and small diameter (~300nm) aligned scaffolds induced a relative activation of tenocytes. A more profound transcriptional response was observed for diseased tenocytes which were primed to respond to topographical cues. Despite the ability of scaffold architecture to modify fibroblast activation, no scaffold consistently altered the expression of genes involved in the direct regulation of angiogenesis by fibroblasts.

This thesis has demonstrated that (1) current commercially available rotator cuff patches are not clinically efficacious, (2) endothelial-fibroblast crosstalk influences critical features of rotator cuff pathobiology including immune cell recruitment and fibroblast activation, and (3) the micro-architectural design of electrospun scaffolds modulates the activation status of tenocytes, but, within the parameters used in this work, does not appear to influence fibroblast derived angiogenic signaling.

Truth in science can be defined as the working hypothesis best suited to open the way to the next better one.

Konrad Lorenz

Acknowledgements

This work would not have been possible without the support and guidance of my supervisors and fellow colleagues at the Botnar Research centre. To Andy, Sarah, Steph, Steve, Jolet, Mike, Nav, Ed, Wataru, Hayley, Tonia, Kim, Bridget, Debra and Pierre, simply saying thank you is not enough. I will be forever grateful for the hours you have all spent advising, discussing and guiding my research, but above all thank you for your friendship.

I started this journey as a clinician and leave a, somewhat amateur, scientist. This DPhil has forever changed my clinical perspectives, but these last three years have also blessed me with my wife, Laura, and my son, Harry. More than anything else, it is these experiences that have irrevocably altered my outlook. Without your undiminishing encouragement and patience none of this would have been possible. Lastly, to my parents and sister, your energy, dedication and untiring support are a continual source of inspiration that drives me to always do better.

This thesis is dedicated to my family.

Contents

Abstract **iii**

Chapter 1 Introduction **1**

1.1 Rotator Cuff Anatomy 1

1.2 Tendon Structure 1

1.3 Rotator cuff Injuries 1

1.4 Physiological tendon repair mechanisms 3

1.5 Pathobiology of rotator cuff tendon disease 4

1.6 Tendon Vascularity 6

1.7 Angiocrine signalling 8

1.8 Treatment of Rotator Cuff Tears 9

1.9 Scaffold augmentation of rotator cuff repairs 11

1.9.1 Biological scaffolds – Decellularised ECM 11

1.9.2 Biological scaffolds – Natural Hydrogels 11

1.9.3 Synthetic Scaffolds 12

1.9.4 Modification of Synthetic Scaffolds 13

1.9.4.1 Scaffold anisotropy *14*

1.9.4.2 Cell type *14*

1.9.4.3 Fibre diameter *15*

1.9.4.4 Scaffold Porosity *15*

1.9.4.5 Scaffold Stiffness *16*

1.10 Fabrication of electrospun synthetic scaffolds 16

1.10.1 Electrospinning Process 17

1.10.2 Basic Parameter Alterations 18

1.11 Aims 19

1.12 Hypotheses 20

Chapter 2 Use of implantable meshes for augmented rotator cuff repair - a systematic review and meta-analysis **21**

2.1 Abstract 21

2.1.1 Background 21

2.1.2 Methods 21

2.1.3 Results 21
2.1.4 Conclusions 21
2.2 Introduction 22
2.3 Aims 24
2.4 Hypotheses 24
2.5 Methods 25
2.5.1 Protocol and Registration 25
2.5.2 Eligibility Criteria 25
2.5.2.1 Population *25*
2.5.2.2 Interventions *25*
2.5.2.3 Comparators *26*
2.5.2.4 Outcomes *26*
2.5.2.5 Study types *26*
2.5.3 Search Strategy 26
2.5.4 Study selection 26
2.5.5 Data Extraction 27
2.5.6 Risk of bias assessment 27
2.5.7 Data Analysis 27
2.5.8 Statistical Analysis 28
2.6 Results 30
2.6.1 Study selection 30
2.6.2 Study Characteristics 30
2.6.3 Surgical characteristics 41
2.6.4 Shoulder specific Patient Reported Outcome Measures (PROMs) 41
2.6.5 Repair failure and radiological assessments utilised 48
2.6.6 Shoulder pain 53
2.6.7 Health related quality of life 53
2.6.8 Patch related adverse events 53
2.6.9 Meta-analysis 60
2.6.10 Risk of bias 61
2.7 Discussion 68
2.8 Conclusions 71

Chapter 3 Endothelial-fibroblast crosstalk alters fibroblast activation and endothelial recruitment of immune cells 73

3.1 Abstract 73

3.1.1 Background 73

3.1.2 Methods 73

3.1.3 Results 73

3.1.4 Conclusions 73

3.2 Introduction 74

3.3 Aims 76

3.4 Hypotheses 76

3.5 Methods 77

3.5.1 Isolation and culture of leukocytes, fibroblasts and endothelial cells 77

3.5.1.1 Peripheral blood leukocyte isolation 77

3.5.1.2 Collection and processing of tendon samples 77

3.5.1.3 Isolation and expansion of tendon fibroblasts 77

3.5.1.1 Endothelial cell culture 78

3.5.2 Co-culture of endothelial cells and fibroblasts on transwell filters 78

3.5.3 Gene expression by tendon-fibroblasts and endothelial cells during co-culture 78

3.5.4 Adhesion and migration of leukocytes on HMEC-1 endothelial cells during indirect co-culture with tendon-derived fibroblasts 79

3.5.5 Flow cytometry 82

3.5.6 Statistical Analysis 83

3.6 Results 84

3.6.1 Temporal expression of pro-inflammatory cytokines by tendon fibroblasts during EC co-culture 84

3.6.2 The effect of EC co-culture on the expression of fibroblast activation markers 84

3.6.3 The effect of EC co-culture on the expression of inflammatory cytokines and ECM related genes by tendon fibroblasts 87

3.6.4 The effect of EC co-culture on inflammation activation signatures and cell-cycle regulators 92

3.6.5 Adhesion of leukocytes to endothelial-fibroblast co-culture under static conditions 94

3.6.6 Expression of EC adhesion receptors during tendon-derived fibroblast co-culture 95

3.6.7 Trans-endothelial and trans-fibroblast migration of leukocytes during co-culture 96

3.6.8 HMEC-1 expression of endothelial junctional molecules during tendon-derived fibroblast co-culture 98
3.7 Discussion 103
3.8 Conclusions 109
Chapter 4 The effect of electrospun scaffold architecture on tendon fibroblast activation 110
4.1 Abstract 110
4.1.1 Background 110
4.1.2 Methods 110
4.1.3 Results 110
4.1.4 Conclusions 110
4.2 Introduction 111
4.3 Aims 113
4.4 Hypotheses 113
4.5 Methods 114
4.5.1 Electrospun scaffold fabrication 114
4.5.1.2 PDO solution preparation 114
4.5.1.3 Electrospinning 114
4.5.1.4 Scanning electron microscopy and image analysis 115
4.5.1.5 Characterisation of electrospun scaffold pore size and porosity 115
4.5.2 Collection and processing of tendon samples 116
4.5.2.1 Sample collection 116
4.5.2.2 Isolation and expansion of tendon fibroblasts 117
4.5.3 Culture of tendon fibroblast on electrospun scaffolds 117
4.5.3.1 Preparation of Electrospun scaffolds for in vitro cell culture 117
4.5.3.2 Seeding and culture of tendon fibroblasts 118
4.5.4 Immunocytochemistry of tendon fibroblasts on electropsun scaffolds 118
4.5.5 Bulk mRNA sequencing 119
4.5.5.1 RNA isolation 119
4.5.5.2 Library Construction and sequencing 119
4.5.5.3 RNA-seq analysis 120
4.5.6 Statistical analysis 120
4.5.6.1 Electrospun scaffolds fibre diameter 120

4.5.6.2 Electrospun scaffolds fibre anisotropy *120*

4.5.6.3 RNA-sequencing *121*

4.6 Results 122

4.6.1 Production of electrospun scaffolds with variable fibre diameters 122

4.6.2 Production of electrospun scaffolds with variable fibre orientations 123

4.6.3 Final Production of electrospun scaffolds for in vitro cell culture 124

4.6.4 Characterization of scaffold pore size and porosity 125

4.6.5 Effect of scaffold architecture on the morphology of healthy hamstring fibroblasts 126

4.6.6 Transcriptome sequencing of hamstring and rotator cuff derived fibroblasts 128

4.6.7 Micro-architecture modulates gene expression of healthy tendon fibroblasts 128

4.6.8 Effect of fibre diameter on gene expression of healthy tendon fibroblasts 128

4.6.9 Fibre anisotropy induces differential gene expression 133

4.6.10 Functional analysis using gene set enrichment 133

4.6.11 Micro-architecture influences activation status of healthy tendon fibroblasts 138

4.6.12 Diseased tendon fibroblasts display significant transcriptomic differences, are activated and respond to changes in electrospun scaffold micro-architecuture 142

4.6.13 The fibre diameter of aligned scaffolds can regulate the activation status of diseased tendon fibroblasts, which are primed to respond 149

4.6.14 Scaffold anisotropy regulates the activation status of diseased tendon fibroblasts but not their angiogenic activity 150

4.6.15 PDPN surface expression on activating and resolving scaffolds 151

4.7 Discussion 161

4.8 Conclusions 166

Chapter 5 General Discussion 167

5.1 Introduction 167

5.2 Summary of novel findings 169

5.2.1 Systematic review of the surgical management of rotator cuff repair with an augmentative patch 169

5.2.2 Endothelial-tenocyte crosstalk alters fibroblast activation and endothelial recruitment of immune cells 171

5.2.3 The effect of electrospun scaffold architecture on tendon fibroblast activation 172

5.2 Clinical Relevance 174

5.3 Methodological Improvements 176

5.3.1 Methodological improvements in the systematic review of current rotator cuff augmentative patches 176

5.3.2 Methodological improvements concerning EC and fibroblast co-cultures 177

5.3.3 Methodological improvements concerning cell-material interactions between electrospun scaffolds and tendon derived fibroblasts 177

5.4 Future Work 178

5.4.1 Determining the clinical efficacy of current and future rotator cuff scaffolds 178

5.4.2 Determining the mechanism of tenocyte-endothelial cross-talk and establishing a causal link with tendon healing 179

5.4.3 Further exploring the effect cell-material interactions on angiogenesis through investigation of immune and endothelial cell populations during mono-culture, co-culture and in vivo 180

5.5 Conclusions 182

Chapter 6 References 184

Appendices 206

Appendix A - Additional information for Chapter 2 206

Appendix B Additional information for Chapter 3 208

Appendix C Additional information for Chapter 4 218

List of Figures

Figure 1-1. The hierarchical structure of tendon extracellular matrix 2
Figure 1-2. Schematic diagram illustrating the cross-talk between chronic inflammation and angiogenesis 7
Figure 1-3. Schematic diagram depicting rotator cuff tears and various repair strategies 10
Figure 1-4. Electrospinning of synthetic scaffolds 17
Figure 2-1. PRISMA flowchart of study selection 29
Figure 2-2. Forest plots comparing shoulder specific pain and function outcome scores, pain and re-tear rates at final follow-up between augmented and standard repair 62
Figure 2-3. Forest plots comparing shoulder specific pain and function outcome scores at final follow-up between patch types and standard repair 63
Figure 2-4. Forest plots comparing shoulder pain at final follow-up between patch types and standard repair 64
Figure 2-5. Forest plots comparing re-tear rates at final follow-up between patch types and standard repair 65
Figure 3-1. Schematic depicting the assessment of PBL adherence and migration during co-culture of HMEC-1 endothelial cells with tendon-derived fibroblasts 80
Figure 3-2. Effect of HMEC-1 endothelial cell co-culture on the mRNA expression of NK-κB targets by tendon fibroblasts during a 9-day time course 85
Figure 3-3. Effect of HMEC-1 endothelial cell co-culture on the mRNA expression of fibroblast activation markers by tendon fibroblasts 86
Figure 3-4. Effect of HMEC-1 endothelial cell co-culture on the mRNA expression of inflammatory cytokines by tendon fibroblasts 89
Figure 3-5. Effect of HMEC-1 endothelial cell co-culture on the mRNA expression of collagens I,III,VI and IX by tendon fibroblasts 90
Figure 3-6. Effect of HMEC-1 endothelial cell co-culture on the mRNA expression of tendon matrix proteins by tendon fibroblasts 91
Figure 3-7. Effect of HMEC-1 endothelial cell co-culture on the mRNA expression of ECM proteases by tendon fibroblasts 92
Figure 3-8. Effect of HMEC-1 endothelial cell co-culture on the mRNA expression of NK-κB, IFN and STAT6 pathway genes 93
Figure 3-9. Effect of HMEC-1 endothelial cell co-culture on the mRNA expression of the cell-cycle regulators FOXF2 and HSPB1 by tendon fibroblasts 94
Figure 3-10. Adhesion of peripheral blood leukocytes to HMEC-1 endothelial cells 95
Figure 3-11. Effect of tendon fibroblast co-culture on the mRNA expression of adhesion receptors involved in leukocyte capture by HMEC-1 endothelial cells 97
Figure 3-12. Effect of tendon fibroblast co-culture on the mRNA expression of adhesion receptors involved in leukocyte capture by HMEC-1 endothelial cells 98
Figure 3-13. Trans-endothelial migration of peripheral blood leukocytes through HMEC-1 endothelial cells 100

Figure 3-14. Trans-fibroblast migration of peripheral blood leukocytes through tendon derived fibroblasts 101
Figure 3-15. Effect of tendon fibroblast co-culture on the mRNA expression of endothelial junction molecules involved in the transmigration of leukocytes by HMEC-1 endothelial cells 102
Figure 3-16. Effect of tendon fibroblast co-culture on the mRNA expression of the VE-Cadherin/VE-PTP complex by HMEC-1 endothelial cells 103
Figure 4-1. Protocol for measurement of pore size, number and porosity with ImageJ 117
Figure 4-2. Effect of specific electrospinning parameters on fibre diameter 123
Figure 4-3. Effect of collector speed on fibre alignment 124
Figure 4-4. Characterisation of aligned electrospun fibres for subsequent *in vitro* experiments 125
Figure 4-5. Characterisation of randomly orientated electrospun fibres for subsequent *in vitro* experiments 126
Figure 4-6. Relationship between mean pore size and mean fibre diameter 127
Figure 4-7. Electrospun scaffold architecture modulates the morphology of healthy tenocytes 128
Figure 4-8. Heatmap and Principle component analysis (PCA) 130
Figure 4-9. Scaffold-by-scaffold comparison of differentially expressed genes 131
Figure 4-10. Volcano plot of differentially expressed genes for hamstring tendon fibroblast seeded on aligned scaffolds 132
Figure 4-11. Volcano plot of differentially expressed genes for hamstring tendon fibroblasts seeded on random scaffolds 133
Figure 4-12. Volcano plot highlighting the effect of scaffold anisotropy on healthy tendon fibroblast gene expression 136
Figure 4-13. Volcano plots showing enriched hallmark pathways and leading-edge analysis for hamstring tendon fibroblasts seed on aligned scaffolds 137
Figure 4-14. Volcano plots showing enriched hallmark pathways and leading-edge analysis for hamstring tendon fibroblasts seeded on random scaffolds 138
Figure 4-15. Volcano plots showing enriched hallmark pathways and leading-edge analysis for hamstring tendon fibroblasts seeded on anisotropic scaffolds 140
Figure 4-16. Effect of fibre diameter on gene expression of fibroblast activation markers for healthy tendon fibroblasts seeded on aligned PDO scaffolds 141
Figure 4-17. Effect of fibre anisotropy on gene expression of fibroblast activation markers for healthy tendon fibroblasts 142
Figure 4-18. Volcano plots showing enriched genesets and leading-edge analysis for hamstring tendon fibroblasts seeded on 4000nm aligned scaffolds 144
Figure 4-19. Volcano plots showing enriched genesets and leading-edge analysis for hamstring tendon fibroblasts seeded on 300nm random scaffolds 145
Figure 4-20. Volcano plots showing enriched extracellular matrix/cytoskeleton genesets and leading-edge analysis for hamstring tendon fibroblasts seeded on anisotropic scaffolds 146

Figure 4-21. Volcano plots showing enriched immune genesets and leading-edge analysis for hamstring tendon fibroblasts seeded on anisotropic scaffolds 147
Figure 4-22. Baseline differences in expression between healthy compared with diseased tenocytes 148
Figure 4-23. Volcano plots showing enriched genesets and leading-edge analysis for healthy compared with diseased fibroblasts 149
Figure 4-24. Principle component analysis (PCA) of healthy and diseased tendon fibroblasts 150
Figure 4-25. Scaffold-by-scaffold comparison of differentially expressed genes between diseased rotator cuff tendon fibroblasts cultured on scaffolds of different microarchitectures 151
Figure 4-26. Volcano plot of differentially expressed genes for diseased rotator cuff tendon fibroblasts seeded on aligned scaffolds 153
Figure 4-27. Volcano plots showing enriched genesets and leading-edge analysis for diseased rotator cuff tendon fibroblasts seeded on 4000nm aligned scaffolds 154
Figure 4-28. Volcano plots showing enriched genesets and leading-edge analysis for diseased rotator cuff tendon fibroblasts seeded on 300nm aligned scaffolds 155
Figure 4-29. Effect of fibre diameter on gene expression of fibroblast activation markers for diseased tendon fibroblasts seeded on aligned PDO scaffolds 156
Figure 4-30. Volcano plot highlighting the effect of scaffold anisotropy on diseased rotator cuff tendon fibroblast gene expression 157
Figure 4-31. Effect of fibre anisotropy on gene expression of fibroblast activation markers for diseased tenocytes 158
Figure 4-32. Volcano plots comparing the transcriptional profile of diseased rotator cuff tenocytes cultured on 2000nm aligned versus 2000nm random scaffolds 159
Figure 4-33. Volcano plots comparing the transcriptional profile of diseased rotator cuff tenocytes cultured on 4000nm aligned versus 4000nm random scaffolds 160
Figure 4-34. PDPN surface staining for healthy tendon fibroblast cultured on aligned electrospun scaffolds 161
Figure 5-1. Graphical summary of key findings 183
Figure B-1. Schematic diagram depicting co-culture method and mRNA extraction for cultures of tendon-derived fibroblasts and HMEC-1 endothelial cells 208
Figure B-2. Effect of exogenous IL-1β and IL-4 on inflammatory cytokine expression by EC co-cultured tendon fibroblasts 209
Figure B-3. Effect of endothelial cell co-culture on tendon fibroblasts collagen III:I ratio 210
Figure B-4. Effect of exogenous IL-1β and IL-4 on collagen expression by EC co-cultured tendon fibroblasts 211

Figure B-5. Effect of exogenous IL-1β and IL-4 on tendon matrix protein expression by EC co-cultured tendon fibroblasts 212
Figure B-6. Effect of exogenous IL-1β and IL-4 on ECM protease expression by EC co-cultured tendon fibroblasts 213
Figure B-7. Effect of exogenous IL-1β and IL-4 on NF-κB, IFN and STAT6 pathway genes by EC co-cultured tendon fibroblasts 214
Figure B-8. Effect of exogenous IL-1β and IL-4 on FOXF2 and HSPB1 by EC co-cultured tendon fibroblasts 215
Figure B-9. Effect of exogenous IL-1β and IL-4 on peripheral blood leukocytes to HMEC-1 endothelial cells during co-culture with tendon-derived fibroblasts 216
Figure B-10. Effect of co-culture with tendon-derived fibroblasts on the expression of inhibitors of leukocyte adhesion by HMEC-1 endothelial cells 217
Figure C-1. RNA-sequencing quality control metrics for tendon fibroblasts isolated from human hamstring 219
Figure C-2. RNA-sequencing quality control metrics for tendon fibroblasts isolated from human massive rotator cuff 220
Figure C-5. Scaffold anisotropy displays a limited ability to modulate healthy tendon fibroblast expression of genes involved in the regulation of angiogenesis 228
Figure C-6. Scaffold anisotropy displays a limited ability to modulate healthy tendon fibroblast expression of genes involved in the regulation of cytokine or chemokine production and activity 230
Figure C-8. Heatmap and dendrogram of healthy and diseased tendon fibroblasts cultured on 8 scaffolds with different microarchitectures 238
Figure C-9. In response to the variation of fibre diameter for randomly orientated scaffolds, the gene expression of diseased tendon fibroblast is largely unchanged 239
Figure C-10. Heatmap and PCA of diseased tendon fibroblasts cultured on scaffolds with different microarchitectures 240

List of Tables

Table 1-1 Electrospinning paraments with effect on fibre diameter or alignment. 19
Table 2-1 Summary of Study Designs 32
Table 2-2 Patch type and population demographics 39
Table 2-3 Functional Outcome Scores 42
Table 2-4 Risk of re-tear and complications 49
Table 2-5 Pain Scores 55
Table 2-6 Quality of Life Scores 58
Table 2-7 Risk of Bias (Randomised Trials) 66
Table 2-8 ROBINS-I Risk of Bias (Non-randomised Comparative trials) 67
Table 3-1 Primers used during qRT-PCR assessment of fibroblasts during endothelial cell co-culture 81
Table 3-2 Primers used during qRT-PCR assessment of HMEC-1 endothelial cells during co-culture with tendon-derived fibroblasts 82
Table 3-3 Antibodies used for extracellular staining of peripheral blood leukocytes
Table 3-4 Matched isotype controls 83
Table 4-1 Parameters utilised to produce aligned electrospun scaffolds for *in vitro* culture 114
Table 4-2 Parameters utilised to produce random electrospun scaffolds for *in vitro* culture 115
Table 4-3 Secondary antibodies used in imaging validation of RNAseq data 119
Table C-3.1 Leading edge genes contributing to enriched hallmark pathways for healthy fibroblasts cultured on 300nm aligned scaffolds compared with 1000nm aligned 221
Table C-3.2 Leading edge genes contributing to enriched hallmark pathways for healthy fibroblasts cultured on 4000nm aligned scaffolds compared with 1000nm aligned 221
Table C-3.3 Leading edge genes contributing to enriched hallmark pathways for healthy fibroblasts cultured on 300nm random scaffolds compared with 1000nm random 222
Table C-3.4 Leading edge genes contributing to enriched hallmark pathways for healthy fibroblasts cultured on 1000nm aligned scaffolds compared with 1000nm random 222
Table C-3.5 Leading edge genes contributing to enriched hallmark pathways for healthy fibroblasts cultured on 2000nm aligned scaffolds compared with 2000nm random 223
Table C-3.6 Leading edge genes contributing to enriched hallmark pathways for healthy fibroblasts cultured on 4000nm aligned scaffolds compared with 4000nm random 224
Table C-4.1 Leading edge genes contributing to enriched genesets describing immune system regulation for healthy fibroblasts cultured on 4000nm aligned scaffolds compared with 1000nm aligned 225
Table C-4.2 Leading edge genes contributing to enriched genesets describing immune system regulation for healthy fibroblasts cultured on 2000nm aligned scaffolds compared with 2000nm random 225

Table C-4.3 Leading edge genes contributing to enriched genesets describing immune system regulation for healthy fibroblasts cultured on 4000nm aligned scaffolds compared with 4000nm random 226
Table C-4.4 Leading edge genes contributing to enriched genesets describing regulation of immune response for healthy fibroblasts cultured on 300nm random scaffolds compared with 1000nm random 227
Table C-5.1 Leading edge genes contributing to enriched genesets describing regulation of angiogenesis for healthy fibroblasts cultured on 1000nm aligned scaffolds compared with 1000nm random 229
Table C-6.1 Leading edge genes contributing to enriched genesets describing regulation of cytokine or chemokine production by healthy fibroblasts cultured on 2000nm random scaffolds compared with 2000nm random 231
Table C-6.2 Leading edge genes contributing to enriched genesets describing regulation of cytokine or chemokine production by healthy fibroblasts cultured on 300nm random scaffolds compared with 1000nm random 231
Table C-7.1 Leading edge genes contributing to enriched genesets describing regulation of ECM production and cytoskeletal apparatus for healthy fibroblasts cultured on 1000nm aligned scaffolds compared with 1000nm random 232
Table C-7.2 Leading edge genes contributing to enriched genesets describing regulation of ECM production and cytoskeletal apparatus for healthy fibroblasts cultured on 2000nm aligned scaffolds compared with 2000nm random 233
Table C-7.3 Leading edge genes contributing to enriched genesets describing regulation of ECM production and cytoskeletal apparatus for healthy fibroblasts cultured on 4000nm aligned scaffolds compared with 4000nm random 235

List of Abbreviations

αSMA	Alpha Smooth Muscle Actin
ACAN	Aggrecan
ACK	Ammonium-Chloride-Potassium
ADAM	A Disintegrin and Metalloproteinase
Ang-2	Angiopoietin 2
ANOVA	Analysis of Variance
ASES	American Shoulder and Elbow Surgeons
BMEC	Bone Marrow Endothelial Cells
CAFS	Cancer Associated Fibroblasts
CENTRAL	Central Register of Controlled Trials
COX2	Cyclo-oxygenase-2
CRD	Centre for Reviews and Dissemination
CSF	Colony Stimulating Factor
DARC	Duffy Antigen Receptor
DARE	Database of Abstracts of Reviews of Effects
DBM	Demineralised Bone Matrix
DMEM/F12	Dulbecco's Modified Eagle Medium: Nutrient Mixture F-12
DNA	Deoxyribonucleic Acid
ECM	Extracellular Matrix
ECs	Endothelial Cells
ESAM	Endothelial Surface Adhesion Molecule
FAP	Fibroblast Activation Protein
FCS	Foetal Calf Serum
FGF-2	Fibroblast Growth Factor
GAG	Glycosaminoglycan
GFP	Gene Fluorescence Protein
GO	Gene Ontology
GSEA	Gene Set Enrichment Analysis
HFIP	1,1,1,3,3,3-Hexafluoro-2-propanol

HGF	Hepatocyte Growth Factor
HMEC-1	Human Microvascular Endothelial Cells 1
hMSCs	Human Mesenchymal Stem Cells
ICAM	Intercellular Adhesion Molecule
IFN	Interferon
IGF	Insulin-like Growth Factor
IL	Interleukin
JAMA	Junctional AdhesionMolecule A
MMP	Metalloproteinase
MRI	Magnetic Resonance Imaging
MSD	Mesoscale Discovery
NHS	National Health Service
NHS EED	NHS Economic Evaluation Database
NSAIDS	Non-steroidal Anti-inflammatory Drugs
OSS	Oxford Shoulder Score
PBL	Peripheral Blood Leukocytes
PBS	Phosphate Buffered Saline
PCA	Principle Component Analysis
PCL	Polycaprolactone
PCR	Polymerase Chain Reaction
PDGF	Platelet Derived Growth Factor
PDGF	Platelet Derived Growth Factor
PDO	Polydioxanone
PDPN	Podoplanin
PENN	Pennsylvannia
PGA	Polyglycolic Acid
PLGA	Poly(lactic-co-glycolic-acid)
PLLA	Poly-L-lactic acid
POA	Percentage Open Area
PRISMA	Preferred Reporting Items for Systematic Reviews and Meta-Analyses

PROMS	Patient Reported Outcome Measures
PRP	Platelet Rich Plasma
PVR	Polio Virus Receptor
RCR	Rotator Cuff Repairs
RCT	Rotator Cuff Tears
RNA	Ribonucleic Acid
ROBINS-I	Risk Of Bias In Non-randomised Studies - of Interventions
RPMI	Rosewell Park Memorial Institute 1640 media
SAA	Serum Amyloid Alpha
SELE	Selectin E
SELP	Selectin P
SEM	Scanning Electron Microscope
SIS	Small Intestinal Submucosa
STAT	Signal Transducer and Activator of Transcription
TCP	Tissue Culture Plastic
TGFβ	Tissue Growth Factor Beta
TNFα	Tissue Necrosis Factor Alpha
TNMD	Tenomodulin
UCLA	University of California, Los Angeles
USS	Ultrasound Scan
VAS	Visual Analogue Scale
VCAM1	Vascular Adhesion Molecule 1
VE-PTP	Vascular Endothelial cell-specific phosphotyrosine phosphatase
VEGF	Vascular Endothelial Growth Factor

Chapter 1 Introduction

1.1 Rotator Cuff Anatomy

The human shoulder's wide range of movement permits complex upper limb movements in multiple planes, allowing us to interact and influence the World around us. A low bony congruence between the humerus and glenoid fossa has evolved to facilitate this function, but at the cost of joint stability.[1,2] Unlike most other synovial joints, soft tissue constraints instead provide a series of static and dynamic tightropes that prevent glenohumeral subluxation during routine shoulder movements.[3] The key dynamic stabiliser is the rotator cuff, a set of 4 muscles; supraspinatus(SS), infraspinatus (IS), teres minor (TM) and subscapularis, that arise from the scapula before the tendons of the three postero-superior muscles (SS,IS and TM) condense to form a common cuff that inserts into the proximal humerus.[4]

1.2 Tendon Structure

Tendons efficiently transfer tensile forces from the muscles to the skeleton.[5] While the overall cellular content of tendon tissue is low, tendon fibroblasts, or tenocytes, are responsible for the production and maintenance of the ECM, the structure of which is critical to tendon function.[6,7] The most abundant constituent of the ECM is type 1 collagen which constitutes around 60% of the dry mass.[8] Type 1 collagen molecules self-assemble into highly organised hierarchical fibrils.[9] In turn, these aggregate into fibril bundles and fascicles which are the principle determinant of a tendon's mechanical strength (Figure 1-1).[10,11] In common with other soft tissues, proteoglycans (PGs) and their attached glycosaminoglycans (GAGs) make up the remaining non-cellular component of tendon and play a critical role in collagen fibrillogenesis and presentation of growth factors.[12,13]

1.3 Rotator cuff Injuries

Injury to this complex framework is a common occurrence. Shoulder pain is the third most common cause of musculoskeletal pain, with an estimated prevalence of 16-26% in the United Kingdom.[14] Rotator cuff disease, which progresses from tendinitis through to massive tears, constitute a large proportion of the disease burden, resulting in pain, disability and a significant

socioeconomic cost.[15–17] Indeed, tears of the rotator cuff affect around 50% of those over 66 years of age.[18] Ageing populations and increasing rates of obesity are expected to further amplify this problem.[19]

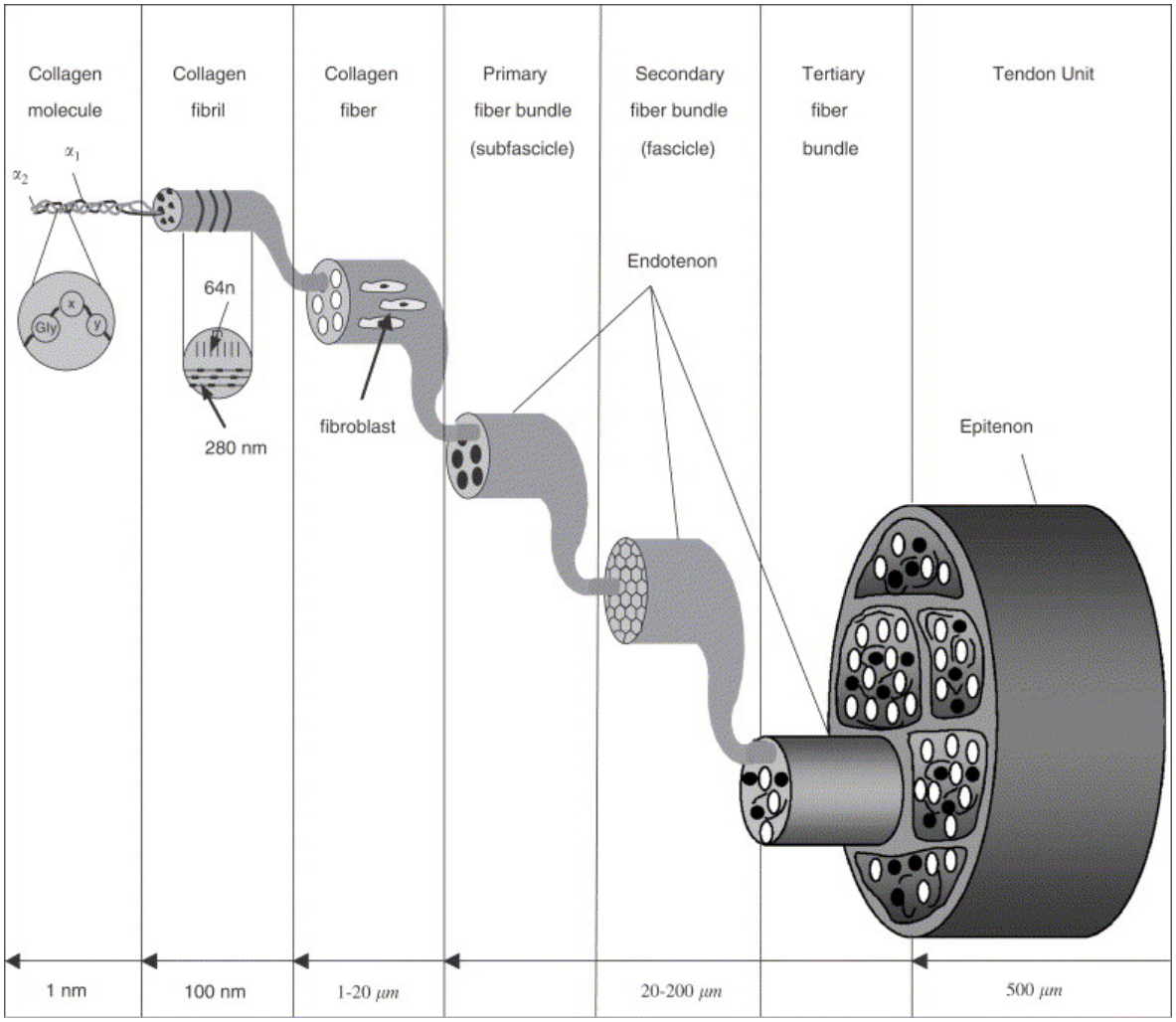

Figure 1-1 The hierarchical structure of tendon extracellular matrix. This hierarchical structure of collagen confers considerable mechanical strength to tendons. The fibril is the smallest structural unit of tendon with diameters ranging from 100nm-500nm. Fibres are the next level of a tendon structure with diameters from 1-20m. Fibres are bound by loose connective tissue (endotenon) that also containing nerves, vessels and lymphatics. Bundles of fibres form fascicles which are surrounded another layer of loose connective tissue, nerves, vessels and lymphatics - the epitenon. Reproduced with permission from Wang *et al. 2005.*[5]

Although spontaneous healing can occur, the morphological and mechanical properties of healed tendons never match those of a normal tendon.[20,21] Moreover, many tendon injuries demonstrate little capacity for successful repair and surgical intervention is frequently required. As such, the management of tendon injuries represents a substantial, and growing, economic burden. Over 10,000 rotator cuff repairs are performed annually in the UK and over 200,000 in the United States.[16] While resolution of symptoms correlates with rotator cuff

healing[22], our current surgical techniques result in functionally incompetent scar tissue with over 40% of rotator cuff repairs failing within 2 years of surgery.[22] This is in stark contrast with the low failure rates observed in other arenas of Orthopaedics, for example joint replacement surgery, in which the use of biomaterials to replace damaged tissue has revolutionised patient care.[23,24] Thus, there is a clear need to deliver a new generation of biomaterials that are capable of improving the healing rate of tendon.

1.4 PHYSIOLOGICAL TENDON REPAIR MECHANISMS

Healing is thought to progress through three overlapping stages of tissue inflammation, cellular proliferation and remodelling.[25–28] After injury the release of chemotactic and pro-inflammatory factors attracts neutrophils, monocytes and macrophages to the wound site, with the release of angiogenic factors stimulating the concomitant formation of a primitive vascular network.[29] Tenocytes are gradually recruited, and their rapid proliferation is responsible for the synthesis of a disordered ECM composed mostly of type III collagen.[30] The subsequent remodelling stage is characterised by a decreased in cellularity, decreased vascularity and a switch from type III to type I collagen synthesis.[31,32] While the extent of remodelling is dependent on anatomical location, species and disease model, in general there in an incomplete recapitulation of a tendons ECM structure and mechanical properties.[31,33]

The identity of cells contributing to tendon healing is not fully understood but is hypothesised to arise from intrinsic or extrinsic origins. Intrinsic cells are typically defined as the tenocytes within the collagen fascicles, whereas extrinsic populations reside within the surrounding paratenon and perivascular regions. In an attempt to determine the relationship and contribution of these populations to repair, lineage tracing experiments with transgenic ScxGFP$^+$ mice have been undertaken following patellar tendon injury.[34] After one week the paratenon had thickened and the defect infiltrated by numerous cells that expressed the tenogenic differentiation marker Scleraxis (Scx). Concurrently, these infiltrating cells also expressed the paratenon and perivascular cell marker αSMA.[34] Similar findings have also been reported in an murine model of achilles rupture.[35] To determine if the expanded SMA$^+$ population differentiated into ScxGFP$^+$ tenocytes a tamoxifen-inducible SMA9 reporter mouse (αSMA-CreERT2; R26-TdTomato) crossed with ScxGFP$^+$ mice were injured and the

percentage of double positive SMA9/Scx cells analysed. [36] At day 7, 12.5% of cells express both $SMA9^+/Scx^+$ which increased to 65% at day 14, suggesting that amplification of $SMA9^+$ cells are the main contributor of tendon healing in this particular model.[36] However, it is unclear whether the paratendon or perivascular niche is the source of these $SMA9^+$ progenitors.

In a novel model of Achilles transection in the neonatal mouse there is a complete recovery of the tendons mechanical properties with significantly improved collagen matrix organisation when compared with adult murine injury.[37] Lineage tracing with a Scleraxis Cre reporter system (Scx-CreERT2;R26-TdTomato) confirmed that in adult mice there is an abundant proliferation of intrinsic Scx^+ cells within the injured tendon stubs, but that these do not contribute to repair, with repair tissue instead expressing αSMA. In contrast, at 2 and 4 weeks after neonatal injury the repair site was mostly composed of Scx-lineage tenocytes recruited from the tendon stubs. Further, while adult Scx+ tenocytes were activated they demonstrated abnormal differentiation along chondrogenic lines, suggesting that aberrant differentiation of adult tenocytes may contribute to the failure of intrinsic repair mechanisms.[37] Unfortunately, while SMA^{+ve} fibroblasts are critical to dermal wound healing[38], the cellular mechanisms underpinning human tendon healing remains largely unknown.

1.5 PATHOBIOLOGY OF ROTATOR CUFF TENDON DISEASE

While several theories on the aetiology of tendinopathy have been proposed[39], it is increasingly evident that inflammatory mechanisms play a critical role in the pathogenesis of tendon disease.[40] A surgically induced rat model of Achilles tendon injury demonstrates a transient accumulation of neutrophils, followed by an increased macrophage infiltration between 1-28 days post-injury.[41] A failure of this inflammatory infiltrate to resolve has been implicated in human tendinopathy, with a persistent accumulation of macrophages and mast cells observed in painful human tendinopathic versus healthy tissue.[42] Other studies have also reported the persistence of NK cells and T lymphocytes in tendinopathic human Achilles biopsy samples.[43] However, the total size of the immune cell infiltrate appears to be dependent on disease stage with the number of mast cells and macrophages increasing as the size of rotator cuff tears (RCTs) increases.[44] Inflammatory pathway activation signatures are also influenced by the stage of disease – NKκB target genes were overexpressed in small RCTs,

whilst STAT6 pathways dominate in end-stage massive RCTs.[45] Interestingly, immunostaining for phosphorylated NF-kB–p65 was predominately localised to non-immune populations, implicating the stromal compartment of tendons in the persistence of the chronic inflammation.[45]

Indeed, fibroblasts in diseased tendon show increased expression of markers of fibroblast activation including Podoplanin (PDPN), Vascular Cell Adhesion Molecule 1 (VCAM-1/CD106) and Endosialin (CD248), which persists during *in vitro* culture.[46] The term 'activated' refers to the observation that αSMA^{+} fibroblasts associated with wound healing display an increased migratory and proliferative capacity, increase their production of ECM constituents and cytokines and are thought to be fundamental to injury resolution.[38,47,48] However, the aberrant accumulation of activated fibroblasts has also been implicated in several chronic inflammatory diseases such as rheumatoid arthritis (RA),[49,50] as well as fibrotic renal disease[51] and cancer metastasis.[52] Accumulating evidence also suggests that activated fibroblasts are in fact a highly heterogenous population with distinct functions. In the context of cancer associated fibroblasts, cells expressing Fibroblast Activation Protein (FAP) promote angiogenesis and immunosuppression, whilst αSMA^{Hi} fibroblasts seem to be responsible for collagen synthesis and the desmoplastic stromal reaction observed around tumors.[53] Similarly, in an elegant single-cell transcriptomic assessment of FAP^{+} fibroblasts isolated from a murine model of RA, two functionally distinct subsets were identified.[54] $FAP\alpha^{+}THY1^{+}$ fibroblasts were located in the synovial sub-lining and mediated persistent immune cell infiltration, while $FAP\alpha^{+}THY1^{-}$ fibroblasts were restricted to the synovial lining layer and mediated bone and cartilage destruction. It is not yet known whether the sub-populations of activated fibroblasts observed in tendon disease display similar heterogenicity. Nonetheless, activated tendon fibroblasts display increased cytokine production, a hyper-responsive state to further inflammatory stimuli and an increased capacity for the inactivation of protective pro-resolving lipid mediators via 15-Prostaglandin Dehydrogenase degradation.[46,55] Together, these studies strongly support the notion that resident tendon fibroblasts are implicated in the persistence of chronic inflammation in human tendon disease.

1.6 TENDON VASCULARITY

An association between tendon vascularity and rotator cuff disease was first suggested over 80 years ago. Codman postulated that regional hypovascularity, in the so-called 'watershed' or 'critical' zone, was responsible for cumulative age-related attritional damage that ultimately led to rotator cuff rupture.[56] Presumably, the biological premise underpinning this theory was that vascularity is critical to tendon healing.

More recent *in-vivo* studies utilising doppler ultrasound have cast doubt on the existence of a watershed area[57], with one systematic review concluding that the critical zone is an artefact caused by a failure of vascular casting techniques to adequately delineate the microvasculature.[57] Irrespective of whether regional hypovascularity is responsible for tendon ruptures, there is a clear response of the vascular bed to tendon injury. Vessel density is a key component of the Bonar histological scoring system[58], a research tool utilised for grading tendinopathy severity. Similarly, Matthews *et al*. in a histological characterisation of 40 small to massive RCTs reported hypervascularity in samples taken from the tear edge, with a sequential decrease in vessel density as tear size increased.[44] Similar results have been reported by studies utilising doppler ultrasound, with an increase in intra-tendinous blood flow observed across the whole tendon and not just at the tear site.[59] Vessel number may also increase following rotator cuff tendon repair and biomaterial implantation[60], raising the possibility that angiogenesis can be modulated.

The cellular and molecular mechanisms underpinning pathological angiogenesis in tendon disease are yet to be fully elucidated. However, in the context of other chronic inflammatory diseases, including RA and psoriasis, there is a well-recognised co-dependence between inflammation and angiogenesis.[61] Sprouting angiogenesis is a complex multistep process involving ECM degradation, proliferation, survival, migration, and anastomosis of endothelial cells (ECs), with each stage co-ordinated by a careful balance of anti- and pro-angiogenic factors.[62] Vascular endothelial growth factor (VEGF) is a critical pro-angiogenic growth factor that is produced by macrophages and fibroblasts in an NF-κB dependent manner[63,64] and can be upregulated by Cyclo-oxygenase-2 (COX2) induction.[65] Disease rotator cuff tendon displays upregulated NF-κB, COX2 and VEGF, although the relative contributions of different

cell types to the production of VEGF is not yet known.[45,55,66] Further, many inflammatory mediators including prostaglandins E_1 and E_2, TNFα, IL-1β, IL-6 and IL-8, which are elevated in tendon disease,[66] can induce angiogenesis *in vitro* through either direct action on ECs, or through the modulation of VEGF production by immune and stromal cell populations.[61]

While inflammatory mediators can promote new vessel formation, angiogenesis can in turn sustain inflammation (Figure 1-2).[67] For example, angiopoietins act as regulators of vessel maturation but also play crucial roles during inflammation. Mice deficient in Angiopoietin 2(Ang-2) failed to mount an inflammatory response to Staphylococcus aureus induced peritonitis, a phenotype that was rescued on administration of recombinant Ang-2.[68]

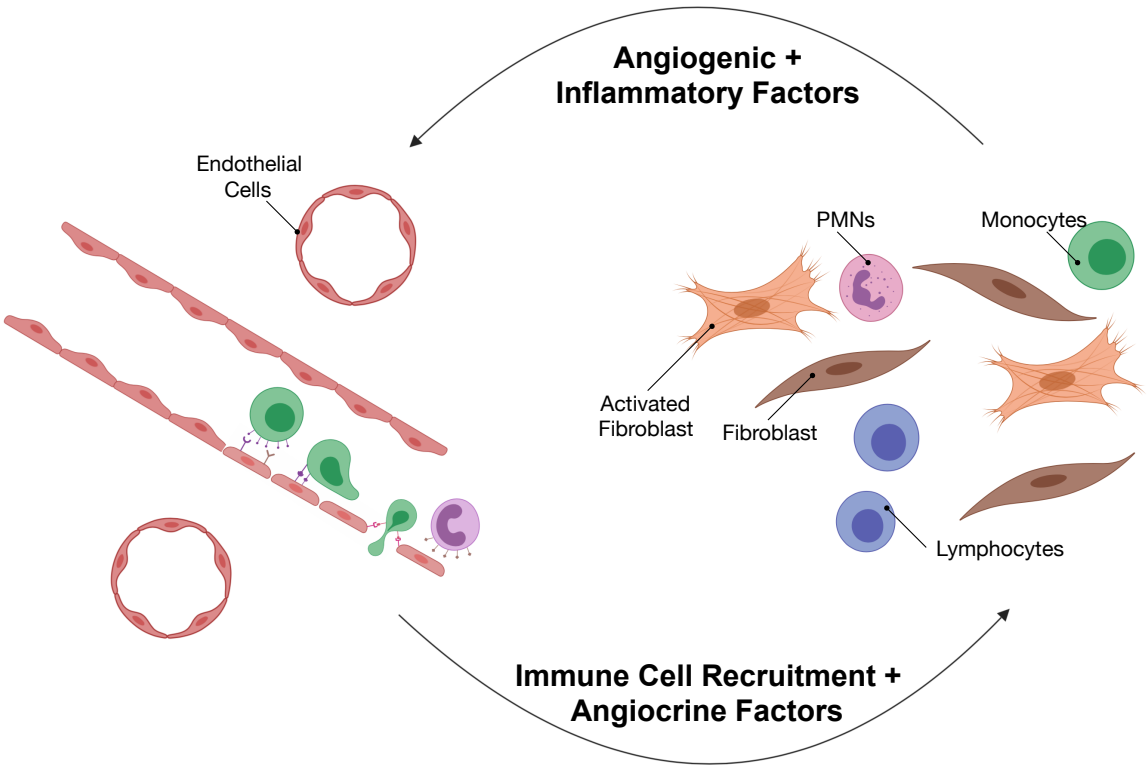

Figure 1-2 Schematic diagram illustrating the cross-talk between chronic inflammation and angiogenesis. Immune and stromal inflammatory cells secrete cytokines and proteases that causes ECM degradation and permit endothelial cell sprouting, migration and tube formation. In turn, endothelial cells are also able to recruit immune cells and regulate tissue repair through the production of Angiocrine factors. Abbreviations: Polymorphoneutrophils (PMNs)

Indeed, many pro-inflammatory cytokines are potent activators of neighbouring ECs, causing endothelial expression of adhesion molecules that facilitate leukocyte extravasation through a series of well-defined steps known as capture, rolling, leukocyte arrest and transmigration through the ECs, pericytes and basement membrane.[69] Endothelial selectins, E-selectin and

P-selectin, are induced on the surface of endothelial cells in inflamed tissues and mediate leukocyte capture from flowing blood.[70] Chemokines, generated by ECs or tissue resident inflammatory cells, activate the rolling leukocytes and enable binding to members of the immunoglobulin superfamily, such as Intercellular Adhesion Molecule 1 (ICAM1) and VCAM1.[70] The expression of these adhesion molecules is induced on endothelial cells by pro-inflammatory cytokines and mediate the firm adhesion of immune cells.[70] Leukocytes are then able to crawl on the luminal surface of vessels until they are able to migrate between transiently opened endothelial cell junctions. It is not yet known whether the endothelium in tendon disease undergoes a similar phenotypic change to inflammatory cytokines.

The molecular mechanisms that control diapedesis are less well understood but involve the opening of endothelial junctions through the dissociation of VE-PTP from VE-cadherin, as well as the sequential interaction of a large number of endothelial cell surfaces receptors with leukocytes.[70] These receptors include the junctional adhesion molecules JAMA, JAMB, JAMC, the related endothelial surface adhesion molecule (ESAM) as well as ICAM2, CD99, CD99L2, CD47 and Polio Virus Receptor (PVR). These have all been implicated in leukocyte diapedesis in a variety of *in vitro* and *in vivo* studies.[69]

Fibroblast-EC interactions are critical to this process with the exact phenotype of the fibroblast population controlling immune cell recruitment.[71,72] In the context of RA, diseased synovial fibroblasts lose their immune-suppressive function causing an increase in the number of adherent lymphocytes,[73] an effect that was in part dependent on IL-6.[74] In summary, persistent angiogenesis appears to be both a consequence and a potential cause of chronic inflammation, with mounting evidence that diseased fibroblasts playing a critical role in orchestrating these co-dependent processes.

1.7 ANGIOCRINE SIGNALLING

The vascular bed is not just a passive transport network. As well as delivering oxygen, nutrients and inflammatory cells, microvascular ECs can also regulate the homeostasis of tissues through the production of angiocrine factors.[75] For many organs, tissue-specific stem cells are often positioned in close proximity to capillary ECs, with the size and activation state

of the EC niche being a direct determinant of a tissues capacity for repair. [76,77] Murine derived bone marrow endothelial cells (BMECs) are able to direct haematopoietic stem cell renewal and expansion ex vivo.[78] Moreover, after lethal irradiation, mice receiving transplantations BMECs demonstrated accelerated haematopoietic recovery.[78]

More recently, angiocrine signalling has been shown to be critical to musculoskeletal tissue repair. In murine skeletal systems specialised type H vessels, that are positive for CD31 and Endomucin, have been described.[76] Through the angiocrine release of Noggin, type H ECs act as critical regulators of both osteogenesis and chondrogenesis.[79] Similarly, the co-culture of ECs with striated-muscle precursor cells, supported stem cell proliferation through the production of Insulin-like Growth Factor 1 (IGF1), Hepatocyte Growth Factor (HGF), Fibroblast Growth Factor 2 (FGF-2), Platelet Derived Growth Factor BB (PDGF-BB) and VEGF-A.[80] Whilst a link between vascularity and tendon healing has long been suggested[39], the existence of a tendon-specific angiocrine response has not yet been investigated. There is evidence to suggest that the healing of murine ligaments can be improved by artificially increasing vessel formation.[81,82] Nonetheless, other authors have found an association between neovascularisation and foreign body reactions following dermal implantation of electrospun scaffolds in mice,[83] suggesting that vessel formation must be phenotypically and temporally appropriate.

1.8 Treatment of Rotator Cuff Tears

Non-surgical approaches in the management of rotator cuff tears include physiotherapy, oral non-steroidal anti-inflammatories (NSAIDs) and injections of corticosteroid into the subacromial bursa. However, no randomised controlled trials have yet been undertaken to support the use of exercise therapy[84] and a similar paucity of evidence exists for the use of NSAIDs and corticosteroids in rotator cuff tears.[85] In fact, *in vitro* data has questioned whether these medications may in fact be harmful – reducing tendon fibroblast viability, collagen synthesis and dampening production of pro-resolving prostaglandins.[86,87]

After 12 months of non-operative management, approximately 40% of patients will continue to experience pain, with many requiring surgical repair of the tear.[88] To this end, a multitude

of surgical strategies have been developed that aim to oppose the free edge of the tendon back onto the insertion site on the humeral head.[89] Recent variations, including a double-row suture technique or administration of platelet rich plasma onto the repair, all aim to improve the mechanical[84] or biological environment[84] of healing tendons. Unfortunately, these approaches have not improved the outcome of rotator cuff repair[90–92] with over 40% of repairs failing within 24 months of surgery.[22]

More recently, the use of biomaterial patches to augment the surgical repair site has gained popularity. To provide structural and biological support scaffolds are either surgically sutured over the top of the tendon-to-bone repair, or interposed between the tendon and bone to fill any residual defect in an otherwise irreparable tear (Figure 1-3).

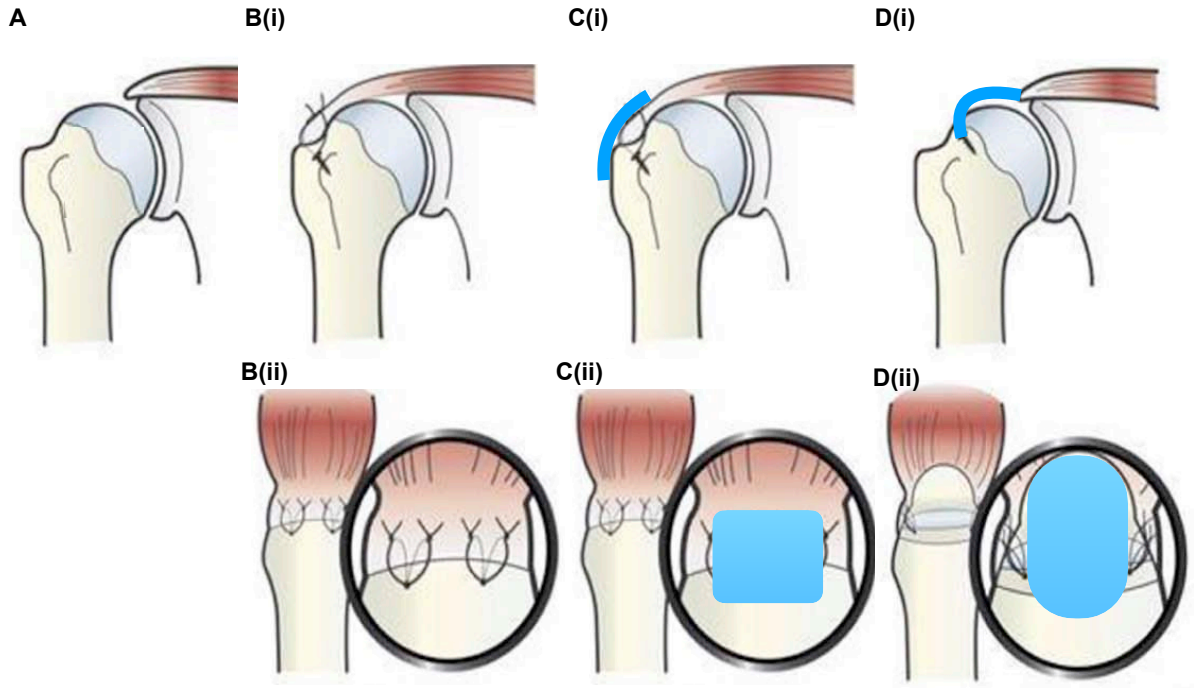

Figure 1-3 Schematic diagram depicting rotator cuff tears and various repair strategies (A)Torn rotator cuff tendons retract from their insertion position on the greater tuberosity - the rotator cuff footprint (B)Traditional suture repair of the rotator cuff utilising a single or double row of bone anchored sutures that provide compression of the torn tendon back onto the footprint - repair demonstrated in coronal and axial orientations by images (i) and (ii) respectively (Ci + ii) Coronal and sagittal images depicting *on-lay* augmented rotator cuff repair in which the biomaterial is secured over the top of the traditional suture repair (Di + ii) Coronal and axial images depicting *interposition* augmented rotator cuff repair in which the biomaterial is used to fill any residual defect of an otherwise irreparable tear. Modified from Jeong *et al.*[91] with permissions.

1.9 SCAFFOLD AUGMENTATION OF ROTATOR CUFF REPAIRS

The number of patches, or scaffolds, available for use in rotator cuff surgery is increasing and can be broadly grouped into two categories based on the materials used – biological and synthetic. The removal of cellular components from xeno- or allografts to produce a decellularized extracellular matrix is a common method of biological scaffold production. Alternatively, synthetic scaffolds can be produced from a variety of polymers.

1.9.1 Biological scaffolds – Decellularised ECM

The removal of cellular components from xeno- or allografts to produce a decellularised ECM, is a common method of biological scaffold production. It aims to retain proteins and the three-dimensional architecture of the original tissue to provide instructive chemical and structural signals, but without causing implant rejection.[93] The implantation of demineralised bone matrix (DBM) demonstrates sufficient bioactivity to induce new bone formation *in vivo*,[94] an effect that is maintained even when implanted into muscle.[95] However, in the context of trauma and orthopaedic surgery, the clinical evaluation of DBM has failed to demonstrate efficacy.[96] Despite this, the use of ECM derived scaffolds have been translated into the tendon arena and are one of the most commonly used methods for augmenting tendon repair.[97,98] Promising results have been reported in animal models[99], but with highly variable clinical results, including concerns surround biocompatibility for the Restore® patch.[100]

1.9.2 Biological scaffolds – Natural Hydrogels

Natural hydrogels constitute another major class of biological scaffold. These are water-swollen polymeric networks formed from numerous hydrophilic proteins or polysaccharides.[101] Given that collagen is a key and ubiquitous component of the ECM, it is not surprising that collagen based hydrogels have been extensively studied for cardiac[102], ophthalmic[103] as well as musculoskeletal applications.[104] However, in the context of tendon repair, rather than being utilised independently they are often used as a vehicle for cell delivery or as a means of functionalising a synthetic scaffold.[105,106]

In comparison to Tissue Culture Plastic (TCP), collagen hydrogels provide a preferential *in vitro* environment for the culture of tenocytes.[107] Additionally, Human Mesenchymal Stem

Cells (MSCs) cultured in collagen hydrogels demonstrate greater proliferation and differentiation into tenocytes, than when cultured on TCP.[107] Few studies have assessed *in vivo* the efficacy of unseeded hydrogels in tendon repair. In a rabbit model of Achilles tendon rupture a collagen hydrogel improved the histological and biomechanical properties of healing tendons over standard repair. Nevertheless, the biomechanical properties remained far below those of a normal Achilles tendon.[108] Conversely, a fibrin hydrogel failed to demonstrate any biomechanical or clinical advantage over standard repair in a rabbit flexor tendon injury model.[109]

The poor mechanical properties of hydrogels remain a major limitation and arises from their failure to fully recapitulate natural ECM structure. Crosslinking is commonly employed to improve the mechanical properties but may reduce sites for cellular attachment and can result in toxicity[110] and fibrous encapsulation.[111] Other processing methods include the production of aligned collagen fibres[112] and the incorporation of other ECM components.[113] However, the mechanical properties remain far below those of native tendon.

1.9.3 Synthetic Scaffolds

Both degradable and non-degradable synthetic scaffolds are currently under development for rotator cuff repair. The latter approach, similar to hernia repair, aims to permanently support the diseased tendon and negates the need for complete tissue regeneration. Polycarbonate polyurethane patches are currently under investigation with promising early results. In a non-randomised case series, 90% of patients had an intact repair at 12 months with no adverse events reported.[114] Similar results have been reported for polyethylene terephthalate (Dacron).[115] However, there remain concerns over a higher infection risk[116] and long-term toxicity. Carbon-fibre implants, once utilised in the treatment of rotator cuff tears[117], can shed carbon debris that elicits a foreign body response in tissues distant from the initial implantation site.[118,119] A failure to stimulate adequate regeneration, with consequential fatigue of the polymer, has been cited as a plausible causative mechanism.[120]

Degradable polyesters, including poly-L-lactic acid (PLLA)[121], poly(lactic-co-glycolic acid) (PLGA)[122], polycaprolactone (PCL)[123,124] and polydioxanone (PDO)[125,126] are among the most

promising candidates currently under development. Interestingly, different polymers have diverse effects on the cellular response. Although PLLA, PLGA and polyglycolic acid (PGA) are all poly-α-hydroxyesters, variations in cellular attachment, morphology and proliferation are observed.[127]

Aside from polymer type, several strategies including manipulation of porosity, fibre alignment, fibre diameter and surface roughness can produce new biomaterials through a targeted and precise 'bottom-up' design process. One such approach employs biomimicry, the synthetic replication of biophysical stimuli normally provided by the healthy tissue niche, to alter cellular phenotypes and drive an improved healing response.

1.9.4 Modification of Synthetic Scaffolds

Engineering of materials with optimal properties for cellular ingrowth and differentiation requires an understanding of the complex relationship between a material's surface properties, micro-architecture and cellular response. The effect of modifications to a material's surface properties, including hydrophobicity, charge and incorporation of bioactive molecules, on the response of stromal cells has been reviewed elsewhere.[128] This thesis will concentrate on the modulation of a scaffold's physical properties.

The nanoscale architecture of native ECM provides a natural network that structurally supports cells and guides their behaviour.[129] Through the formation of focal adhesions, cells can transmit mechanical signals into the nucleus, resulting in epigenetic modifications and altered protein expression.[130] Synthetic biomaterials can be modified so as to recapitulate aspects of this complex biophysical environment. A material's dimensionality[131], stiffness[132], and topography[133,134] have all been shown to influence cell behaviour.

As the primary constituent of tendon ECM, collagen fibrils are a critical determinant of a tenocytes physical and mechanical environment. Fibril diameter (50-200 nm)[135,136], anisotrophy[137] and nanotropography created by repeating D-bands[138] all contribute to a tendons biophysical signature. Tendinopathy changes many of these parameters[8] and in turn, this may contribute to the phenotypic shift that diseased tenocytes undergo.[139] Thus, by adjusting the microscale and nanoscale architecture of synthetic materials to mimic those of

a healthy tendons ECM niche, it might be possible to manipulate the phenotype of diseased tenocytes.

1.9.4.1 Scaffold anisotropy

Collagen anisotropy is fundamental to the function of tendon.[140] If we are to effectively imitate native tendon ECM it follows that a scaffold's microscale architecture must also be highly aligned. Several techniques can modulate scaffold anisotropy of which electrospinning is one of the most widely investigated. It provides a relatively easy and cost effective way of producing a 3D network of aligned ultrafine polymer fibres.[141] Refinement of this technology has enabled the efficient adjustment of the degree of fibre alignment.[142]

Murine NIH3T3 Fibroblasts, seeded onto aligned electrospun PCL fibres orientate and proliferate in the direction of the fibres.[143] An increase in proliferation,[144] migration[145], and upregulated expression of genes linked to adhesion and actin polymerisation is also observed.[143] Similar results have been reported for tenocytes cultured on aligned PDO fibres.[146] Fibre orientation has also been found to influence the fate of hMSC differentiation.[147] Likewise, aligned PLLA scaffolds support proliferation and tenogenic differentiation of tendon derived stem cells.[148]

Deposition of newly produced ECM is also sensitive to fibre alignment. Using second harmonic generation it has been demonstrated that collagen deposition on aligned microfibres displays greater organisation.[149] Biomechanical testing found improved tensile properties for aligned scaffolds, a difference that was amplified as appropriately aligned collagen was laid down during prolonged culture. Early *in vivo* work has also demonstrated that aligned PLLA scaffolds, seeded with human tendon stem cells and implanted subcutaneously into nude mice, caused an improvement in cellular and ECM alignment than when random scaffolds were implanted.[148]

1.9.4.2 Cell type

The vast majority of studies have utilised 'healthy' tendon cells, yet tenocytes isolated from tendon tears demonstrate an altered phenotype.[45] Furthermore, although external biomechanical cues also influence the orientation[150] and proliferation rate of diseased rotator cuff tenocytes, their response at the mRNA level does not precisely mirror that of healthy

cells.[146] Clearly, when investigating the effects of biomechanical cues on tendon healing, the target tissue niche must always frame our enquires. Disease specific changes in a tendon fibroblast phenotype[151] will adjust this niche and is likely to significantly influence cell-material interactions.

1.9.4.3 Fibre diameter

In addition to fibre anisotropy, electrospun fibre diameter can also be manipulated to produce scaffolds with nanoscale (<1000nm) or microscale (>1000nm) fibres.[152] However, how these parameters interact to elicit the cell response most favourable for tendon repair remains to be fully determined. On randomly orientated PLGA scaffold fibre diameter has no discernible effect on the proliferation of murine MSCs.[153] In contrast, for aligned scaffolds with fibre diameters ranging from 150-6000nm, human dermal fibroblast proliferation and collagen expression demonstrated fibre diameter dependency.[154,155] Other work has suggested that the morphological changes observed for NIH3T3 murine fibroblasts cultured on aligned scaffolds only occur above a critical fibre diameter of ~300nm.[152] This cellular response may also be cell type specific, regardless of anisotropy, fibre diameters >2μm consistently influenced the tenogenic differentiation of C3H10T1/2 stem .[156] Importantly, diseased rotator cuff tenocytes demonstrated higher rates of proliferation, collagen and GAG production when cultured on aligned electrospun scaffolds with submicron fibre diameters [157] - raising the possibility that the behaviour of diseased tenocytes can be further tuned through the manipulation of fibre diameter.

1.9.4.4 Scaffold Porosity

The spacing between fibres within a scaffold can also provide cells with topographical information. Smaller pore sizes, (<150 μm) seem to increase the adhesion of fibroblasts isolated from the human dermis and equine digital flexor tendons.[158,159] An effect that may be driven by an increase in a materials surface area[160], roughness[159] or through modulation of micromechanical properties.[158] However, pore size is also intimately related to overall porosity with large pore size generally resulting in an increased porosity.[160] Higher porosity improves the mass transport of nutrients and increases fibroblast proliferation, migration and enables deeper penetration into the scaffold.[161–164] For osteoblasts the increased proliferative rate associated with large pore, high porosity scaffolds overcomes the initial advantage offered by

an increased attachment rate for scaffolds with small pore sizes.[165] The degree of connectivity between pores is also important. Scaffolds that demonstrate higher degrees of interconnectivity, but constant porosity, facilitate increased migration of fibroblasts into the scaffold.[166]

1.9.4.5 Scaffold Stiffness

Substrate stiffness also plays an important role in fibroblast biology, however it has, to date, seen only limited translation into the tissue engineering arena.[167–169] Microarray analysis has demonstrated that hydrogel stiffness modulates cellular phenotype, with an increased expression of ECM genes and a decreased expression of matrix degrading enzymes, characterising human dermal fibroblasts grown in less compliant environments.[170] Bovine tenocytes demonstrate a similar responsiveness to the stiffness of silicone micropillars.[171] Unfortunately, with many of the methodologies previously utilised it is often difficult to separate the influence of changes in stiffness from the concurrent changes in other biophysical parameters.

1.10 Fabrication of Electrospun Synthetic Scaffolds

Several fabrication techniques including 3D-printing[172] and electrospinning[172] allow the production of synthetic scaffolds with varied and manipulable biophysical parameters. Amongst these, electrospinning has several advantages including cost effectiveness, scalability and fine control over scaffold architecture – allowing the tailoring of properties for optimal cellular differentiation, proliferation and migration. These characteristics make electrospun scaffolds ideal for tissue engineering and regenerative medicine with electrospun materials now under development for cardiac[172], dermal[172] and musculoskeletal applications.[172] These include the Biopatch[125] and BioYarn[126] which are currently under commercial development for use in rotator cuff tendon repair.

1.10.1 Electrospinning Process

The basic electrospinning setup consists of three major components (i) a high voltage power supply (ii) a syringe and spinneret to feed the solution and (iii) a collector to deposit the electrospun fibres. A typical setup is illustrated in figure 1-4.

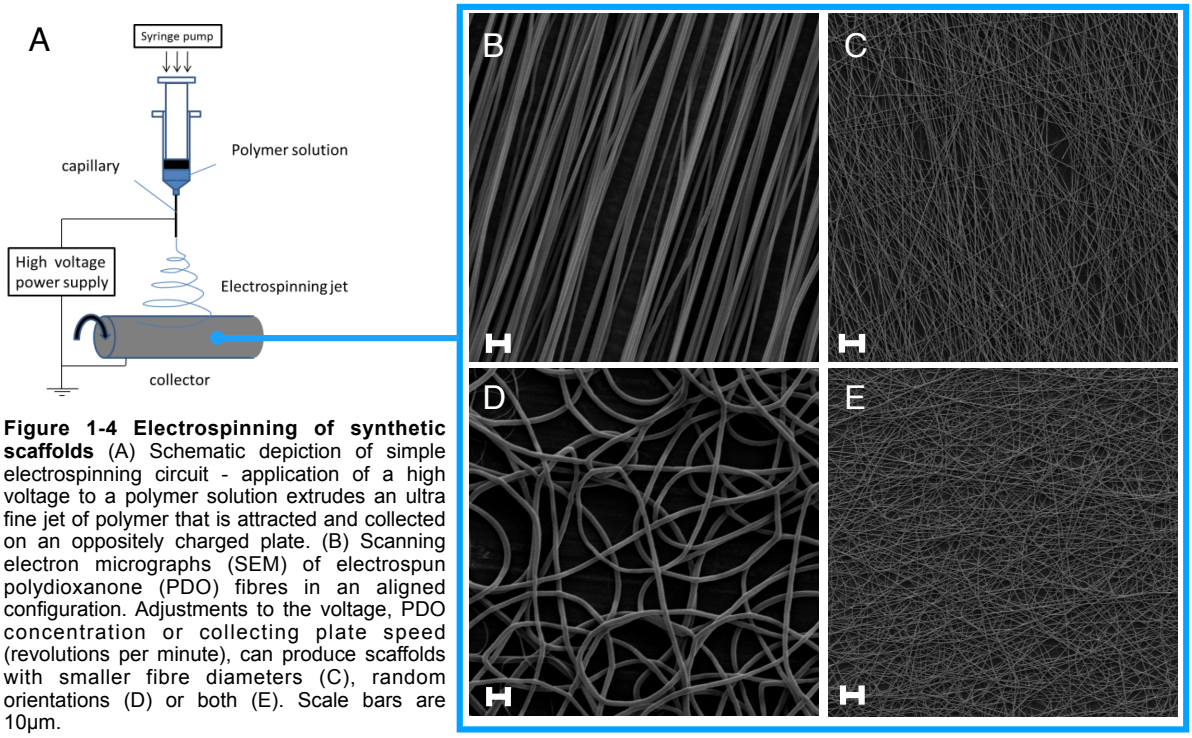

Figure 1-4 Electrospinning of synthetic scaffolds (A) Schematic depiction of simple electrospinning circuit - application of a high voltage to a polymer solution extrudes an ultra fine jet of polymer that is attracted and collected on an oppositely charged plate. (B) Scanning electron micrographs (SEM) of electrospun polydioxanone (PDO) fibres in an aligned configuration. Adjustments to the voltage, PDO concentration or collecting plate speed (revolutions per minute), can produce scaffolds with smaller fibre diameters (C), random orientations (D) or both (E). Scale bars are 10μm.

A polymer is first dissolved in a highly volatile solvent and slowly extruded from the syringe to form a droplet at the tip of the spinneret. When the positive pole of a high voltage DC power supply is connected to this nozzle, positive ions within the solution are repelled and concentrate towards the centre of the solution.[173] Accumulation of these positive charges and their respective forces of attraction on the negatively charged collector increase as the amount of external voltage is increased. Ultimately, these electrostatic forces are able to overcome the surface tension of the fluid droplet, forming a conical-shaped droplet known as the Taylor cone.[174] At the apex, where surface tension becomes minimal, a jet of solution escapes and is drawn towards the collector. In accordance with Earnshaw's theorem, electrostatic repulsions within the jet then induce a series of bending or whipping instabilities resulting in a series of spiral motions that allow entangled polymer chains to be stretched out.[175] As the volatile solvent evaporates, small diameter polymer fibres are received by the collector.

1.10.2 Basic Parameter Alterations

Many parameters can affect the electrospinning process and the resulting architecture of the scaffolds produced. These are summarised in table 1-1.

The concentration of the polymer solution plays an important role in fibre formation. At low concentrations a high surface tension tends to pull the solution together, resulting in the formation of small droplets – a technique known as electrospraying.[176] As the concentration is increased there is a gradual transition from beads to smooth, uniform, nanoscale fibres.[177] Beyond this threshold, incremental increases in polymer concentrations will results in larger diameter fibres.[176,178]

A threshold voltage is also required for the ejection of charged polymer jets from the Taylor cone. Higher voltages increase the electrostatic forces and several groups have reported reductions in fibre diameter until bead formation is observed at very high voltages.[179,180] Higher voltages can also result in multiple jets causing an increase in fibre branching and cross-linking.[180] However, these effects appear to be dependent on polymer type, with higher voltages having no effect or increasing the diameter of polyethylene oxide or poly(vinyl alcohol) fibres respectively.[181,182] The polymer flow rate also offers a means of controlling fibre diameter. Higher flow rates allow less time for polymer polarisation, resulting in large fibre diameters but with greater diameter variability and an increased rate of beading.[183]

Replacing the collector plate with a rotating mandrel is a common method of modifying fibre anisotropy.[184,185] If the velocity of the rotating collector is higher than the flight velocity of the electrospun fibre aligned fibres are collected, but increases in collector speed also reduce fibre diameter.[186] Indeed, many of the adjustable electrospinning parameters are not independent of each other[174] and attention has recently turned to the use of machine learning to develop algorithms capable of predicting fibre diameter.[187,188]

Table 1-1 Electrospinning paraments with effect on fibre diameter or alignment.

Parameter	Effect
Solution	
- Polymer Type[189]	Determines size + fibre morphology
- Polymer Concentration[176–178,190]	Related to viscosity. Low → beading, further increases → larger fibre diameters
- Molecular Weight[191,192]	Related to polymer concentration. Low molecular weight → beading. Further increased → larger fibre diameters
- Conductivity[193,194]	Addition of salts or pyridine to polymer solution → increased conductivity → reductions in fibre diameter
- Solvent[191,192]	Different solvents alter surface tension, reducing beading and/or fibre diameter
Processing	
- Voltage[179–182]	Relationship with fibre diameter dependent on polymer type
- Polymer Flow Rate[183]	Increased flow rate → increased fibres but with larger variance. Beading at high rates
- Collector-Tip distance[180,181]	Increased distance → reduced diameters and/or beading
- Collector Motion[184]	Higher tangential velocities increase fibre alignment
Ambient	
- Temperature[190]	Higher temperatures → reduced diameters
- Humidity[195]	Higher humidity → increased diameters and surface pitting on fibres.

1.11 AIMS

This thesis aims to establish the clinical need for a new generation of biomaterials that are capable of modulating the pathobiology of rotator cuff tears, understand the role endothelial cells play in tendon disease and produce electrospun materials that are able to modulate vessel growth. Specifically, this thesis aims to:

1. Identify, critically appraise and undertake evidence synthesis for studies reporting on the augmented repair of rotator cuff tears in terms of clinical effectiveness and safety
2. Investigate the role of the endothelium in the pathogenesis of human tendon disease with respect to fibroblast phenotype and recruitment of immune cells
3. Investigate how a scaffold's microscale topographical features can modulate the angiogenic signalling of resident tendon fibroblasts

1.12 HYPOTHESES

1. Current rotator cuff patch designs do not sufficiently improve clinical outcomes, but that patch type can influence outcomes
2. Endothelial-tenocyte crosstalk will influence the activation signature of tenocytes and this interaction will be modulated by the disease status of tendons from which tenocytes are derived
3. Endothelial-tenocyte crosstalk will influence the recruitment of peripheral blood leukocytes and this interaction will be modulated by the disease status of tendons from which tenocytes are derived
4. Alterations in the micro-architectural features of an electrospun scaffold will modulate the activation status of tendon fibroblasts and this will alter the angiogenic transcriptional profile of tenocytes.

Chapter 2 Use of implantable meshes for augmented rotator cuff repair - a systematic review and meta-analysis

2.1 ABSTRACT

2.1.1 Background

Surgical repair of rotator cuff tears has a high failure rate (~40%).Implanted surgical meshes are being increasingly used in an attempt to improve the integrity and healing of Rotator Cuff Repairs (RCR), a technique known as 'patch augmentation'. The objective of this review was to appraise studies reporting on the clinical effectiveness and safety of patch augmented RCR and to identify the most effective and safe materials in use.

2.1.2 Methods

Medline, Embase and Cochrane databases were searched between April 2006 and August 2018, according to a previously published search strategy. All randomised and non-randomised (comparative and single-intervention group) studies evaluating adults (≥ 18 years) undergoing rotator cuff surgery were considered. No restriction was placed on language. Risk of bias assessment was carried out for all randomised (RoB2, Cochrane) and comparative studies (ROBINS-I, Cochrane).

2.1.3 Results

We included 52 studies involving 1596 participants, consisting of 4 Randomised Controlled Trials (RCTs), 11 observational comparative studies and 37 observational case series with a variety of patch materials utilised (human allo/autograft [46%]; xenograft [33%]; synthetic [20%]). 14 comparative studies reported on shoulder specific functional outcome scores, 13 on the radiographic occurrence of re-tear and 11 on pain score metrics. Only one comparative study did not use standard, non-augmented repair, as a comparator arm.

Compared with non-augmented repair, a small improvement in shoulder function or pain scores was observed for synthetic patches with a mean improvement of 9.8 points on the UCLA shoulder score (95% CI, 9.10 to 10.51) and 0.46 point reduction on the VAS (95% CI -0.74 to -0.17) respectively. A reduced likelihood of radiologically observed re-tear was observed for synthetic (RR 0.40, 95% CI 0.25 to 0.64) and allograft (RR 0.34, 95% CI 0.18 to 0.64) derived patches. A total of 42 studies provided information about the occurrence of complications. A similar complications rate was observed for patch augmented (2.3%) and standard repair (2.1%).

2.1.4 Conclusions

There was little or no published evidence on the clinical effectiveness or safety of a number of patches in clinical use. While several studies suggest a decreased failure rate and some improvements in shoulder function and pain following augmented RCR, a lack of rigorous clinical evaluation prevents firm recommendations on this technology. There is a need for both well-designed multi-centre RCTs capable of robustly evaluating the effectiveness of patches of different types, and for large observational registry cohorts to assess the safety of these types of implants.

PROSPERO REGISTRATION: CRD42017057908

2.2 INTRODUCTION

Shoulder pain is the third most prevalent musculoskeletal disorder and is responsible for prolonged periods of disability, absence from work and a significant health-economic burden.[88,196,197] Rotator cuff problems account for a large proportion of shoulder pain and results in pain, weakness, reduced shoulder mobility and sleep disturbance. It is estimated that the overall prevalence of full-thickness tears is between 15-20% with the rate set to increase as populations age.[198,199] Unfortunately, symptoms in the elderly are particularly persistent with almost half of over 60's seeking recurrent medical attention and many experiencing continued problems over 2 years after initial presentation.[88,196] Many symptomatic full-thickness tears will often require surgical repair, with successful repair though to be correlating with symptom resolution.[22] Indeed, 9,000 rotator cuff repairs (RCRs) are performed each year in the NHS in England alone, at a cost of £6,500 per operation.[16] Unfortunately, RCRs have demonstrated a failure rate of up to 40%, with increasing patient age and tear size both predictive of failure.[22,200] While various surgical techniques have attempted to improve the outcome of RCR, there remains a real need to improve healing rates.[90]

One approach is the use of an implant called a surgical mesh, or patch, to augment the repair. A patch made from Teflon was first described over 30 years ago[201], but recently, the number and types of patch specifically for rotator cuff surgery has increased significantly and can be broadly grouped into several categories based on the materials used. The removal of cellular components from xeno- or allografts, derived from animal or human cadaveric tissue respectively, to produce a decellularized Extracellular Matrix (ECM) is a common method of biological scaffold production. Alternatively, autografts are a patient's own whole tendon harvested from various anatomical site. Finally, synthetic patches can be produced from a variety of bio-inert polymers that are commonly employed as suture materials. Patch augmentation can also be classified based on the method of application into 'on-lay' or 'bridging'. The former refers to the application of a synthetic or biological patch over the top of a standard repair to provide mechanical stability and biological stimulation, reducing the likelihood of failure and improving patient outcomes.[202,203] In contrast, 'bridging' refers to the

use of a patch as an interposition graft to fill any residual defect of an otherwise irreparable tear, providing a scaffold for the regeneration of tendon and/or scar tissue formation.[204] *Ex vivo* testing has demonstrated that patches differ in their mechanical properties as well as their ability to stimulate healing.[205]

Recent debates surrounding medical device regulation has emphasized the need for robust clinical evaluations of safety, efficacy and surveillience.[206] Unfortunately, in the context of patch augmentation, the growing number of available patches, mixed results and recent concerns over safety, including adverse immunological responses[207], have generated a clouded and uncertain landscape.

2.3 AIMS

The aim of this systematic review was to identify and critically appraise those studies reporting on the clinical effectiveness and safety of patch augmented surgical repair in adults with rotator cuff tears. The key objectives were to:

1. Undertake evidence synthesis using systematic review methodologies, including meta-analysis, to evaluate the relative effectiveness of patch augmented rotator cuff repair
2. Undertake a review of adverse events associated with all identified patches
3. To identify the most clinically effective and safe patch sub-type, as well as other key parameters, that can inform a future definitive randomised controlled trial

2.4 HYPOTHESES

This work hypothesises that patch augmented rotator cuff repair is a safe procedure, but that current patch designs, thus far, have failed to deliver sufficiently large improvements in clinical outcomes.

The specific hypotheses of this chapter are that:

1. Patch augmented rotator cuff repair demonstrates some, albeit small, improvements in the rate of re-tear, patient reported outcomes and pain.
2. Complications after patch augmented rotator cuff repair are comparable to those of standard, non-augmented, repair
3. Patch type influences the clinical effectiveness and safety of augmented surgical repair of the rotator cuff

2.5 METHODS

2.5.1 Protocol and Registration

Evidence synthesis was carried out according to the recommendations of the Cochrane Handbook for Systematic Reviews[208], the Centre for Reviews and Dissemination (CRD) guidance for undertaking reviews in health care[209] and was reported according to the Preferred Reporting Items for Systematic Reviews and Meta-Analyses (PRISMA).[210] The review protocol and search strategy has been previously been registered (PROSPERO Registration: CRD42017057908) and published in full.[211]

2.5.2 Eligibility Criteria

2.5.2.1 Population

The review incorporated studies of adult (≥18 years) patients who required surgical repair of a rotator cuff tear. No restrictions were applied to tear type (partial or full thickness), size (small through to massive), tendon involvement (supraspinatus, infraspinatus, teres minor or subscapularis), primary or recurrent tears or the presence of medical comorbidities. For the purpose of this review small (<1cm), medium (1-3cm) and large (3-5cm) tears were classified according to the DeOrio and Cofield classification[212]. Due to the large number of classification systems available, tears were considered massive if they met 1 of following criteria: (1) Measured >5cm in the anterior-posterior dimension[212], (2) involved ≥2 tendons[213], or were (3) described as being massive by the study authors.

2.5.2.2 Interventions

All studies where at least one treatment arm included the use of patches to augment rotator cuff surgery were included. A patch was defined as an implantable human, synthetic, or animal material which is used with the aim of improving tissue healing and/or patient outcome via some form of mechanical support. Patches were grouped in to xenograft, allograft, autograft or synthetic. There was no restriction placed on the type of surgery received or the experience of the surgeon. The type of patch surgery was classified as either (1) 'on-lay' or (2) 'bridging' in accordance with previously reported definitions[214]. We excluded studies that investigated

the use of sutures or anchors in isolation, or studies investigating drug therapy or physiotherapy, except when used as a comparator group or in addition to patch augmentation.

2.5.2.3 Comparators

No restriction was placed on the type or number of control groups.

2.5.2.4 Outcomes

The primary outcomes of interest in this review were (1) Shoulder specific function and pain scores – measured using a previously validated scale (2) Patch related adverse events (3) Shoulder pain outcomes – measured using validated tools such as the Visual Analog Scale (VAS) or non-validated scales. (4) Health related quality life – measured using tools such as Short Form-36 (SF-36), EuroQol- 5D (EQ-5D) or other assessment measures. The main secondary outcome was the radiological assessment of post-operative rotator cuff integrity.

2.5.2.5 Study types

All relevant randomised controlled trials (RCTs) and observational studies (comparative and single group) involving ≥5 patients were considered. No language restrictions were applied. In vitro studies, animal studies, review articles, editorials and studies involving ≤5 patients were all excluded. Economic evaluations were permitted, although none were identified

2.5.3 Search Strategy

A previous Cochrane systematic review had carried out a comprehensive search prior to April 2006.[90] Based on this search, we searched the following databases between the dates of April 2006 to February 2017 (and updated our search in August 2018): (1) EMBASE (2) MEDLINE (3) The Cochrane Library, incorporating; Central Register of Controlled Trials (CENTRAL), Cochrane Database of Systematic Reviews, Database of Abstracts of Reviews of Effects (DARE), The health technology assessment database, NHS Economic Evaluation Database (NHS EED). In addition, the reference list of all identified articles and reviews identified, were checked for relevant articles.[214–218] The search strategy was initially developed for Embase (Appendix A-1) and has previously been published.[211] Our strategy was subsequently modified for use in Medline and Cochrane Library databases.

2.5.4 Study selection

Two reviewers independently screened all titles and abstracts identified from the search strategy. Full reports for all relevant studies identified were then reviewed and assessed against the eligibility criteria. A third independent reviewer was available to resolve any disagreements regarding study inclusion. Reasons for exclusion are detailed in the PRISMA flow diagram (Figure 2-1).

2.5.5 Data Extraction

Two reviewers extracted the following data from all eligible studies: general study information (authors, publication year, study location), study population (sample size, age, gender, tear size), study characteristics (study design, inclusion/exclusion criteria, duration of clinical and radiological follow-up, surgical technique, patch characteristics), all primary and secondary outcomes for each study and adverse events or complications. Each reviewer independently checked the results of the data extraction process.

2.5.6 Risk of bias assessment

The risk of bias was independently assessed by two reviewers and discrepancies discussed with a third reviewer allowing resolution based on unanimous decision. RCTs were assessed using the ROB2 (2011 update) provided by the Cochrane Collaboration.[219] Each domain was rated as a 'low', 'high' or an 'unclear' risk of bias before the study as a whole was assessed. Observational comparative studies were assessed using the ROBINS-I tool.[220] The risk of bias for each domain was judges as low, moderate, serious, critical or no information, followed by an overall judgement of biases based around the judgements from each individual domain. Single-arm studies were not formally assessed for risk of bias.

2.5.7 Data Analysis

Identified studies were stratified (RCTs, observational comparative studies, single-arm studies) and a narrative summary of results from RCTs and observational comparative studies reported in accordance with the standards set out in the PRISMA-P checklist.[210] Data from single-arm studies were only utilised in the quantification of complications. All studies that compared the outcomes of RCR with graft augmentation versus standard RCR were considered for meta-analysis. A meta-analysis was conducted only for outcomes consistently

reported across studies and reported using Review Manager v5.3 (RevMan, Cochrane Collaboration). Regardless of the observed statistical heterogeneity, we conducted an analysis for each patch type (xenograft, allograft, autograft or synthetic) when each type was represented by at least two studies. Given the known controversy surrounding xenograft isolated from Small Intestinal Submucosa (SIS), the analysis for xenografts was further divided into SIS-derived and non-SIS. There were insufficient study numbers to permit subgrouping based on graft configuration (on-lay or bridging).

2.5.8 Statistical Analysis

For dichotomous parameters included in the meta-analysis the Risk Ratio (RR) with 95% CI was calculated for each graft type. For continuous variables, such as shoulder specific functional outcome scores, the effect was reported as the mean difference with 95% CI. Due to significant heterogeneity in the specific functional shoulder scores utilised between studies, a meta-analysis was conducted using the most frequently used score across all studies at final follow-up. Within each patch type, if no single functional outcome score was consistently used, we combined scores and reported a standard mean difference (95% CI). Studies in which no standard deviation was calculable, or where only subcomponents of functional outcome scores were reported, were excluded. Heterogeneity was characterised by use of the I^2 statistic and a random-effect analysis used to incorporate heterogeneity among studies.

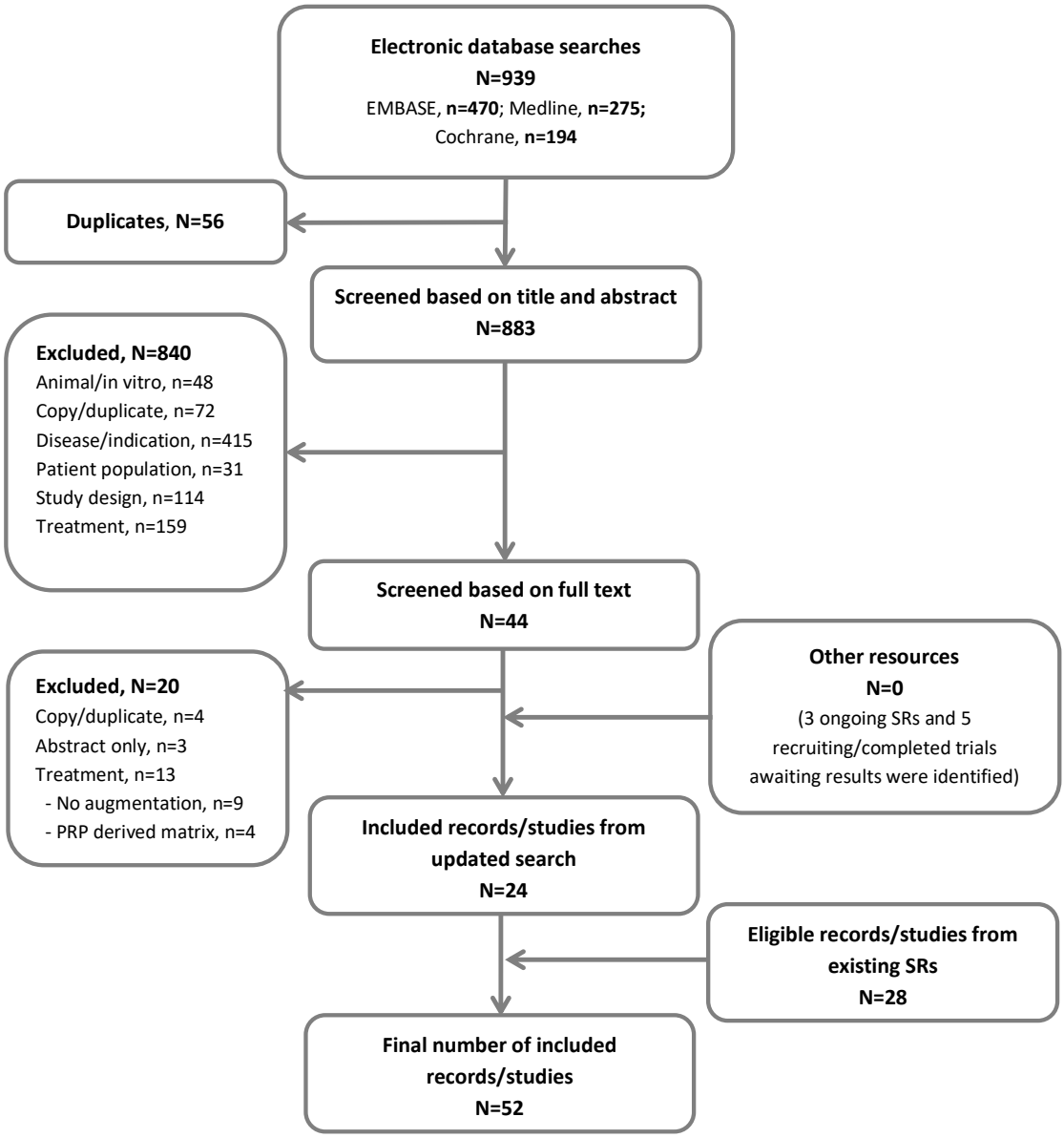

Figure 2-1 - PRISMA flowchart of study selection A total of 939 studies were identified after initial searches of EMBASE, Medline and Cochrane databases. Following review by two independent reviewers a total of 52 studies were selected for inclusion in the systematic review. Abbreviations: N, number; PRISMA, Preferred Reporting Items for Systematic Reviews and Meta-Analyses; SR, systematic review

2.6 RESULTS

2.6.1 Study selection

The search strategy identified 939 articles, of which 56 were duplicates (Figure 2-1). A total of 882 abstracts were reviewed in detail with 44 appearing to meet inclusion criteria. After full text review 27 articles were excluded based on the following criteria: included an abstract only (n=3), treatment was a Platelet Rich Plasma (PRP) derived matrix lacking the structural properties of patch augmentation (n=4), rotator cuff repair did not involve any form of augmentation (n=9), the article was a duplicate (n=4).A further 28 articles were identified from existing systematic reviews, generating a total of 52 studies for inclusion. No economic evaluations of patch augmented rotator cuff surgery were identified.

2.6.2 Study Characteristics

Comparative studies: Four RCTs and eleven observational comparative studies involving 896 patients were identified. Most comparative studies assessed a single patch against standard repair, with some studies having up to three treatment arms.[221,222,223] Study population sizes ranged from 30-89 patients for RCTs (age range 29-82), and 21-152 patients (age range 36-83) amongst observational comparative studies, with a predominance of male participants across all studies. Only two studies included the full spectrum of full thickness tear sizes, with most studies instead restricting recruitment to large or massive tears of the supraspinatus and infraspinatus. Other eligibility criteria were highly heterogeneous but with the exclusion of patients with significant glenohumeral osteoarthritis (n=10) emerging as a common theme (Tables 2-1 and 2-2).

The RCTs employed various time points of data collection. One RCT collected data preoperatively, and at six weeks, three, six 12 and 24 months post-operatively, another collected at 12 and 24 months, and a third at 14 months.

Non-comparative studies: 37 observational case-series involving 700 patients were identified. The study populations ranged from 5-61 patients (ages range 26-89) with the majority (n=28) only recruiting patients with large or massive full thickness tears. Petricciolo *et al.* was the only study to have reported on the use of patch augmentation in the treatment of isolated

subscapularis tears,[224] while Schlegel *et al.* recruited only patients with partial thickness supraspinatus tears.[225]

Table 2-1 | Summary of study designs

Study	Design	Intervention(s)	Stated eligibility criteria	Size		Follow-up	Outcomes	
				Recruited*	Analysed		Primary	Secondary
Randomised Comparative Studies								
Barber 2012[226], USA	RCT	Graftjacket® augmented repair **vs** no augmentation	(1) Aged 18-75 years (2) Large (>3cm width + 2-tendon involvement) RC tears (3) Primary RC repair (4) Amenable to arthroscopic repair (5) Good preoperative movement of contralateral arm (6) Ability to perform postoperative exercises (7) Ability to read and understand English for PROMs (8) Willingness to participate in post-operative follow-up (9) No massive (>5cm) or subscapularis tears (10) No inflammatory, autoimmune disease, cancer, highly communicable disease or active infection (11) Non-smokers only	NR	42	MRA, 12 or 24 months Clinical evaluation, 6 and 12 months, annually thereafter	Repair failure	Constant, UCLA, ASES
Bryant 2016[227], Canada	RCT	Restore® augmented repair **vs** no augmentation	(1) All patients scheduled for RC repair (2) Able to repair defect with a residual defect of ≤1cm or <1cm of medialization (3) No other shoulder disease; Grade II-IV SLAP lesion, Bankart lesion, Hill Sachs Lesion, ≥ grade 3 OA† (4) No significant shoulder girdle paralysis (5) No systemic or active joint infection (6) No major medical or psychiatric illness, or developmental handicap (7) No previous shoulder surgery (except acromioplasty or diagnostic arthroscopy) (8) Ability to read and understand English (9) Willingness to be assessed for 1 year after surgery	62	62	MRA, 12 months Clinic evaluation, 1.5, 3, 6,12, 18 and 24 months	Repair failure	WORC, ASES, Constant, SST, SF-36
Iannotti 2006[228], USA	RCT	Restore® augmented repair **vs** no augmentation	(1) Large or massive tears of supraspinatus and infraspinatus tendons on pre-op MRI (2) Age > 18 years (3) Tear ≥ 3 months' duration (4) Fully repairable tear – determined intraoperatively (5) No prior shoulder surgery (6) No glenohumeral arthritis, frozen shoulder or cervical spine disease	32	30	MRA, 12 months Clinical Scores, Mean 14 months (range 12-26.5)	Repair failure	PENN, SF-36
Leuzinger 2016[221], Switzerland	RCT	Graftjacket® **vs** Artelon® **vs** Restore®	(1) Primary or revision RC repair (2) Stage >2 fatty degeneration of supraspinatus according to Goutallier *et al.*‡ (3) No history of glenohumeral OA (4) Repairable tear not requiring bridging with a patch (5) At least 3 years follow-up	92	89	MRI, 6 months Clinical evaluation 6 and 36 months	Repair failure, Constant, SSV	-
Non-Randomised Comparative Studies								
Ciampi 2014[222], Italy	Comparative observational study	Repol Angimesh augmented repair **vs** Tutopatch augmented repair **vs** no augmentation	(1) Pre-op MRI evidence of a full-thickness tear involving 2 tendons (2) Postoperative residual retraction of 2 cm (3) Stage 1 or 2 fatty degeneration according to Goutallier *et al.*‡ (4) Failure of 6-months non-operative management consisting of physical therapy and anti-inflammatory medications (4) Duration of symptoms for at least 3 months (5) No other shoulder pathology requiring additional procedures; Grade II-IV SLAP lesion, Bankart lesion, biceps tenodesis (6) No glenohumeral OA, inflammatory arthritis or any rheumatic condition (7) No cortisone injections within 12 weeks of surgery (8) No contralateral shoulder injuries	N/A	152	US, 12 months Clinical Scores, 2 and 35 months	UCLA	VAS, Repair failure
Gilot 2015[229], USA	Comparative observational study	Arthroflex® augmented repair **vs** no augmentation	(1) Patient is scheduled for primary RC repair (2) Large to massive rotator cuff tear on MRI (3) Aged 18-85 years (4) Patient is willing and able to provide scores for the study (5) No known allergy to the augmentation material (6) No drug, solvent or alcohol addiction (7) No bacteremia, systemic or surgical site infection	40	35	US and Clinical Score, 1.5,3,6,12 and 24 months	Repair failure	SF-12, ASES, VAS, WORC, shoulder activity level survey

			(8) No pregnant or nursing patients (9) No history of autoimmune disease (10) No personal beliefs prohibiting use of grafts					
Ito 2003[230], Japan	Comparative observational study	Fascia lata allograft **vs** no augmentation	(1) Large or massive cuff tears on MRI or pneumo-arthrogram (2) Pain and loss of function despite conservative therapy	28	21	Final follow-up (range 2-8 years)	Japanese Orthopaedic Association shoulder surgery score, ROM (degrees)	-
Jeon 2017[231], South Korea	Comparative observational study	Long head of biceps **vs** no augmentation	(1) L-shaped rotator cuff tears (2) Minimum follow-up period of 2 years (3) No revision surgery (4) No subscapularis tendon tears (5) No glenohumeral OA or instability	N/A	64	MRI, 6 months US, 12 months Clinical evaluation, 3,6,12 and final follow-up (range 24-40 months)	ASES, Constant, VAS, Strength (NR)	-
Maillot 2018[223], France	Comparative observational study	Conexa™ **vs** standard repair **vs** debridement only	(1) Large to massive RC tear on MRI or CTA (2) Failure of non-operative management consisting of a period of relative rest, nonsteroidal anti-inflammatory medication, physiotherapy > 3 months and >2 corticosteroid (3) Functional impairment or unacceptable pain for a minimum of 3 months (4) Stage 2 or 3 fatty degeneration according to Goutallier *et al.*‡ (5) No glenohumeral OA or prior ipsilateral shoulder surgery	32	32	Clinical evaluation, 3,6,12 and 24 months	Constant	VAS, ROM (degrees)
Mori 2013[232], Japan	Comparative observational study	Tensor Fascia Lata **vs** no augmentation	(1) Irreparable large or massive RC tear with pain and functional disability refractory to conservative treatment (2) Stage 3-4 fatty degeneration of supraspinatus + stage 1-2 degeneration of infraspinatus according to Goutallier *et al.* ‡ (3) Intact teres minor tendon (4) Availability of MRI to evaluate the integrity of the rotator cuff tendons and/or autografts pre- and post-operatively (5) Minimum follow-up period of 24 months (6) Absence of the drop-arm sign (7) Absence of stage 3 or 4 fatty degeneration of infraspinatus (8) Stage 1 or fatty degeneration of supraspinatus were excluded (9) Absence of full thickness subscapularis tendons (10) No history of; surgery, nerve palsy, glenohumeral OA, diabetes, symptom onset following motor vehicle accident	N/A	48	MRI, not reported Clinical evaluation, 6, 12 and 24 months	Repair failure	Constant, ASES, UCLA, VAS
Mori 2015[204], Japan	Comparative observational study	Tensor Fascia Lata + grade 1-2‡ infraspinatus fatty atrophy **vs** Tensor Fascia Lata + grade 3-4‡ infraspinatus fatty atrophy	(1) Irreparable large to massive RC tear (2) Pain + disability refractory to nonsurgical treatment (oral anti-inflammatory medications, corticosteroid injections + physical therapy) (3) Stage 3 -4 fatty degeneration of supraspinatus according to Goutallier *et al.* ‡ (4) Intact teres minor tendon (5) <75% fatty degeneration of infraspinatus (6) Availability of MRI to evaluate the integrity of the rotator cuff tendons and/or autografts pre- and post-operatively (7) Minimum follow-up period of 24 months (8) Absence of the drop-arm sign (9) No history of; surgery, nerve palsy, glenohumeral OA, diabetes, symptom onset following motor vehicle accident (10) No full subscapularis tears	N/A	45	MRI, not reported Clinical evaluation, 6, 12 and 24 months	Repair failure	Constant, ASES, ROM
Tempelaere 2017[233], France	Comparative observational study	Quadriceps tendon **vs** no augmentation	(1) Massive RC tears (2) Patients < 70 years old (3) Pain + loss of strength refractory to medical treatment (≥1 injection, rehabilitation session) (4) No stage 3 -4 fatty degeneration of supraspinatus or infraspinatus according to Goutallier *et al.* ‡ (5) No history of ipsilateral; shoulder surgery, dislocation, fracture, glenohumeral OA, diabetes, symptom onset following motor vehicle accident	80	50	Final follow up – range 12-116 months	Constant, Subjective shoulder value (SSV), Strength(kg)	-
Vitali 2015[234], Italy	Comparative observational study	Repol Angimesh + Long head of Biceps augmented repair **vs** no augmentation	(1) MRI evidence of a full-thickness tear involving 2 tendons, (2) Stage 1 or 2 fatty degeneration according to Goutallier *et al.* ‡ (3) Patients with pain and a deficit in elevation, not responding to physiotherapy (4) Intraoperative evidence of irreparable rotator cuff lesion (5) Minimum follow-up of 3 years after surgery (6) Active and motivated patients (7) No other shoulder pathology requiring additional procedures; Grade II-IV SLAP lesion, Bankart lesion, biceps tenodesis	N/A	120	MRI, 12 months Clinical evaluation, 3 and36 months	UCLA	Repair failure, VAS, range of motion (degrees), Strength(kg)

			(8) No glenohumeral OA, inflammatory arthritis or any rheumatic condition (9) No cortisone injections within 12 weeks of surgery (10) No contralateral shoulder injuries					
Walton 2007[100], Australia	Comparative observational study	Restore® augmented Repair **vs** no augmentation	(1) Poor-quality tendon or a large-to-massive full-thickness tear of a tendon that could be attached to the greater tuberosity after appropriate mobilization techniques (2) Intact subscapularis tendon	NR	31	MRI, 24 months 3 months, 6 months, and 24 months	Repair failure, Pain and function questionnaire[#], systematic shoulder examination[¶], strength(N)	-
Yoon 2016[235], South Korea	Comparative observational study	Bone Marrow Stimulation + Allocover™ augmented repair **vs** no augmentation	(1) Massive RC tears (2) Persistent severe pain and disability (3) Unresponsive to ≥ 6 months of non-operative treatment (4) Repairable RC tears (5) Minimum follow-up of 1 year after surgery (6) No advanced glenohumeral OA (≥ stage 4, Hamada *et al.*)[§] (7) No prior surgery to affect shoulder (8) No contralateral shoulder lesions	87	75	MRI, 12 months Clinical evaluation, 12 months + final follow-up (range 14-43)	VAS, UCLA. Constant, ASES, SST, Repair failure	-
Non-comparative studies								
Agrawal 2012[236], USA	Non-comparative observational study	Allopatch HD™	(1) Primary RC tears ≥ 3 cm (2) Recurrent RC tears of any size (3) Arthroscopic repair undertaken	N/A	14	MRI, 1-2 years Clinical evaluation, 12 months	Repair failure, Constant, Flex SF	-
Audenaert 2006[237], Belgium	Non-comparative observational study	Mersilene®	(1) Primary massive full-thickness tears of ≥ 2 tendons, measuring >4cm in maximal diameter (2) Irreparable by simple suture (3) Open repair undertaken (4) Inability to elevate arm beyond 90º after 3 months, despite maximal conservative treatment	41	41	US and Clinical evaluation, Mean 43 months (range 24–86)	Repair failure, Constant	-
Badhe 2008[238], UK	Non-comparative observational study	Zimmer® collagen repair patch	(1) MRI or US evidence of RC tears ≥5cm involving both the supraspinatus and infraspinatus tendons (2) Refractory to a trial of nonoperative management, including physiotherapy and steroid injections	10	10	MRI + USS, 'final follow-up'- Mean 54 months (range 36-60) Clinical evaluation, 12 months + 'final follow-up'	Constant, Repair failure	-
Bektafier 2010[239], Turkey	Non-comparative observational study	Corocoacromial ligament	[Eligibility criteria not explicitly stated] (1) Treated for a rotator cuff tear between 2003-2009	N/A	46	Clinical evaluation, 1, 3 + 12 months (range NR)	Constant, Acromio-humeral distance	-
Bond 2008[240], USA	Non-comparative observational study	Graftjacket®	(2) MRI evidence RC tears ≥5cm and/or 2 tendon tears (3) Irreparable tears – determined at prior arthroscopy	N/A	16	MRI, 3 + 12 months Clinical evaluation, 3, 6, 12 months and 'final follow-up' - Mean 26.7 months (range 12-38)	UCLA, Constant, SST, Pain Score, Repair failure	-
Burkhead 2007[241], USA	Non-comparative observational study	Graftjacket®	(1) Massive (≥ 2 tendon + ≥ 5 cm) or recurrent RC tears (2) Repairable tears only (3) No active infection	N/A	17	MRI/CTA and Clinical evaluation, Mean 14.4 months (range NR)	UCLA, Pain, Repair failure	-
Cho 2014[242], South Korea	Non-comparative observational study	Permacol™	(1) Posterosuperior massive RC tear (≥ 5 cm or ≥ 2 tendon), confirmed by MRI and arthroscopy (2) Inability to reduce the residual cuff to the anatomic (3) Active individuals ≤ 60 years (4) Unresponsive to > 3 months of non-operative treatment (5) No prior shoulder surgery (6) Able to comply with the post-op rehabilitation programme (7) Anterosuperior massive RC tears were excluded (8) No irreparable RC tears - could be only partially repaired despite full mobilisation (9) No superior humeral head migration (10) No stage 3-4 fatty degeneration according to Goutallier *et al.*[‡]	5	5	MRI, 6 months Clinical evaluation, 'final follow-up' - Mean 20.6 months (range 14-27)	VAS, UCLA, ASES, Repair failure	-
Consigliere 2017[243], UK	Non-comparative observational study	DX reinforcement matrix	(1) Large (>3cm) + Massive (>2 tendon) RC tears (2) Repairable RC tears only (3) Poor tissue quality only	10	10	Clinical evaluation, 3,6 and 12 months	Constant, OSS, VAS	-

			(4) Patients will achievable objectives (pain relief + improved function) (5) No evidence of cuff arthropathy (6) No signs of glenohumeral OA (7) No stage 4 fatty degeneration according to Goutallier *et al.* ‡ (8) No active infections					
Encalada-Diaz 2011[244], Mexico	Non-comparative observational study	Polycarbonate polyurethane patch	(1) Full-thickness tear of supraspinatus or infraspinatus tendon and intact subscapularis	10	10	MRI + US, 6 and 12 months Clinical evaluation, 0.5,1,3,6 +and 12 months	SST, VAS, ASES, UCLA, SF-12, Repair failure	-
Flury 2012[245], German	Non-comparative observational study	Graftjacket® Arthroflex	(1) Symptomatic revision RC tear with poor quality tendon (degeneration or delamination) (2) Aged > 60 years with unfavourable co-morbidities (massive rupture, diabetes, steroid therapy) (3) No Irreparable RC tear	N/A	8	USS or MRI – 6 months Clinical evaluation, 6 or 9 months	Constant, OSS, SSV	-
Giannotti 2014[246], Italy	Non-comparative observational study	Zimmer® Collagen Repair Patch	[Eligibility criteria not explicitly stated] (1) Massive RC tear with minimum follow-up of 30 months	N/A	9	US, MRI and clinical evaluation, Mean 36 months (Range 30-45)	Repair failure, ASES, Constant, Strength (BMRC), Electromyography	-
Gupta 2012[247], USA	Non-comparative observational study	Graftjacket®	(1) Full thickness RC tear with >5cm retraction on pre-op MRI (2) Unresponsive to > 6 months of non-operative treatment, including physiotherapy + nonsteroidal anti-inflammatories (3) Inability to reduce the residual cuff to the anatomic (4) Ability to fully participate in the postoperative rehabilitation (5) No glenohumeral OA and/or cuff tear arthropathy (6) No stage 3-4 fatty degeneration according to Goutallier *et al.* ‡ (7) No prior rotator cuff repair	24	24	US, Mean 36 months (range NR) Clinical evaluation, Mean 36 months (range 29-42)	VAS, ASES, SF-12, ROM (degrees), Strength (BMRC), Repair failure	-
Gupta 2013[248], USA	Non-comparative observational study	Conexa™	(1) Full thickness RC tear with >5cm retraction and/or >2 tendon full-thickness RC tear visualised during arthroscopy (2) Unresponsive to > 6 months of non-operative treatment, including physiotherapy + nonsteroidal anti-inflammatories (3) Inability to reduce the residual cuff to the anatomic (4) Ability to fully participate in the postoperative rehabilitation (5) No glenohumeral OA and/or cuff tear arthropathy (6) No stage 3-4 fatty degeneration according to Goutallier *et al.* ‡	26 patients, 27 shoulders	26 patients, 27 shoulders	US + Clinical evaluation, Mean 32 months (range 24-40)	VAS, ASES, SF-12, ROM (degrees), Strength (BMRC), Repair failure	-
Hirooka 2002[249], Japan	Non-comparative observational study	Gore-tex® Expanded PTFE patch	NR	27 patients, 28 shoulders	27 patients, 28 shoulders	Clinical evaluation, Mean 44 months (range 24-72)	Japanese Orthopaedic Association shoulder surgery score, strength (kg)	-
Lederman 2016[250], USA	Non-comparative observational study	Conexa™	(1) Aged 40-70 years (2) Repairable primary large (3-5cm) RC tears (3) ≥90° movement of the non-operative arm (4) Able to perform postoperative exercises (5) Able to return for all scheduled and required study visits (6) No Irreparable tears – inability to approximate the tendon to the tuberosity without tension (7) No subscapularis tears (8) No stage 3-4 fatty degeneration ‡ (9) No prior RC repair on the affected shoulder (10) No patients with: inflammatory disease, autoimmune disease, cancer, insulin-dependent diabetes, chronic steroid use, malnourishment, active infection, history of alcohol or drug abuse, significant mental illness, tobacco user within last 6 months, ASA class 4 or 5 (11) Can walk without aids (12) No known allergy to the augmentation material	68	61	MRI, 6 + 12 months Clinical evaluation, 6,12 + 24 months	ASES, Constant, SST, Repair failure	-
Lenart 2015[251], USA	Non-comparative observational study	X-repair	(1) Massive RC tears (≥2 tendons) repaired with X-repair patch (2) Primary or revision RC surgery	N/A	13	Clinical evaluation, Mean 18 months	ASES, PENN, SANE, Repair failure	-

			(3) No history of instability, moderate-severe glenohumeral OA, shoulder surgery within the follow-up period			(range 14.4-20.4)		
Malcarney 2005[207], Australia	Non-comparative observational study	Restore®	(1) A poor-quality of deficient tendon (2) 5 patients also met the criteria for a concurrent comparative trial (Walton *et al.* 2007)	N/A	25	NR	Early complications	-
Marberry 2012[252], USA	Non-comparative observational study	Artelon®	(1) Large or massive RC tear diagnosed on MRI (2) Pain and insufficient muscle function for ≥t 3 months (3) Reparable tendon of poor quality, determined at the time of surgery (4) No evidence of active infection, significant osteoarthritis in the shoulder, chronic dislocation or glenohumeral OA (5) No systemic corticosteroids, chemotherapeutics or major medical conditions	17	16	MRI, NR Clinical evaluation, 3,6 +12 months	Constant, WORC, SF36, Repair failure	-
Metcalf 2002[253], USA	Non-comparative observational study	Restore®	[Eligibility criteria not explicitly stated] (1) Massive RC tears (>5cm^2) with retraction medial to glenoid (2) Significant atrophy of supraspinatus and infraspinatus on pre-operative MRI.	N/A	12	Clinical evaluation, 2 years	UCLA, SST, SF-36. ROM (degrees), Strength (BMRC)	-
Modi 2013[254], UK	Non-comparative observational study	Graftjacket®	(1) Irreparable large or massive RC tears (≥3 cm) (2) No history of inflammatory or autoimmune disease (3) Patients undergoing RC repair after arthroplasty were excluded	61	61	Clinical evaluation 3, 6, 12 months + yearly thereafter	OSS, VAS, ROM (degrees), Strength (BMRC)	-
Moore 2006[255], USA	Non-comparative observational study	Cadaveric allograft	(1) Irreparable, massive RC tears (≥ 2 tendons)	N/A	32	MRI, Mean 33.7 months (range 3-124) Clinical evaluation, Mean 31.3 months (range 1 – 123)	Repair failure, UCLA	-
Nada 2010[115], UK	Non-comparative observational study	Dacron	(1) Full-thickness massive RC tear (>5cm + ≥ 2 tendons) on MRI (2) Pain + disability despite conservative treatment (3) A functional deltoid muscle (4) Primary or revision (3 cases) RC repairs (5) Compliance with post-operative rehabilitation (6) No history of; cuff tear arthropathy with stiffness, infection, any neurological condition effecting the shoulder girdle	21	21	MRI + Clinical evaluation, Mean 36 months (range 30-46)	Constant, VAS, ROM(degrees), Strength (BMRC), Satisfaction	-
Neumann 2017[256], USA	Non-comparative observational study	Conexa™	(1) Irreparable massive RC tear (>5cm) on MRI (2) Primary or revisions (8 cases) RC repairs (3) Failure of 6 months non-operative management (non-steroidal anti-inflammatories and/or physical therapy) (4) Able to participate in post-operative physical therapy (5) No glenohumeral OA, cuff arthropathy, >50% fatty infiltration of supraspinatus on MRI,	85 shoulders 84 patients	61 shoulders 60 patients	US + Clinical evaluation, Mean 50.3 months (range 24-63)	Modified ASES, VAS, ROM(degrees), Strength (BMRC)	-
Petrie 2013[257], UK	Non-comparative observational study	LARS™	(1) Symptomatic massive RCT clinically and radiologically (2) Stage 3-4 fatty degeneration according to Goutallier *et al.* ‡ (3) Not amenable to primary arthroscopic repair (4) No patients over 75 years with arthritis	53 shoulders 50 patients	31 shoulders 28 patients	Clinical evaluation 4 + 24 months	OSS	-
Petri 2016[258], USA	Non-comparative observational study	Arthroflex®	(1) Open revision of large to massive posterosuperior RC tears with biological augmentation (2) Patients with concomitant SLAP tears, OA, biceps pathology or subscapularis tears were included (3) No stage 3-4 fatty degeneration according to Goutallier *et al.* ‡ (4) Patient who underwent primary augmented repair, arthroscopic augmented repair or revision of a prior augmented repair were excluded	N/A	13	MRI, Mean 9.9 months (range 0.3-26.3) Clinical evaluation, Mean 30 months (range 24 -48)	ASES, QuickDASH, SANE, SF-12, Repair failure	-
Petricciolo 2013[224], Italy	Non-comparative observational study	SportMesh™	[Eligibility criteria not explicitly stated] (1) Open repair of subscapularis tendon	N/A	10	US + Clinical evaluation, Mean 23 months (range 12-34)	Constant, DASH, VAS, Repair failure	-
Phipatanakul 2009[259], USA	Non-comparative observational study	Restore®	(1) Rotator cuff tears that could not be advanced to the native footprint or to reinforce thin attritional tissues	11	11	MRA, Mean 25 months (range 14-38) Clinical evaluation, Mean 26 months (range 14-38)	UCLA, ASES, Repair failure	-
Proctor 2014[260], USA	Non-comparative observational study	X-repair	(1) Massive RC tears (≥ 2 tendon tears), (2) Failure of non-operative treatment (3) No evidence of adhesive capsulitis	18	18	US or MRI, NR	ASES, Repair failure	-

						Clinical evaluation, 3,6,12 months + 'final follow-up'- Mean 42 months (range 35-47)		
Rhee 2008[261], South Korea	Non-comparative observational study	Long head of biceps	(1) Massive (>5cm) RC tears at arthroscopy (2) No history of SLAP lesion, acromioclavicular arthritis requiring distal clavicle resection, glenohumeral OA, neural damage, prior shoulder surgery	N/A	31	MRI, NR Clinical evaluation, 1.5,3,6,12 months + 'final follow-up' – Mean 32 months (range 24-67)	Constant, UCLA, SST, VAS, ROM (Degress), Strength (kg)	-
Rotini 2011[262], Italy	Non-comparative observational study	Acellular Human Dermal Matrix	(3) Aged <55 (4) Healthy with high functional demands (3) Large to massive tears^ (4) Tendon retraction < 3 according to Thomazeau *et al.* [‡] (5) No stage 3-4 fatty degeneration according to Goutallier *et al.* [‡] (6) ≥1 year follow-up (7) No OA degeneration (even mild), frozen shoulder, symptomatic acromioclavicular arthritis, autoimmune connective tissue disease, allergy to penicillin or pork (8) Able to engage with rehabilitation regimen	N/A	5	MRI, NR Clinical evaluation, Mean; NR (range 12-18 months)	Repair failure, Constant	-
Sano 2010[263], Japan	Non-comparative observational study	Long head of biceps	[Eligibility criteria not explicitly stated] (1) Irreparable massive RC tears (≥ 2 tendons) with concomitant long head of biceps pathology (2) > 12 months follow-up available	N/A	14	MRI + clinical evaluation, Mean; 28 months (range 48-79)	Repair Failure, Japanese Orthopaedic Association shoulder surgery score	-
Schlegel 2017[225], USA	Non-comparative observational study	Collagen Sheet	(1) Chronic, degenerative partial (≥ 25%) thickness tear of supraspinatus tendon (2) ≥ 21 years old (3) Unresponsive to conservative therapy (analgesia, physiotherapy or injections) for > 3 months (4) No; full-thickness tears, acute injuries, previous surgery on same shoulder, shoulder instability, chondromalacia (>grade 3), > grade 2 cuff muscle fatty infiltration, severe calcification, IDDM, Workers' Compensation, smokers, hypersensitivity to bovine collagen, genetic collagen disease, autoimmune, immunodeficiency, chronic inflammatory disorders patients (5) No oral steroid use for 2months (or IM steroid use for 1 month)	33	33	MRI+ clinical evaluation, 3 months and 1 year'	Repair failure, Constant, ASES	-
Scheibel 2007[264], Germany	Non-comparative observational study	Humeral Periosteum	(1) Degenerative symptomatic full-thickness supraspinatus tears (2) High functional demand (3) Tendon retraction < 3 according to Thomazeau *et al.* [‡] (4) No stage 3-4 fatty degeneration according to Goutallier *et al.* [‡] (5) No; partial RC tears, traumatic history, prior surgery to affected shoulder, cuff tear arthropathy (acromiohumeral distance <6mm)	20	20	MRI, 12 months Clinical evaluation, Mean 14.4 months (range 12-21)	Repair failure, Constant, SST	-
Sclamberg 2004[265], USA	Non-comparative observational study	Restore®	(1) Symptomatic, atrophic, retracted large and massive (≥2-tendon) RC tears on MRI and confirmed at surgery	N/A	11	MRI + clinical evaluation, Mean; NR (range 6-10 months)	ASES, Repair Failure	-
Sears 2014[266], USA	Non-comparative observational study	GraftJacket®or Tissuemend or Conexa™	[Eligibility criteria not explicitly stated] (1) Full thickness rotator cuff repairs (2) Revision surgery	31	24	MRI or US, Mean 4.2 years (range, NR) Clinical evaluation, Mean 4.2 years (range 30-112)	Repair failure, ASES and SANE	-
Venouziou 2013[267], USA	Non-comparative observational study	Graftjacket®	(1) Massive (>5cm) RC tear (2) Not capable of mobilisation (3) ≥18 months follow-up was available	N/A	14	Clinical evaluation, 1.5, 3,6,12 months + 'final follow-up'- Mean 30.2 months (range 18-52)	VAS, ASES, ROM (degrees), Strength (BMRC)	-
Wong 2010[268], USA	Non-comparative observational study	Graftjacket®	[Eligibility criteria not explicitly stated] (1) Large and massive RC tears (2) Motivated, intelligent, younger patients with disabling pain but intact biceps tendons (3) Functioning subscapularis muscle (4) No glenohumeral OA, immunocompromise or heavy smokers	N/A	45	Clinical evaluation, Mean;NR, (range 24-68)	UCLA, WORC, ASES	-

Abbreviations*:* ASA, American Society of Anaesthesiologists; ASES, American Shoulder and Elbow Surgeons standardised tool; BMRC, British Medical Research Council Scale; CTA, Computed Tomography Arthrogram; DASH, Disabilities of the Arm, Shoulder and Hand; SF, Flexilevel scale of Shoulder Function; MRA, Magnetic Resonance Arthrogram; MRI, Magnetic Resonance Imaging; NR, Not Reported; OA, Osteoarthritis; OSS, Oxford Shoulder Score; PTFE, Polytetrafluoroethylene; QuickDASH, Quick

Disabilities of the Arm, Shoulder and Hand; RC, Rotator Cuff; ROM, Range of Motion; SANE, Single Assessment Numerical Evaluation; SLAP, Superior Labrum from Anterior to Posterior; SST, Simple Shoulder Test; SF-12, 12-item Short Form health survey; SF-36, 36-Item Short Form health survey; UCLA, shoulder rating scale of the University of California Los Angles; US, Ultrasonography; VAS, Visual Analogue Scale; WORC, Western Ontario Rotator Cuff **Footnotes***:* [*]Recruited number of patients only refers to studies reporting a prospective design. [†]Osteoarthritis defined according to Kellgren *et al* (Ann Rheum Dis 1957;16:494-502); [‡] Goutellier *et al.* (Clin Orthop Relat Res 1994; 304:78); [§] Hamada *et al.* (Clin Orthop Relat Res 2011; 469:2452-60); [#]L'Insalata *et al.* (J Bone Joint Surg Am 1997;79:738-48); [¶] Hayes *et al.* (Aust J Physiother 2001:47:289-94); [^]Gerber *et al.* (J Bone Joint Surg Am 2000;82:505-15); [ǁ] Thomazeau *et al.* (Acta Orthop Scand 1996; 67: 264-268)

Table 2-2 | Patch type and population demographics

Study	Patch Type							Brand	Surgical approach	Surgical Patch Technique	Patient Demographics		
	Xenograft			**Human**		**Synthetic**					Age at Surgery, Mean (range or ±SD)	Gender, n Male(%)	Tear Size
	Dermal	Intestinal	Other	Allograft[‖]	Autograft	Resorbable	Non-resorbable						
Randomised Comparative Studies													
Barber, 2012				✓				Graftjacket®	Arthroscopic	On-lay	56 (43-69)	18(82)	Small-to-massive‡
								Control			56 (34-72)	13(65)	Small-to-large‡
Byrant, 2016		✓						Restore®	Open	On-lay	55 (29-40)	29(85)	Small-to-massive‡
								Control			58 (40-81)	22(79)	Small-to-massive‡
Ianotti, 2006		✓						Restore®	Open	On-lay	58 (NR)	11(73)	Large-to-Massive‡
								Control			57 (NR)	12(80)	Large-to-Massive‡
Leuzinger, 2016				✓				Graftjacket	Arthroscopic		66 (51-81)	20(71)	Massive§
						✓		Artelon		On-lay	68 (52-79)	23(22)	Massive§
		✓						Restore			68 (50-82)	20(69)	Massive§
Non-Randomised Comparative Studies													
Ciampi, 2014							✓	Repol Angimesh	Open	On-lay	66 (57-77)	41(79)	Massive§
			✓†					Tutopatch			66 (58-76)	38(78)	Massive§
								Control			67 (58-77)	35(69)	Massive§
Gilot, 2015				✓				Arthroflex®	Arthroscopic	On-lay	58 (±6.2)	8(60)	Large-to-massive‡
								Control			62 (±4.6)	7(47)	Large-to-massive‡
Ito, 2003				✓				Fascia Lata	Open	Bridging	63 (49-70)	6(67)	Large-to-massive‡
								Control			52 (36-66)	10(83)	Large-to-massive‡
Jeon, 2017					✓			Biceps (long head)	Arthroscopic	Bridging	62 (46-82)	14(45)	Medium‡
								Control			63 (46-82)	16(48)	Medium-to-large‡
Maillot, 2018	✓							Conexa™	Open	On-lay	56 (46-63)	5(45)	Medium-to-massive‡
								Standard Repair	Arthroscopic		58 (45-71)	5(42)	Medium-to-massive‡
								Debridement	Arthroscopic		60 (54-76)	3(33)	Medium-to-massive‡
Mori, 2013					✓			Fascia Lata	Arthroscopic	Bridging	65 (±8.9)	17(71)	Medium-to-massive‡
								Control			65 (±9.2)	10(42)	Medium-to-massive‡
Mori, 2015					✓			Fascia Lata + grade 1-2 atrophy	Arthroscopic	Bridging	65(±9.0)	18(69)	Large-to-massive‡
					✓			Fascia Lata + grade 3-4 atrophy			67(±6.2)	11(58)	Large-to-massive‡
Tempelaere, 2017					✓			Quadriceps tendon	Open	Bridging	NR	18(78)	Massive^
								Control	Arthroscopic		NR	15(56)	Massive^
Vitali, 2015					✓		✓	Repol Angimesh + Biceps (long-head)	Open	Bridging	66 (55-78)	15(25)	Massive§
								Control			67 (56-77)	18(30)	Massive§
Walton, 2007		✓						Restore®	Open	On-lay	60 (±3.5)	10(67)	Large-to-massive¶
								Control			59 (±3.1)	11(69)	Large-to-massive¶
Yoon, 2016				✓				Allocover™	Arthroscopic	Bridging	64 (±8.7)	9(43)	Large-to-massive‡
								Control			62 (±6.7)	26(48)	Large-to-massive‡
Non-comparative studies													
Agrawal, 2006				✓				Allopatch HD™	Arthroscopic	On-lay	54 (47-69)	10(71)	Large-to-massive‡
Audenaert, 2006							✓	Mersilene®	Open	Bridging	67 (51-80)	23(56)	Massive§
Badhe, 2008	✓							Zimmer® Collagen repair patch	Open	Bridging	66(46-80)	5(50)	Massive‡§

Bektafier, 2010					✓				Coricoacromial ligament	Open	On-lay	54.3 (39-66)	4(8.6)	Medium-to-massive‡
Bond, 2008				✓					Graftjacket®	Arthroscopic	Bridging	54 (39-74)	13(81)	Massive‡§
Burkhead, 2007				✓					Graftjacket®	Open	On-lay	56(NR)	12(71)	Massive§
Cho, 2014	✓								Permacol™	Open	On-lay	53(45-57)	3(60)	Massive‡§
Consigliere, 2017	✓								DX reinforcement matrix	Arthroscopic	On-lay	74 (65-82)	6 (40)	Large-to-massive§
Encalada-Diaz, 2011								✓	Polycarbonate polyurethane patch	Open	On-lay	56 (44-65)	0	Small-to-large‡
Flury, 2012				✓					Graftjacket® or Arthroflex®	Arthroscopic	On-lay	57 (50-68)	5(63)	Medium-to-large‡
Giannotti, 2014	✓								Zimmer® Collagen repair patch	Open	Mixed	66 (50-80)	4(44)	Massive¶
Gupta, 2012				✓					Graftjacket®	Open	Bridging	63 (45-83)	12(50)	Massive¶
Gupta, 2013	✓								Conexa™	Open	Bridging	60 (45-77)	12(46)	Massive§
Hirooka, 2002								✓	Gore-tex® PTFE	Open	Bridging	62 (44-75)	20(74)	Small-to-massive‡
Lederman, 2016	✓								Conexa™	Open	On-lay	56 (40-69)	NR	Large‡
Lenart, 2015						✓			X-repair	Open	On-lay	57 (42-68)	9(69)	Massive§
Malcarney, 2005		✓							Restore®	Open	Mixed	NR	NR	NR
Marberry, 2012						✓			Artelon®	Open	On-lay	65 (45-76)	5(29)	Massive§
Metcalf, 2002		✓							Restore®	Open	On-lay	NR	NR	Massive¶
Modi, 2013				✓					Graftjacket®	Open	Bridging	62 (47-72)	41(67)	Large-to-Massive‡
Moore, 2006				✓#					Cadaveric	Open	Bridging	59 (34-81)	23(72)	Massive§
Nada. 2010								✓	Dacron	Arthroscopic	Bridging	66 (55-85)	14(67)	Massive‡§
Neumann, 2017	✓								Conexa™	Open	Bridging	62 (38-82)	21(35)	Massive‡§
Petrie, 2013								✓	LARS™	Open	Bridging	67 (NR)	21(70)	Massive¶
Petri, 2016				✓					Arthroflex®	Open	On-lay	57 (26-68)	11(85)	Large-to-Massive¶
Petricciolo, 2013						✓			SportMesh™	Open	On-lay	61 (51-68)	8(80)	Subscapularis tears
Phipatanakul, 2009		✓							Restore®	Open	On-lay	48 (31-62)	9(82)	Massive¶
Proctor, 2014						✓			X-Repair	Arthroscopic	On-lay	66 (52-89)	NR	Massive§
Rhee, 2008					✓				Biceps (long-head)	Mixed	Bridging	61 (46-79)	11(35)	Massive‡§
Rotini, 2011				✓					Acellular Human Dermal Matrix	Mixed	On-lay	48 (37-55)	5(100)	Large-to-Massive¶
Sano, 2009					✓				Biceps (long-head)	Open	Bridging	64 (48-79)	12 (86)	Massive§
Scheibel, 2007					✓				Periosteum	Open	On-lay	59 (44-71)	16(70)	NR
Schlegel, 2017			✓†2						Collagen Sheet	Arthroscopic	On-lay	54 (34-75)	19(58)	N/A - Partial thickness
Sclamberg, 2004		✓							Restore®	Open	Mixed	67 (52-79)	7(64)	Large-to-Massive‡
Sears, 2014				✓					Graftjacket®	Arthroscopic	On-lay			
	✓								Tissuemend			50 (37-70)	NR	NR
	✓								Conexa™					
Venouziou, 2013				✓					Graftjacket®	Open	Bridging	54 (33-64)	9(64)	Massive¶
Wong, 2010				✓					Graftjacket®	Arthroscopic	Bridging	53 (39-67)	36(80)	Massive¶

Abbreviations: NR, Not reported; PTFE, Polytetrafluoroethylene **Definitions:** Control refers to rotator cuff repair without augmentation. For definitions of 'On-lay' and 'Bridging' see methods section. **Footnotes:**†Patch constructed from decellularised bovine pericardium; †2 Patch derived from bovine achilles; ‖ Allograft patches constructed from decellularised human dermis; # Cadaveric source of allograft, irradiated but not decellularized; § Gerber *et al.*[6] (J Bone Joint Surg Am 2000;82:505-15) ‡ DeOrio et al.[8] (J Bone Joint Surg Am 1984:66:563-7) ¶ size of tear as reported by study authors - no details provided on classification utilised and insufficient detail to enable post-hoc classification ^defined as grade 3 retraction according to Patte classification[9] (Clin Orthop Relat Res 1990;254:81-6)

2.6.3 Surgical characteristics

Comparative studies: Across all the comparative studies a total of twelve different patches were utilised. Decellularised xenograft patches were the most commonly investigated (n=6; Restore® n=4). Surgical techniques could be classified as fully arthroscopic (46%, n=7), open (40%, n=6) or a mixture of both (13%, n=2). The method of patch utilisation was split fairly evenly between the categories of 'on-lay' (53%, n=8) or 'bridging' (47%, n=7).

Non-comparative studies: A full spectrum of patch materials (human allograft [32%, n=12]; human autograft [11%, n=4]; xenograft dermal [22%, n=8]; xenograft intestinal[11%, n=4];synthetic [24%, n=9]) and surgical techniques were reported (on-lay [51%, n=19], bridging [41%, n=15], mixed [8%, n=3]).

2.6.4 Shoulder specific Patient Reported Outcome Measures (PROMs)

Comparative studies: Eight different outcomes scores were used to assess shoulder function (Table 2-1). The Constant Scale (60%), ASES Score (47%) and the UCLA Scale (33%) were most commonly reported with most studies reporting multiple functional scores.

Amongst RCTs, only one study found a statistically meaningful improvement in ASES and Constant scores, but not UCLA scale, following implantation of an allograft patch (Table 3).[226] The two RCTs investigating decellularised porcine small intestine submucosa (Restore®)[227,228] failed to demonstrate an improvement in patient-reported outcomes at 1-2 year follow-up, while the study by Leuzinger *et al.*[221] only undertook intra-group comparisons between pre- and post-operative Constant scores, reporting similar improvements following implantation of an allograft, xenograft or synthetic patch.

For the non-randomised comparative studies, only three reported a significant improvement in functional shoulder scores for synthetic[222], human allograft[229] and fascia-lata autografts[230]. The remaining studies found no significant improvement, whilst the studies by Ito *et al.*[231] and Vitali *et al.*[232] did not undertake inter-group comparisons.

Non-comparative studies: Of the case series, 35 collected patient-reported outcome scores, with 25 reporting a statistically significant temporal improvement (Table 2-3).

Table 2-3 | Functional outcome scores

Study		Shoulder Specific Functional Scores																				
		ASES, Mean (±SD or range)			**Constant**, Mean (±SD or range)			**OSS**, Mean (±SD or range)			**PENN**, Mean (±SD or range)			**SST**, Mean (±SD or range)			**UCLA**, Mean (±SD or range)			**WORC**, Mean (±SD or range)		
		Baseline	Intermediate	Final†	Baseline	Intermediate	Final†	Baseline	Intermediate	Final†	Baseline	Intermediate	Final†	Baseline	Intermediate	Final†	Baseline	Intermediate	Final†	Baseline	Intermediate	Final†
Randomised Comparative Studies																						
Barber 2012	Graftjacket®	48.5 (±NR)		2 yrs: 98.9 (±4.2)	41.0 (±NR)		2 yrs: 91.9 (±9.2)										13.3 (±NR)		2 yrs: 28.2 (±2.1)			
	Control	46.0 (±NR)		2 yrs: 94.8 (±14.2)	45.8 (±NR)		2 yrs: 85.3 (±11)										15.9 (±NR)		2 yrs: 28.3 (±3.0)			
				p= 0.035			p= 0.008												p= 0.43			
Bryant 2016	Restore®	52.2 (±3.3)	1 yr: 83.3 (±2.6)	2 yrs: 84.6 (±2.9)	58.4 (±3.9)	1 yr: 72.8 (±3.0)	2 yrs: 79.3 (±3.5)							47.2 (±4.3)	1 yr: 78.5 (±3.2)	2 yrs: 78.5 (±3.6)				40.2 (±NR)	1 yr: 78.6 (±NR)	2 yrs: 78.8 (±NR)
	Control	54.6 (±3.7)	1 yr: 84.8 (±2.9)	2 yrs: 87.9 (±3.1)	46.8 (±4.2)	1 yr: 79.5 (±3.1)	2 yrs: 87.5 (±3.7)							40.7 (±4.8)	1 yr: 82.1 (±3.6)	2 yrs: 85.4 (±4.0)				40.1 (±NR)	1 yr: 79.8 (±NR)	2 yrs: 82.2 (±NR)
			p= 0.69	p= 0.44		p=0.14	p=0.13								p= 0.48	p= 0.21					p= 0.73	p= 0.46
Iannotti 2016	Restore®										42 (±NR)		14 mnths: 83 (IQR 70-92)									
	Control										34 (±NR)		14 mnths: 91 (IQR 81-99)									
													p=0.07									
Leuzinger 2016	Graftjacket®				47.3 (±7.3)		6 mnths: 81.4 (±11.4)															
	Artelon®				46.2 (±9.6)		6 mnths: 81.3 (±11.1)															
	Restore®				41.0 (±9.6)		6 mnths: 78.5 (±12.3)															
							p= NR															
Non-Randomised Comparative Studies																						
Ciampi 2014	Repol Angimesh																10.9 (± 1.5)	2 mnths: 19.1 (± 2.0)	36 mnths: 24.6 (± 3.2)			
	Tutopatch																10.4 (± 1.2)	2 mnths: 11.4 (± 1.5)	36 mnths: 14.7 (± 2.0)			
	Control																10.7 (± 1.1)	2 mnths: 11.3 (± 1.5)	36 mnths: 14.9 (± 2.0)			
																			p<0.001‡			
Gilot 2015	Arthroflex®	63.8 (±13.8)	12 wks: 60.6 (±8.3) 24 wks: 64.3 (±7.8)	96 wks: 88.9 (±4.8)																54 (±8)	12 wks: 52 (±6) 24 wks: 81 (±12)	96 wks: 84(±4)

	Control	60.3 (±9.5)	12 wks: 57.6 (±8.8) 24 wks: 60.4(±10.1)	96 wks: 72.6 (±11.9)									58 (±5)	12 wks: 59 (±8) 24 wks: 64 (±6)	96 wks: 66(±5)
			p=0.59; p=0.08	p= 0.048										p=0.36; p=0.05	p= 0.04
Ito 2003	Fascia Lata														
	Control														
Jeon 2017	Biceps tendon	52.8 (±10.6)	12 wks: 60.1 (±15.8) 24 wks: 76.3 (±10.6)	29 mnths: 88.2 (±6.9)	43.2 (±9.9)	12 wks: 54.9 (±12.8) 24 wks: 72.2 (±12.8)	29 mnths: 86.8 (±6.2)								
	Control	53.0 (±11.8)	12 wks: 63.0 (±10.2) 24 wks: 75.7 (±11.5)	29 mnths: 87.4 (±7.2)	44.3 (±11.3)	12 wks: 56.1 (±10.8) 24 wks: 71.6 (±9.7)	29 mnths: 84.0 (±7.9)								
				p=0.901			p=0.742								
Maillot 2018	Conexa™				43.6 (±11.0)	12 wks: 49.4 (±14.1) 24 wks: 59.0 (±18.8)	24 mnths: 75.8 (±8.6)								
	Repair only				45.7 (±11.6)	12 wks: 52.4 (±10.2) 24 wks: 64.1 (±8.5)	24 mnths: 74.7 (±4.3)								
	Debridement				44.1 (±11.6)	12 wks: 54.9 (±10.0) 24 wks: 62.2 (±5.9)	24 mnths: 64.2 (±5.0)								
							p=1.0[§]; p= 0.002[‖]								
Mori 2013	Fascia Lata	40.8 (±13.0)	12 mnths: 84.9 (±8.1)	35 mnths: 94.1 (±5.4)	37.4 (±8.1)	12 mnths: 73.6 (±6.6)	35 mnths: 81.1 (±5.7)				14.3 (±2.9)	12 mnths: 28.6 (±4.3)	35 mnths: 32.6 (±3.4)		
	Control	41.8 (±11.3)	12 mnths: 84.2 (±19.7)	35 mnths: 85.7 (±14.1)	36.3 (±9.9)	12 mnths: 72.9 (±16.8)	35 mnths: 69.9 (±10.3)				13.7 (±3.1)	12 mnths: 27.3 (±6.1)	35 mnths: 29.8 (±5.3)		
				p= 0.021			p= 0.001						p= 0.094		
Mori 2015	Fascia Lata + grade 1-2 infraspinatus atrophy	41.6 (±13.0)		41mnths: 91.3 (±6.7)	38.7 (±9.1)		41mnths: 78.4 (±5.7)								
	Fascia Lata + grade 3-4 infraspinatus atrophy	39.9 (±9.9)		67 mnths: 73.6 (±10.1)	40.7 (±0.7)		67 mnths: 63.9 (±8.0)								
					p<0.001			p<0.0001							
Tempelaere 2017	Quadriceps tendon				42.9 (17-72)		58 mnths: 67.5 (41-87)								
	Control				45.7 (22-63)		55 mnths: 72.1 (21-90)								
							p=NS								

Vitali 2015	Repol Angimesh															10.8 (±1.4)	3 mnths: 20.9 (±1.3)	36 mnths: 24.6 (±3.3)	
	Control															10.9 (±1.2)	3 mnths 11.3 (±1.4)	36 mnths: 14.7 (±2.0)	
																		p= Unclear	
Walton 2007	Restore®																		
	Control																		
Yoon 2016	Allocover™	50.4 (± 15.3)	1 yr: 84.5 (±12.2)	2 yrs:82.5 (±11.2)	56.3 (±9.4)	1 yr: 79.0 (±9.5)	2 yrs: 78.3 (±12.8)				4.1 (±2.3)	1 yr: 8.8 (±2.9)	2 yrs: 8.8 (±2.9)	23.0 (±5.5)	1 yr: 29.5 (±4.1)	2 yrs: 29.5 (±4.1)			
	Control	48.9 (±16.0)	1 year: 84.2 (±13.1)	2 yrs:82.0 (±15.3)	53.6 (±13.2)	1 yr: 80.0 (±11.6)	2 yrs: 75.7 (±15.7)				4.1 (±2.6)	1 yr: 10.0 (±2.7)	2 yrs: 10.0 (±2.7)	23.7 (±5.6)	1 yr: 29.8 (±4.5)	2 yrs: 29.8 (±4.5)			
			p= 0.92	p= 0.88		p= 0.72	p= 0.47					p= 0.09	p= 0.60		p= 0.79	p= 0.10			
Non-comparative studies																			
Agrawal 2012	Allopatch™				49.7 (13-74)		1yr: 81.1 (45-92)												
							p= 0.009												
Audenaert 2006	Mersilene®				25.7 (20-39)		43 mnths: 72.1 (34-89)												
							p< 0.001												
Badhe 2008	Zimmer® Collagen Repair Patch				41.5 (13-78)	1 yr: 62.5 (50-97)	4.5 yrs: 62.2 (50-80)												
						p= 0.0003	p=NR												
Bektafier 2010	Coraco-humeral Ligament				45 (±NR)		1 yr: 80 (±NR)												
							p=NR												
Bond 2008	Graftjacket®	53.8 (39-70)		27 mnths: 84 (69-100)										18.4 (11-25)		27 mnths: 30.4 (22-35)			
				p= 0.0001												p= 0.0001			
Burkhead 2007	Graftjacket®													9.06 (±NR)		1.2 yrs: 26.12 (±NR)			
																p <0.001			
Cho 2014	Permacol™	39.4 (±NR)		21 mnths: 86.4 (±NR)										15.4 (±NR)		21 mnths: 31.2 (±NR)			
				p=0.04												p= 0.04			

Consiglier e 2017	DX reinforceme nt matrix				54(±4)	3 mnths: 65 (±12)	7 mnths: 75 (±11)	30 (±8)	3 mnths: 38.7 (±12.7)	7 mnths: 47 (±10)								
						p <0.05	p <0.05		p >0.05	p <0.05								
Encalada-Diaz 2011	Polycarbona te polyurethan e patch	44 (±NR)	6 mnths: 61.3 (±NR)	12 mnths: 73.3 (±NR)								3.6 (±NR)	6 mnths: 6.5 (±NR)	12 mnths: 7.7 (±NR)				
			p= 0.008	p< 0.001									p= 0.02	p= 0.004				
Flury 2012	Graftjacket® or Artelon®				51 (29-74)		6 mnths: 57 (43-71)	21 (7-38)		6 mnths: 38 (19-45)								
							p> 0.05			p< 0.05								
Giannotti 2014	Zimmer® Collagen Repair Patch	38 (±NR)		34 mnths: 79 (±NR)	42 (±NR)		34 mnths: 73 (±NR)											
				p= NR			p= NR											
Gupta 2012	Graftjacket®	66.6 (±NR)		3 yrs: 88.7 (±NR)														
				p= 0.0003														
Gupta 2013	Conexa™	62.7		32 mnths: 91.8 (±13.3)														
				p= 0.0007														
Hirooka 2002	Gore-tex® PTFE																	
Lederman 2016	Conexa™	48.7 (±20.2)	1 yr: 85.4 (±18.4)	2 yrs: 90.4 (±15.3)	45.4 (±15.2)	1 yr: 68.7 (±11.3)	2 yrs: 71.7 (±9.6)					5.0 (±2.6)	1 yr: 9.9 (±2.7)	2 yrs: 10.6 (±2.2)				
			p< 0.0001	p< 0.0001		p< 0.0001	p< 0.0001						p< 0.0001	p< 0.0001				
Lenart 2015	X-repair	32.8 (±9.5)		18 mnths: 74.2 (±5.0)					50.9 (±4.2)		18 mnths: 77.6 (±5.3)							
				p= 0.0001							p< 0.005							
Malcarney 2005	Restore®																	
Marberry 2012	Artelon®				17.1 (±6.4)		1 yr: 67.1 (±11.6)										34(±18)	1 yr: 86 (±12)
							p= 0.002											p= 0.002
Metcalf 2002	Restore®											NR		NR	9.3 (±NR)		24 mnths: 19.9 (±NR)	
														p= 0.01			p= 0.01	

Modi 2013	Graftjacket®			26 (8-40)	1 yr: 42 (21-48)				
					p=0.001				
Moore 2006	Cadaveric							12.1 (±NR)	31 mnths: 26.1 (±NR)
									p< 0.001
Nada 2010	Dacron		46.7 (39-61)	36 mnths: 84.5 (52-96)					
			p< 0.001						
Neumann 2017	Conexa™	NR	50 mnths: 87.8						
		p=NR							
Petrie 2013	LARS™			46.7 (±NR)	3.3 yrs: 30.6 (±NR)				
					p<0.0001				
Petri 2016	Arthroflex®	64.5 (±10.0)	2.5 yrs: 86.0(±12.3)						
		p= 0.005							
Petricciolo 2013	SportMesh ™		47.0 (±NR)	23 mnths: 69.0 (±NR)					
			p= NR						
Phipatanakul 2009	Restore®	36.3 (±NR)	26 mnths: 71.8 (±NR)					13.9 (±NR)	26 mnths: 25.7 (±NR)
		p< 0.01							p< 0.01
Proctor 2014	X-Repair	26 (±NR)	3 mnths: 57 6 mnths: 68 12 mnth: 71	42 mnths: 70 (±NR)					
		p< 0.05ˆ	p< 0.05ˆ						
Rhee 2008	Biceps tendon		48.4 (8-70)	32 mnths: 81.8 (37-96)			4.2 (1-8)	32 mnths: 10.2 (8-12)	12.5 (6-19)	32 mnths: 31.1 (9-35)
			p< 0.001						p< 0.001
Rotini 2011	Acellular Human Dermal Matrix		64 (55-75)	>1 yr: 88 (77-95)					
			p= NR						
Sano 2009	Biceps tendon								
Scheibel 2007	Periosteum		51.8 (25-68)	14 mnths: 80.9 (73-89)			4.5 (1-8)	14 mnths: 10.7 (8-12)	

| | | |

2.6.5 Repair failure and radiological assessments utilised

Integrity of the surgical repair was assessed by all RCTs and seven observational comparative studies, with a re-tear rate ranging from 10-73% following patch implantation and 18-65% following a standard RCR (Table 2-4). MRI was the commonest imaging modality (62%) utilised to diagnose recurrent tears, with an MR arthrogram utilised in a further 23% of studies. The majority of studies undertook post-operative imaging after 1 to 2 years but with considerable heterogeneity existing in the radiological classification of re-tears and with 4 studies not providing any details. Definitions of re-tears could be broadly categorised into two themes, the presence of any tear or the presence of tears greater than residual intra-operative defects. Five studies also attempted to subcategorise recurrent tears into 'partial' or 'complete'. For example, the study by Iannotti *et al*. described a third, 'partially healed' group, defined as a smaller rotator cuff lesion than that observed during preoperative imaging.

While the RCT investigating human allograft (Graftjacket®)[226], demonstrated a significantly lower failure rate in the augmentation arm, neither of the RCTs investigating the xenograft patch Restore®[227,228] patch found any reduction in re-tear rate. In conflict with these findings, a multi-patch comparative study[221] found no difference in failure rate between three different patches; xenograft (Restore®), human allograft (Graftjacket®) or synthetic (Artelon®). Amongst the observational comparative studies significantly lower rates of re-tears were reported after augmentation with synthetic (Repol Angimesh)[222], autograft (Fascia Lata)[204] or allograft patches (Arthroflex® and Allocover™)[229,233], while no improvement in re-tears was observed following augmentation with long-head of biceps tendon autograft[234] or for the Restore®[100] patch.

Non-comparative studies: Re-tear rate was assessed by 31 non-comparative studies with a wide range of re-tear rates reported for each graft type (human allograft [0-25%, n=7]; human autograft [7-100%, n=4]; xenograft dermal [0-63%, n=8]; xenograft intestinal [8-90%, n=4]; synthetic [7-62%, n=8]

Table 2-4 | Risk of re-tear and complications

Study		Safety Population, n	Recurrence of rotator cuff tears (%)					Complications (%)				
			Definition	Imaging	Time of imaging, months (range)	Absolute risk of re-tear %	p-value	Reported? (Yes/No)	Superficial Infection, n(%)	Deep Infection, n(%)	Inflammatory Response, n(%)	Other, n(%)
Randomised Comparative Studies												
Barber 2012	Graftjacket®	22	Incomplete excursion of the repaired tendon to the greater tuberosity with gadolinium leakage.	MRA	14.5 (12-14)	15	<0.01	Yes	0 (0)	0 (0)	0 (0)	Shoulder Bursitis 1(5)
	Control	20				60			2(10)	0 (0)	0 (0)	Biceps Rupture, 1(5) Post-traumatic fibrosis, 1(5)
Byrant 2016	Restore®	34	>5mm increase in size of any immediate postoperative defect	MRA	12 (NR)	53	0.33	Yes	0 (0)	1(3)	0 (0)	Biceps Rupture,1(3) Unexplained fever, 2(6)
	Control	28				65			1(4)	0 (0)	0 (0)	Shoulder manipulation, 1(4)
Ianotti 2006	Restore®	15	*Not healed:* Tear size ≥ size on pre-op MRI	MRA	12 (NR)	73	0.11	Yes	0 (0)	0 (0)	2(13)	Wound erythema, 1(8)
	Control	15	*Partially healed:* Smaller tear than preoperative MRI			40			0 (0)	0 (0)	0 (0)	0 (0)
Leuzinger 2016	Graftjacket®	29	Complete integrity of the repair with no tendon retraction	MRI	6 (NR)	23	0.08	Yes	0 (0)	0 (0)	1(3)	0 (0)
	Artelon®	33				27			0 (0)	0 (0)	1(3)	0 (0)
	Restore®	30				39			0 (0)	0 (0)	1(3)	0 (0)
Non-Randomised Comparative Studies												
Ciampi 2014	Repol Angimesh®	52	NR	US	12 (NR)	17	0.001‡	Yes	0 (0)	0 (0)	0 (0)	0 (0)
	Tutopatch®	49				51			0 (0)	0 (0)	0 (0)	0 (0)
	Control	51				41			0 (0)	0 (0)	0 (0)	0 (0)
Gilot 2015	Arthroflex®	20	NR	US	24 (NR)	10	0.048	Yes	1(5)	0 (0)	0 (0)	0 (0)
	Control	15				26			0 (0)	0 (0)	0 (0)	0 (0)
Ito 2003	Fascia Lata	30	NR	MRI	NR	0	NR	Yes	0 (0)	0 (0)	0 (0)	0 (0)
	Control	17				18			0 (0)	0 (0)	0 (0)	0 (0)
Jeon 2017	Biceps tendon	31	Complete tendon detachment from the footprint of the	MRI	6 (NR)	32	0.55	No	-	-	-	-

	Control	33	greater tuberosity or loss of continuity in the midsubstance portion			39			-	-	-	-
Maillot 2018	Conexa™	11	N/A	N/A	N/A	N/A	N/A	Yes	0 (0)	1(9)	0 (0)	Shoulder stiffness, 4(4)
	Repair alone	12							1(8)	0 (0)	0 (0)	0 (0)
	Debridement	9							0 (0)	0 (0)	0 (0)	0 (0)
Mori 2013	Fascia Lata	24	High signal intensity or tendon discontinuity on ≥1 T2-weighted image	MRI	NR	21	0.015	Yes	0 (0)	0 (0)	0 (0)	0 (0)
	Control	24				42			0 (0)	0 (0)	0 (0)	0 (0)
Mori 2015	Fascia Lata + grade 1-2 infraspinatus atrophy	26	High signal intensity or tendon discontinuity on ≥1 T2-weighted image (complete defect) or insufficient thickness (partial defect)	MRI	NR	27	<0.001	Yes	0 (0)	0 (0)	0 (0)	0 (0)
	Fascia Lata + grade 3-4 infraspinatus atrophy	19				89			0 (0)	0 (0)	0 (0)	0 (0)
Tempelaere 2017	Quadriceps tendon	23	N/A	N/A	N/A	N/A	N/A	Yes	0 (0)	0 (0)	0 (0)	Knee pain, 12(52) Patellar fracture, 2(8) Quads tendon tear, 1(4) Nerve injury, 1(4) Knee Stiffness, 1(4)
	Control	27							0 (0)	0 (0)	0 (0)	0 (0)
Vitali 2015	Repol Angimesh®	60	NR	MRI	12 (NR)	15	NR	Yes	0 (0)	0 (0)	0 (0)	0 (0)
	Control	60				40			0 (0)	0 (0)	0 (0)	0 (0)
Walton 2007	Restore®	16	Thickness of supraspinatus immediately medial to insertion. 0mm if re-torn.	MRI	24 (NR)	60	NR	Yes	0 (0)	0 (0)	4(21)	0 (0)
	Control	16				58			0 (0)	0 (0)	0 (0)	0 (0)
Yoon 2016	Allocover™	21	Sugaya classification grades 4 and 5 were considered re-tears¶	MRI	12 (NR)	19	0.036	Yes	0 (0)	0 (0)	0 (0)	0 (0)
	Control	54				46			0 (0)	0 (0)	0 (0)	0 (0)
Non-comparative studies												
Agrawal 2006	Allopatch®	14	Sugaya classification grades 4 and 5¶	MRI	16.8 (12-24)	14	N/A	Yes	0 (0)	0 (0)	0 (0)	0 (0)
Audenaert 2006	Mersilene®	41	NR	US	NR	7	N/A	No	-	-	-	-
Badhe 2008	Zimmer® Collagen Repair Patch	10	An identifiable gap between the greater tuberosity and the graft	US/MRI	54 (36-60)	20	N/A	Yes	0 (0)	0 (0)	0 (0)	0 (0)
Bektafier 2010	Coracromial ligament	46	N/A	N/A	N/A	N/A	N/A	No	-	-	-	-

Bond 2008	Graftjacket®	16	NR	MRI	12 (NR)	19	N/A	Yes	0 (0)	0 (0)	0 (0)	0 (0)
Burkhead 2007	Graftjacket®	17	NR	MRI/CTA	14 (NR)	25	N/A	Yes	0 (0)	0 (0)	0 (0)	0 (0)
Cho 2014	Permacol™	5	Fluid-equivalent signal or discontinuity of the rotator cuff in ≥1 T2- weighted images	MRI	8 (6-12)	20	N/A	Yes	0 (0)	0 (0)	0 (0)	0 (0)
Consigliere 2017	DX reinforcement matrix	10	N/A	N/A	N/A	N/A	N/A	No	-	-	-	-
Encalada-Diaz 2011	Polycarbonate polyurethane patch	10	NR	MRI	12 (NR)	10	N/A	Yes	0 (0)	0 (0)	0 (0)	0 (0)
Flury 2012	Graftjacket® or Arthroflex®	8	NR	US/MRI	6 (NR)	Full: 13 Partial: 25	N/A	Yes	0 (0)	0 (0)	0 (0)	0 (0)
Giannotti, 2014	Zimmer® Collagen Repair Patch	9	NR	US/MRI	34 (30-45)	0	N/A	No	-	-	-	-
Gupta 2012	Graftjacket®	24	*Not intact:* A full thickness defect at the graft-tendon or graft-humerus interface *Partially intact:* A partial thickness defect at the graft-tendon or graft-humerus interface.	US	36 (NR)	Full:0 Partial: 26	N/A	Yes	0 (0)	0 (0)	0 (0)	0 (0)
Gupta 2013	Conexa™	26	As above (Gupta 2012)	US	32 (24-40)	Full: 5 Partial: 22	N/A	Yes	0 (0)	0 (0)	0 (0)	0 (0)
Hirooka 2002	Gore-tex® PTFE	27	NR	Arthrography	NR	11	N/A	Yes	0 (0)	0 (0)	0 (0)	0 (0)
Lederman 2016	Conexa™	61	*Complete:* ≥80% of the size of the original tear in the sagittal plane *Partial:* Tears between 1 cm and 80% of original size	MRI	12 (NR)	Full: 15 Partial: 34	N/A	Yes	1(2)	0 (0)	0 (0)	Superficial haematoma, 1(2)
Lenart 2015	X-Repair	13	NR	MRI	18 (14-20)	62	N/A	No	-	-	-	-
Malcarney 2005	Restore®	25	NR	Arthroscopy	NR	16	N/A	Yes	0 (0)	0 (0)	4(16)	0 (0)
Marberry 2012	Artelon®	17	NR	MRI	NR	18	N/A	Yes	1(6)	1(6)	0 (0)	0 (0)
Metcalf 2002	Restore®	12	NR	MRI	NR	8	N/A	Yes	0 (0)	0 (0)	0 (0)	0 (0)
Moore 2006	Cadaveric	32	NR	MRI	34 (3-124)	100	N/A	Yes	0 (0)	1(3)	1(3)	0 (0)
Modi 2013	Graftjacket®	61	NR	MRI	12	Full: 0 Partial: 17	N/A	Yes	0 (0)	1(2)	0 (0)	Persistent pain, 1(2)
Nada 2010	Dacron	21	NR	MRI	36 (30 – 46)	19	N/A	Yes	0 (0)	1(5)	0 (0)	0 (0)
Neumann 2017	Conexa™	60	*Not intact:* Full thickness defect at graft-tendon or graft-humerus interface	US	50 (24 -63)	Full: 5 Partial: 3	N/A	Yes	0 (0)	0 (0)	0 (0)	0 (0)

			Partial: less than full thickness defect at graft-tendon or graft-humerus interface									
Petrie 2013	LARS™	31	N/A	N/A	N/A	N/A	N/A	Yes	0 (0)	0 (0)	0 (0)	Persistent pain, 1(3) Shoulder stiffness, 1(3)
Petri 2016	Arthroflex®	12	NR	MRI	9.9 (0.3-26.3)	17	N/A	Yes	0 (0)	0 (0)	0 (0)	0 (0)
Petricciolo 2013	SportMesh®	10	(1) Bare area between the edge of subscapularis and the bicipital groove and; (2) Coexistence of fluid in the subacromial subdeltoid bursa and/or fluid in the long head of biceps sheath	US	23 (12-34)	10	N/A	Yes	0 (0)	0 (0)	0 (0)	0 (0)
Phipatanakul 2009	Restore®	11	*Partially intact*: Smaller tear than preoperative imaging. Otherwise not stated.	MRA	25 (14-38)	50	N/A	Yes	1(9)	0 (0)	0 (0)	Skin reaction, 3(27)
Proctor 2014	X-Repair	18	NR	US/MRI	12	17	N/A	No	-	-	-	-
Rhee 2008	Biceps tendon	31	Fluid-equivalent signal or non-visualisation of supra-, infra- or subscapularis tendon in ≥1 T2 weighted images	MRI	NR	Full: 21 Partial: 14	N/A	Yes	0 (0)	0 (0)	0 (0)	'Popeye 'biceps deformity, 2(7)
Rotini 2011	Acellular Human Dermal Matrix	5	NR	MRI	12	20	N/A	Yes	0 (0)	0 (0)	0 (0)	0 (0)
Sano, 2010	Biceps tendon	14	Sugaya classification > grades 4 were considered re-tears¶	MRI	28 (12-51)	7	N/A	Yes	0 (0)	0 (0)	0 (0)	'Popeye 'biceps deformity, 1(7)
Scheibel, 2007	Periosteum	20	Fluid equivalent signal in the way of a tendon, discontinuity or retraction	MRI	12	20	N/A	Yes	0 (0)	1(5)	0 (0)	Ectopic ossification, 4(20)
Schlegel 2017	Collagen sheet	33	NR	MRI	3 + 12 (NR)	N/A	N/A	Yes	1(3)	0 (0)	0 (0)	Persistent pain ,1(3) Cardiac event, 1(3) Possible inflammatory response, 1(3)
Sclamberg 2004	Restore®	11	NR	MRI	(6-12)	90	N/A	No	-	-	-	-
Sears 2014	ECM	16	NR	US/MRI	50 (NR)	63	N/A	No	-	-	-	-
Venouziou 2013	Graftjacket®	14	N/A	N/A	N/A	N/A	N/A	Yes	0 (0)	0 (0)	0 (0)	0 (0)
Wong 2010	Graftjacket®	45	N/A	N/A	N/A	N/A	N/A	Yes	0 (0)	1(2)	0 (0)	0 (0)

Abbreviations: CTA, Computed Tomography Arthrogram; ECM, Extracellular Matrix; MRA, Magnetic Resonance Arthrogram; MRI, Magnetic Resonance Imaging; N/A, Not Applicable; NR, Not Reported; PTFE, Polytetrafluoroethylene; US, Ultrasonography **Footnotes:** ‡ values refers to polyprophylene patch (RepolAngimesh) vs control (standard repair). No p-value reported for Tutopatch® vs control. ¶ Sugaya *et al*. (Arthroscopy 2005;21:1307-16)

2.6.6 Shoulder pain

Comparative studies: Only two studies (Gilot *et al.*, Athroflex®[229]; Mori *et al.*, Fascia Lata[204]) reported significant reduction in pain when compared against standard repair (Table 2-5). The remaining nine studies either did not provide inter-group comparisons (n=3) or found no significant difference in pain scores between treatment arms (n=6). Interestingly, the study by Walton *et al.,* who utilised a 'mean activity pain score', found an increase in pain for the first 3 months following implantation of the Restore® patch, which subsequently normalised by 6 months.[100]

Non-comparative studies: In contrast, of the 24 case-series reported pain scores 22 reported a significant temporal improvement following augmented rotator cuff repair.

2.6.7 Health related quality of life

Comparative studies: Only three comparative trials reported the use of either the SF-12 or SF-36 scores (Table 2-6). When compared with standard repair, two RCTs investigating porcine SIS xenograft (Restore®) found no difference in the physical or mental components of the SF-36.[227,228] Conversely, an observational comparative study using human allograft (Athroflex®) reported a significant improvement in both these components at 6 months and two years post-operatively.[229]

Non-comparative studies: Three case-series reported significant improvements in SF-12 scores at final follow-up (32-36 months post-operatively).[235–237] Conversely, the study by Encalada-Diaz *et al.* found no improvement in physical or mental components of the SF-12 at 12 months, following implantation of a synthetic rotator cuff patch.[114]

2.6.8 Patch related adverse events

A total of 43 studies provided data on complications, of which 21 studies reported the occurrence of complications in a total of seventy-three patients. The more common reported events across the studies included were superficial and deep infections, and inflammatory response (Table 2-4). Other reported complications were shoulder bursistis, biceps rupture, fibrosis, unexplained fever, shoulder manipulation, wound erythema, shoulder stiffness,

persistent pain, skin reaction, biceps deformity, ossification, cardiac event, and possible inflammatory response.

The overall complications rates were 5.5% for patients undergoing any form of patch augmentation and 2.1% following non-augmentative surgery. However, by excluding two studies in the augmentation group which had particularly high rates of complications (74% and 20% of participants following quadriceps tendon or humeral periosteal augmented repair respectively[238,239]), the overall rate of complications following patch augmentation was 2.3%. An inflammatory response or was recorded in ten patients (all reported complication detailed in Table 6). The majority of these events (n=8) occurred in patients who received a SIS xenograft (Restore®) [100,228] patch but with reactions also reported after implantation of bovine derived[225], irradiated[240] or decellularized[221] human allograft, and synthetic patches[221].

Table 2-5 | Pain scores

Study		Pain Scores									
		VAS, Mean (SD or range)					**Other pain scales**, Mean (SD or range)				
		Baseline	Intermediate	p-value	Final†	p-value	Baseline	Intermediate	p-value	Final†	p-value
Randomised Comparative Studies											
Iannotti 2006	Restore®						12.5[I](±NR)			14 mnths 25[I](±NR)	0.18
	Control						12.0[I](±NR)			14 mnths 29[I](±NR)	
Non-Randomised Comparative Studies											
Ciampi 2014	Repol Angimesh	8.3 (±1.0)	2 mnths: 4.9 (±0.9)	<0.001‡	36 mnths: 3.3 (±1.1)	<0.001‡					
	Tutopatch	8.3 (±1.1)	2mnths: 6.45 (±1.0)	0.01‡	36 mnths: 4.1 (±1.0)	<0.001‡					
	Control	8.2 (±1.1)	2 mnths: 7.0 (±1.1)	<0.001‡	36 mnths: 3.7 (±1.1)	<0.001‡					
Gilot 2015	Arthroflex®	6.8 (±1.6)	12 wks: 5.3(±1.6) 24 wks: 3.9(±1.6)	12wks: 0.52 24 wks: 0.04	96wks: 1.3 (±1.2)	0.013					
	Control	6.9 (±1.1)	12 wks: 5.8 (±1.1) 24 wks: 6.8 (±1.1)		96wks: 4.1 (±1.1)						
Ito, 2003	Fascia Lata						10.0*(±5.6)			2.9 yrs: 27.8*(±3.6)	<0.01‡
	Control						9.2*(±2.9)			4.2 yrs: 28.3*(±3.3)	<0.005‡
Jeon 2017	Biceps tendon	5.1 (±1.4)	12 wks: 3.7(±1.5) 24 wks: 2.2(±1.4)	NR	29mnths: 1.0 (±0.8)	0.892					
	Control	5.2 (±1.4)	12 wks: 3.9(±1.6) 24 wks: 2.1(±1.2)	NR	29mnths: 0.9 (±0.8)						

Maillot 2018	Conexa™	7.1 (±1.2)	12 wks: 3.5(±1.3) 24 wks: 1.9(±1.3)	12wks: 1.0^ 24 wks: 1.0^	24 months: 0.6(±0.7)	1.0^					
	Repair only	6.9 (±1.2)	12 wks: 3.0(±1.9) 24 wks: 1.6(±1.3)		24 months: 0.7(±0.8)						
	Debridement	7.2 (±0.8)	12 wks: 3.2(±1.2) 24 wks: 1.4(±1.2)	12wks: 1.0^ 24 wks: 1.0^	24 months: 1.0(±0.8)	0.501^					
Mori 2013	Fascia Lata	7.0 (±0.9)	12 mnths: 1.2 (±0.8)	NR	35 mnths: 0.3 (±0.6)	0.028					
	Control	7.0 (±1.0)	12 mnths: 1.8 (±1.7)		35 mnths: 1.2 (±1.5)						
Tempelaere 2017	Quadriceps tendon						5.5§ (0-14)		58 mnths: 11.9§ (3-15)	NS	
	Control						7.6§ (5 -13)		55 mnths: 12.6§ (5-15)		
Vitali 2015	Repol Angimesh	8.2 (±1.1)	3mnths: 4.9 (±0.9)	NR	36 mnths: 3.2(± 1.1)	Unclear*					
	Control	8.4 (±1.0)	3 mnths: 6.9 (±1.1)		36 mnths: 3.7(± 1.0)						
Walton 2007	Restore®						NR	3 mnths:¶ 9.9 (±1.6)	<0.01	NR	NR
	Control						NR	3 mnths:¶ 4.0 (±1.3)		NR	
Yoon 2016	Allocover™	6.0 (±1.9)	1 yr: 1.5 (±2.1)	0.95	2 yrs: 1.6 (±1.7)	0.68					
	Control	6.1 (±1.5)	1 yr: 1.6 (±1.8)		2 yrs: 1.8 (±1.9)						
Non-comparative studies											
Agrawal 2012	Allopatch™						7.7§ (±NR)		1 yr: 13.6 (±NR)	0.008	
Audenaert 2006	Mersilene®						1.3§(±NR)		43 mnths: 13.1§(±NR)	<0.001	
Badhe 2008	Zimmer® Collagen Repair Patch						6.8§ (±NR)		4.5 yrs: 14 (±NR)	0.00003	
Bond 2008	Graftjacket®						4.6‡ (±NR)		26 mnths: 9.8 (±NR)	0.0001	
Cho 2014	Permacol™	6.8 (±NR)			21 mnths: 0.8 (±NR)	0.041					
Consigliere 2017	DX reinforcement matrix	7.0 (±2)	3 mnths: 0.8(±0.8)	<0.05	6 mnths: 0.6 (±0.8)	<0.05					

Encalada-Diaz 2011	Polycarbonate polyurethane patch	5.7 (2 - 8)	6 mnths: 3.8(NR)	0.009	12 mnths: 2.6 (0 - 4)	<0.001				
Gupta 2012	Graftjacket®	5.4 (±NR)			3 yrs: 0.9 (±NR)	0.0002				
Gupta 2013	Conexa™	5.1 (±NR)			32 mnths: 0.4 (±1.0)	0.002				
Hirooka 2002	Gore-tex® PTFE						9.1*(±NR)		44 mnths: 27.7*(±NR)	<0.0001
Marberry 2012	Artelon®						4.5§ (±2.9)		1 yr: 11.6§ (±3.3)	0.002
Modi 2013	Graftjacket®	7.0 (4 - 10)			3.6 yrs: 0.8 (0-5)	0.001				
Moore 2006	Cadaveric						2.5# (±NR)		31 mnths: 7.9# (±NR)	<0.001
Nada 2010	Dacron	7.0 (5 - 8)			36 mnths: 1.0 (0 – 2)	<0.001				
Neumann 2017	Conexa™	4.0 (±2.5)			50 mnths: 1.0 (±1.6)	<0.001				
Petrie 2013	LARS™	7.7 (±NR)			3.3 yrs: 4.4 (±NR)	<0.0001				
Petri 2016	Arthroflex®						38.6§2(±8.6)		2.5 yrs: 44.6§2(±10.6)	0.506
Petricciolo 2013	SportMesh™	7.9 (±1.1)			23 mnths: 2.0 (±1.9)	NR				
Phipatanakul 2009	Restore®	6.6 (±NR)			26 mnths: 2.2 (±NR)	<0.01				
Rhee 2008	Biceps tendon	At rest: 2.0 (0-7) On exercise: 6.6 (3-10)			32 mnths: 0.3 (0-5) 32 mnths: 1.4(0-10)	<0.001 <0.001				
Sano 2010	Biceps tendon						13.1*(±2.5)		28 mnths: 22.9*(±5.1)	0.002
Scheibel 2007	Periosteum						7.9§ (6-12.5)		14 mnths: 14.0§ (12-15)	<0.001
Schlegel 2017	Collagen Sheet	4.2§2 (±0.4)†2	3 mnths: 1.5§2 (±0.3) †2	<0.001	12 mnths: 0.6§2(±0.2) †2	<0.0001				
Venouziou 2013	Graftjacket®	7.4 (4-9)			30 mnths: 1.7 (0-5)	0.001				

Abbreviations: mnth, month; NR, Not Reported; NS, Not Significant; SD, Standard Deviation; SEM, Standard Error of Mean; wk, week; yr, year **Footnotes:** †Average final follow-up; ‖Pain subcomponent of PENN score reported. ‡Comparison is between pre- and post-treatment values and does not refer to statistical differences between groups. ¶Pain and function questionnaire developed by L'Insalata *et al.* (J Bone Joint Surg Am 1997;79:738-48); §Pain subcomponent of the Constant score reported; §2Pain subcomponent of the ASES score reported; #Pain subcomponent of the UCLA score reported; *Pain subcomponent of Japanese orthopaedic association shoulder score reported; ^p-value refers to comparison of Conexa™ or debridement against standard repair; †2 Standard error of mean reported

Table 2-6 | Quality of Life Scores

Study		Quality of Life Outcome Score									
		SF-12, Mean (±SD or range)					**SF-36**, Mean (±SD or range)				
		Baseline	Intermediate	p-value	Final†	p-value	Baseline	Intermediate	p-value	Final†	p-value
Randomised Comparative Studies											
Bryant 2016	Restore®						PCS 40.1 (±1.3)	1 yr: 46.6 (±1.4)	PCS: 0.50	1 yr: 47.3 (±1.6)	PCS: 0.56
							MCS 48.8 (±2.2)	1 yr: 55.7 (±1.4)	MCS: 0.52	1 yr: 55.0 (±1.2)	MCS: 0.83
	Control						PCS 40.5 (±1.5)	1 yr: 48.1 (±1.7)		1 yr: 48.7 (±1.7)	
							MCS 52.8 (±2.4)	1 yr: 54.3 (±1.6)		1 yr:55.0 (±1.2)	
Iannotti 2016	Restore®						PCS 50.3 (±NR)			14 mnths: NR	NS
							MCS 56.3 (±NR)			14 mnths: NR	
	Control						PCS 51.8 (±NR)			14 mnths: NR	
							MCS 51.9 (±NR)			14 mnths: NR	
Non-Randomised Comparative Studies											
Gilot 2015	Arthroflex®	PCS 29.2 (±6.4)	12 wks: 29.2 (±5.1) 24 wks: 36.2 (±4.4)	PCS: 12 wks: 0.68 24 wks: 0.05	96 wks: 42.6 (±10.8)	PCS: 0.05					
		MCS 42.2 (±12.1)	12 wks: 45.7(±10.8) 24 wks: 47.3 (±6.5)		96 wks: 64.1 (±9.3)						
	Control	PCS 30.7 (±6.0)	12 wks: 30.3 (±5.7) 24 wks: 30.4 (±5.0)	MCS: 12 wks: 0.71 24 wks: 0.06	96 wks: 31.7 (±9.5)	MCS: 0.04					
		MCS 43.1 (±8.2)	12 wks: 47.1(±11.8) 24 wks: 41.1 (±8.2)		96 wks: 42.9 (±10.8)						
Non-comparative studies											
Encalada-Diaz 2011	Polycarbonate polyurethane patch	PCS 35.6 (±NR)	6 mnths: 42.5 (±NR)	0.03	12 mnths: 40.4 (±NR)	0.13					

		MCS	45.4 (±NR)	6 mnths: 53.1 (±NR)	0.10	12 mnths: 51.1 (±NR)	0.32	
Gupta 2012	Graftjacket®		48.8 (±NR)			3yrs: 56.8 (±NR)	0.03	
Gupta 2013	Conexa™		48.4 (±NR)			32 mnths: 56.6 (±6.1)	0.04	
Marberry 2012	Artelon®		NR			1 year: 'Positive change for physical component'	NR	
Petri 2016	Arthroflex®	PCS	44.5 (±8.9)			2.8 yrs: 52.9 (±5.7)	0.005	
		MCS	NR			NR	NR	

Abbreviations: MCS, Mental Component Score; mnth, month; PCS, Physical Component Score; NR, Not Reported; NS, Not Significant; SD, Standard Deviation

2.6.9 Meta-analysis

Shoulder pain and function scores: Of the fifteen comparative studies, nine (8 observational and one RCT) provided sufficient data on postoperative functional outcome scores to be included in the meta-analysis (Figure 2-2). A 9-point improvement on the UCLA shoulder scale was observed for synthetic patches at 36-months post-operatively (mean difference 9.81, 95% CI 9.10 to 10.51, I^2 =0%) but not in the ASES score of studies of autografts (mean difference 4.18, 95% CI -3.22 to 11.58, I^2 =78%) (Figure 2-3). Studies of allografts or xenografts derived from dermis or pericardium (non-SIS) used differing measures. No difference was found when the allograft studies were combined (standardised mean difference 0.54, 95% CI -0.23 to 1.31, I^2=80%). There did not appear to be a difference between the sole RCT (Barber 2012) in this meta-analysis and the other studies.[226] For studies of xenografts versus surgery, there was also no evidence of a difference (standardised mean difference -0.05, 95% CI -0.41 to 0.30, I^2=0%, respectively). Insufficient data was available for xenografts derived from intestinal submucosa (SIS).

Shoulder pain: Eight observational comparative studies had sufficient data for a meta-analysis of post-operative pain (Figures 2-2 and 2-4). A small, non-clinically significant,[241] improvement in post-operative pain was only observed for synthetic patches (mean difference -0.46, 95% CI -0.74 to -0.17, I^2=0%) (Figure 2-4). For studies of non-SIS xenografts, there was no evidence of a difference in post-operative pain scores (standardised mean difference 0.26, 95% CI -0.16 to 0.68, I^2=16%). There was substantial statistical heterogeneity between the studies of autograft and allograft patches (mean difference -0.37, 95% CI -1.35 to 0.61, I^2=86% and standardised mean difference -0.75, 95% CI -2.15 to 0.64, I^2=91% respectively). Insufficient data was reported for a meta-analysis of shoulder pain following augmentation with xenograft patches derived from SIS.

Health related Quality of Life: Only three comparative studies (two RCTs and one observational study) provided data on health-related quality of life though there was insufficient data available to meta-analyse.[227–229]

Surgical Re-tear rate: Eleven (four RCTs and seven observational) comparative studies could be included in a meta-analysis for re-tear rate (Figures 2-2 and 2-5). A significantly lower re-tear rate was seen for an allograft patch (RR 0.34 95% CI 0.18 to 0.64, I^2=0%). The one RCT (Barber 2012) evaluating an allograft appears to have a consistent finding with the three observational studies.[226] There was evidence from two observational study for a lower re-tear rate with synthetic patches (RR 0.40, 0.25 to 0.64, I^2=0%). There was no evidence of a difference for autografts (RR 0.69 95% CI 0.40 to 1.18, I^2=0) based upon two observational studies, or SIS derived xenografts (RR 0.97 95% CI 0.72 to 1.30, I^2=0%) based upon two RCTs and one observational studies (the three studies having consistent findings). Insufficient data was available for non-SIS derived xenografts to meta-analyse.

2.6.10 Risk of bias

Assessment of bias was conducted for all RCTs and comparative studies (Tables 2-7 and 2-8). Only the study by Bryant et al.[227] showed a low risk of bias with the remaining RCTs assessed as having an unclear risk. These findings are based on a lack of study methodology detail, in particular surrounding blinding of patients and outcome assessors. All observational comparative studies had a serious risk of bias, centring around the potential for confounding, bias in patient selection and outcome measurement.

a.

Study or Subgroup	Patch Augmentation Mean	SD	Total	Standard Repair Mean	SD	Total	Weight	Std. Mean Difference IV, Random, 95% CI
Ito, 2003	-91.7	7	9	-92	7.6	12	9.6%	0.04 [-0.83, 0.90]
Maillot, 2018	-75.8	8.6	11	-74.7	4.3	12	9.7%	-0.16 [-0.98, 0.66]
Gilot 2015	-88.9	4.8	20	-72.6	11.9	15	9.7%	-1.86 [-2.67, -1.05]
Ciampi 2014	-24.6	3.2	52	-14.9	2	51	10.0%	-3.60 [-4.23, -2.97]
Barber 2012	-98.9	4.2	22	-94.8	14.2	20	10.0%	-0.39 [-1.00, 0.22]
Mori 2013	-94.1	5.4	24	-85.7	14.1	24	10.1%	-0.77 [-1.36, -0.19]
Vitali 2015	-24.6	3.3	60	-14.7	2	60	10.1%	-3.61 [-4.19, -3.02]
Yoon 2016	-82.5	11.2	21	-82	15.3	54	10.2%	-0.03 [-0.54, 0.47]
Jeon 2017	-88.2	6.9	31	-87.4	7.2	33	10.2%	-0.11 [-0.60, 0.38]
Ciampi 2014	-14.7	2	49	-14.9	2	51	10.3%	0.10 [-0.29, 0.49]
Total (95% CI)			**299**			**332**	**100.0%**	**-1.04 [-1.95, -0.13]**

Heterogeneity: $Tau^2 = 2.04$; $Chi^2 = 213.68$, df = 9 ($P < 0.00001$); $I^2 = 96\%$
Test for overall effect: Z = 2.24 (P = 0.02)

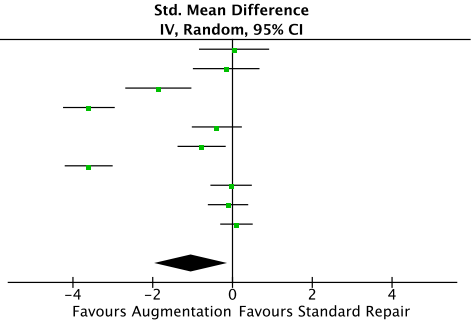

b.

Study or Subgroup	Patch augmentation Mean	SD	Total	Standard Repair Mean	SD	Total	Weight	Std. Mean Difference IV, Random, 95% CI
Gilot 2015	1.3	1.2	20	4.1	1.1	15	8.4%	-2.36 [-3.25, -1.47]
Ito 2003	-27.8	3.6	9	-28.3	3.3	12	8.6%	0.14 [-0.73, 1.01]
Maillot 2018	0.6	0.7	11	0.7	0.8	12	9.0%	-0.13 [-0.95, 0.69]
Mori 2013	0.3	0.5	24	1.2	1.5	24	11.1%	-0.79 [-1.38, -0.20]
Yoon 2016	1.6	1.7	21	1.8	1.9	54	11.9%	-0.11 [-0.61, 0.40]
Jeon 2017	1	0.8	31	0.9	0.8	33	12.0%	0.12 [-0.37, 0.61]
Ciampi 2014	4.1	1	49	3.7	1.1	51	12.9%	0.38 [-0.02, 0.77]
Ciampi 2014	3.3	1.1	52	3.7	1.1	51	12.9%	-0.36 [-0.75, 0.03]
Vitali 2015	3.2	1.1	60	3.7	1	60	13.1%	-0.47 [-0.84, -0.11]
Total (95% CI)			**277**			**312**	**100.0%**	**-0.34 [-0.74, 0.05]**

Heterogeneity: $Tau^2 = 0.27$; $Chi^2 = 39.64$, df = 8 ($P < 0.00001$); $I^2 = 80\%$
Test for overall effect: Z = 1.72 (P = 0.09)

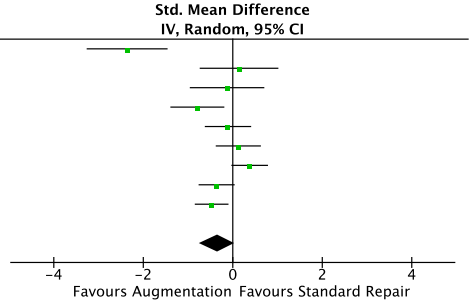

c.

Study or Subgroup	Patch Augmentation Events	Total	Standard Repair Events	Total	Weight	Risk Ratio M-H, Fixed, 95% CI
Ito, 2003	0	13	3	17	2.0%	0.18 [0.01, 3.27]
Gilot 2015	2	20	4	15	3.0%	0.38 [0.08, 1.78]
Walton 2007	6	10	7	12	4.1%	1.03 [0.51, 2.06]
Iannotti 2016	11	15	9	15	5.8%	1.22 [0.73, 2.04]
Mori 2013	5	24	10	24	6.5%	0.50 [0.20, 1.25]
Barber 2012	3	20	9	15	6.7%	0.25 [0.08, 0.77]
Jeon 2017	10	31	13	33	8.2%	0.82 [0.42, 1.59]
Yoon 2016	4	21	24	54	8.7%	0.43 [0.17, 1.09]
Bryant 2016	18	34	17	26	12.5%	0.81 [0.53, 1.24]
Ciampi 2014	25	49	21	51	13.3%	1.24 [0.81, 1.90]
Ciampi 2014	9	52	21	51	13.7%	0.42 [0.21, 0.83]
Vitali 2015	9	60	24	60	15.5%	0.38 [0.19, 0.74]
Total (95% CI)		**349**		**373**	**100.0%**	**0.66 [0.55, 0.81]**
Total events	102		162			

Heterogeneity: $Chi^2 = 26.24$, df = 11 ($P = 0.006$); $I^2 = 58\%$
Test for overall effect: Z = 4.07 ($P < 0.0001$)

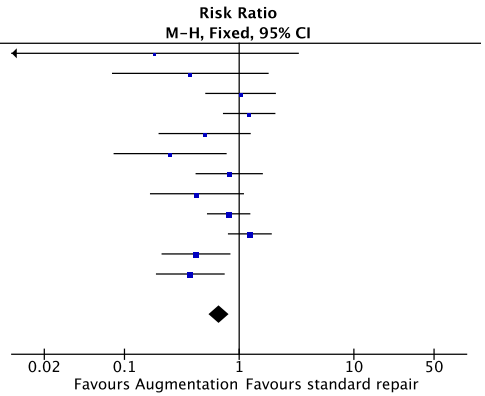

Figure 2-2: Forest plots comparing shoulder specific pain and function outcome scores, pain and re-tear rates at final follow-up between augmented and standard repair. A: Shoulder pain and function scores B: Shoulder pain C: Surgical Re-tear rate

a

Study or Subgroup	Human autograft patch Mean	SD	Total	Standard repair Mean	SD	Total	Weight	Mean Difference IV, Random, 95% CI
Jeon 2017	-88.2	6.9	31	-87.4	7.2	33	55.5%	-0.80 [-4.25, 2.65]
Mori 2013	-94.1	5.4	24	-85.7	14.1	24	44.5%	-8.40 [-14.44, -2.36]
Total (95% CI)			**55**			**57**	**100.0%**	**-4.18 [-11.58, 3.22]**

Heterogeneity: Tau² = 22.58; Chi² = 4.58, df = 1 (P = 0.03); I² = 78%
Test for overall effect: Z = 1.11 (P = 0.27)

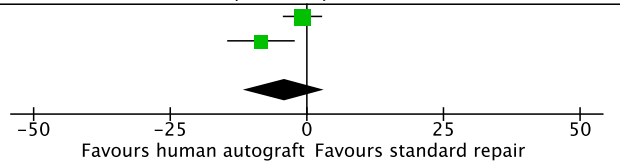

b

Study or Subgroup	Human allograft patch Mean	SD	Total	Standard Repair Mean	SD	Total	Weight	Std. Mean Difference IV, Random, 95% CI
Barber 2012	-98.9	4.2	22	-94.8	14.2	20	26.3%	-0.39 [-1.00, 0.22]
Gilot 2015	-88.9	4.8	20	-72.6	11.9	15	23.3%	-1.86 [-2.67, -1.05]
Ito, 2003	-91.7	7	9	-92	7.6	12	22.6%	0.04 [-0.83, 0.90]
Yoon 2016	-82.5	11.2	21	-82	15.3	54	27.8%	-0.03 [-0.54, 0.47]
Total (95% CI)			**72**			**101**	**100.0%**	**-0.54 [-1.31, 0.23]**

Heterogeneity: Tau² = 0.49; Chi² = 15.36, df = 3 (P = 0.002); I² = 80%
Test for overall effect: Z = 1.37 (P = 0.17)

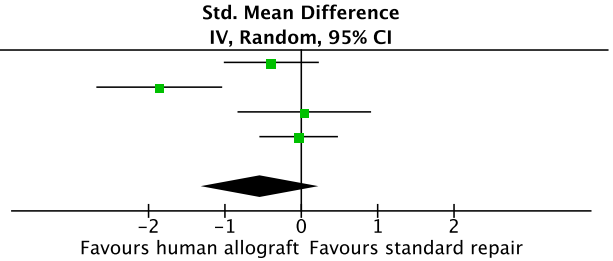

c

Study or Subgroup	Xenograft (non-SIS) patch Mean	SD	Total	Standard repair Mean	SD	Total	Weight	Std. Mean Difference IV, Random, 95% CI
Ciampi 2014	-14.7	2	49	-14.9	2	51	81.4%	0.10 [-0.29, 0.49]
Maillot, 2018	-75.8	8.6	11	-74.7	4.3	12	18.6%	-0.16 [-0.98, 0.66]
Total (95% CI)			**60**			**63**	**100.0%**	**0.05 [-0.30, 0.41]**

Heterogeneity: Tau² = 0.00; Chi² = 0.31, df = 1 (P = 0.58); I² = 0%
Test for overall effect: Z = 0.28 (P = 0.78)

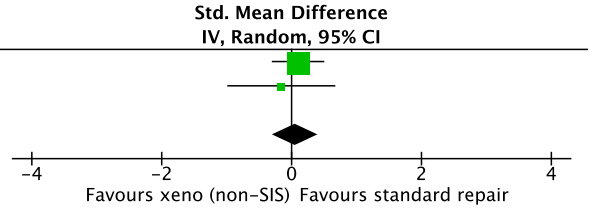

d

Study or Subgroup	Synthetic patch Mean	SD	Total	Standard repair Mean	SD	Total	Weight	Mean Difference IV, Random, 95% CI
Ciampi 2014	-24.6	3.2	52	-14.9	2	51	47.4%	-9.70 [-10.73, -8.67]
Vitali 2015	-24.6	3.3	60	-14.7	2	60	52.6%	-9.90 [-10.88, -8.92]
Total (95% CI)			**112**			**111**	**100.0%**	**-9.81 [-10.51, -9.10]**

Heterogeneity: Tau² = 0.00; Chi² = 0.08, df = 1 (P = 0.78); I² = 0%
Test for overall effect: Z = 27.14 (P < 0.00001)

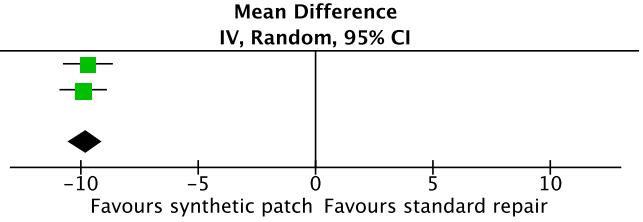

Figure 2-3: Forest plots comparing shoulder specific pain and function outcome scores at final follow-up between patch types and standard repair. A: autograft patches. B: allograft patches. C: Xenografts (non-small intestine submucosa). D: synthetic patches.

a.

Study or Subgroup	Human autograft patch Mean	SD	Total	Standard repair Mean	SD	Total	Weight	Mean Difference IV, Random, 95% CI	Year
Mori 2013	0.3	0.5	24	1.2	1.5	24	46.8%	−0.90 [−1.53, −0.27]	2013
Jeon 2017	1	0.8	31	0.9	0.8	33	53.2%	0.10 [−0.29, 0.49]	2017
Total (95% CI)			**55**			**57**	**100.0%**	**−0.37 [−1.35, 0.61]**	

Heterogeneity: $Tau^2 = 0.43$; $Chi^2 = 6.93$, df = 1 (P = 0.008); $I^2 = 86\%$
Test for overall effect: Z = 0.74 (P = 0.46)

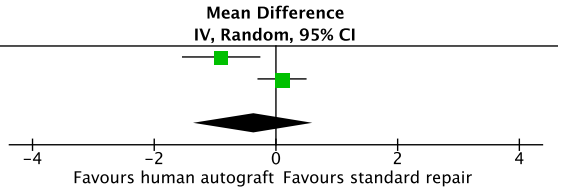

b.

Study or Subgroup	Human allograft patch Mean	SD	Total	Standard repair Mean	SD	Total	Weight	Std. Mean Difference IV, Random, 95% CI	Year
Ito 2003	−27.8	3.6	9	−28.3	3.3	12	32.4%	0.14 [−0.73, 1.01]	2003
Gilot 2015	1.3	1.2	20	4.1	1.1	15	32.2%	−2.36 [−3.25, −1.47]	2015
Yoon 2016	1.6	1.7	21	1.8	1.9	54	35.3%	−0.11 [−0.61, 0.40]	2016
Total (95% CI)			**50**			**81**	**100.0%**	**−0.75 [−2.15, 0.64]**	

Heterogeneity: $Tau^2 = 1.37$; $Chi^2 = 21.21$, df = 2 (P < 0.0001); $I^2 = 91\%$
Test for overall effect: Z = 1.06 (P = 0.29)

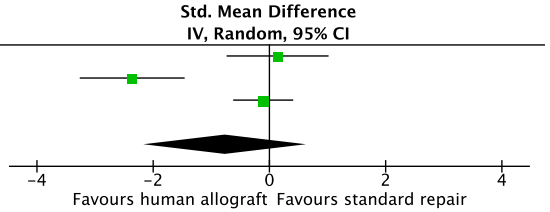

c.

Study or Subgroup	Xenograft (non-SIS) patch Mean	SD	Total	Standard repair Mean	SD	Total	Weight	Std. Mean Difference IV, Random, 95% CI	Year
Ciampi 2014	4.1	1	49	3.7	1.1	51	76.2%	0.38 [−0.02, 0.77]	2014
Maillot 2018	0.6	0.7	11	0.7	0.8	12	23.8%	−0.13 [−0.95, 0.69]	2018
Total (95% CI)			**60**			**63**	**100.0%**	**0.26 [−0.16, 0.68]**	

Heterogeneity: $Tau^2 = 0.02$; $Chi^2 = 1.18$, df = 1 (P = 0.28); $I^2 = 16\%$
Test for overall effect: Z = 1.20 (P = 0.23)

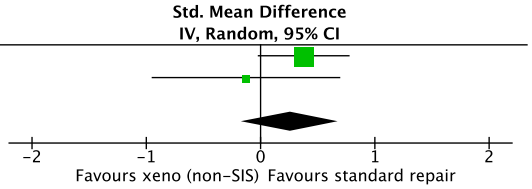

d.

Study or Subgroup	Synthetic patch Mean	SD	Total	Standard repair Mean	SD	Total	Weight	Mean Difference IV, Random, 95% CI	Year
Ciampi 2014	3.3	1.1	52	3.7	1.1	51	43.9%	−0.40 [−0.82, 0.02]	2014
Vitali 2015	3.2	1.1	60	3.7	1	60	56.1%	−0.50 [−0.88, −0.12]	2015
Total (95% CI)			**112**			**111**	**100.0%**	**−0.46 [−0.74, −0.17]**	

Heterogeneity: $Tau^2 = 0.00$; $Chi^2 = 0.12$, df = 1 (P = 0.73); $I^2 = 0\%$
Test for overall effect: Z = 3.17 (P = 0.002)

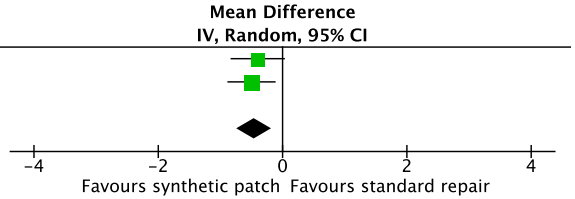

Figure 2-4: Forest plots comparing shoulder pain at final follow-up between patch types and standard repair. A: autograft patches. B: allograft patches. C: Xenografts (non-small intestine submucosa). D: synthetic patches.

a.

Study or Subgroup	Human autograft patch Events	Total	Standard repair Events	Total	Weight	Risk Ratio M-H, Random, 95% CI	Year
Mori 2013	5	24	10	24	34.5%	0.50 [0.20, 1.25]	2013
Jeon 2017	10	31	13	33	65.5%	0.82 [0.42, 1.59]	2017
Total (95% CI)		**55**		**57**	**100.0%**	**0.69 [0.40, 1.18]**	
Total events	15		23				

Heterogeneity: $Tau^2 = 0.00$; $Chi^2 = 0.74$, df = 1 (P = 0.39); $I^2 = 0\%$
Test for overall effect: Z = 1.35 (P = 0.18)

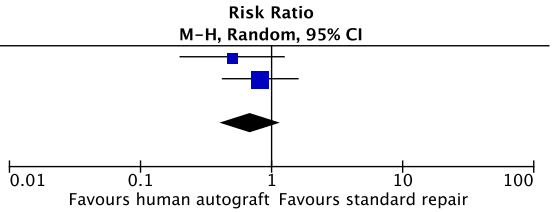

b.

Study or Subgroup	Human allograft patch Events	Total	Standard repair Events	Total	Weight	Risk Ratio M-H, Random, 95% CI	Year
Ito, 2003	0	13	3	17	4.9%	0.18 [0.01, 3.27]	2003
Barber 2012	3	20	9	15	32.0%	0.25 [0.08, 0.77]	2012
Gilot 2015	2	20	4	15	16.6%	0.38 [0.08, 1.78]	2015
Yoon 2016	4	21	24	54	46.5%	0.43 [0.17, 1.09]	2016
Total (95% CI)		**74**		**101**	**100.0%**	**0.34 [0.18, 0.64]**	
Total events	9		40				

Heterogeneity: $Tau^2 = 0.00$; $Chi^2 = 0.72$, df = 3 (P = 0.87); $I^2 = 0\%$
Test for overall effect: Z = 3.34 (P = 0.0008)

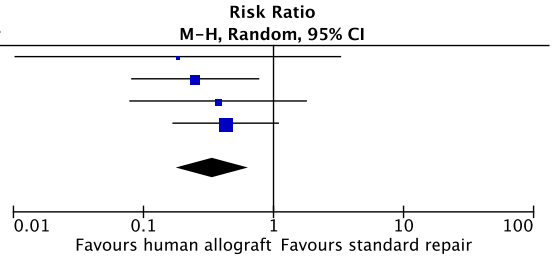

c.

Study or Subgroup	Xenograft (SIS) patch Events	Total	Standard repair Events	Total	Weight	Risk Ratio M-H, Random, 95% CI	Year
Walton 2007	6	10	7	12	18.0%	1.03 [0.51, 2.06]	2007
Bryant 2016	18	34	17	26	48.9%	0.81 [0.53, 1.24]	2016
Iannotti 2016	11	15	9	15	33.1%	1.22 [0.73, 2.04]	2016
Total (95% CI)		**59**		**53**	**100.0%**	**0.97 [0.72, 1.30]**	
Total events	35		33				

Heterogeneity: $Tau^2 = 0.00$; $Chi^2 = 1.51$, df = 2 (P = 0.47); $I^2 = 0\%$
Test for overall effect: Z = 0.21 (P = 0.83)

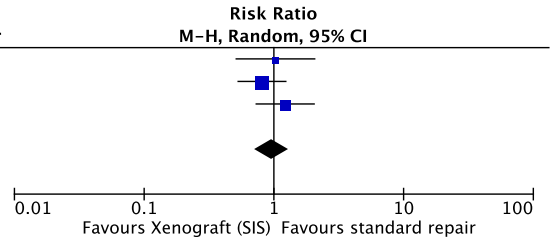

d.

Study or Subgroup	Synthetic patch Events	Total	Standard repair Events	Total	Weight	Risk Ratio M-H, Random, 95% CI	Year
Ciampi 2014	9	52	21	51	49.9%	0.42 [0.21, 0.83]	2014
Vitali 2015	9	60	24	60	50.1%	0.38 [0.19, 0.74]	2015
Total (95% CI)		**112**		**111**	**100.0%**	**0.40 [0.25, 0.64]**	
Total events	18		45				

Heterogeneity: $Tau^2 = 0.00$; $Chi^2 = 0.05$, df = 1 (P = 0.82); $I^2 = 0\%$
Test for overall effect: Z = 3.78 (P = 0.0002)

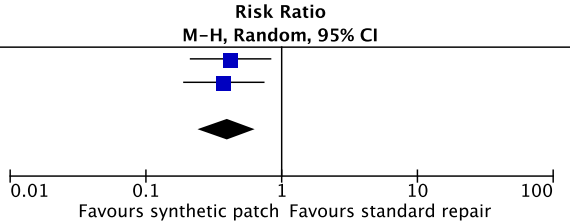

Figure 2-5: Forest plots comparing re-tear rates at final follow-up between patch types and standard repair. A: autograft patches. B: allograft patches. C: Xenografts (small intestine submucosa). D: synthetic patches.

Table 2-7 | Risk of bias (Randomised Trials)

Study	Type of Bias							
	Random sequence generation	Allocation concealment	Blinding of participants and personnel	Blinding of outcome assessors	Incomplete outcome data	Selective reporting	Other sources of Bias	Overall Assessment
Barber 2012	Unclear	High	Unclear	Unclear	Unclear	Low	High†	Unclear
Byrant 2016	Low	Low	Low	Low	Low	Low	Low	Low
Ianotti 2006	Low	Unclear	Unclear	Unclear	Unclear	Unclear	Unclear	Unclear
Leuzinger 2016	Unclear	Unclear	Unclear	Unclear	Low	High	Low	Unclear

Footnotes: † Classified as 'high' due to risk of sponsor bias

Table 2-8 | ROBINS-I Risk of bias (Non-randomised Comparative Trials)

Study	Type of Bias							Overall Assessment
	Bias due to confounding	Bias in participant selection	Bias in classification of interventions	Bia due to deviation from intended interventions	Bias due to missing data	Bias in measurement of outcomes	Bias in selection of the reported results	
Ciampi 2014	Serious	Moderate	Low	Low	No information	Serious	No information	Serious
Gilot 2015	Serious	Serious	Low	Low	Serious	Serious	Serious	Serious
Ito 2003	Serious	Serious	Moderate	No information	No information	Serious	Moderate	Serious
Jeon 2017	Moderate	Serious	Moderate	No information	No information	Serious	Moderate	Serious
Maillot 2018	Moderate	Serious	Low	No information	Low	Serious	Serious	Serious
Mori 2013	Serious	Serious	Low	Low	Serious	Serious	Serious	Serious
Mori 2015	Serious	Serious	Moderate	Low	Moderate	Serious	Serious	Serious
Tempelaere 2017	Serious	Serious	Moderate	No information	Serious	Serious	Moderate	Serious
Vitali 2015	Serious	Serious	Low	No information	Serious	Serious	Serious	Serious
Walton 2007	Moderate	Serious	Low	No information	Serious	Serious	Low	Serious
Yoon (2016)	Serious	Serious	Low	No information	Serious	Serious	Serious	Serious

2.7 DISCUSSION

Surgical repair with patch augmentation has been proposed as a method of improving rates of rotator cuff tendon healing. To date, this is the largest and most comprehensive systematic review to examine the clinical effectiveness and safety of patch augmented rotator cuff repair. However, despite safety concerns associated with specific patches (Restore®)[100] or techniques (Quadriceps allograft)[238], the evidence to support the use of a particular patch type, let alone individual patches, currently remains very weak.

Most studies reported on the use of patch augmentation for large-to-massive tears in patients aged 50-70 years of age. This demographic is similar to that reported by British shoulder surgeons, in which only 10% of respondents would consider augmentation for small and medium sized tears (unpublished data under review). Only 4 studies were identified that included patients with small and medium sized tears and none assessed the effect of tear size on outcome. It is therefore unclear why a dichotomy between small-medium and large-massive tears has emerged. It is interesting to note that small tears in patients aged 80 years are predicted to have a similar chance of repair failure as massive tears in patients aged 50 years.[200] Rather than viewing the degree of structural incompetence as the primary indication for patch augmentation, a biological perspective should instead be encouraged, applying augmentation to cases in which tendon healing is the most impaired.

Across the 52 studies, there was substantial variation in surgical technique and graft type. While previously research has found no difference in clinical effectiveness between open or arthroscopic repair of degenerative rotator cuff tears[22], the effect of graft type is not yet known. Only one study has directly compared multiple graft types, the trial by Ciampi *et al.*[222] found that a polypropylene patch (Repol Angimesh) had a lower rate of re-tear and improved UCLA scores at 3 years, than both a xenograft patch and standard repair. While this suggests that patch type could be important to outcome, the study by Leuzinger *et al.* found no difference in re-tear rate between patients randomised to receive human allograft (Graftjacket®), synthetic (Artelon®) or xenograft augmentation (Restore®). Unfortunately, this study did not provide any analysis on the effect of patch type on functional outcome score, pain or quality of life.[221]

MRI was the commonest imaging modality (62%) utilised to diagnose re-tears, with an MR arthrogram utilised in a further 8% of studies. The majority of studies undertook post-operative imaging after 1 to 2 years but with considerable heterogeneity existing in the radiological classification of what constituted a recurrent tear, and many (n=24) studies did not providing any details. Definitions of re-tears could be broadly categorised into two themes, the presence of any tear or the presence of tears greater than any residual intra-operative defect. Five studies also attempted to subcategorise recurrent tears into 'partial' or 'complete'. For example, the study by Iannotti *et al*. described a 'partially healed' group, defined as a smaller rotator cuff lesion than that observed during preoperative imaging.[228] Amongst studies investigating xenograft augmentation four reported that neither porcine small intestine submucosa or bovine pericardium patches resulted in improved rates of cuff re-tear over conventional repairs. A fifth study reported a trend towards a higher rate of re-tear with the Restore® patch than both Graftjacket® and Artelon®, although this result failed to reach statistical significance (p=0.08).[221] While a variety of porcine dermal xenografts are available, only one comparative studies to-date has assessed efficacy and did not report on the rate of re-tear.[223] Conversely, allografts and synthetic patches have all been reported to significantly reduce failure rates.[222,226,229,231,232]

Amongst the studies included in the meta-analysis there were significant differences in surgical techniques, with patches being used in both an 'on-lay', and 'bridging ' fashion.[204,242] It should be noted that differences in terminology makes comparison of these surgical techniques challenging - many studies use the terms *irreparable*, *bridging*, *interposition* or *reconstruction* interchangeable. This is particularly important when considering the biological processes that underpin the success of each technique. While on-lay patches seek to reinforce and stimulate tendon repair, a bridging scaffold provides a framework for potential tendon regeneration. Further, it is likely that each technique reflects different patient cohorts, with the use of bridging scaffolds probably representing larger, more chronic and even recurrent rotator cuff tears. A uniform approach to terminology is needed to facilitate the correct interpretation and synthesis of future studies. To this end, and in close agreement with previous work[214], we would recommend that the term *on-lay augmentation* is used to describe techniques in which a patch overlies a successful primary repair, and the term *bridging*

reconstruction be used when a patch is used to fill a residual defect for tears that cannot be repaired at or near their anatomical insertion site. Since multiple *post-hoc* comparisons risk finding false associations, a further subgroup analysis based around 'on-lay' or 'bridging' techniques was not undertaken.

Patient reported outcome measures seemed to closely echo radiological findings. Amongst the comparative studies, five found no significant improvement in either patient reported outcome measures or rate of re-tear for Restore®[100,227,228], biceps autograft[234] and Tutopatch[222]. A further six studies reported significant improvements in both functional outcomes scores and radiologically defined repair failure.[204,222,226,229,232,242] This lends support to the notion that repair success is intimately linked with symptom resolution. Indeed, in a subgroup analysis Iannotti *et al.* identified a significant association between tendon healing and post-operative improvements in the PENN score and SF-36 physical component.[228] Similar findings have previously been reported by the UKUFF study, in which those with healed repairs had a better Oxford Shoulder Score (OSS) than patients with re-tears, but with the worst results amongst those with an irreparable tear.[22] Nonetheless, while a correlation exists, the magnitude of change in PROMS following successful repair, compared with re-tear, is unlikely to be clinically meaningful. It is likely that the scar tissue, formed after successful repair, is not biologically normal. It is tempting to speculate that patches capable of restoring tendon biology will produce superior results. Of note, amongst the comparative studies and regardless of the type of patch utilised, there was a consistent temporal improvement in shoulder function, reinforcing the fundamental importance of selecting appropriate comparator groups when assessing patch efficacy.

In comparison with previous systematic reviews[216,217,243], we have included one additional RCT[221] and three observational comparative studies[231,233,234], representing 278 patients, not otherwise identified. Results from our meta-analysis are, in part, consistent with a previous analysis which found an overall reduction in re-tear rate and improved ASES scores following patch augmentation.[216] The substantial number of additional studies included in this current review provide greater precision and, while a subgroup analysis was not originally specified in our protocol, they have allowed us to hypothesise that patch type may have an effect on

patient outcomes. The occurrence of adverse events with only certain patch types add some credibility to this notion. Previous reviews of augmented RCR have, on the basis of a presumed effect on patient outcome, excluded studies based on the size of rotator cuff tear or surgical technique (on-lay or bridging).[243] It is possible that each technique reflects different patient cohorts, for example the use of bridging scaffolds may represent larger, more chronic or even recurrent rotator cuff tears. However, we did not formally assess whether there are differences in patient reported outcomes, re-tear rate or pain scores between studies reporting on-lay or bridging techniques.

Strengths of this this review include *a priori published* protocol[211]; a comprehensive search strategy; inclusion of non-English language articles and duplicate assessment of eligibility, risk of bias and data extraction. Nonetheless, there remain several limitations to the current review, which are mainly a reflection of the quality of published primary research available. Only four RCTs have been published, of which two refer to a product (Restore®) that has now been withdrawn from market due to safety concerns.[226] Secondly, substantial heterogeneity between studies was observed with the majority of studies also judged to have a high risk of bias, seriously limiting our ability to draw firm recommendations. An exhaustive exploration of the heterogeneity has not been undertaken and indeed such an analysis was not declared *a priori* in the protocol paper.[211] However, separating studies by patch type did influence the degree of heterogeneity and we would therefore recommend patch type should be considered in the design of future reviews.

2.8 CONCLUSIONS

There are a growing number of patches available for the augmentation of rotator cuff repair. Despite the safety related withdrawal of certain patches[100], as well as wider concerns surrounding medical device[244] and mesh implantation[244], rigorous clinical evaluation of patch augmentation is lacking. It is particularly concerned that several patches currently in clinical use (e.g. d-cell® and Leeds-Kuff™) lack any publicly available research. While some studies have indicated promise for specific patches (e.g. synthetic), firm recommendations in terms of patch type or surgical technique, cannot be made at present. Rigorous clinical evaluation of this technology is currently lacking, and the accurate interpretation of trial data is further

hampered by unclear and inconsistent reporting, in particular regarding tear size, definition of re-tear and surgical technique. There remains a need for well-designed comparative (preferably multi-centre RCTs) studies that are capable of robustly evaluating the effectiveness and safety of multiple patch types. Furthermore, routine reporting of registry data patch could address the current lack of robust safety data for cuff augmented rotated cuff repair.[245]

Chapter 3 Endothelial-fibroblast crosstalk alters fibroblast activation and endothelial recruitment of immune cells

3.1 ABSTRACT

3.1.1 Background

An increased immune cell infiltrate and activation of resident fibroblasts are key features of inflammation during acute wound healing. However, their failure to resolve has been implicated in several chronic inflammatory diseases, including human tendon disease. The identification of fibroblast-endothelial cell crosstalk has been pivotal to understanding the biological mechanisms underpinning the accumulation of leukocytes in inflammatory arthritis. However, it remains unclear whether endothelial cell activation by tendon derived fibroblasts is also a contributing factor in the sustained inflammatory cell infiltration observed in tendon disease. Growing evidence also supports a key role for activated endothelial cells (ECs) in the regulation of musculoskeletal tissue repair. Fibroblast activation a key feature of acute wound repair but when persistent can drive chronic inflammation. This experiment sought to investigate if dysregulated tenocyte-endothelial cell crosstalk altered the endothelial-driven recruitment of immune cells in tendon disease. Additionally, the effect of endothelial derived paracrine signalling on the activation status of tendon derived fibroblasts was considered.

3.1.2 Methods

Tendon fibroblasts were isolated from healthy hamstring (n=4 donors) and massive rotator cuff tears (n=4 donors). Transwell™ co-cultures with microvascular endothelial cells (HMEC-1) were undertaken for up to 9 days in either basal culture media or stimulated with IL-1β or IL-4. Transwell™ layers were separated, and a panel of genes assessed by qRT-PCR for relevant biological processes. In a variant of this assay, HMEC-1 and fibroblasts were cultured on 24-well and 12-well Transwell™ inserts respectively to produce three distinct chambers, and peripheral blood leukocytes added to the uppermost chamber. Within each chamber flow cytometry was used to count key leukocyte subsets and endothelial adhesion, trans-endothelial migration and trans-fibroblast migration subsequently calculated.

3.1.3 Results

During extended (day 9) co-culture with microvascular ECs, hamstring derived tendon fibroblasts displayed an activated phenotype. Co-culture increased the expression of the fibroblast activation markers *CD248*, *PDPN* and *VCAM-1*, with a corresponding increase in the expression of pro-inflammatory cytokines, extracellular matrix proteins and matrix proteases also observed. A smaller and non-significant response was observed for diseased tendon fibroblasts. Fibroblasts derived from healthy comparator tendons inhibited the adhesion of lymphocytes and monocytes to the endothelium. This effect was lost during co-cultures with diseased tendon fibroblasts and following the addition of exogenous IL-4,and was not attributable to differential expression of endothelial adhesion receptors.

3.1.4 Conclusions

In human tendon disease, resident fibroblasts undergo a distinct change in phenotype. This includes a lost immunosuppressive effect that results in the increased endothelial cell recruitment of immune cells. However, this cross-talk is not simply unidirectional. The endothelial bed is also capable of providing complementary signalling that influences the activation status of healthy tendon fibroblasts, suggesting an important role for the vasculature in the initiation and persistence of fibroblast derived inflammatory signalling. For the first time, these findings provide a unique insight into the role of the endothelium in the pathobiology of rotator cuff tendon disease.

3.2 INTRODUCTION

The histological characterisation of human tendinopathy has identified a chronic infiltration of monocytes, macrophages and lymphocytes, with the total size of these expanded immune populations dependent on disease stage.[42,246] These persistent leukocyte populations can induce cellular damage and extra-cellular matrix degradation directly, whilst also inducing resistant stromal fibroblasts to turn on pro-inflammatory cellular programmes[247,248], thereby amplifying the inflammatory milieu within the tissue microenvironment. However, it is now clear that fibroblasts are not just passive bystanders, they respond directly to tissue damage[249] and act as important sentinels of the innate immune system.[250] Further, in many chronic inflammatory diseases, fibroblasts acquire persistent phenotypic alterations in which they fail to switch off production of pro-inflammatory cytokines, and continually synthesise and remodel newly created matrix – a state termed 'fibroblast activation'.[251] Recent evidence has also demonstrated a role for fibroblast activation in the pathogenesis of tendinopathy.[252] Biopsies from patients with rotator cuff tendonitis demonstrated an upregulation of PDPN, CD248 and VCAM-1 (CD106) by diseased tendon fibroblasts, a phenotype that persists during *in vitro* culture. The activation of NF-κB, interferon and STAT-6 pathways have all been implicated in the phenotype of diseased tendon fibroblasts.[45]

Vascular endothelial cells (ECs) act as critical regulators of leukocyte adhesion and extravasation. The original model of leukocyte adhesion proposed a sequential three-step cascade involving selectin-mediated capture, chemokine activation of captured leukocytes and integrin-dependent arrest.[253] Subsequent modifications to this model have also considered the molecular events that underpin trans-endothelial leukocyte migration.[254] This multi-step process requires the precise expression of EC receptors and chemokines, a signature often referred to the recruitment postcode[72] - thereby ensuring that leukocytes are delivered to the correct organ at the appropriate time. Importantly, local cytokines and inflammatory agonists are able to modulate the EC phenotype.[255] Since tissue resident fibroblasts play an important role in defining the stromal cytokine environment, they can in turn condition the response of ECs. If, as in the case of many inflammatory joint diseases, the resident fibroblasts are constitutively pro-inflammatory, a chronic inflammatory milieu is

created and sustained.[256] For instance, during *in vitro* co-culture with rheumatoid arthritis synovial fibroblasts ECs, through the expression of Duffy Antigen receptor (DARC), demonstrate an increased capacity to transport and present stromal derived CXCR5, facilitating an increased recruitment of neutrophils from flowing culture media.[74] However, in the context of tendon disease, whether changes to the stromal postcode are responsible for increased immune cell infiltrates is unknown.

Fibroblast-endothelial cell cross-talk is not unilateral. Paracrine factors produced by activated endothelial cells provides signals to quiescent tissue-specific stem cells to drive regeneration and repair.[75] In the skeletal system, type H vessels that are positive for CD31 and Endomucin regulate osteoblasts and skeletal repair via Notch dependent production of Noggin by ECs.[79] Moreover, a combination of EC derived cytokines has been shown to support the proliferation of muscle satellite-cells.[80] An increase in vascularity is a prominent feature of rotator cuff tendon disease[44,246] and also increases in response to surgery.[257] However, whether this expanded endothelial cell population has a direct role in tendon healing is as yet unclear.

To date, the pathobiological role of the endothelium in tendon disease has not been considered. This chapter aims to examine the effect of tenocyte-endothelial cell paracrine crosstalk and assess the transcriptional and/or functional response on both cell types during indirect co-culture.

3.3 AIMS

The overarching aim was to to investigate if paracrine interactions between endothelial cells (HMEC-1) and diseased or healthy human tendon fibroblasts (tenocytes) influence either the phenotype of tenocytes, or the endothelial recruitment of immune cells. Specifically, this work aimed to:

1. Determine if tenocyte-endothelial cell co-culture modulates expression of fibroblast activation markers by tenocytes, comparing responses of healthy and diseased tendon cells
2. Investigate how tendon-endothelial cell co-culture influences fibroblast activation, release of pro-inflammatory cytokines and extracellular matrix turnover, comparing responses of healthy and diseased tendon cells
3. Determine if tendon-derived fibroblasts modulate endothelial mediated recruitment of immune cells, comparing responses of healthy versus diseased tendon donors

3.4 HYPOTHESES

This work hypothesises that tenocyte-endothelial cell crosstalk regulates fibroblast activation and that the inflammatory milieu of diseased tenocytes promotes leukocyte recruitment mediated by the endothelium.

The specific hypotheses of this chapter are that:

1. Endothelial cell-derived paracrine signaling influence the activation signature of tenocytes
2. Endothelial cell-derived paracrine signaling modulates expression of tendon extracellular matrix proteins, matrix proteases and/or pro-inflammatory cytokine release
3. Diseased tenocytes promote the endothelial attachment of immune cells via upregulation of endothelial adhesion receptors
4. Diseased tenocytes promote trans-endothelial migration of immune cells through the upregulation of junctional adhesion molecules.
5. Diseased tenocytes reduce trans-fibroblast migration of immune cells

3.5 METHODS

3.5.1 Isolation and culture of leukocytes, fibroblasts and endothelial cells

3.5.1.1 Peripheral blood leukocyte isolation

Venous blood isolated from a single healthy individual was collected in EDTA tubes (BD Biosciences, Berkshire, UK). Peripheral blood leukocytes (PBLs) were isolated by red cell lysis. Ammonium-Chloride-Potassium (ACK) buffer was added to anticoagulated blood in a 14:1 ratio and then agitated at room temperature for 10 minutes prior to centrifugation at 300*xg* for 5 minutes. The supernatant was discarded, and the procedure repeated to minimise red cell contamination. Isolated cells were then washed, counted (TC20, Bio-rad, Hertforshire, UK) and adjusted to the desired concentration ($10x10^6$ cells/ml) in RPMI-1640 (Sigma Aldrich, Dorset, UK), supplemented with 1% Fetal Bovine Serum (FBS) (Labtech, Uckfield, UK) and 1% penicillin-streptomycin (ThermoFischer Scientific, Waltham, MA, USA).

3.5.1.2 Collection and processing of tendon samples

Biopsies of diseased rotator cuff tendons were collected from patients undergoing tendon repairs (n=4, 3 male 1 female, average age 62.5 yrs). All tendon tears had been classified at massive (>5cm in anterior-posterior diameter) by the operative surgeon. Healthy controls were obtained from patients undergoing anterior cruciate ligament reconstruction during which residual autologous hamstring tendon graft was collected (n=4, 3 male 1 female, average age 22.5 yrs). Informed consent was provided by all donor and samples collected through Oxford Musculoskeletal Biobank (REC 09/H0606/11), in full compliance with national and institutional ethical requirements including the Declaration of Helsinki (2013) and the Human Tissue Act (2004). Tendon samples were immediately placed in D10 culture media and underwent laboratory processing to isolate tendon-derived fibroblasts.

3.5.1.3 Isolation and expansion of tendon fibroblasts

Under aseptic conditions tendon samples were divided into 2-mm^3 sections and between 4 and 6 explants transferred into each well of a 6-well plate. Samples were initially cultured in D50 culture media (DMEM/F12 containing 50% FCS and 1% PS) in a tissue culture incubator at 37^oC and 5% CO2. Phase contrast microscopy was used to determine the migration of fibroblasts out of tendon explants, at which point whole tissue samples were removed and the

culture medium changed to D10 media. At 80-90% confluence cells were enzymatically detached (TrypLE^{TM}, ThermoFischer Scientific, Waltham, MA, USA) and expanded in polystyrene tissue culture dishes (CELLSTAR, Greiner, Frickenhausen, Germany). All subsequent experiments were undertaken on cells at passage 2.

3.5.1.1 Endothelial cell culture

The immortalised human microvascular endothelial cell line, HMEC-1 (ATCC, Manassas, VA, USA) was utilised in place of primary endothelial cells. HMEC-1 cells were cultured in MCDB131 (ThermoFischer Scientific, Waltham, MA, USA) and supplemented with 10ng/ml recombinant human epidermal growth factor (Sigma Aldrich, Dorset, UK), 10mM L-glutamine (ThermoFischer Scientific, Waltham, MA, USA) and FBS to a final concentration of 10% during cellular expansion or 1% during co-culture.

3.5.2 Co-culture of endothelial cells and fibroblasts on transwell filters

Tendon-derived fibroblasts from healthy hamstring or diseased supraspinatus were seeded at a density of 150,000 cells per well into a 24-well plate, whilst HMEC-1 cells (1.5 x10^5 cell/filter) were cultured separately on the surface of a 24-well 0.4µm transwell filter inserts (Corning Inc., Corning, NY, USA). After 48 hours, the 24-well inserts were fitted into the 24-well plate and co-cultured together in 1% FBS supplemented endothelial cell media for 1 to 9 days. During extended culture media was changed every 3 days. In some experiments human recombinant IL-1β(Sigma Aldrich, Dorset, UK) or IL-4(Sigma Aldrich, Dorset, UK) each at 10ng/ml was added to the culture media for the full duration of co-culture. For comparison, tendon-derived fibroblasts or HMEC-1 cells were cultured alone.

3.5.3 Gene expression by tendon-fibroblasts and endothelial cells during co-culture

After 1,3,6 and 9 days in co-culture HMEC-1 and tendon-fibroblasts layers were separated, culture media removed, and each layer gently washed with PBS prior to the addition of 300µl Trizol (Invitrogen, Paisley, UK) to each mono-layer (Appendix B-1). Specimens were then stored at -80^{o}C before RNA extraction. RNA extraction, which included a DNAse treatment step, was performed using the Direct-Zol RNA Microprep Kit (Zymo Research, Irvine, CA, USA) according to manufacturer's instructions. RNA quantity was determined using

spectrophotometry (ND1000, Nanodrop Technologies, Willington, DE, USA) and the ratio of 260/280nm absorbance was used to determine RNA quality. All samples had a minimum 260/280nm ratio of 1.8. RNA was then diluted with nuclease free water (Invitrogen, Waltham, MA, USA) to a concentration of 1.25ng/µl before cDNA synthesis using a high capacity cDNA reverse Transcription kit (Applied Biosystems, Waltham, MA, USA) and a 9902 Veriti 96-well thermal cycler (Applied Biosystems, Waltham, MA, USA) set according to the manufacture's protocol. RT-qPCR was performed with Fast SYBR Green Master Mix (Applied Biosystems, Waltham, MA, USA), using an Applied Biosystems ViiA7 Real-time PCR system (Life Technologies, Carlsbad CA, USA). Reactions consisted of 5ng cDNA (4µl), 5 µl SYBR Green and 0.2-0.5 µl primer to a total volume of 10µl with nuclease free water. A list of primers is available in table 3-1 and 3-2. Reference genes with the most stable expression across experimental conditions were selected from a panel of 12 candidate reference genes with qbase+ software (Primer Design, Camberley, UK). Gene expression was calculated based on the comparative CT method.[258]

3.5.4 Adhesion and migration of leukocytes on HMEC-1 endothelial cells during indirect co-culture with tendon-derived fibroblasts

Tendon-derived fibroblasts and HMEC-1 cells were cultured in endothelial media on the surface of 24-well and 12-well 3.0 µm pore Transwell filter inserts (Corning Inc., Corning, NY, USA) respectively. Fibroblasts were seeded at 2 $x10^5$ cells/filter and HMEC-1 at 1 $x10^5$ cells/filter to yield confluent monolayers within 48 hours. After 48 hours, culture media was removed and the 24-well inserts placed into the 12-well insert, 1.5ml endothelial media was added to the lowest chamber and a further 200µl to the surface of each filter. In some experiments, cytokine stimulation with human recombinant IL-1β or IL-4 was undertaken. To provide appropriate comparisons, parallel cultures of fibroblast or HMEC-1 mono-cultures, with and without cytokine stimulation, were maintained.

Cells were co-cultured together for 24 hours (37°C and 5% CO_2) prior to the addition of PBLs (1 $x10^6$ cell/ml in 200µ)l. Co-cultures were returned to the incubator and PBLs allowed to adhere for 30 minutes, after which non-adherent cells were collected as previously described.[259]In brief, upper chamber media was collected and the 24-well filter washed twice

with PBS (Fraction A). Fresh media (200μl) was added to the upper chamber and co-cultures returned to the incubator. After 36 hours, each filter was transferred into a fresh well and the cells that had migrated through both filters collected (Fraction C). Media between the 12-well and 24-well filter was collected, and the 12-well filter washed twice prior to treatment with Accutase (ThermoFischer Scientific, Waltham, MA, USA) for 3 minutes to dissociate cells adherent to the fibroblast monolayer. Together, these cells represented fraction B (Figure 3-1). For comparison, PBLs were added to mono-cultures of endothelial cells or fibroblasts.

Flow cytometry was used to count the number of PBLs and the proportion of cells calculated as follows:

1) PBL adherence (%): For each major PBL population, the total number of adherent cells was inferred by subtracting fraction A from the total number added. Adhesion was then expressed as a percentage of the total number of cells added.
2) PBL trans-endothelial migration (%): The total number of cells in fractions B and C, expressed as a percentage of the total number of adherent cells.
3) PBL trans-fibroblast migration (%): The total number of cells in fraction C, expressed as a percentage of the total number of cells in fractions B and C combined.

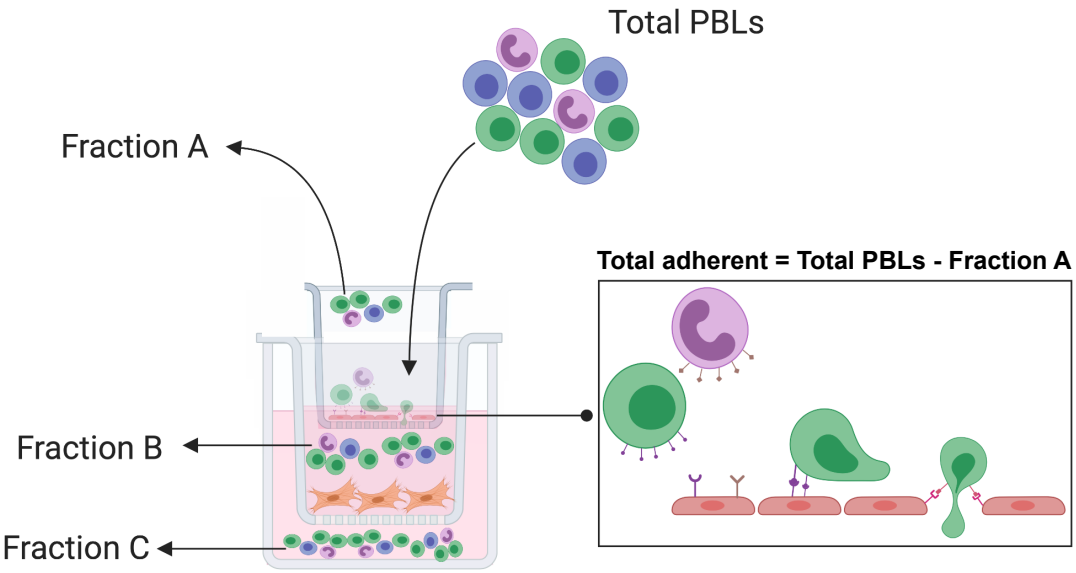

Figure 3-1. Schematic depicting the assessment of PBL adherence and migration during co-culture of HMEC-1 endothelial cells with tendon-derived fibroblasts. HMEC-1 and tendon-derived fibroblasts were cultured on 12-well and 24-well Transwell inserts respectively for 48 hours. The 12-well filter was then inserted into the 24-well filter, as depicted, and allowed to equilibrate for 24 hours prior to addition of a fixed number of peripheral blood leukocytes (PBLs). After 30 minutes non-adherent PBLs were removed and counted with flow cytometry (Fraction A). Leukocytes that had migrated through the endothelial monolayer, but not the fibroblast layer constituted fraction B. Finally, cells in the lowest chamber that had undergone trans-endothelial and trans-fibroblast migration, were collected and counted with flow cytometry (Fraction C).

Gene	Supplier	Forward	Reverse	Volume (µl)
CD248	Primer Design	TGTCCCGTGACCACCAGATC	GGAGGCTGTGCTGAATGAGAG	0.5
VCAM1	Primer Design	CAGGCTAAGTTACATATTGATGACAT	GAGGAAGGGCTGACCAAGAC	0.5
PDPN	Primer Design	CCGAAGATGATGTGGTGACTC	CGATGCGAATGCCTGTTACA	0.5
FAP	Primer Design	CCAAAGACCCAGGAGCATATAG	TGTAGCCATCCTTGTCACTAAATA	0.5
COL1A1	Primer Design	AGACAGTGATTGAATACAAAACCA	GGAGTTTACAGGAAGCAGACA	0.5
COL3A1	Primer Design	GTCCCGCTGGCATTCCTG	CTCTCCTTTGGCACCATTCTTAC	0.5
COL5A2	Primer Design	GCCAAGACACATCGACAATGAG	GCAGGATCAGCCATTACTTCAAG	0.5
COL9A3	Primer Design	ACGGTGCTCCGGGAGAGAA	ACCCAGCTCCCCAGCTCTG	0.5
ACAN	Primer Design	CCAACCAGCCTGACAACTTT	GTGAAGGGGAGGTGGTAATTG	0.5
TNMD	Primer Design	TACCAAGGAGGACGAGTCATC	GCCAGCAGTTTAAGCATTTGAG	0.5
SAA1	Primer Design	CCAGAGAGAATATCCAGAGATTCTTTG	CCCATTCATTGGCAGCCTGA	0.5
MMP3	Primer Design	ATGATGAACAATGGACAAAGGATAC	AGTGTTGGCTGAGTGAAAGAG	0.5
ADAMS12	Primer Design	GGCAAGCAGATAACCAAGGT	TTCTTATTTGTAAACAGCAGTCGTA	0.5
IL1β	Primer Design	CACGATGCACCTGTACGATCA	TGGAGAGCTTTCAGTTCATATGGA	0.5
IL2	Primer Design	CCTATCACTCTCTTTAATCACTACTC	GTTTGTGACAAGTGCAAGACT	0.5
IL4	Sigma Aldrich	CGAGTTGACCGTAACAGACAT	CGTCTTTAGCCTTTCCAAGAA	0.2
IL6	Primer Design	CGTCTTTAGCCTTTCCAAGAA	ACCTCAAACTCCAAAAGACCA	0.5
IL8	Sigma Aldrich	TGCTAAAGAACTTAGATGTCAGTGCAT	TGGTCCACTCTCAATCACTCTCA	0.2
IL10	Sigma Aldrich	TACGGCGCTGTCATCGATT	GGCTTTGTAGATGCCTTTCTCTTG	0.2
IL12β	Sigma Aldrich	AGAAGATGGTATCACCTGGACC	GAACCTCGCCTCCTTTGTGAC	0.2
TNFα	Primer Design	GGCCAAGCCCTGGTATGAG	TAGTCGGGCCGATTGATCTC	0.5
IFNɣ	Primer Design	TCAACTTCTTTGGCTTAATTCTCTC	ATATGGGTCCTGGCAGTAACA	0.5
TGFβ	Primer Design	CAATTCCTGGCGATACCTCAG	GCACAACTCCGGTGACATCAA	0.5
CSF2	Primer Design	AACAAGAGCTAGAAACTCAGGATG	ATTCTTCTGCCATGCCTGTATC	0.5
PTGS2	Primer Design	CAGGCTTCCATTGACCAGAG	TTTCTCCTGTAAGTTCTTCAAATGAT	0.5
IRF1	Sigma Aldrich	CTGTGCGAGTGTACCGGATG	ATCCCCACATGACTTCCTCTT	0.2
TGM2	Sigma Aldrich	GCCACTTCATTTTGCTCTTCAA	TCCTCTTCCGAGTCCAGGTACA	0.2
FOXF2	Primer Design	CACCTGCCACTTAGCCAGAA	TTGGGGAACGCTACCTTGC	0.5
HSPB1	Primer Design	AGGATGGCGTGGTGGAGAT	GGGGGCAGCGTGTATTTCC	0.5
GAPDH	Primer Design	GAAGGTTGAAGGTCGGAGTC	GAAGATGGTGATGGGATTTC	0.5
TOP1	Primer Design	-	-	0.5

Table 3-1. Primers used during qRT-PCR assessment of fibroblasts during endothelial cell co-culture

Gene	Supplier	Forward	Reverse	Volume (µl)
SELE	Primer Design	TTCTTGCCTACTATGCCAGATG	AGGAAAGGGAACACTGAGTCT	0.5
SELP	Primer Design	TTCCTGTCCCACCTCTTCTC	GTCTCTTTGGTTCACTGGTATTTC	0.5
PODXL	Primer Design	CTGGCTCAGCAAGTCTCAGG	GATGGTGGTAGTAGGGTTGCC	0.5
300LG	Primer Design	CGATGGTCCGCATACTGGC	TCTCCACAGGAGCAGGTGG	0.5
EMCN	Primer Design	CACTGATGTCAGGAAGAATGACTC	GGAACTTTGTAATGTTGAAACAGCA	0.5
GLYCAM1	Primer Design	CCTGCTACAGCTCCACCATG	CCAGATTCAACATCAAGGATGGC	0.5
ICAM1	Primer Design	CCTATGGCAACGACTCCTTC	TCTCCTGGCTCTGGTTCC	0.5
MCAM	Primer Design	CAGACTGTGGAGTCGAGTGG	ACTGGGCATCTTTGTCTTCTTTAAC	0.5
VCAM1	Primer Design	CAGGCTAAGTTACATATTGATGACAT	GAGGAAGGGCTGACCAAGAC	0.5
ICAM2	Primer Design	CAGTGGAAACATTACTTGGTCTCAA	CGCTGACGTTGGAATTCATTGA	0.5
F11R	Primer Design	ACCTGAAGTCAGAATTCCTGAGAATA	TGGTGGTGTCTCCTTGGTCA	0.5
JAM2	Primer Design	GGAAGAGGATACAGTCACTCTGG	CCAGTGTATTCAGGAGCTGGA	0.5
JAM3	Primer Design	ACCGCACTCCGGCTCTG	TCCTGTACCACTGGGGTTCG	0.5
ESAM	Primer Design	CCGCTGTCCAATACCAGTGG	GCAGACATAGACTCCAGCCATG	0.5
CD99	Primer Design	GGGGAGTATCTGTCCTGCC	CGACCAGAACACCCAGCAG	0.5
CD99L2	Primer Design	GCTCGGCGTTCCTTGTCTG	GCATCCTCCAGGTTAAAATCATCAA	0.5
CD47	Primer Design	AGGAGATGCCTCTTTGAAGATGG	CCTTCTCTGGTTAATTCTGTTACTTCA	0.5
PVR	Primer Design	AGAGCTTTGAGAAGCCTCAG	GCCAAGGTACCAGTTGTTATCATA	0.5
AOC3	Primer Design	CGGAGCTGCTGGAGATGG	CCACTTGTTGCTGTGGTTGC	0.5
PTPRB	Primer Design	GCAACAACTTCAGAAGAGAATACATTG	CCTTCTCAACACACTGGGTCAC	0.5
CDH5	Primer Design	CGGAGTTTGCCAAGCCCTA	CGTGGTGTTATGTCCTTGTCTATT	0.5
ICAM5	Primer Design	GCGAGGCGGTCAAGGACG	CGAGGCTTCTGTTCCCTCCAGC	0.5
EDIL3	Primer Design	AGGGAAATTTTGACAATGACACTCA	CAGCTCTGACCGCAATGTGA	0.5
SDHA	Primer Design	-	-	0.5
TBP	Primer Design	GTTTGCCAAGAAGAAAGTGAAC	GGGTCAGTCCAGTGCCAT	0.5
TOP1	Primer Design	-	-	0.5

Table 3-2. Primers used during qRT-PCR assessment of HMEC-1 endothelial cells during co-culture with tendon-derived fibroblasts

3.5.5 Flow cytometry

Each co-culture PBL fraction, as well as total PBLs that had not been added to the co-culture system, were transferred into a round-bottom 96-well plate, centrifuged, washed twice in stain buffer (BD Biosciences, Berkshire, UK) and cells incubated with 5µl FcR Blocking reagent (TruStain FcX, Biolegend, London, UK) for 10 minutes at room temperature. Cells were then labelled with a combination of the antibodies or isotype controls as listed in tables 3-3 and 3-4 for 30 minutes on ice. After washing twice in stain buffer, cells were fixed using Cytofix fixation buffer (BD Biosciences, Berkshire, UK) at room temperature for 20 minutes, washed

and suspended in 150µl of stain buffer (BD Biosciences). Flow cytometry was performed the following day using a BD LSR Fortessa calibrated with BD cytometer setup and tracking beads. Analysis of cell populations was performed with FlowJo v10 (FlowJo LCC, Ashland, Oregon, USA), isotype controls were used to optimise gating strategies.

Surface Markers	Supplier	Fluorochrome	Isotype	Clone	Dilution
CD3	BioLegend	Pe-Cy7	Mouse IgG1, kappa	SK7	1:20
CD4	BioLegend	PerCP/Cy5.5	Mouse IgG1, kappa	RPA-T4	1:20
CD8	BD Biosciences	APC	Mouse IgG1, k	RPA-T8	1:12.5
CD14	BioLegend	AlexFlour700	Mouse IgG2a, kappa	M5E2	1:25
CD15	BD Biosciences	BV650	Mouse IgM, kappa	HI98	1:20
CD19	BD Biosciences	PE-CF594	Mouse IgG1, k	HIB19	1:20
CD45	Biolegend	BV711	Mouse IgG1, κ	HI30	1:50
Live/Dead	eBioScience	BV780	-	-	1:250

Table 3-3. Antibodies used for extracellular staining of peripheral blood leukocytes

Supplier	Fluorochrome	Isotype	Clone	Dilution
BioLegend	Pe-Cy7	Mouse IgG1, kappa	MOPC-21	1:20
BioLegend	PerCP/Cy5.5	Mouse IgG1, kappa	MOPC-21	1:40
BD Biosciences	APC	Mouse IgG1, k	MOPC-21	1:250
BioLegend	AlexFlour700	Mouse IgG2a, kappa	MOPC-173	1:25
BD Biosciences	BV650	Mouse IgM, kappa	G155-228	1:160
BD Biosciences	PE-CF594	Mouse IgG1, k	X40	1:80
Biolegend	BV711	Mouse IgG1, κ	MOPC-21	1:50

Table 3-4. Matched isotype controls

3.5.6 Statistical Analysis

Statistical analyses were performed using GraphPad Prism 7.0 (GraphPad Software Inc, California, USA). All multivariant data were analysed using a two-way analysis of variances with post hoc Tukey's or Dunnett's testing. $p < 0.05$ was considered as statistically significant.

3.6 RESULTS

3.6.1 Temporal expression of pro-inflammatory cytokines by tendon fibroblasts during EC co-culture

The effect of indirect EC co-culture on the mRNA expression of NF-κB regulated pro-inflammatory cytokines was assessed over a 9-day time course (Figure 3-2). Compared with mono-cultured fibroblast controls, co-culture fibroblasts from healthy tendon showed significantly increased mRNA expression of *IL-1β, IL-6 and IL-8* after 9 days (Figure 3-2 A(ii)-D(ii)). A similar trend was observed at days 3 and 6 but did not reach statistical significance. Fibroblasts isolated from diseased massive rotator cuff tears also demonstrated a significant upregulation of *IL-8* mRNA expression after extended EC co-culture for 9 days. A similar trend was observed for *IL-1β* and *IL-6* (Figure 3-2 A(i)-D(i)).

3.6.2 The effect of EC co-culture on the expression of fibroblast activation markers

The observed upregulation of NF-κB regulated pro-inflammatory cytokines mRNA raised the possibility that EC co-culture modified fibroblast activation status. Figure 3-3 shows the effect of co-culture on the differential gene expression of the fibroblast activation markers; *PDPN, CD248, VCAM1* and *FAP* after 9 days in co-culture. Fibroblasts isolated from healthy tendons demonstrated an upregulation of *PDPN*, *CD248* and *VCAM1* with a similar trend also observed for diseased fibroblasts after 9 days in co-culture.

As IL-1β induces NF-κB target genes, that are highly expressed in early stage tendon disease we investigated if the exogenous addition of IL-1β EC-tendon fibroblast co-cultures could induce a more profound activation of tendon derived fibroblasts. Conversely, IL-4 induces STAT6 target genes that are highly expressed in late stage tendon disease.[45] The addition of IL-4 sought to induce the chronic inflammatory environment seen during the later stages of disease. However, treatment with IL-1β or IL-4 abrogated the effect of EC co-culture on the expression of fibroblast activation markers.

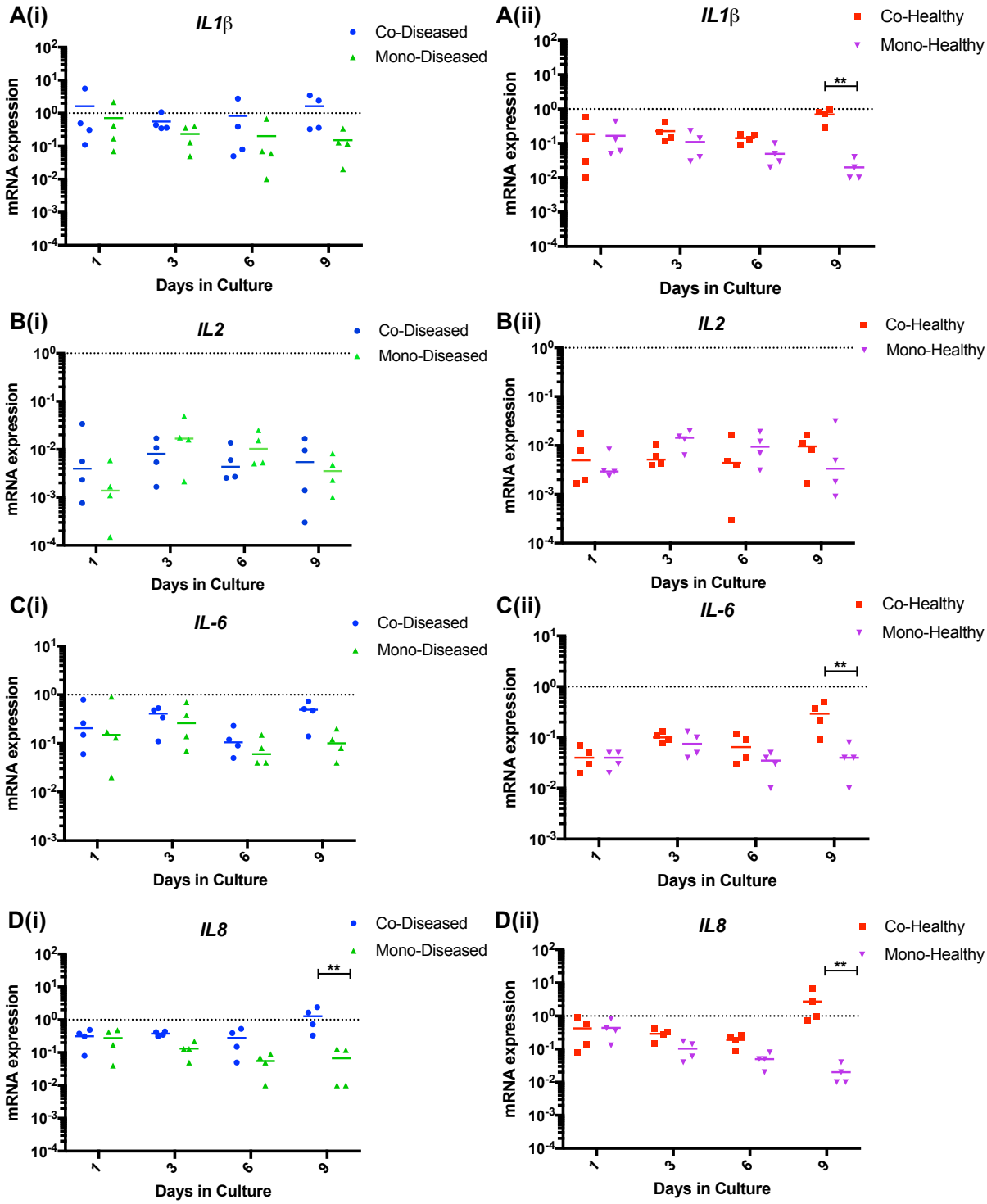

Figure 3-2 . Effect of HMEC-1 endothelial cell co-culture on the mRNA expression of NK-κβ targets by tendon fibroblasts during a 9-day time course. mRNA was isolated from tendon fibroblasts derived from massive rotator cuff tears (diseased) or healthy hamstring (healthy) that had been co-cultured for up to 9 days with HMEC-1 cells. Gene expression was assessed by qRT-PCR and values were expressed as relative expression units (REU) compared with housekeepers (GAPDH and TOP1) according to the $2^{-\Delta CT}$ method. Data are mean of three technical replicated for explant derived fibroblasts from 4 healthy and 4 diseased tendons. **p<0.005 compared to tendon fibroblast mono-culture by 2-way ANOVA with Sidak's correction for multiple testing.

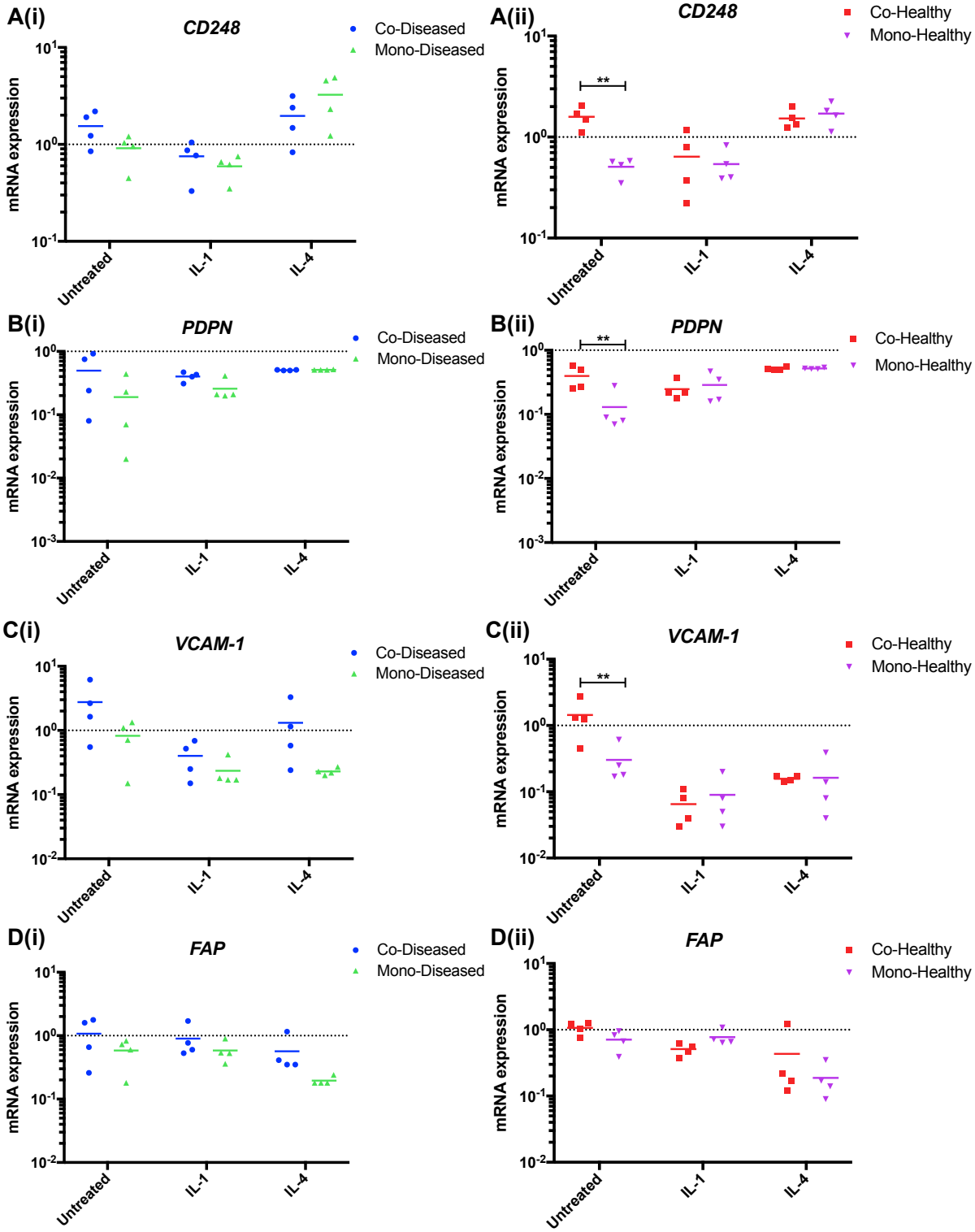

Figure 3-3 . Effect of HMEC-1 endothelial cell co-culture on the mRNA expression of fibroblast activation markers by tendon fibroblasts. mRNA was isolated from tendon fibroblasts derived from massive rotator cuff tears (diseased) or healthy hamstring (healthy) that had been co-cultured with HMEC-1 cells in either an unstimulated state or following treatment with cytokines (IL-1 or IL-4 each at 10ng/ml). Gene expression was assessed by qRT-PCR and values were expressed as relative expression units (REU) compared with housekeepers (GAPDH and TOP1) according to the $2^{-\Delta CT}$ method. Data are mean of three technical replicated for explant derived fibroblasts from 4 healthy and 4 diseased tendons. *p<0.05, **p<0.005 compared to tendon fibroblast mono-culture by 2-way ANOVA with Sidak's correction for multiple testing.

3.6.3 The effect of EC co-culture on the expression of inflammatory cytokines and ECM related genes by tendon fibroblasts

To further investigate the influence of EC co-culture on the activation status of tendon fibroblasts we interrogated biological processes that are associated with fibroblasts activation including cytokine production and extracellular matrix turnover. During unstimulated co-culture conditions, fibroblasts isolated from healthy hamstring tendon demonstrated an increased expression of *IL-1β*, *IL-2*, *IL-6*, *IL-8* and *TGF-β* (Figure 3-4). A similar response was observed for fibroblasts from diseased tendon and reached significance for *IL-6*, *IL-8* and *TGF-β*. Interestingly, co-cultures of diseased tendon fibroblasts induced high expression of *IL-10*, an effect not seen during healthy fibroblast co-culture.

Stimulation with IL-1β amplified the effect of co-culture on the expression of *CSF2* and *TGF-β* by diseased tendon cells (Figure 3-4 A(v) and A(ix)), but removed the effect of endothelial cell co-culture on the expression of *IL-6, IL-8, IL-10* by diseased tendon fibroblasts during unstimulated co-culture. A similar effect was observed for co-cultures containing healthy tendon fibroblasts.

When compared with unstimulated controls the expression of *IL-1β*, *IL-6* and *IL-8* by both diseased and healthy tendon fibroblasts was markedly reduced during co-culture conditions that contained exogenous IL-1β (Appendix B-2). When compared to unstimulated co-cultures, stimulation with IL-4 also resulted in a significant reduction of *IL-1β*, *IL-2*, *IL-6*, *IL-8* and *TGF-β* expression, for both healthy and diseased cells, during co-culture (Appendix B-2). The inhibitory effect of *IL-1β* or IL-4 stimulation during mono-cultures of fibroblasts, from both diseased and healthy tendons, was less pronounced than during co-cultures with ECs (Appendix B-2). This differential response of mono- and co-cultured fibroblasts to cytokine stimulation, served to abrogate any effect of co-culture.

During unstimulated conditions the co-culture of healthy tendon fibroblasts with endothelial cells resulted in an upregulation of *COL1A1, COL5A2* and *COL9A3* but with no significant effect on *COL3A2* or the collagen III:I ratio (Figure 3-5 A(ii)-D(ii) and Appendix B-3). Again,

similar but non-significant trends were observed for diseased tendon fibroblasts during co-culture (Figure 3-5 A(i)-D(i)).

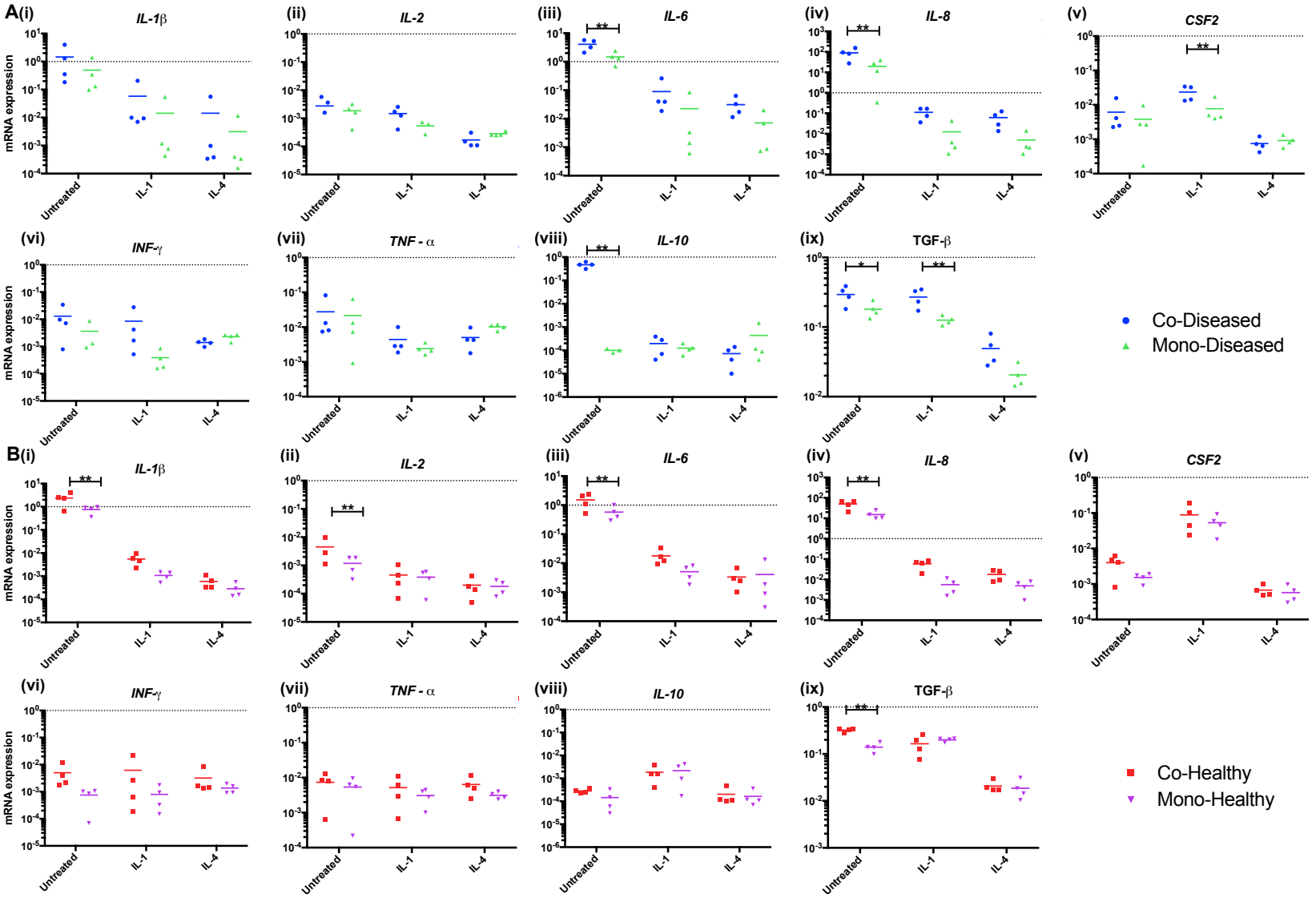

Figure 3-4. Effect of HMEC-1 endothelial cell co-culture on the mRNA expression of inflammatory cytokines by tendon fibroblasts. Fibroblast mRNA was isolated from massive rotator cuff tears (diseased) or healthy hamstring (healthy) that had been cultured with HMEC-1 cells in either an unstimulated state or following treatment with cytokines (IL-1 or IL-4 each at 10ng/ml). *p<0.05, **p<0.005 compared to fibroblast mono-culture by 2-way ANOVA with Sidak's correction for multiple testing.

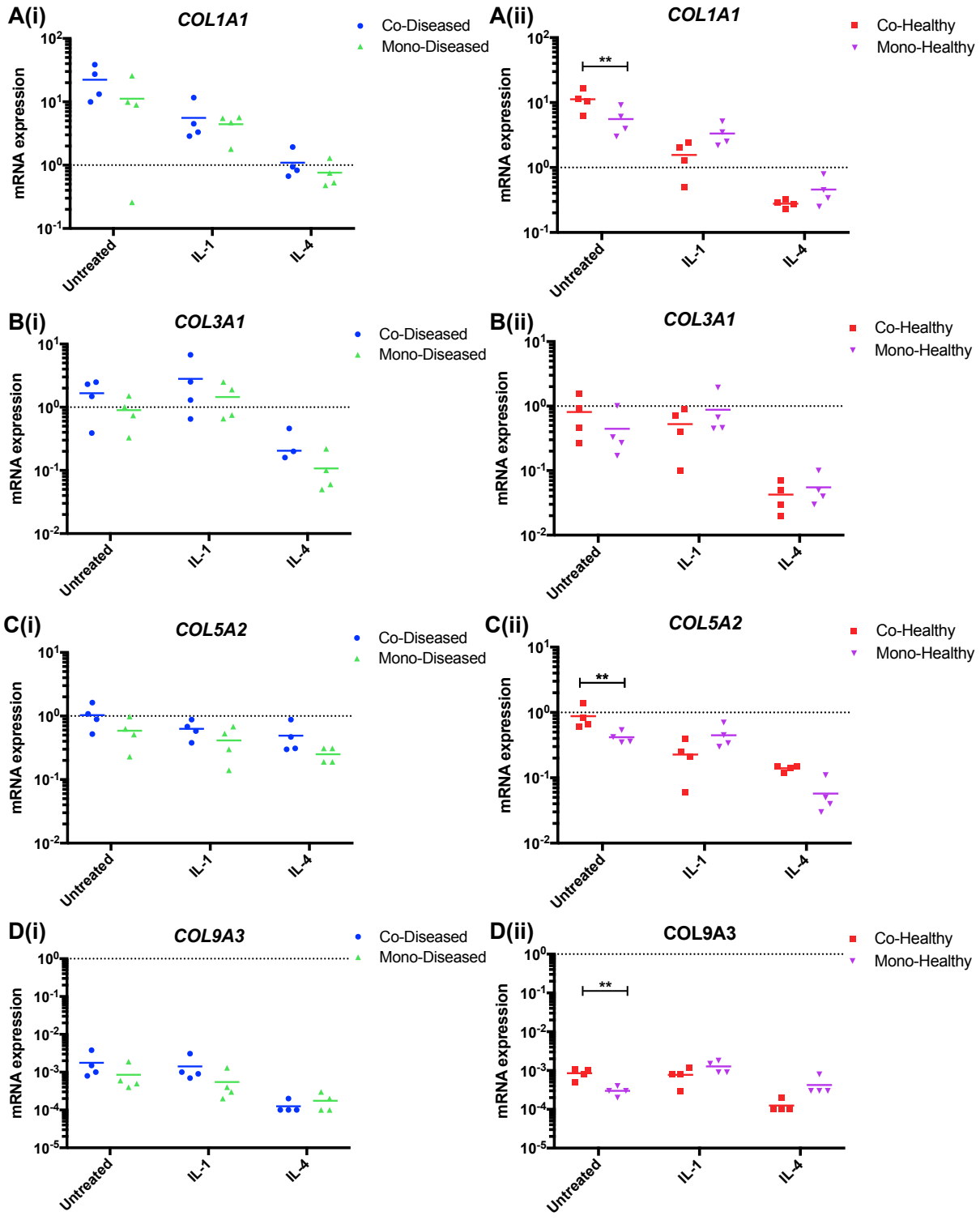

Figure 3-5. Effect of HMEC-1 endothelial cell co-culture on the mRNA expression of collagens I,III,VI and IX by tendon fibroblasts. mRNA was isolated from tendon fibroblasts derived from massive rotator cuff tears (diseased) or healthy hamstring (healthy) that had been co-cultured with HMEC-1 cells in either an unstimulated state or following treatment with cytokines (IL-1 or IL-4 each at 10ng/ml). Gene expression was assessed by qRT-PCR and values were expressed as relative expression units (REU) compared with housekeepers (GAPDH and TOP1) according to the $2^{-\Delta CT}$ method. Data are mean of three technical replicated for explant derived fibroblasts from 4 healthy and 4 diseased tendons. *p<0.05, **p<0.005 compared to tendon fibroblast mono-culture by 2-way ANOVA with Sidak's correction for multiple testing.

Co-culture had no effect on the ECM proteins *ACAN*, *TNMD* and *SAA1* (Figure 3-6) but significantly increased the expression of the ECM protease *ADAM12* by healthy tendon fibroblasts in unstimulated conditions and *MMP3* by diseased tendon fibroblasts following IL-1β stimulation (Figure 3-7). Overall, during both mono- and co-culture, the administration of IL-1β and IL-4 decreased collagen and matrix protein gene expression, but with a more profound reduction seen during co-culture (Appendix B-4 and B-5). Consequently, the differential effect of co-culture observed for collagen expression during unstimulated conditions was masked.

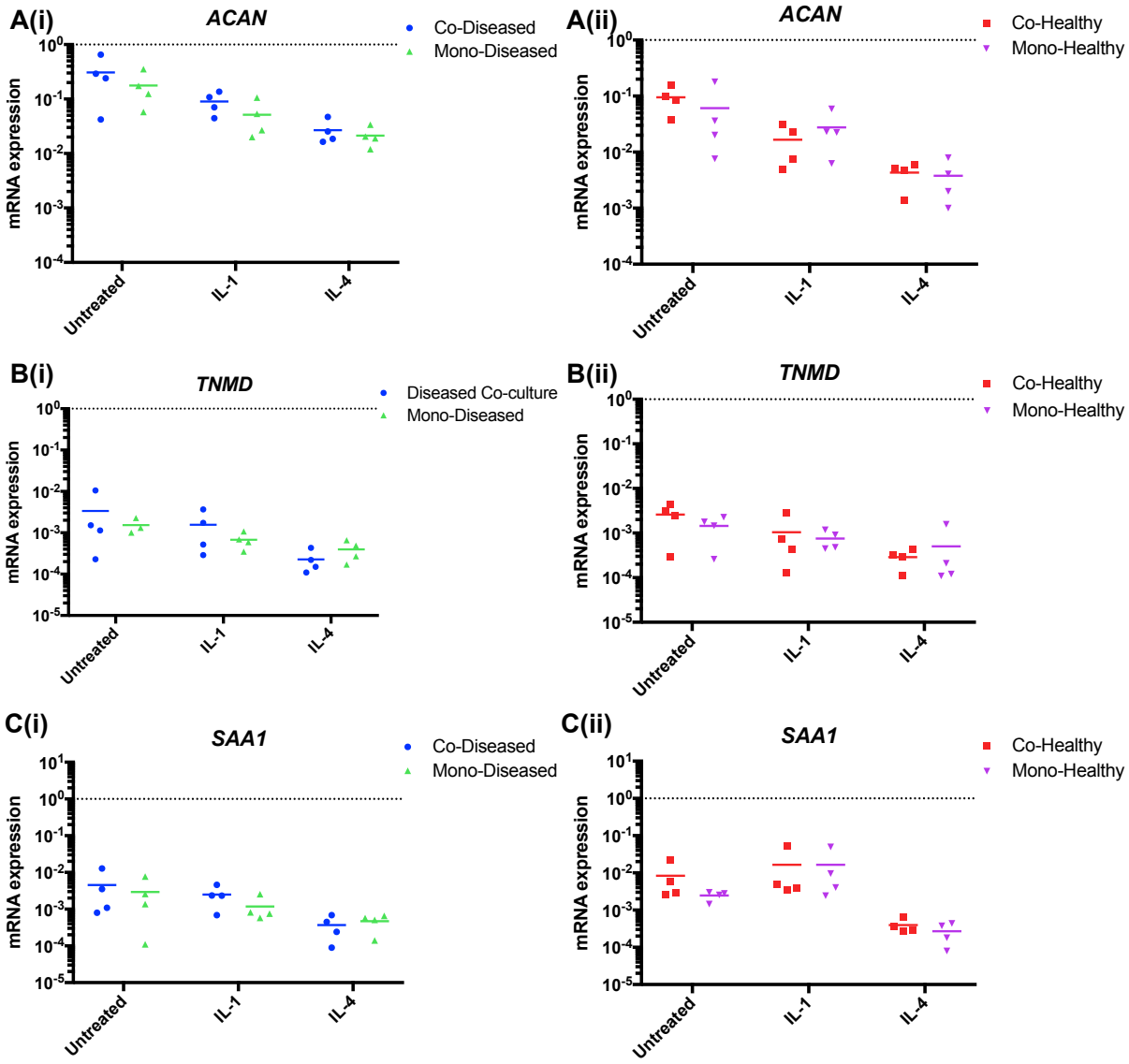

Figure 3-6. Effect of HMEC-1 endothelial cell co-culture on the mRNA expression of tendon matrix proteins by tendon fibroblasts. mRNA was isolated from tendon fibroblasts derived from massive rotator cuff tears (diseased) or healthy hamstring (healthy) that had been co-cultured with HMEC-1 cells in either an unstimulated state or following treatment with cytokines (IL-1 or IL-4 each at 10ng/ml). Gene expression was assessed by qRT-PCR and values were expressed as relative expression units (REU) compared with housekeepers (GAPDH and TOP1) according to the $2^{-\Delta CT}$ method. Data are mean of three technical replicated for explant derived fibroblasts from 4 healthy and 4 diseased tendons. *p<0.05, **p<0.005 compared to tendon fibroblast mono-culture by 2-way ANOVA with Sidak's correction for multiple testing.

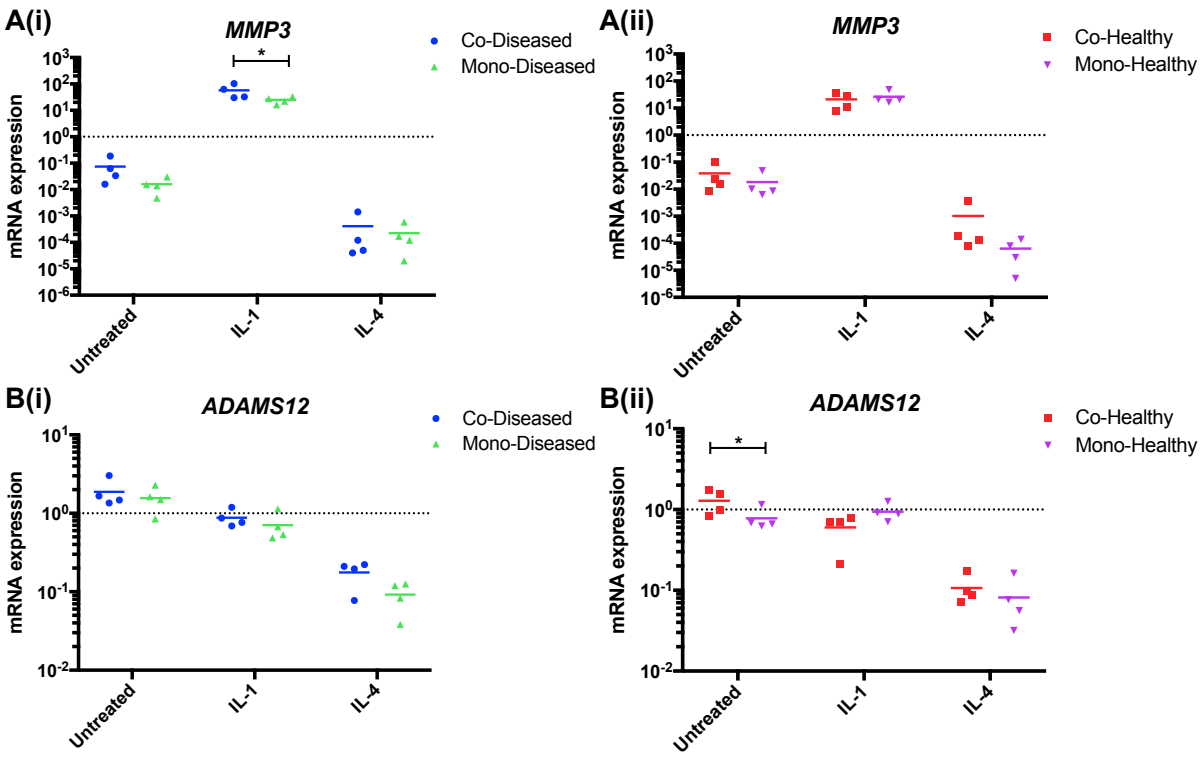

Figure 3-7 . Effect of HMEC-1 endothelial cell co-culture on the mRNA expression of ECM proteases by tendon fibroblasts. mRNA was isolated from tendon fibroblasts derived from massive rotator cuff tears (diseased) or healthy hamstring (healthy) that had been co-cultured with HMEC-1 cells in either an unstimulated state or following treatment with cytokines (IL-1 or IL-4 each at 10ng/ml). Gene expression was assessed by qRT-PCR and values were expressed as relative expression units (REU) compared with housekeepers (GAPDH and TOP1) according to the $2^{-\Delta CT}$ method. Data are mean of three technical replicated for explant derived fibroblasts from 4 healthy and 4 diseased tendons. *p<0.05, **p<0.005 compared to tendon fibroblast mono-culture by 2-way ANOVA with Sidak's correction for multiple testing.

3.6.4 The effect of EC co-culture on inflammation activation signatures and cell-cycle regulators

NF-κB, IFN and STAT6 inflammatory pathways are important regulators of fibroblast activation for tendon fibroblasts explanted from intermediate-advanced stage rotator cuff disease.[45] Following 9 days in co-culture with HMEC-1 endothelial cells tendon derived fibroblasts from both healthy and diseased tendons showed increased expression of the NF-κB inducible, and prostaglandin biosynthetic gene, *PTGS2* (Figure 3-8A). Tendon-derived fibroblasts from healthy tendons also showed increased expression of the IFN pathway gene *IRF1* during co-culture (Figure 3-8B(ii)), but neither healthy or diseased tendon-derived fibroblasts during unstimulated EC co-culture demonstrated differential expression of the STAT6 pathway gene *TGM2*.

Heat shock binding protein 1 (HSP1) promotes cell cycle progression of human fibroblasts.[260] During HMEC-1 co-culture healthy tendon-derived fibroblasts displayed a significant upregulation of the *HSP1* gene, which failed to reach significance for diseased tendon

fibroblasts (p=0.24). However, no differences in expression were observed for the metabolic and cell-cycle transcription factor *FOXF2* (Figure 3-9).

Similar, to the previously observed effect of IL-1β and IL-4 on expression of cytokine and ECM gene expression, prolonged cytokine stimulation with either IL-1β or IL-4 inhibited the expression of both NK-κB and IFN pathway genes (Appendix B-7) as well as *FOXF2* and *HSBP1* cell cycle regulators (Appendix B-8).

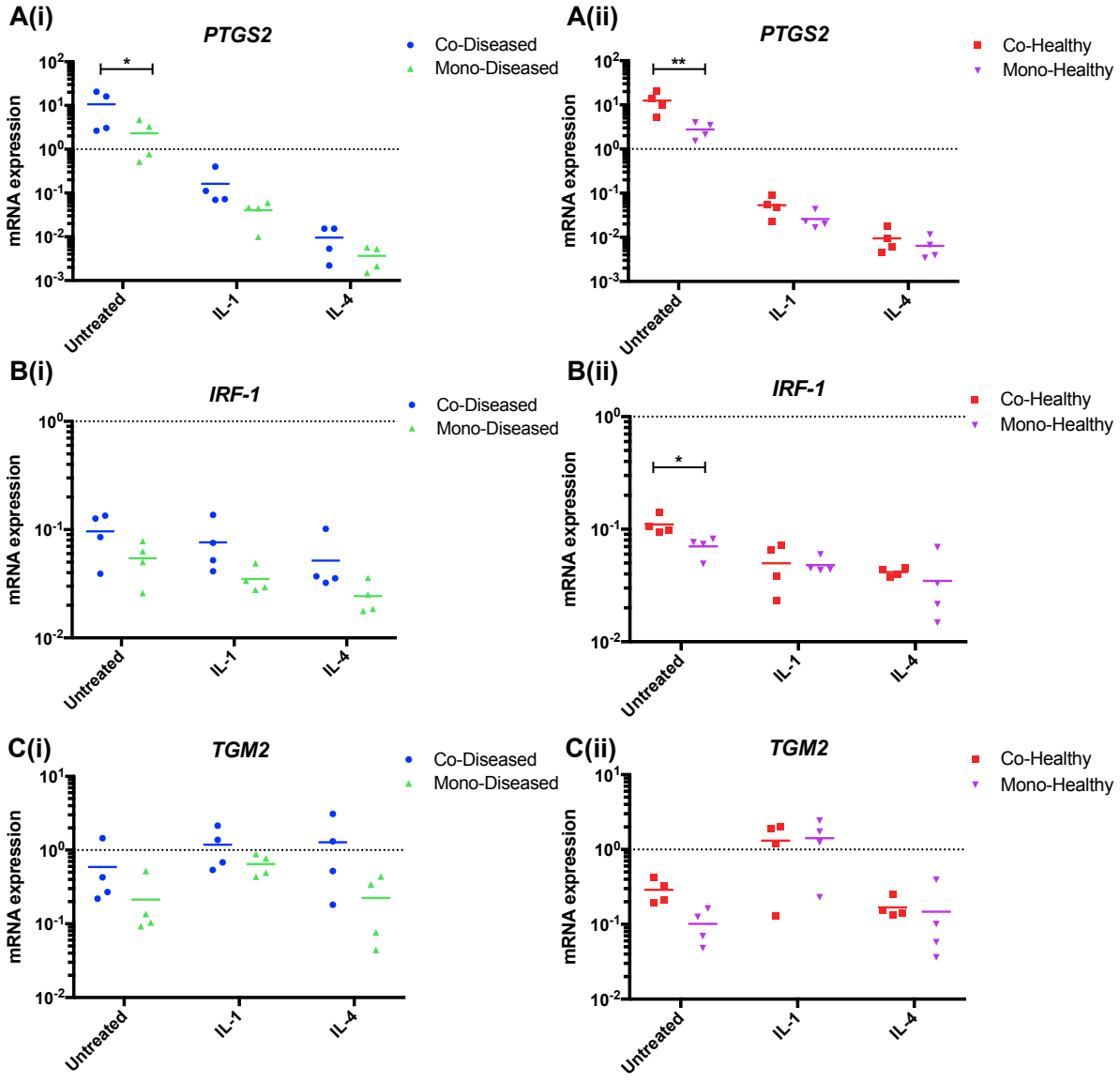

Figure 3-8 . Effect of HMEC-1 endothelial cell co-culture on the mRNA expression of NK-κB, IFN and STAT6 pathway genes by tendon fibroblasts. mRNA was isolated from tendon fibroblasts derived from massive rotator cuff tears (diseased) or healthy hamstring (healthy) that had been co-cultured with HMEC-1 cells in either an unstimulated state or following treatment with cytokines (IL-1 or IL-4 each at 10ng/ml). Gene expression was assessed by qRT-PCR and values were expressed as relative expression units (REU) compared with housekeepers (GAPDH and TOP1) according to the $2^{-\Delta CT}$ method. Data are mean of three technical replicated for explant derived fibroblasts from 4 healthy and 4 diseased tendons. *p<0.05, **p<0.005 compared to tendon fibroblast mono-culture by 2-way ANOVA with Sidak's correction for multiple testing.

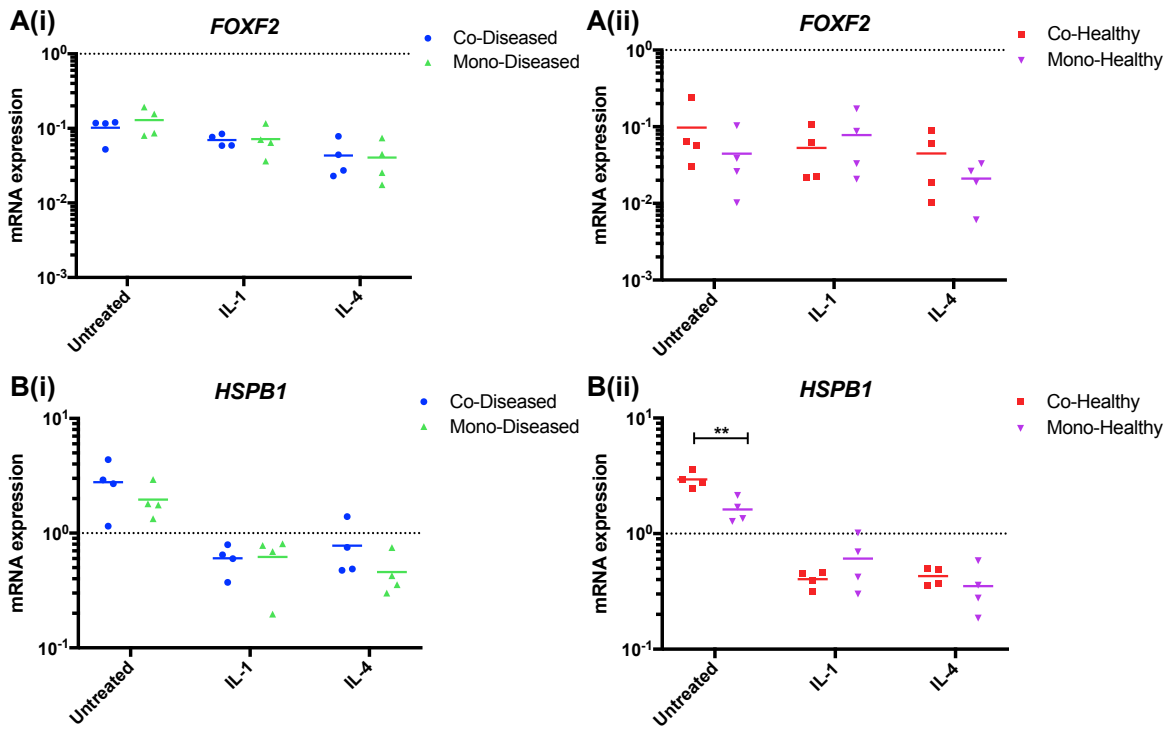

Figure 3-9. Effect of HMEC-1 endothelial cell co-culture on the mRNA expression of the cell-cycle regulators FOXF2 and HSPB1 by tendon fibroblasts. mRNA was isolated from tendon fibroblasts derived from massive rotator cuff tears (diseased) or healthy hamstring (healthy) that had been co-cultured with HMEC-1 cells in either an unstimulated state or following treatment with cytokines (IL-1 or IL-4 each at 10ng/ml). Gene expression was assessed by qRT-PCR and values were expressed as relative expression units (REU) compared with housekeepers (GAPDH and TOP1) according to the $2^{-\Delta CT}$ method. Data are mean of three technical replicated for explant derived fibroblasts from 4 healthy and 4 diseased tendons. *p<0.05, **p<0.005 compared to tendon fibroblast mono-culture by 2-way ANOVA with Sidak's correction for multiple testing.

3.6.5 Adhesion of leukocytes to endothelial-fibroblast co-culture under static conditions

Endothelial cells and fibroblasts were co-cultured on the surface of 24-well and 12-well transwell inserts respectively (Figure 3-1). Peripheral blood leukocytes were then added into the top (24-well) insert. $CD45^{+ve}$ leukocytes adhesion to HMEC-1 ECs was similar for both EC mono-cultures and co-cultures with unstimulated fibroblasts from diseased tendons. In contrast, during co-culture with healthy tendon-derived fibroblasts $CD45^{+ve}$ leukocytes adherence to the endothelial monolayer was significantly lower (Figure 3-10A).

The effect of co-culture on the adherence of specific $CD45^{+ve}$ leukocyte sub-populations was then explored. A marked reduction in the EC adherence of $CD4^{+ve}$ and $CD8^{+ve}$ T-cells was observed during co-culture with healthy tendon-derived fibroblasts. A reduction in adherence was also observed for $CD14^{+ve}$ monocytes but this was not significant (p=0.09).

The ability of tendon derived fibroblasts to modify the adhesion of leukocytes to ECs was then assessed following activation of fibroblasts with IL-1β or IL-4 cytokine treatment. During mono-

culture of ECs the presence of cytokines had no effect on the adhesion of any leukocyte subset (Figure B-9). However, following the addition of IL-4, healthy tendon fibroblasts no-longer suppressed leucocyte recruitment but rather supported the attachment, of all subsets, at a similar level as that observed for diseased fibroblast co-cultures (Figure 3-10 A-F).

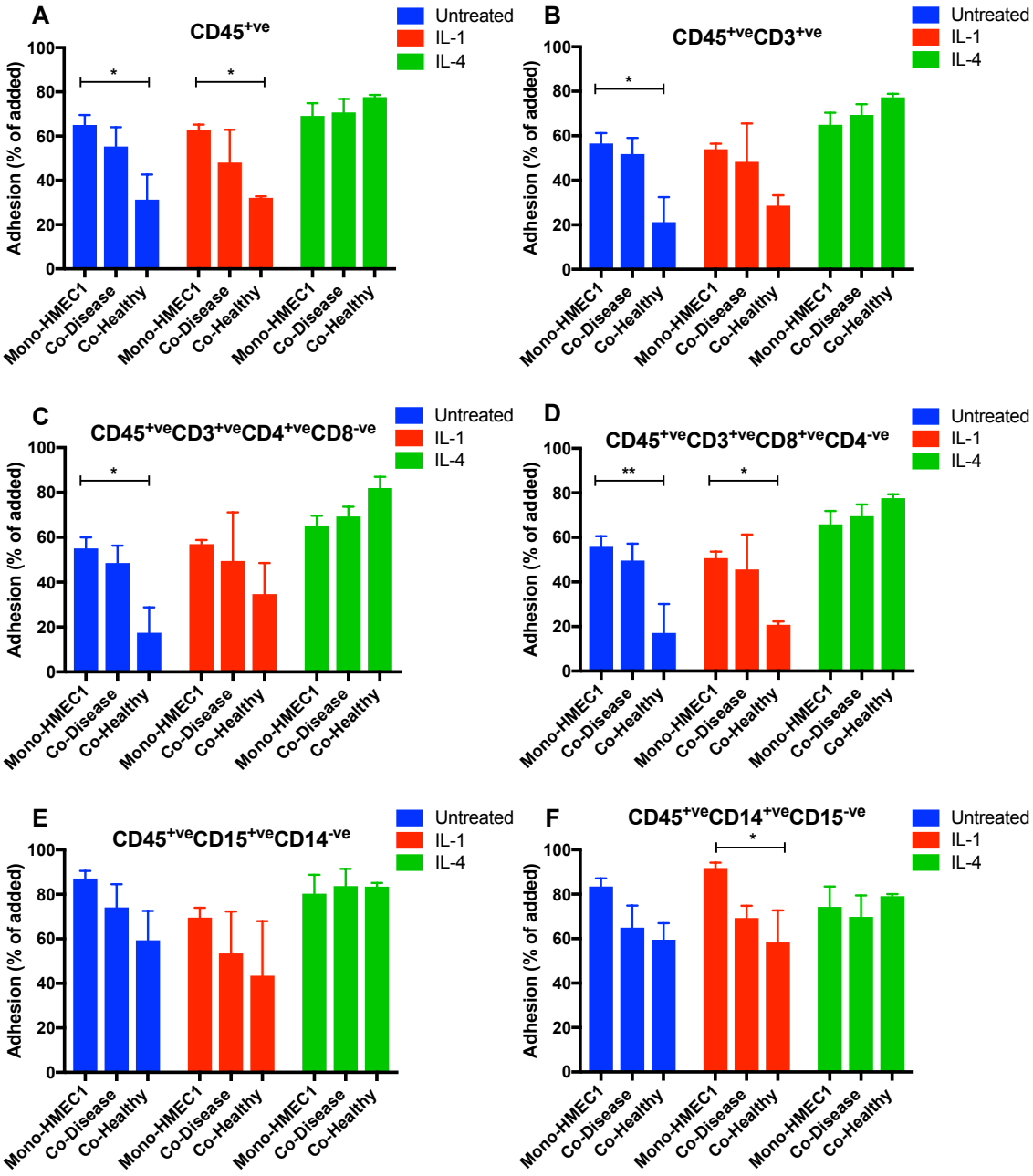

Figure 3-10 . Adhesion of peripheral blood leukocytes to HMEC-1 endothelial cells Co-cultures were established by inserting a confluent monolayer of HMEC-1 cells cultured on a 24-well filter, into a fibroblast coated 12-well filter and allowed to equilibrate for 24-hours in the presence or absence of IL-1 (10ng/ml) or IL-4 (10ng/ml). Fibroblasts were derived from hamstrings (Healthy) or massive rotator cuff tears (Diseased). Leukocytes were allowed to settle for 30-minutes after which non-adherent cells were washed off and analysed using flow cytometry for (A) $CD45^{+ve}$ Peripheral blood leukocytes, (B) $CD3^{+ve}$ T-cells, (C) $CD4^{+ve}$ T-cells, (D) $CD8^{+ve}$ T-cells, (E) $CD15^{+ve}$ Neutrophils and (F) $CD14^{+ve}$ Monocytes. Total adherent cells were calculated by subtracting each fraction of non-adherent from the total added. For each population data were expressed as a percentage of the cells added. Data are mean +/- SEM for explant derived fibroblasts from 3 healthy and 3 diseased tendons. *p<0.05, **p<0.005 compared to HMEC-1 mono-culture by 2-way ANOVA with Dunnett's correction for multiple testing.

3.6.6 Expression of EC adhesion receptors during tendon-derived fibroblast co-culture

To test whether the observed inhibition of leukocyte adhesion to ECs during co-culture with healthy tenocytes was due to changes in EC expression of adhesion receptors, we assessed the mRNA levels of receptors involved in both the capture and firm adhesion phases of leucocyte migration. Co-culture with both healthy and diseased tendon fibroblasts, tended to increase the expression of the capture receptors *SELP*, *300LG*, *PODXL* and *EMCN* on endothelial cells, an effect that was accentuated during IL-4 stimulation (Figure 3-11). A similar response was also observed for the receptors *ICAM1* and *MCAM* involved in firm adhesion (Figure 3-12). There was no difference in the expression of receptors involved in leucocyte capture or firm adhesion, between co-cultures of healthy and diseased tendon-derived fibroblast with ECs. Similarly, no differences in the expression of leukocyte adhesion inhibitors were detected (Appendix B-10) Hence, the functional loss of leukocyte adhesion observed during healthy fibroblast co-culture could not be explained by changes in HMEC-1 adhesion receptor expression.

3.6.7 Trans-endothelial and trans-fibroblast migration of leukocytes during co-culture

The migration of the adherent $CD45^{+ve}$ leukocytes through the EC monolayer was augmented during co-culture with healthy, but not diseased, tendon-derived fibroblasts (Figure 3-13). To assess if distinct $CD45^{+ve}$ leukocytes subsets behaved differently we assessed the total number of T-cells, neutrophils and monocytes that had been collected in the fractions beneath the endothelial monolayer. During unstimulated conditions healthy tendon fibroblasts promoted trans-endothelial migration for both $CD4^{+ve}$ and $CD8^{+ve}$ T-cell subsets, as well as $CD14^{+ve}$ monocytes, but with no effect on $CD15^{+ve}$ neutrophils.

In contrast, for the cytokine stimulated co-cultures no significant difference in migration was observed for T-cells or monocytes. However, a marked increase in trans-endothelial migration was observed for $CD15^{+ve}$ neutrophils during IL-1 stimulated co-culture with either diseased or healthy tendon derived fibroblasts.

To provide an assessment of leukocyte retention, onward migration through the fibroblast layer was then analysed. When tendon-derived fibroblasts were cultured alone, very little trans-fibroblast migration of leukocytes was observed, an effect that was not influenced by the leukocyte subpopulation or by addition of cytokines (Figure 3-14). Both stimulated and unstimulated co-culture with ECs caused a significant increase in trans-fibroblast migration but with no clear differences between healthy or diseased tendon-derived fibroblast co-cultures.

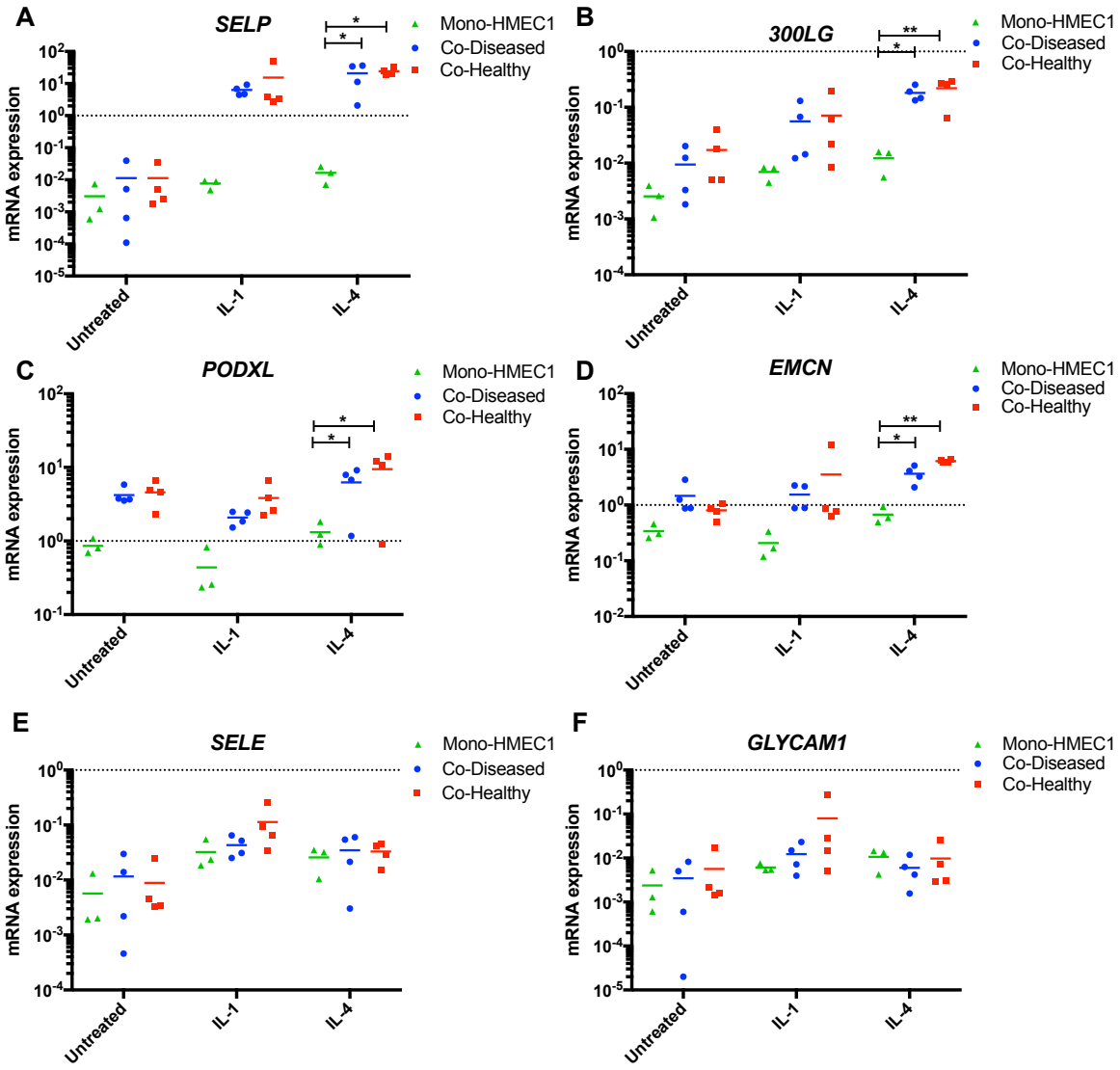

Figure 3-11. Effect of tendon fibroblast co-culture on the mRNA expression of adhesion receptors involved in leukocyte capture by HMEC-1 endothelial cells. Endothelial mRNA was isolated from HMEC-1 endothelial cells cultured indirectly with tendon fibroblasts derived from massive rotator cuff tears (diseased) or healthy hamstring (healthy) in either an unstimulated state or following treatment with cytokines (IL-1 or IL-4 each at 10ng/µl). Gene expression was assessed by qRT-PCR and values were expressed as relative expression units (REU) compared with housekeepers (TOP1, TBP and SDHA) according to the $2^{-\Delta CT}$ method. Data are mean of three technical replicated for explant derived fibroblasts from 4 healthy and 4 diseased tendons. *p<0.05, **p<0.005 compared to HMEC-1 mono-culture by 2-way ANOVA with Sidak's correction for multiple testing.

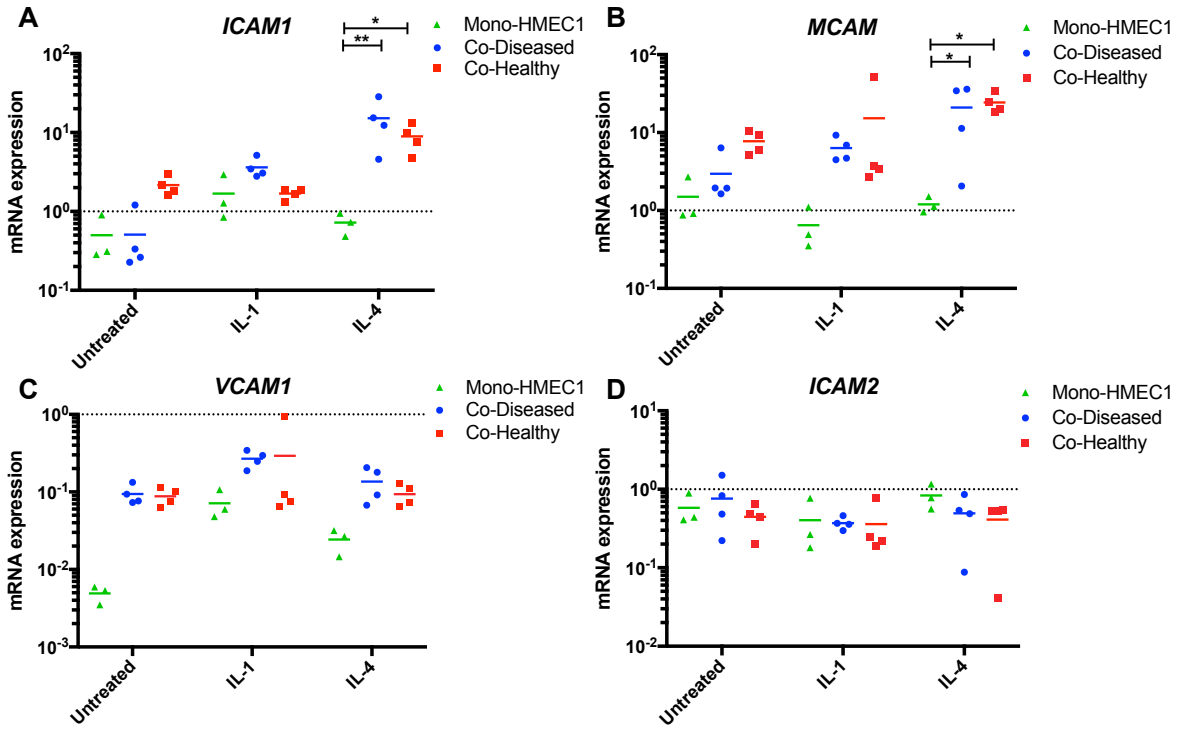

Figure 3-12. Effect of tendon fibroblast co-culture on the mRNA expression of adhesion receptors involved in leukocyte capture by HMEC-1 endothelial cells. Endothelial mRNA was isolated from HMEC-1 endothelial cells cultured indirectly with tendon fibroblasts derived from massive rotator cuff tears (diseased) or healthy hamstring (healthy) in either an unstimulated state or following treatment with cytokines (IL-1 or IL-4 each at 10ng/ml). Gene expression was assessed by qRT-PCR and values were expressed as relative expression units (REU) compared with housekeepers (TOP1, TBP and SDHA) according to the $2^{-\Delta CT}$ method. Data are mean of three technical replicated for explant derived fibroblasts from 4 healthy and 4 diseased tendons. *p<0.05, **p<0.005 compared to HMEC-1 mono-culture by 2-way ANOVA with Sidak's correction for multiple testing.

3.6.8 HMEC-1 expression of endothelial junctional molecules during tendon-derived fibroblast co-culture

To determine if differences in leukocyte migration could be explained by changes in the gene expression of endothelial junctional molecules, the EC expression of receptors regulating endothelial-leukocyte interactions during leukocyte transmigration was assessed. While no significant differences between mono- and co-culture were observed during unstimulated co-cultures, differences tended to be amplified following IL-1β or IL-4 stimulation, with increased EC expression of *JAM2*, *JAM3*, *ESAM*, *CD99* and *CD47* during co-culture with both healthy and diseased tendon-derived fibroblasts (Figure 3-15).

Since reduced inter-endothelial contact is also a critical requirement for leukocyte extravasation, the mRNA expression of the VE-cadherin/VE-PTP complex[261] was assessed (Figure 3-16). During unstimulated conditions co-culture with diseased tendon fibroblasts significantly increased the expression of *PTPRB* (VE-PTP), but with no significant differences (p=0.1) between co-cultures with healthy or diseased tendon-derived fibroblasts. No significant

differences were observed for *CDH5* (VE-cadherin) expression during co-culture. Overall, the above findings suggest that co-culture induced a generalised activation of HMEC-1 endothelial cells, but that the previously observed functional differences in trans-endothelial migration during co-culture with healthy and diseased tenocytes, cannot be explained by changes in endothelial junctional adhesion molecule expression.

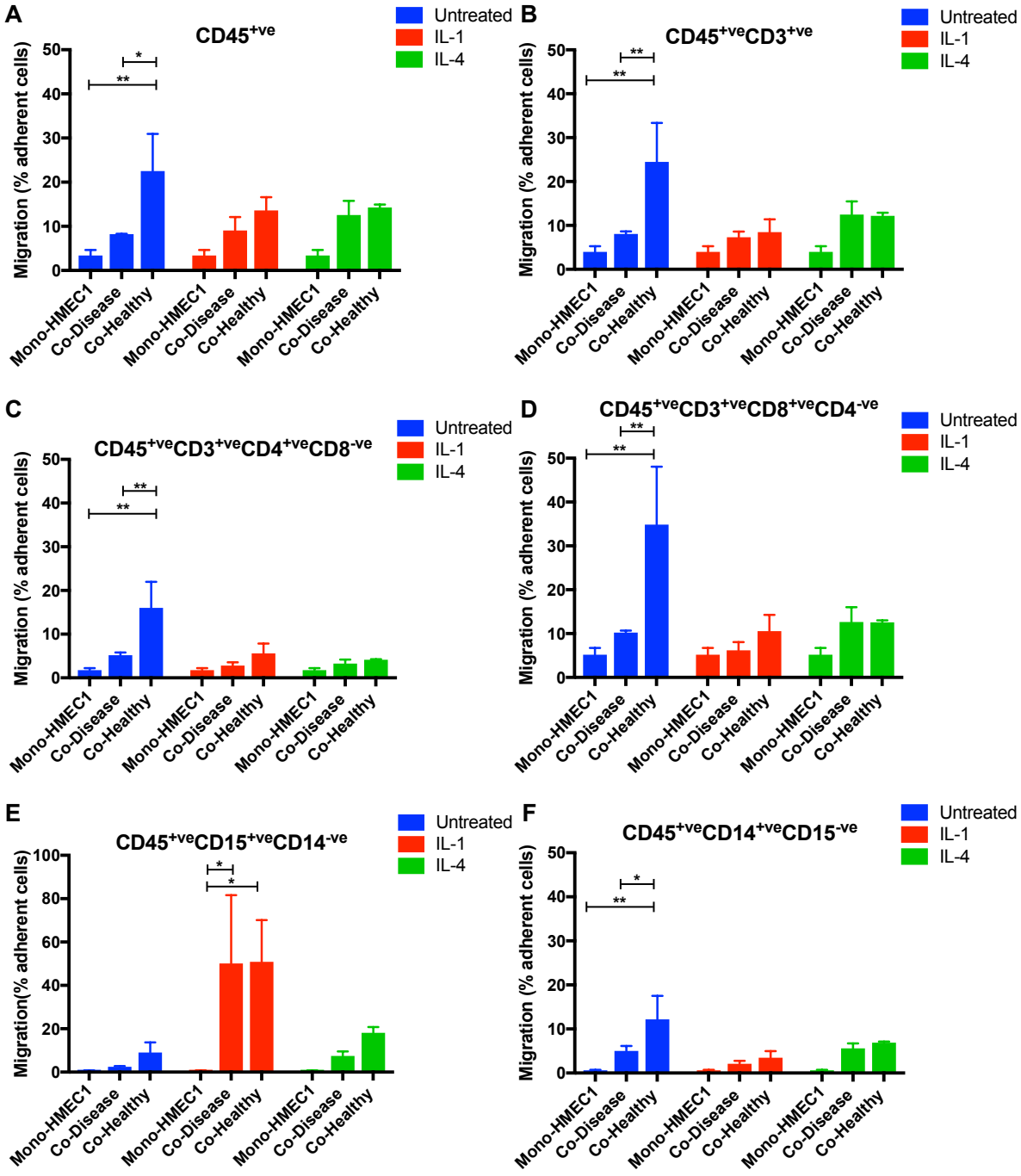

Figure 3-13 . Trans-endothelial migration of peripheral blood leukocytes through a HMEC-1 endothelial cells. Co-cultures were established by inserting a confluent monolayer of HMEC-1 cells cultured on a 24-well filter, into a fibroblast coated 12-well filter and allowed to equilibrate for 24-hours in the presence or absence of IL-1 (10ng/ml) or IL-4 (10ng/ml). Fibroblasts were derived from hamstrings (Healthy) or massive rotator cuff tears (Diseased). Leukocytes were allowed to migrate for 24-hours after which cells beneath the endothelial layer were collected and analysed using flow cytometry for (A) $CD45^{+ve}$ Peripheral blood leukocytes, (B) $CD3^{+ve}$ T-cells, (C) $CD4^{+ve}$ T-cells, (D) $CD8^{+ve}$ T-cells, (E) $CD15^{+ve}$ Neutrophils and (F) $CD14^{+ve}$ Monocytes. For each population, the total number of leukocytes that had undergone trans-endothelial migration were calculated by adding the number of cells beneath the endothelial and fibroblast layers. For each population data were expressed as a percentage of adherent cells. Data are mean +/- SEM for explant derived fibroblasts from 3 healthy and 3 diseased tendons. *p<0.05, **p<0.005 compared to HMEC-1 mono-culture by 2-way ANOVA with Dunnett's correction for multiple testing.

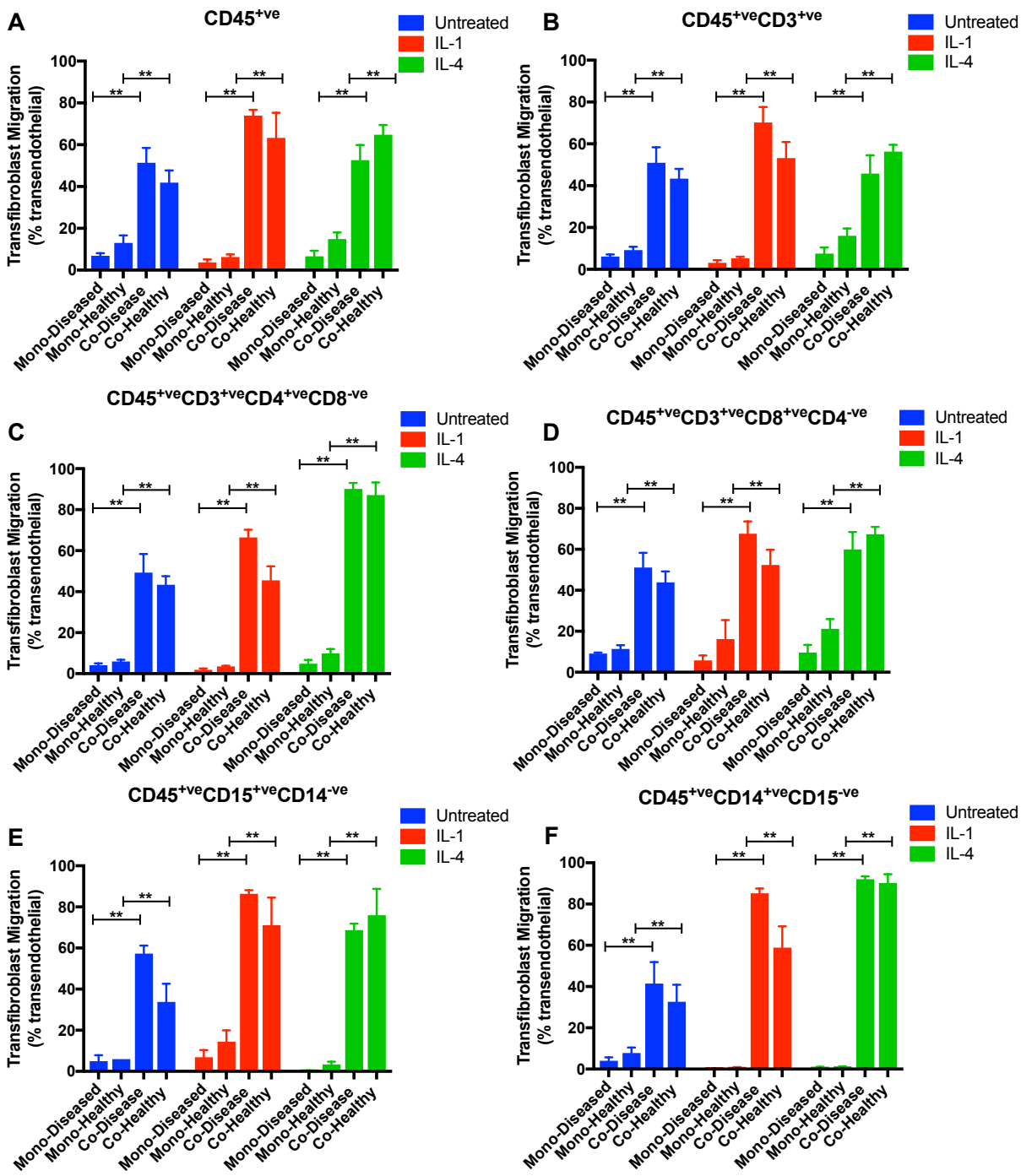

Figure 3-14 . Trans-fibroblast migration of peripheral blood leukocytes through tendon derived fibroblasts. Co-cultures were established by inserting a confluent monolayer of HMEC-1 cells cultured on a 24-well filter, into a fibroblast coated 12-well filter and allowed to equilibrate for 24-hours in the presence or absence of IL-1 (10ng/ml) or IL-4 (10ng/ml). Fibroblasts were derived from hamstrings (Healthy) or massive rotator cuff tears (Diseased). Leukocytes were allowed to migrate for 24-hours after which cells beneath the fibroblast layer were collected and analysed using flow cytometry for (A) $CD45^{+ve}$ Peripheral blood leukocytes, (B) $CD3^{+ve}$ T-cells, (C) $CD4^{+ve}$ T-cells, (D) $CD8^{+ve}$ T-cells, (E) $CD15^{+ve}$ Neutrophils and (F) $CD14^{+ve}$ Monocytes. For each population data were expressed as a percentage of leukocytes that had undergone trans endothelial migration. In the case of migration through fibroblast mono-cultured , data were expressed as the number of cells that were adherent to fibroblasts in the mono-cultures. Data are mean +/- SEM for explant derived fibroblasts from 3 healthy and 3 diseased tendons. *p<0.05, **p<0.005 compared to HMEC-1 mono-culture by 2-way ANOVA with Tukey's correction for multiple testing.

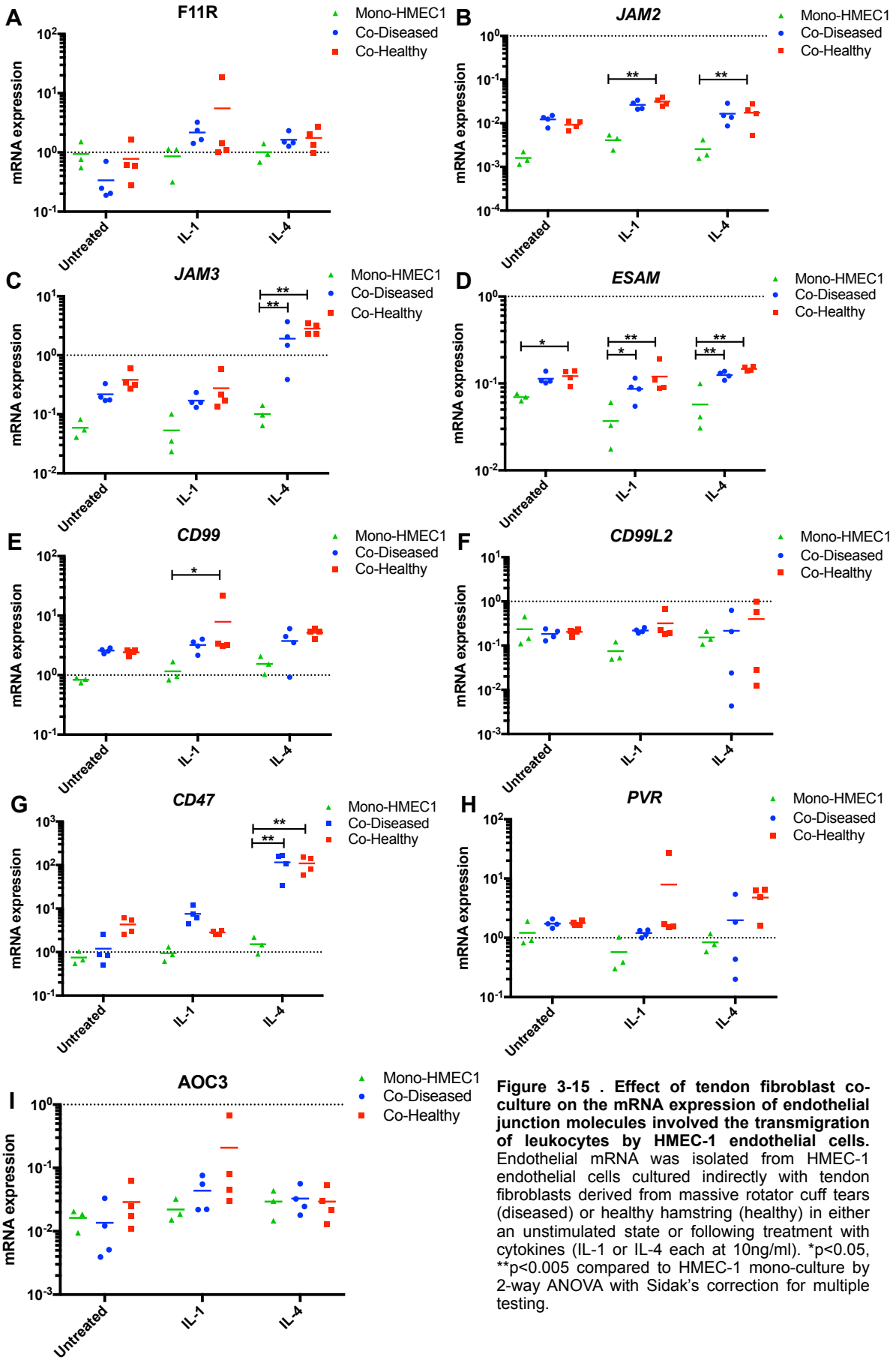

Figure 3-15 . Effect of tendon fibroblast co-culture on the mRNA expression of endothelial junction molecules involved the transmigration of leukocytes by HMEC-1 endothelial cells. Endothelial mRNA was isolated from HMEC-1 endothelial cells cultured indirectly with tendon fibroblasts derived from massive rotator cuff tears (diseased) or healthy hamstring (healthy) in either an unstimulated state or following treatment with cytokines (IL-1 or IL-4 each at 10ng/ml). *p<0.05, **p<0.005 compared to HMEC-1 mono-culture by 2-way ANOVA with Sidak's correction for multiple testing.

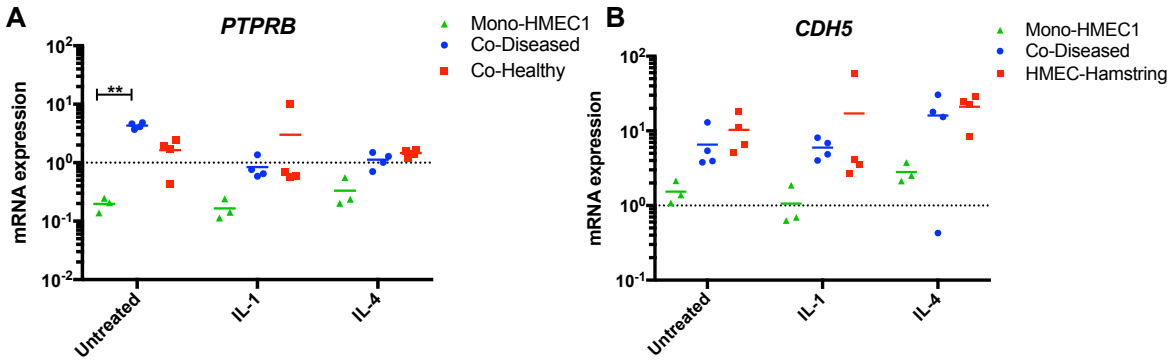

Figure 3-16. Effect of tendon fibroblast co-culture on the mRNA expression of the VE-Cadherin/VE-PTP complex by HMEC-1 endothelial cells. Endothelial mRNA was isolated from HMEC-1 endothelial cells cultured indirectly with tendon fibroblasts derived from massive rotator cuff tears (diseased) or healthy hamstring (healthy) in either an unstimulated state or following treatment with cytokines (IL-1 or IL-4 each at 10ng/ml). *p<0.05, **p<0.005 compared to HMEC-1 mono-culture by 2-way ANOVA with Sidak's correction for multiple testing.

3.7 Discussion

Following injury the microvascular circulation is critical to the restoration of tissue homeostasis – acting as a gatekeeper to inflammatory cell infiltration, and supplying a milieu of instructive angiocrine factors that regulate tissue repair by tissue resident stem cells.[75] In musculoskeletal tissues endothelial-fibroblast crosstalk can drive the proliferation of human striated-muscle stem cells[80], while type H vessels, that are positive for both CD31 and endomucin, are fundamental to murine bone homeostasis.[76] Conversely, the persistent EC recruitment of leukocytes observed in rheumatoid arthritis is, in part, due to immunostimulatory crosstalk derived from diseased synovial fibroblasts, that display an 'activated' pro-inflammatory phenotype.[73] A similar accumulation of inflammatory cells is seen in painful human tendinopathy however the mechanisms underlying the accumulation is unknown.[42] This thesis examines the effect of fibroblast-endothelial cell crosstalk, in the context of human tendon disease. Co-culture with endothelial cells induced an activated phenotype in fibroblasts derived from healthy tendon, and to a lesser extent, accentuated the activation of diseased tendon fibroblasts. A reciprocal effect on endothelial cells was also observed, where co-cultures of ECs with healthy but not diseased tendon fibroblasts inhibited the adhesion of leukocytes to an endothelial monolayer.

Traditionally, fibroblasts have simply been viewed as 'caretakers' of the extracellular matrix. Whilst this is undoubtedly true, activated fibroblasts play a critical role in the initiation and modulation of the inflammatory response to injury. Persistent fibroblast activation has also

been implicated in the pathogenesis of numerous inflammatory conditions including rheumatoid arthritis[54], tendinopathy[46], adhesive capsulitis[262] and several malignancies.[263] While the precise cellular mechanisms that determine initiation, maintenance or reversal of fibroblast activation remain obscure, cellular crosstalk appears to play a role. The calcium binding protein S100A4, produced by lung macrophages, activates human lung fibroblasts *in vitro* and triggers lung fibrosis following adoptive transfer of S100A4+ macrophages into S100A4$^{-/-}$ mice.[264] This cross-talk is likely to be tissue and disease type specific. In the context of tendon disease, the co-culture of macrophages with tendon derived fibroblasts did not alter the phenotype of tendon fibroblasts.[45] However, the ability of other prominent cellular populations to influence fibroblast activation has not previously been explored. Several cytokines, such as IL-1β, IL-4 IL-6, IL-13 and PDGF are accepted inducers of fibroblast activation[265–267] and are increased in patients with rotator cuff disease.[66] Microvascular endothelial cells are an overlooked source of such cytokines, demonstrating secretion of both IL-6 and IL-8 in their resting state, and to an even greater extent once activated.[268] Indeed, vessel formation is a cardinal feature of tendon disease[58] and single nucleotide polymorphisms in VEGF and VEGFR2 have been implicated in the development of tendinopathy.[269–271] This chapter provides new insights into the role of the endothelium in fibroblast activation. During indirect co-culture with HMEC-1 endothelial cells, tendon derived fibroblasts, from healthy and diseased donors, increased their expression of several pro-inflammatory cytokines, including IL-1β, IL-6 and IL-8 that are regulated by the NF-κB pathway. Since activation of NF-κB pathways is a critical feature of fibroblast activation[268], it is perhaps unsurprising that a corresponding upregulation of the activation markers *PDPN*, *CD248* and *VCAM1* was also observed. This finding is supported by recent work demonstrating that the addition of conditioned media from activated endothelial cells increased the production of IL-6, IL-8 and CCL2 by dermal fibroblasts.[272] Future work, including cytokine immunoassays and selective antibody blockade of candidate molecules, will help to delineate the identity of the paracrine factors responsible for activation of tendon fibroblasts by the microvasculature.

Whilst the effect of ECs on diseased tendon fibroblasts was less pronounced, similar responses were observed to those seen following co-culture with fibroblasts from healthy

tendon. A larger variance in mRNA expression between fibroblasts isolated from diseased donors and a smaller effect size, itself a consequence of higher baseline expression for several inflammatory cytokines, will have resulted in a larger beta-error and an underpowering of the results. To this end, exogenous cytokines are often added to increase the effect size, previous work demonstrating an accentuation of NF-κB, IFN and STAT6 pathway genes following cytokine stimulation.[45,252] In contrast, this current work demonstrates a significant downregulation of activation markers and inflammatory cytokines following the stimulation of both healthy and diseased tendon fibroblasts with IL-1β or IL-4. This discrepancy may be explained by the extended duration of cytokine stimulation, with the expression of cytokine mRNA by fibroblasts known to be time-dependent. In duodenal fibroblasts, with the exception of GM-CSF (CSF2), cytokine expression during *in vitro* culture with exogenous IL-1β peaked follow 6 and 24 hours exposure.[273] It is likely that 9 days of cytokine stimulation produced a similar response, with only the expression of *CSF2* observed to increase after such prolonged IL-1β stimulation. Whilst the mechanisms underpinning this loss of function are unclear, the observed phenotype closely echoes the exhaustion state observed in T and NK cells following continuous antigenic stimulation.[274,275] Exhausted immune cells are characterised by a significant decrease in cytokine production, such as IL-2, IFN-ɣ and TNF-α and eventual cell cycle arrest.[276] Given the known immunoregulatory function of fibroblasts, it is tempting to speculate that a similar phenotypic state exists for stromal cells.

Dysregulated ECM production is a hallmark feature of activated fibroblasts.[277] Endothelial cell co-culture with healthy tendon fibroblasts appeared to recapitulate this phenotype, upregulating fibroblast expression of collagen as well as matrix proteases. This finding is supported by previous work that found the endothelial cell derived molecule, endothelin-1, induced an activated myofibroblast phenotype in healthy dermal and lung fibroblasts.[278,279] Since EC monolayers lack any contact with mural cells (i.e. pericytes, fibroblasts or smooth muscle cells), they best mimic a situation of immature microvessels.[280] It is perhaps unsurprising that immature vessels are able to activate fibroblasts, thereby facilitating EC invasion through the production of cytokines, matrix proteins and the proteolytic processing of the extracellular matrix to reveal cryptic binding sites.[278,279] Such a paracrine loop would act to amplify the initial physiological stimulus for angiogenesis. Whether dysregulation of this EC-

fibroblast cross-talk is, in part, responsible for the switch from acute to chronic inflammation remains an area for future research.

An increased number of macrophages, mast cells and lymphocytes is observed in painful human tendon disease, and closely follows observed changes in vessel numbers.[42,281] However little is known about the role of diseased tendon fibroblasts in the persistence of this chronic inflammatory infiltrate. Upon co-culture with microvascular ECs, fibroblasts derived from healthy tendon suppressed leucocyte adhesion. This immunoprotective effect was lost in fibroblasts isolated from advanced rotator cuff disease. Similar results have been seen in the context of non-inflammatory synovial fibroblasts co-cultured with endothelial cells under conditions of dynamic flow.[259,282] Interestingly, this immunoprotective effect was not due to the differential expression of EC adhesion receptors. Endothelial cells in co-culture demonstrated an activated state[283] with a generalised upregulation of adhesion receptors. However, despite diseased tenocytes demonstrating an effect on PBL attachment, no differences in the expression of EC adhesion receptors were observed between healthy and diseased co-culture. This is consistent with previous reports, in which there was no correlation between the functional differences observed during co-culture and EC expression of adhesion molecules.[284,285] Instead, previous micro-array analysis has revealed a distinct signature for ECs that depended on their co-culture with inflammatory or non-inflammatory synovial fibroblasts.[71] Future work, utilising bulk RNA sequencing will assess if clustering of EC transcriptomic profiles is dependent on the disease status of tendon fibroblasts during co-culture.

The use of an indirect co-culture system implies that paracrine factors are responsible for the observed immunoprotective effect of healthy tendon fibroblasts. Paracrine driven alterations in endothelial cell STAT activation, through differential expression of suppressor of cytokine signalling 3 (SOSC3), have previously been implicated in the immunoprotective effects of non-inflammatory synovial fibroblasts during co-culture, albeit the responsible cytokines are yet to be determined.[73] Interestingly, during co-culture of ECs with healthy tendon fibroblasts, the addition of exogenous IL-4, a known activator of STAT6[286], removed their immunoprotective effect. This raises the possibility that a common mechanism, mediated through STAT

activation, underpins the ability of both diseased tendon fibroblasts and rheumatoid synovial fibroblasts to recruit leukocytes. While it is tempting to suggest that the observed response to IL-4 was due to the upregulation of endothelial adhesion molecules, a similar trend was also seen following the addition of IL-1β but without any functional effect. Thus, the mechanism by which co-culture and endothelial STAT activity modulates leukocyte attachment to the endothelium remains to elucidated. Investigating the effects of co-culture on the expression of leukocyte integrins, or the expression of chemokines, such as the CXCL10/CXCR3 axis that are fundamental to the stable attachment of lymphocytes,[287] remain exciting areas for future research.

The increase in immune cell populations observed in tendon disease might also be explained by the ability of diseased fibroblasts to stimulate leukocyte diapedesis or their retention in tissues.[251] This hypothesis was tested through the dual assessment of trans-endothelial and trans-fibroblast migration. Unexpectedly, we observed that a greater proportion of adherent T-cells and monocytes migrated through the endothelial monolayer when cultured with healthy, but not diseased, tendon-derived fibroblasts. Tenocyte-endothelial cell crosstalk had relatively little effect on the migration of neutrophils. These findings are consistent with previous reports of an increased trans-endothelial migration of lymphocytes, but not neutrophils, during co-culture with dermal derived fibroblasts.[282] However, this group found no differences in lymphocyte migration when co-culture was undertaken with inflammatory synovial fibroblasts. The mechanisms underpinning differential diapedesis remain unclear, with no correlation between the expression of endothelial junctional adhesion molecules and the observed functional changes. Furthermore, previous work examining antibody blockage of suspected cytokines also failed to reverse the effect of co-culture on lymphocyte migration.[285]

When considering the equilibrium that determines the size of inflammatory infiltrates, immune cell retention within tissues must also be considered. However, no differences in trans-fibroblast migration, a measure of leukocyte retention, was observed between healthy and diseased tenocyte co-cultures. Taken together, these latter findings for trans-endothelial and trans-fibroblast migration, seem at odds with notion that aberrant tenocyte signalling is responsible for the persistent immune infiltrates observed in tendinopathy. Alternatively, the

current *in vitro* model may not be fully recapitulating the physiological environment of tendon. In particular, the effect of the ECM on leukocyte migration has not been investigated – given that matrix is a major constituent of tendon this is an important future consideration. The duration of culture must also be considered, the observed effects may be reversed or lost during prolonged cultures. Thirdly, since immune cells also exit tissues via lymphatics, future models of leukocyte retention must also take account the lymphatic endothelium. Lastly, the role of differential apoptosis or preferential proliferation as causes for immune cell persistence needs to be built into future iterations of this *in vitro* model.

There are several other limitations to this work. Firstly, functioning of the endothelial barrier was not formally tested and we cannot exclude that observed differences in leukocyte adhesion or transmigration were not due to differential permeability of monolayers between the experimental conditions. Future work would assess the initial electrical impedance of EC monolayers and also seek to assess if real-time differences in trans-endothelial migration during co-culture with healthy tendon fibroblasts are explained by endothelial hyperpermeability.[288] Secondly, we cannot exclude that the observed activation of tenocytes during extended co-culture was not a consequence of an increased cellular mass and altered metabolic load within the culture media. Additional co-cultures, with fibroblasts seeded into both the upper and lower transwell chambers, would add support to the notion that microvascular endothelial cells exert a specific paracrine action. Further, endothelial cells are known to display transcriptional and functional heterogeneity that is dependent on the organ of isolation.[289] The phenotype of tendon-derived endothelial cells is yet to be described and future research must unravel whether tenocytes respond in a similar manner to tendon specific ECs. Ultimately, a detailed understanding of how endothelial-fibroblast cross-talk effects fibroblast phenotype and tendon repair, will require the identification of candidate paracrine factors and subsequent generation of a transgenic murine strain.

Finally, the attachment of leukocytes has only been considered in the context of static conditions and not the dynamic flow experienced by leukocytes during physiological, or indeed pathological, recruitment into tissues. Confirmation that hamstring derived tendon cells exert

an immunoprotective role when compared to diseased tendon derived fibroblasts will also require co-culture under dynamic conditions.

3.8 CONCLUSIONS

The indirect co-culture of endothelial cells with tendon-derived fibroblasts from healthy and diseased tendons provides a unique opportunity to examine the effect of cellular cross-talk on tendon disease pathogenesis. Extended indirect co-culture with an immature endothelial monolayer induced an activated phenotype in healthy, and to a lesser extent, diseased tendon fibroblasts. In the context of acute injury, this crosstalk may represent beneficial angiocrine signalling that facilitates fibroblast mediated wound healing. Conversely, vessel persistence in the chronically inflamed tendon may perpetuate activation and, in part, contribute to a failure of resolution. Moreover, this work has also demonstrated that the inflammatory infiltrate is modulated by the phenotype of tendon fibroblasts. It appears that fibroblasts from non-inflamed tendon reduce the adhesion of T-cell and monocytes. Loss of this protective mechanism may explain the increased number of inflammatory cells observed in tendinopathy. Thus, the model described here provides a relevant and relatively easy means of studying both the pathobiology and therapeutic manipulation of human tendon disease.

Chapter 4 The effect of electrospun scaffold architecture on tendon fibroblast activation

4.1 ABSTRACT

4.1.1 Background

The extracellular matrix (ECM) is a natural topographical blueprint that guides cellular shape and behaviour. Through the careful manipulation of parameters such as fibre alignment and diameter, synthetic electrospun materials can recapitulate this environment and enable modulation of the aberrant cellular phenotypes that are present within diseased tendon. In the context of human rotator cuff tendon disease, fibroblasts demonstrate an activated, pro-inflammatory phenotype and display characteristic morphological changes. Growing evidence also supports a key role for activated fibroblasts in pathological angiogenesis. However, the effect of electrospun material on the activation status of tendon derived fibroblasts has not been assessed. This experiment sought to characterise and compare the effect of fibre alignment and diameter on the transcriptome of fibroblasts isolated from healthy and diseased tendons. The expression of biological processes associated with activation, including regulation of pro-angiogenic pathways, was assessed at a computational level.

4.1.2 Methods

Tendon fibroblasts were isolated from healthy hamstrings (n=3) and massive rotator cuff tendon tears (n=3). Electrospun scaffolds were produced with fibres in aligned or random orientations, but with matching fibre diameters of approximately 300,1000,2000 and 4000nm. Fibroblasts were cultured on scaffolds for 7 days prior to harvesting for bulk mRNA sequencing.

4.1.3 Results

Diseased tendon fibroblasts demonstrated an upregulation of *PDPN*, *FAP*, *VCAM1* and *CD248*, corresponding to a positive enrichment for gene-sets describing inflammatory regulation, cytokine release, ECM production and immune cell activation. Angiogenic pathways were not differentially enriched. Aligned electrospun scaffolds with diameters above 1000nm resulted in a downregulation of these gene-sets, with a profound response observed for diseased tendon fibroblasts. Conversely, small diameter (~300nm) aligned and randomly orientated scaffolds produced a relative activation. Changes in electrospun scaffold architecture did not consistently alter the expression of genes involved in the direct regulation of angiogenesis by fibroblasts.

4.1.4 Conclusions

Electrospun scaffolds are capable of modulating the shape and activation status of both healthy and diseased tenocytes but, at a computational level, this did not correspond with differences in the angiogenic output of tendon fibroblasts. Scaffolds resembling smaller diameter, disordered, collagen III typically present during the earlier phases of wound healing, resulted in tenocyte activation. Conversely, scaffolds mimicking aligned larger diameter collagen I fibrils, present during tissue remodelling, did not activate tendon derived fibroblasts. This has implications for the design of scaffolds used during rotator cuff repair augmentation. It is tempting to speculate that synthetic scaffold designs should avoid persistent stromal activation, a characteristic feature of failed tendon healing, and instead provide tissue-resident fibroblasts with temporally appropriate signals. Future work will correlate long-term *in vivo* outcomes with scaffold induced changes to the activation signature of tendon fibroblasts.

4.2 INTRODUCTION

The nanoscale structure of the ECM provides a natural network of physical and chemical cues that supports cells and guides their behaviour.[129] Through the formation of focal adhesions, mechanical signals are transmitted to the nucleus, resulting in epigenetic modifications and alterations to the expression of genes and proteins.[130] As the primary constituent of tendon ECM, collagen fibres (1-20μm), are a critical determinant of a tendon fibroblasts' physical and mechanical environment. Fibril diameter (50 – 200 nm),[136,290] anisotrophy[137] and nanotopography created by repeating D-bands[138], all contribute to the global biophysical profile each collagen fibre presents to the surrounding tendon fibroblasts.

Tendinopathy alters the ECM niche.[8] Diseased tendon exhibits an overall reduction in collagen content, a relative increase in collagen II and III and a loss of matrix organisation.[66] In turn, these changes may contribute to the phenotypic shift that diseased tenocytes undergo.[139] Tendon fibroblasts isolated from rotator cuff tears exhibit altered collagen synthesis, a constitutive pro-inflammatory profile and become hyper-responsive to subsequent inflammatory stimuli – a phenotype that persists despite multiple rounds of cell culture.[45,252,291] Indeed, persistent fibroblast activation is a hallmark feature of many chronic fibrotic and inflammatory conditions,[292] and describes a diverse cellular response that includes proliferation, migration, synthesis of extracellular matrix, secretion of cytokines and chemokines, recruitment of immune cells and the modification of tissue architecture through cytoskeletal alterations. This activated phenotype is in marked contrast with quiescent or resting status of fibroblasts isolated from healthy tissue which, in an unstimulated state, exhibit negligible transcriptional and metabolic activity.[47] Crucially, activated fibroblasts also play a critical role in pathological angiogenesis, acting as major source of soluble angiogenic growth factors, including VEGF, TGF-β, FGF-2 and PDGF, as well as secreting numerous matrix proteins that are fundamental to endothelial cell lumen formation.[293] Several markers that identify activated fibroblasts have now been described and include, Fibroblast Activation Protein (FAP), Endosialin (CD248), Podoplanin (PDPN), VCAM1 (CD106) and Thy1 (CD90).[262,294]

Inflammation and angiogenesis are two closely coupled processes. Indeed, diseased rotator cuff tendons display an increased vascularity, which is greatest during the early stages of disease and closely mirrors the size of the chronic inflammatory infiltrate.[44] Growing evidence supports that the endothelium is not a passive bystander, but is itself capable of defining the tissue microenvironment. Divergent theories currently hold that the endothelium has a role in the perpetuation of chronic inflammation[67], or conversely that endothelial cells can also drive tissue regeneration through the production of angiocrine signalling.[75] In any event, the manipulation of angiogenesis is now a key consideration of contemporary implant design.[295]

The surgical implantation of electrospun scaffolds provides cells with an alternative extra-cellular niche. Through modifications to a synthetic biomaterial's microarchitecture we aim to recapitulate a 'healthy' biophysical environment, and in doing so redirect diseased tendon fibroblasts toward a healthy phenotype. Indeed, a material's dimensionality[131], stiffness[296], and topography[134,297] have all been shown to influence the behaviour of cardiac fibroblasts and mesenchymal stem respectively. This biophysical reprogramming appears to be driven by epigenetic mechanisms.[298] Interestingly, epigenetic dysregulation has also been implicated in persistent fibroblast activation,[299] raising the possibility that appropriate topographical alterations can manipulate fibroblast activation status.

It is likely that cell-material interactions are heavily influenced by the type of fibroblast under study. The transcriptional profile of fibroblasts isolated from the skin, bone marrow and synovium is determined by the anatomical location and disease status of the original tissue.[292] Indeed, fibroblasts isolated from healthy hamstring tendons and seeded onto aligned electrospun polydioxanone fibres, elongated along the direction of the fibres and reduced their surface expression of VCAM-1 relative to tissue culture plastic. Diseased tendon fibroblasts, isolated from rotator cuff tears, demonstrated a much slower, albeit similar morphological response, but without any change in surface phenotype.[291]

To date, studies have focused on a limited number of architectural modifications and not considered their global effect on cellular phenotype, using only a small repertoire of genes or surface proteins to define a favourable response. Consequently, the ideal microarchitectural properties of synthetic scaffolds has remained elusive. This chapter aims to robustly

interrogate a broad range of microarchitectural properties, assessing their effect on both the global and angiogenic transcriptional profiles of fibroblasts isolated from healthy and diseased tendons.

4.3 AIMS

This project aimed to develop a comprehensive library of topographically diverse electrospun scaffolds and investigate, at a transcriptional level, the effect of topography on the phenotype of tendon derived fibroblasts. Specific aims were to:

1. Develop a library of electrospun materials, with variable fibre alignment and/or diameter, for subsequent *in vitro* testing
2. For healthy and diseased tendon fibroblasts, undertake an unbiased transcriptional characterisation of the biological processes affected by fibre anisotropy and diameter, and specifically determine if alterations to microarchitecture modulates angiogenesis

4.4 HYPOTHESES

This work hypothesised that electrospun scaffolds most closely mimicking the natural architecture of human tendon would favourably modulate the transcriptional phenotype of tendon-derived fibroblasts.

The specific hypotheses of this chapter were that:

1. The manipulation of electrospinning parameters would allow the production of scaffolds with fibres in random or aligned configurations, but with matched fibre diameters covering a spectrum of sizes that mimicked the size of collagen fibrils (300nm) through to collagen fibres (4000nm)[5]
2. Biomimetic aligned scaffolds would modulate the activation status of tendon fibroblasts, and that disease status would alter their responsiveness to biophysical stimuli
3. Scaffold induced activation of fibroblasts would result in a pro-angiogenic transcriptional profile

4.5 METHODS

4.5.1 Electrospun scaffold fabrication

4.5.1.2 PDO solution preparation

Variable quantities of PDO resin (Riverpoint Medical, Portland, USA) were dissolved in Hexafluoro-2-propanol (Apollo Scientific Ltd, Cheshire, UK) to obtain the required mass concentration (% w/v) of PDO solution. To achieve small diameter fibres, pyridine (Sigma, Dorset, UK) was also added to PDO solutions at a fixed concentration of 1µl/ml.[300] Prior to use all solutions underwent gentle agitation at room temperature for 24 hours.

4.5.1.3 Electrospinning

PDO Solutions were loaded into a PHD 2000 syringe pump (Harvard Apparatus, Kent, UK) and supplied to an environmentally-controlled (20^{oc} and 30% humidity) IME electrospinning device (IME Technologies, Spaarpot, Netherlands) at a constant flowrate. A voltage was then applied between a stainless-steel nozzle and rotating collector coated in a single sheet of aluminium foil. Variations of; flowrate, voltage, collector speed, chamber temperature, chamber humidity and distance between the nozzle and collector, enabled the production of scaffolds with different fibre diameters and alignments. The final parameters utilised in the production of scaffolds for *in vitro* culture are outlined in tables 4-1 and 4-2. Following production, scaffolds were stored in a desiccator to slow hydrolytic breakdown and utilised within 30 days.

Scaffold	300nm aligned	1000nm aligned	2000nm aligned	4000nm aligned
PDO concentration (%w/v)	7	12	14	15
Pyridine Concentration (µl/ml)	1	0	0	0
Flow rate (ml/hr)	0.5	0.5	1.5	3
Voltage (kv)	20	8	12	6
Collector Speed (rpm)	2000	2000	2000	1500
Nozzle-collector distance (cm)	20	20	20	20
Total time (hours)	4	4	4	3

Table 4-1. Parameters utilised to produce aligned electrospun scaffolds for *in vitro* culture

Scaffold	300nm random	1000nm random	2000nm random	4000nm random
PDO concentration (%w/v)	7	10	10	13
Pyridine Concentration (μl/ml)	1	1	0	0
Flow rate (ml/hr)	0.5	0.5	0.5	0.75
Voltage (kv)	25	8	10	8
Collector Speed (rpm)	50	50	50	50
Nozzle-collector distance (cm)	20	20	20	20
Total time (hours)	4	4	4	3

Table 4-2. Parameters utilised to produce random electrospun scaffolds for *in vitro* culture

4.5.1.4 Scanning electron microscopy and image analysis

A 1cm x 1cm section of electrospun scaffold was cut and mounted on aluminium stubs (Agar Scientific, Essex, UK) using carbon tape (Agar Scientific). Samples were then gold/palladium coated for 120 seconds (SC7620 Mini Sputter Coater, Quorum Technologies, Laughton, UK) and images acquired with an EVO LS15 Scanning Electron Microscope (SEM) (Zeiss, Oberkochen, Germany). To enable accurate image quantification images were taken at high magnification (5000x - 10,000x) and at least 5 separate images acquired for each sample.

The diameter and alignment electrospun fibres ($n > 50$) were characterized using Image J software (National Institutes of Health, Bethesda, USA) using an in-house protocol. In brief, measurements were first calibrated against each image's scale bar. The diameter of all consecutive images fibres were measured perpendicular to the longitudinal access of the fibre. ImageJ concurrently provides an angle of measurement, relative to the vertical axis of the image, the addition of 90 degrees transforms this measurement relative to the longitudinal axis of each fibre.

4.5.1.5 Characterisation of electrospun scaffold pore size and porosity

Porosity and pore size measurement were initially undertaken using mercury intrusion with an AutoPore IV 9500 mercury porosimeter (Micromeritics Instrument Co, Norcross, GA, USA) with 100mg of each scaffold, a mercury filling pressure of 0.49 psia and an equilibration time of 10 seconds. Due to failure of this methodology, porosity and pore size were quantified from SEM image analysis in ImageJ. SEM images were first segmented to produce a binary black and white image (Figure 4-1A). This was produced through global thresholding, in which a

single constant threshold was applied. All pixels greater than or equal to the threshold were defined as electrospun fibres and the remaining belonged to the background. The optimal threshold differed between images and was chosen based on observer judgement. To improve segmentation quality, manual correction of each segmented image was then undertaken (Figure 4-1B). The pore size and number of pores was then estimated using the built-in "Analyse Particle" plugin in ImageJ (Figure 4-1C). Percent open area (POA), a two-dimensional approximation of porosity,[301] was calculated by dividing the number of pixels contributing to all pores, by the total number of pixels in the image. Measurements were then calibrated to the scale bar associated with each original SEM image. For each scaffold, this was undertaken for a minimum of five discrete images and values averaged.

4.5.2 Collection and processing of tendon samples

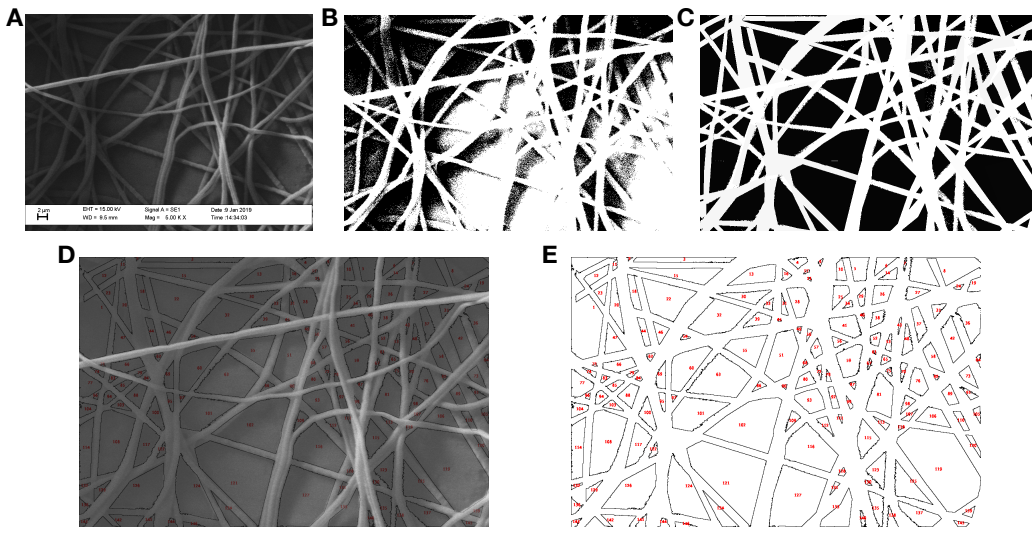

Figure 4-1 Protocol for measurement of pore size, number and porosity with ImageJ. SEM images were imported into image J and the scale bar used to provide a conversion ratio for pixel size to micrometers (A). Automated segmentation of each image was undertake based on a global threshold, set according to observer judgement (B). Inhomogeneities in the grey-level distribution of objects (fibres) and background was then corrected through manual segementation of each image (C). The "Analyse Particles" plugin for ImageJ was then able to map the number and size of the pores and provide a calculation of percent open area (POA) (D and E)

4.5.2.1 Sample collection

Biopsies of diseased rotator cuff tendons were collected from patients undergoing tendon repairs (n=3, 2 male 1 female, average age 65.6 yrs). All tendon tears had been classified as massive (>5cm in anterior-posterior diameter) by the operative surgeon. Healthy controls were obtained from patients undergoing anterior cruciate ligament reconstruction during which residual autologous hamstring tendon graft was collected (n=3, 2 male 1 female, average age 21.4 years). Informed consent was provided by all donor and samples collected through

Oxford Musculoskeletal Biobank (REC 09/H0606/11), in full compliance with national and institutional ethical requirements including the Declaration of Helsinki (2013) and the Human Tissue Act (2004). Tendon samples were immediately placed in D10 culture media (Dulbecco's Modified Eagle Medium: Nutrient Mixture F-12 (DMEM/F12) (Lonza, Slough, UK) supplemented with 10% Fetal Bovine Serum (FBS) (Labtech, Uckfield, UK) and 1% penicillin-streptomycin (PS) (ThermoFisher Scientific, Waltham, MA, USA)) and underwent laboratory processing to isolate tendon-derived fibroblasts.

4.5.2.2 Isolation and expansion of tendon fibroblasts

Under aseptic conditions tendon samples were divided into 2-mm^3 sections and between 4 and 6 explants transferred into each well of a 6-well plate. Samples were initially cultured in D50 culture media (DMEM/F12 containing 50% FCS and 1% PS) in a tissue culture incubator at 37^{oc} and 5% CO2. Phase contrast microscopy was used to determine the migration of fibroblasts out of tendon explants, at which point whole tissue samples were removed and the culture medium changed to D10 media. At 80-90% confluence cells were enzymatically detached (TrypLE^{TM}, ThermoFischer Scientific, Waltham, MA, USA) and expanded in polystyrene tissue culture dishes (CELLSTAR, Greiner, Frickenhausen, Germany). All subsequent experiments were undertaken on cells at passage 2.

4.5.3 Culture of tendon fibroblast on electrospun scaffolds

4.5.3.1 Preparation of Electrospun scaffolds for *in vitro* cell culture

1.5cm x 1.5cm sections of scaffolds were cut and sprayed with ethanol, facilitating detachment and sterilisation of the scaffold. Sections were then mounted onto 24-well sized cell crowns (Scaffdex, Tampere, Finland) and a further two rounds of ethanol sterilisation undertaken. Between sterilisation cycles, scaffolds were allowed to air dried in a laminar flow tissue culture cabinet for 60 minutes. Three separate washes with 2mls Phosphate Buffered Saline (PBS, Sigma-Aldrich) was undertaken followed by a visual inspection to detect any macroscopically detective scaffolds. Any such scaffolds were discarded prior to cell seeding.

To facilitate protein adsorption, mounted electrospun scaffolds were placed in 24-well plates with 2mls D10 culture media for 2 hours. Subsequently, to remove non-adsorbed proteins and debris, mounted scaffolds underwent three wash cycles with 2mls PBS.

4.5.3.2 Seeding and culture of tendon fibroblasts

Tendon fibroblasts were enzymatically detached from polystyrene tissue culture dishes, counted (Bio-Rad, Hertfordshire, UK) and diluted in D10 media to a concentration of 0.5 x10^6 cells/ml. Mounted scaffolds were placed in the bottom of a 12-well polystyrene plate (Costar®, Corning Inc, Corning NY, USA) and 100µl of cell suspension added to the surface of each scaffold (total scaffold area is 0.79cm^2), equating to a seeding density of ~40,000 cells/cm^2. Cells were left to adhere for 2 hours prior to transfer of cell-laden scaffolds to 24-well plates (Costar®, Corning Inc, Corning NY, USA) containing 1.5mls of fresh D10 media. To ensure full immersion, an additional 500µl of D10 media was then added to the upper surface of each scaffold. Media was changed every 4 days for the duration of each experiment.

4.5.4 Immunocytochemistry of tendon fibroblasts on electropsun scaffolds

Healthy tendon fibroblasts were cultured on scaffolds for 7 days before being fixed in 10% formalin for 10 mins. Before and after fixation, all scaffolds were washed twice with 2mls PBS. Scaffolds were stored in PBS at 4ºC prior to staining.

Cells were permeabilised with 0.1% Triton-X (ThermoFisher Scientific) for 3 minutes and washed in PBS. Specimens were then with stained AlexaFluor™ 488 Phalloidin (ThermoFischer Scientific) at 1 in 1000 concentration for 20 minutes at room temperature in the dark. Nuclear counter staining was performed with DAPI (ThermoFischer Scientific) at a concentration of 1µg/ml for a further 10 minutes at room temperature in the dark. Scaffolds were subsequently washed and mounted onto adhesive glass slides using a hard setting fluorescent mounting medium (VectaShield Hardset, Vector Laboratories, CA, USA) and stored at 4°C until image acquisition.

For imaging validation of RNA-sequencing, scaffolds were permeabilised with 0.1% Triton-X for 3 minutes, washed in PBS and then blocked in 5% normal goat serum (Sigma-Aldrich) in PBS for 60 min in a humid chamber at room temperature. Scaffolds were then incubated with the primary antibodies (Table 4-3) diluted in 5% normal goat serum in PBS for 2 hours at room temperature. After incubation with the primary antibody, scaffolds were washed three times with PBSfor 5 min. Slides were incubated with the secondary antibodies detailed in Table 4-3. Scaffolds were washed with PBS and then stained with AlexaFluor™ 633 Phalloidin

(ThermoFischer Scientific) at 1 in 1000 concentration for 20 minutes at room temperature. Scaffolds were washed three times with PBST, incubated with DAPI at a concentration of 1µg/ml for 10 minutes, washed 3 times in PBS, and mounted onto adhesive glass slides.

Imaging was acquired with a confocal laser scanning microscope ZEISS LSM 880 (Carl Zeiss AG, Oberkochen, Germany) with 63 x 1.4 NA oil objective and equipped with an Airyscan detection unit. For each scaffold a 12-part titled scan (Zen 2.0, Carl Zeiss, Germany) was performed with a 15 percent overlap between tiles. Image stitching was undertaken in ImageJ.

Antibody	Supplier	Clone	Isotype	Species	Dilution
PDPN	Abcam (Ab10288)	18H5	IgG1	Mouse	1:500
Anti-Mouse IgG	Abcam (Ab150113)	-	IgG	Goat	1:200

Table 4-3. Primary and secondary antibodies used in imaging validation of RNAseq data

4.5.5 Bulk mRNA sequencing

4.5.5.1 RNA isolation

Scaffolds underwent three wash cycles with 2mls PBS before being removal from the cell-crown and placed in an Eppendorf tube. 300µl of TRIzol (Invitrogen, Paisley, UK) was added to each Eppendorf and specimens were then stored at -80^{oc} until later analysis. mRNA extraction, which included a DNAse treatment step, was performed using the Direct-Zol RNA Microprep Kit (Zymo Research, Irvine, CA, USA) according to manufacturer's instructions. mRNA quantity and integrity was determined using spectrophotometry (ND1000, Nanodrop Technologies, Willington, DE, USA) and Agilent 2200 Bioanalyser (Agilent Technologies, Santa Clara, CA, USA). All samples had a RIN score of 7 or greater and no evidence of DNA contamination.

4.5.5.2 Library Construction and sequencing

A total of 100ng RNA per sample was used to generate sequencing libraries using the NEBNext Ultra II Directional RNA Library Prep Kit for Illumina® (NEB, USA), following the manufacturer's protocol. The method has previously been described by Chen *et al.*[302] In brief, mRNA was purified from total RNA and fragmented to an average size of 300bp using the NEBNext Poly(A) mRNA Magnetic Isolation Module. Following 1st and 2nd strand cDNA synthesis, adaptors and indexes were ligated to double-stranded cDNA via 6 cycles of PCR. Quality of cDNA library was assessed using an Agilent 2200 Bioanalyser and further rounds

of magnetic purification undertaken if primer or adaptor-dimer contamination was detected. Finally, libraries were pooled, and sequencing was performed using the Illumina HiSeq 4000 sequencer using 42 base read lengths in paired-end mode.

4.5.5.3 RNA-seq analysis

Raw reads generated from each RNA sample in fastq format were initially processed using an RNA-seq analysis pipeline developed in Python (version 3.7.2) and available in appendix C-1. RNA-seq data quality was first confirmed using FastQC, and reads were mapped to the Ensembl hg38 release 94 using the splice aware mapper HISAT2 (version 2.1.0)[303]. Alignment quality was assessed with Picard-tools.[304] FeatureCounts[305] was utilised to quantify the abundance of mapped reads and differential expression analysis was performed using DESeq2[306] with shrinkage of logarithmic fold change according to the 'apeglm' methodology.[307] Benjamini-Hochberg correction (false discovery rate of 5%) was applied to determine the P_{adj} and define significance. Geneset enrichment analysis was performed in R (version 3.2.4), using the fgsea package on significantly upregulated genes (P_{adj} <0.05) ranked by the sign of the fold change multiplied by the inverse log10 of the p-value.

4.5.6 Statistical analysis

4.5.6.1 Electrospun scaffolds fibre diameter

Analysis was performed with GraphPad Prism v7 software (GraphPad Software Inc, California, USA). For testing for statistical differences in mean diameter of two scaffolds, an unpaired, two-tailed t test with Welch's correction was used. For testing of more than two scaffolds, a one-way ANOVA with Tukey's multiple comparisons testing was used. A p-value of <0.05 was deemed statistically significance.

4.5.6.2 Electrospun scaffolds fibre anisotropy

Analysis was performed with PAST3 v20 (Oyvind Hammer, Natural History Museum, University of Oslo) and circular arrow plots generated. For each arrow plot a Rayleigh's R value was calculated. For each individual scaffold, Rayleigh's R value tests for a significant unimodal orientation in fibre directionality.[308] A value of R=1 indicates that all data shared the same directionality, whereas a value of R=0 implies that the data is evenly distributed around

a circle. An arbitrary threshold of R>0.7 was taken to mean that a scaffold had aligned fibres, and an R value of <0.3 was deemed to be a scaffold with randomly orientated fibres.

4.5.6.3 RNA-sequencing

All plots were generated using R (v-3.2.4), including the following R packages ggplot2, Enhancedvolcano and ComplexHeatmap for producing PCA plots, volcano plots or heat maps respectively. For heatmaps hierarchical clustering was performed on the top 500 PCA genes in the first three eigenvectors (PC1,PC3 and PC3) across all samples. As previously described, genes are clustered on the basis of Pearsons correlation. Samples are clustered on the basis of a Euclidian distance matrix with complete linkage. [309]

4.6 RESULTS

4.6.1 Production of electrospun scaffolds with variable fibre diameters

Several parameters were assessed for their effect on the diameter of electrospun fibres (Figure 4-2). Increasing concentrations of PDO significantly increased mean fibre diameter, with an increase of 85 ±12nm (R^2= 0.90, p=0.0004) observed for each percentage increase in polymer concentration. Higher polymer flow rates were also observed to increase diameter but with a corresponding increase in fibre diameter variability (Figure 4-2B).

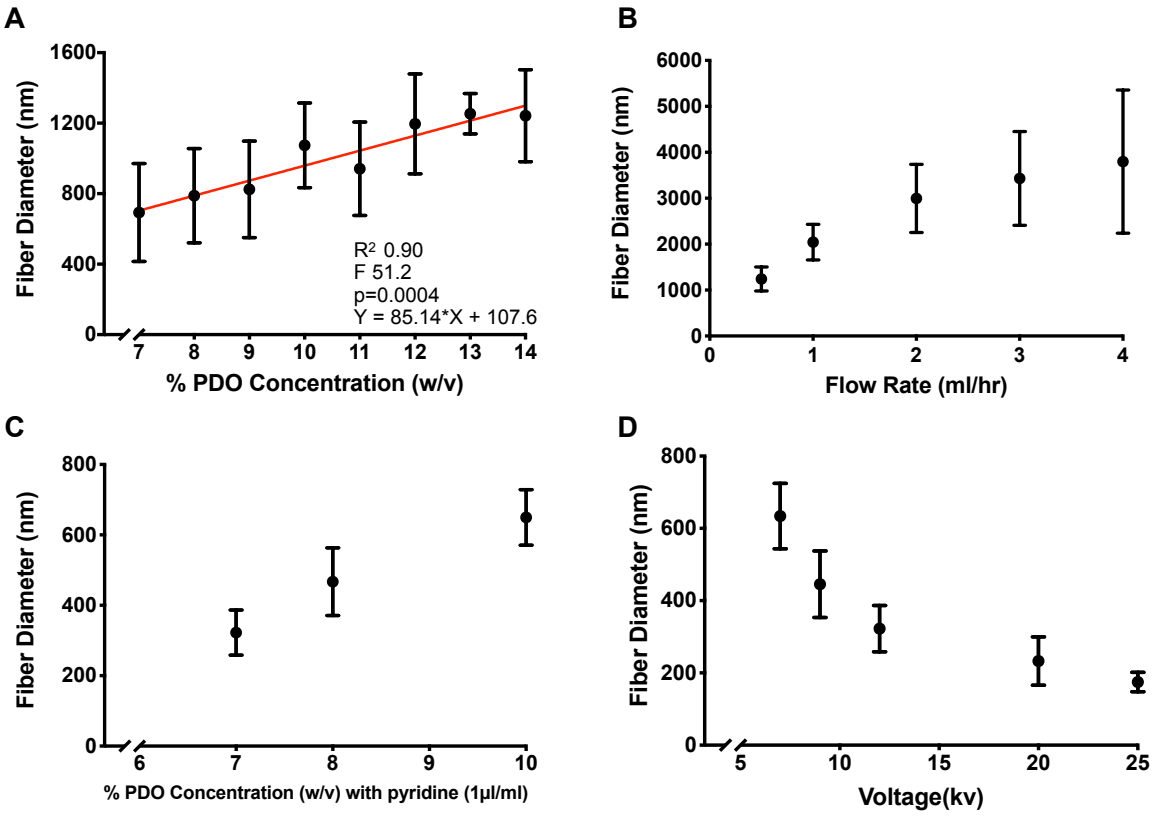

Figure 4-2. Effect of specific electrospinning parameters on fibre diameter. Mean diameter and standard deviation of electrospun scaffolds produced with (A) an increasing concentration of Polydioxanone (PDO) with all other kept variables constant (collector speed 2000rpm, voltage 8kv, and flow rate 0.5ml/hr) (B) varied polymer flow rate with constant PDO concentration (14% w/v), voltage(8kv) and collector speed (2000rpm), (C) addition of a fixed concentration of pyridine (1µl/ml) to increasing concentrations of PDO (constant; voltage 12kv, flow rate 0.5ml/hr, collector speed 2000rpm) and (D) increasing voltages applied to a solution of 7% PDO + pyridine (1µl/ml), collector speed and flow rate were constant at 2000rpm and 0.5ml/hr respectively

The production of fibres with a diameter smaller than ~700nm required addition of pyridine[194] (1µl/ml) to the polymer solution and the use of higher voltages (20-25kv), enabling production of fibres with diameters in the range of 200-300nm (Figure 4-2C and D).

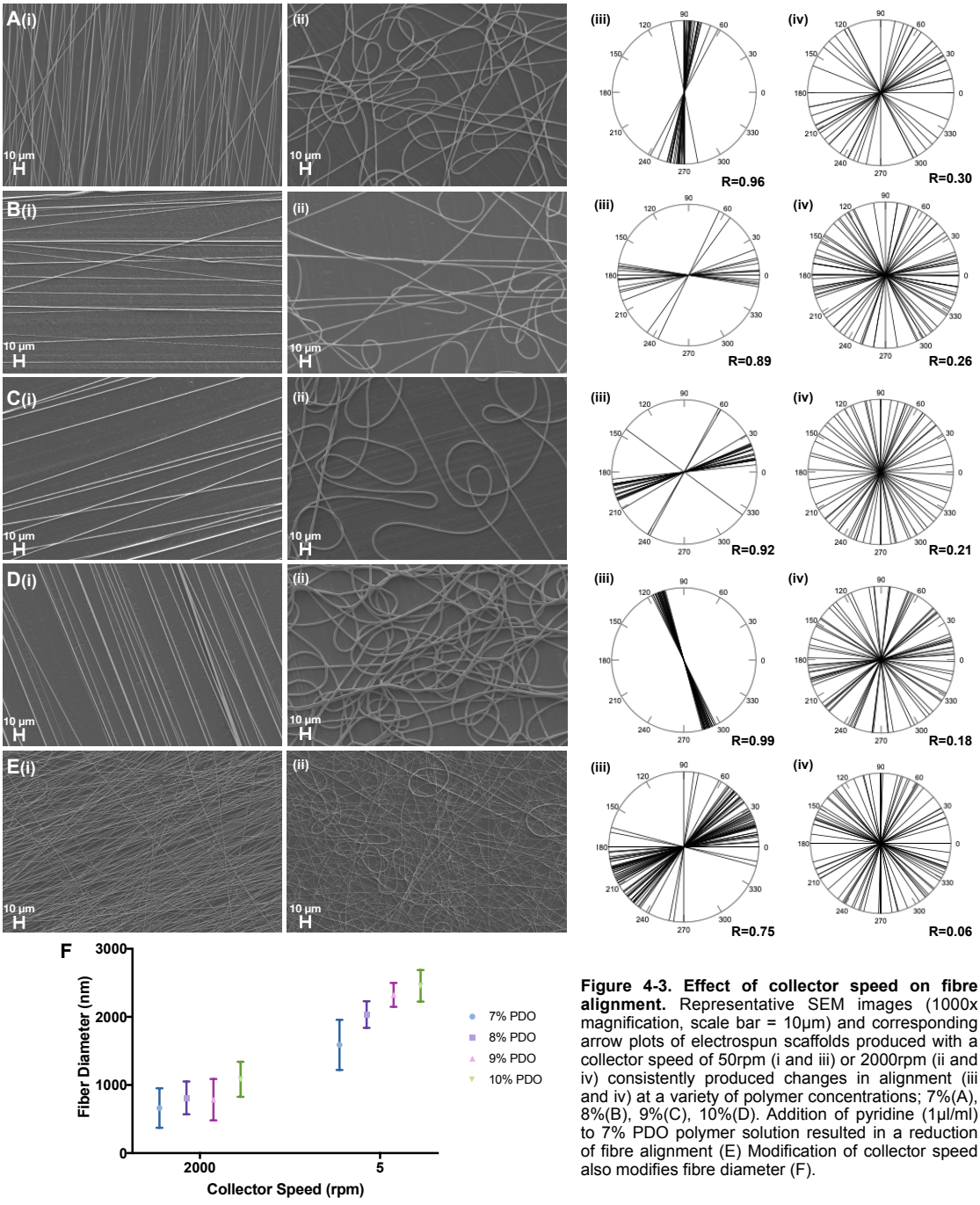

Figure 4-3. Effect of collector speed on fibre alignment. Representative SEM images (1000x magnification, scale bar = 10µm) and corresponding arrow plots of electrospun scaffolds produced with a collector speed of 50rpm (i and iii) or 2000rpm (ii and iv) consistently produced changes in alignment (iii and iv) at a variety of polymer concentrations; 7%(A), 8%(B), 9%(C), 10%(D). Addition of pyridine (1µl/ml) to 7% PDO polymer solution resulted in a reduction of fibre alignment (E) Modification of collector speed also modifies fibre diameter (F).

4.6.2 Production of electrospun scaffolds with variable fibre orientations

Fibre orientation was modified through alterations in the rotational speed of the collector. Across a range of polymer concentrations, scaffolds produced at high collector speeds (2000rpm) displayed a clear directionality (Figure 4-3A(i) - E(i)), but with a corresponding reduction in fibre diameter (Figure 4-3F). For both aligned and random scaffolds, the addition of pyridine to the polymer solution also increased fibre direction variability (Figure 4-3A and E).

4.6.3 Final Production of electrospun scaffolds for in vitro cell culture

Electrospun PDO scaffolds with fibres in an aligned (Rayleigh's R value > 0.7) or random (Rayleigh's R value < 0.3) orientation were produced (Figures 4-4 and 4-5 respectively) with a target mean fibre diameter of 300nm,1000nm,2000nm or 4000nm. The achieved mean fibre diameters were 277(±36), 1204(±102), 2113(±193) and 3584(±207). There was no significant

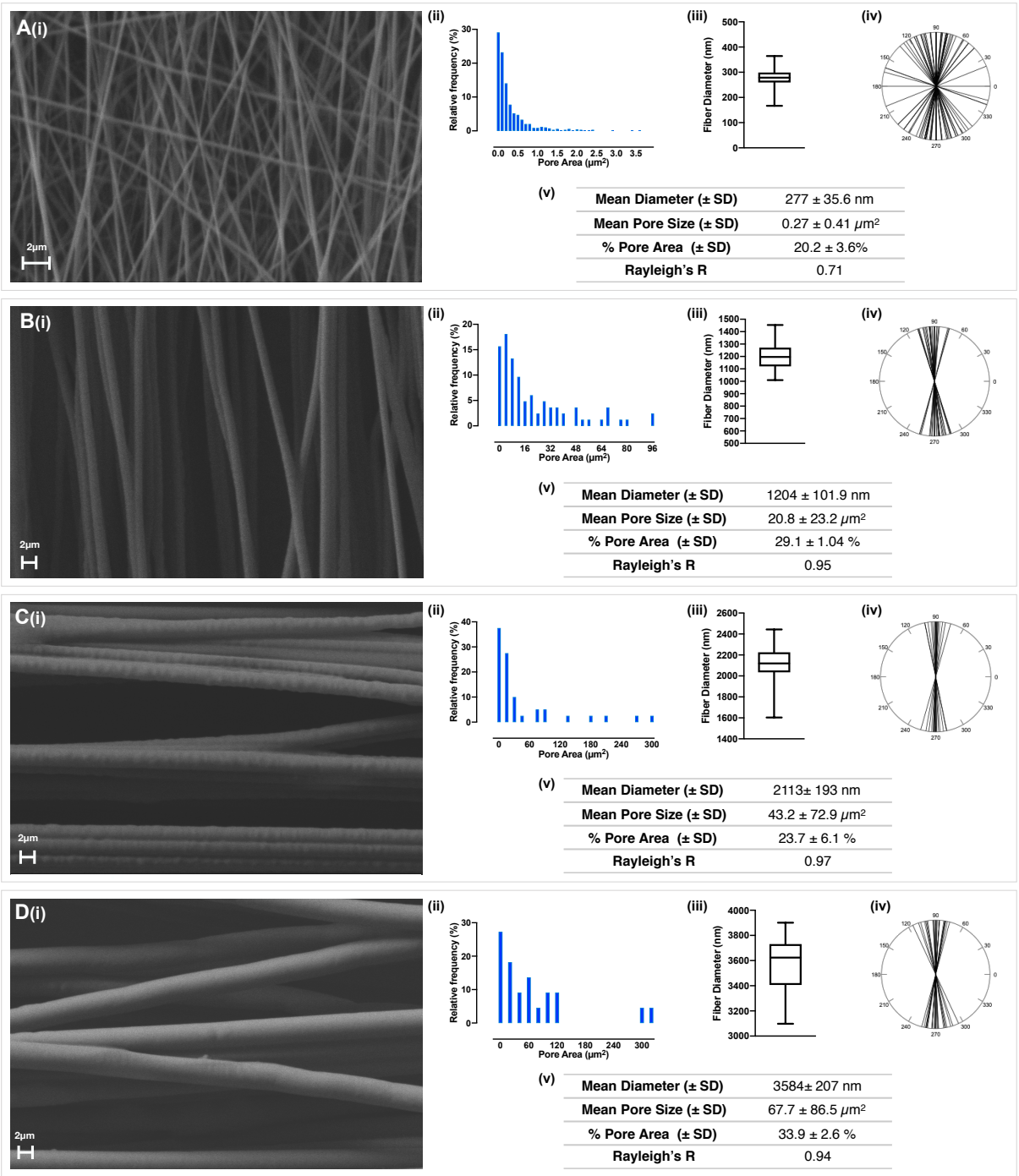

Figure 4-4. Characterisation of aligned electrospun fibres for subsequent *in vitro* experiments. Polydioxanone (PDO) fibres were produced in an aligned configuration and the fibre diameter manipulated to produce scaffolds with approximately (A) 300nm (B) 1000nm (C) 2000 nm and (D) 3500nm fibres. Each panel contains (i) Representative SEM image (5000x - 10,000x magnification, scale bar =2 μm) (ii) Pore size distribution (iii) Fibre diameter distributions (iv) Fibre alignment and (v) Summary statistics.

difference in the mean fibre diameter for scaffolds produced in an aligned or random orientation. For clarify scaffolds will herein be referred to by the targeted, and not the achieved, fibre diameters.

4.6.4 Characterization of scaffold pore size and porosity

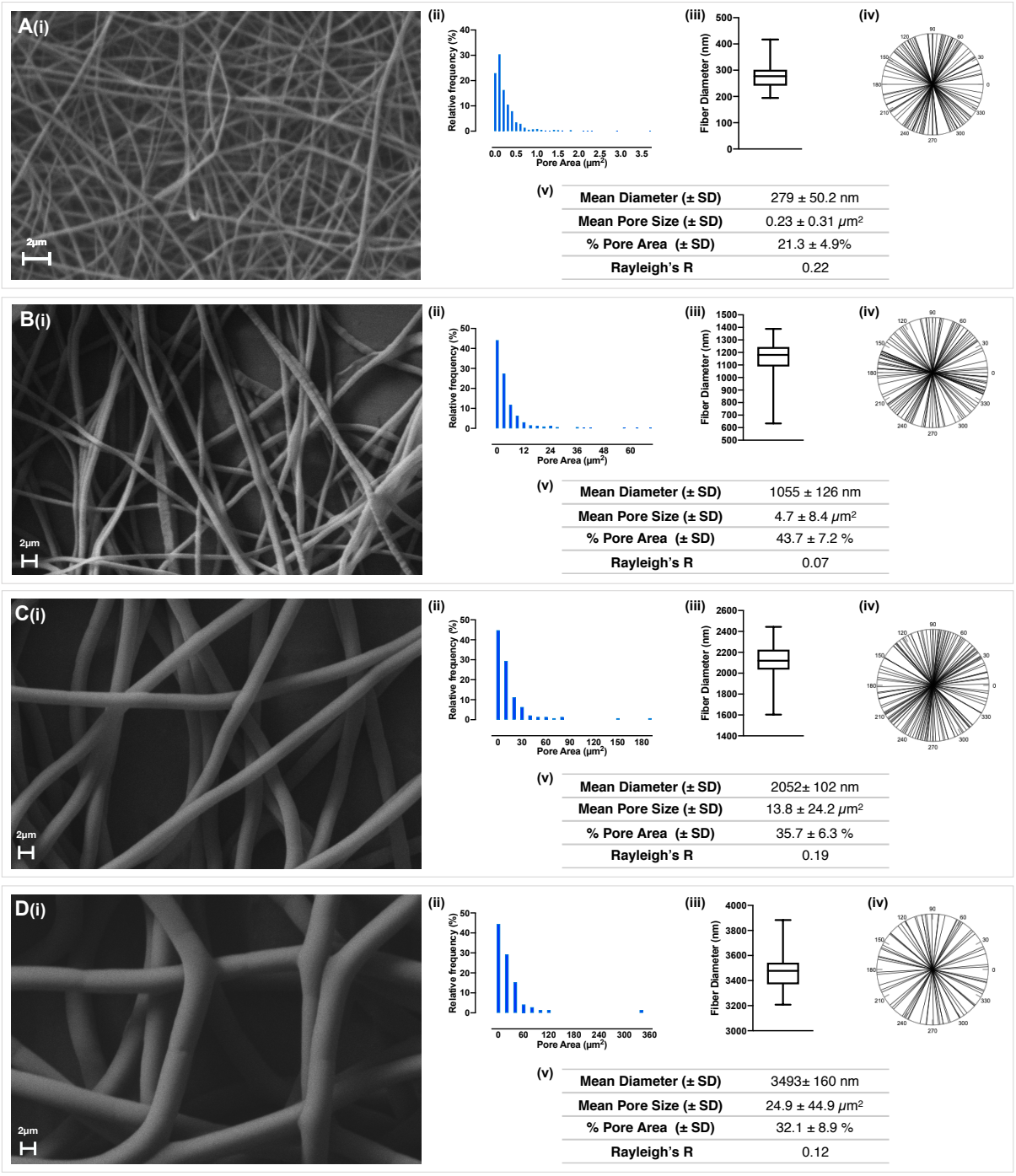

Figure 4-5. Characterisation of randomly orientated electrospun fibres for subsequent *in vitro* experiments. Polydioxanone (PDO) fibres were produced in an aligned configuration and the fibre diameter manipulated to produce scaffolds with approximately (A) 300nm (B) 1000nm (C) 2000 nm and (D) 3500nm fibres. Each panel contains (i) Representative SEM image (5000x - 10,000x magnification, scale bar =2 μm) (ii) Pore size distribution (iii) Fibre diameter distributions (iv) Fibre alignment and (v) Summary statistics.

A linear relationship between mean fibre diameter and mean pore size was observed (Figure 4-6) for scaffolds with both aligned (R^2= 0.99, p=0.0052) and randomly (R^2= 0.99, p=0.0013) orientated fibres However, aligned scaffolds with target fibre diameters of 1000nm (95% CI, 11.0 to 21.2µm, p<0.0001) 2000nm (95% CI, 22.1 to 36.9µm, p<0.0001) and 4000nm (95% CI, 32.7 to 53.0µm, p<0.0001) each demonstrated significantly larger pore sizes than their randomly orientated counterparts. No difference was observed between aligned and randomly orientated 300nm scaffolds.

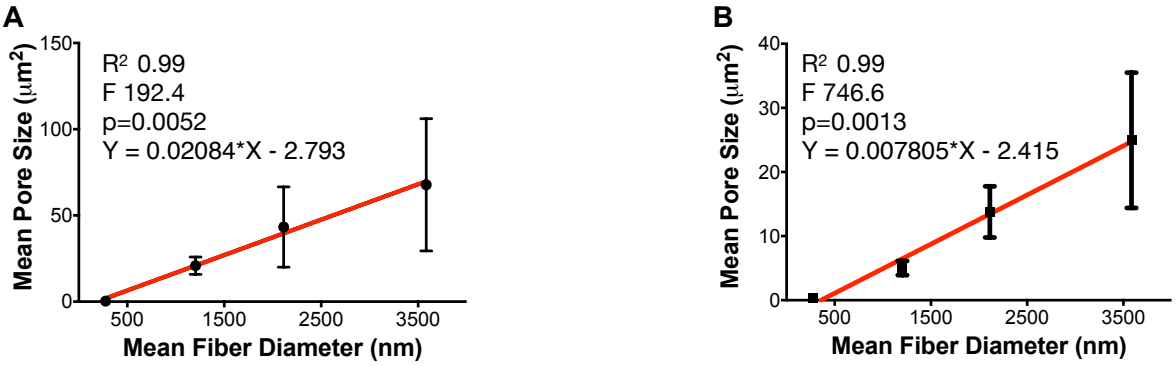

Figure 4-6. Relationship between mean pore size based on mean fibre diameter. A simple linear regression was calculated to predict mean pore size (µm²) base on the mean fibre diameter (nm) of electrospun scaffolds produced with fibres in an aligned (A) or randomly (B) orientated configuration.

Whilst attempts were made to calculate porosity using mercury porosimetry, results were unreliable and inconsistent. However, image analysis enabled calculation of percent open area (POA), an approximation of porosity.[301] All scaffolds with randomly orientated fibres displayed similar POAs, whilst 4000nm aligned scaffolds demonstrated a significantly larger POA than both 300nm (95% CI, 3.13 to 25.28%, p=0.013) and 2000nm (95% CI, 1.3 to 19.83%, p=0.025) aligned scaffolds. At each diameter, no significant differences in POA between random and aligned scaffolds was observed.

4.6.5 Effect of scaffold architecture on the morphology of healthy hamstring fibroblasts

Across the full spectrum of diameters tested, fibroblasts seeded for 7 days on scaffolds with arandomly configured fibres demonstrated a flattened and spread morphology (Figure 4-7Bi-iv). Conversely, at fibre diameters ≥1000nm scaffolds that displayed greater anisotropy

induced a distinctive fibroblast elongation. No difference in morphology was observed for fibroblasts cultured on scaffolds with a 300nm aligned or 300nm random configuration.

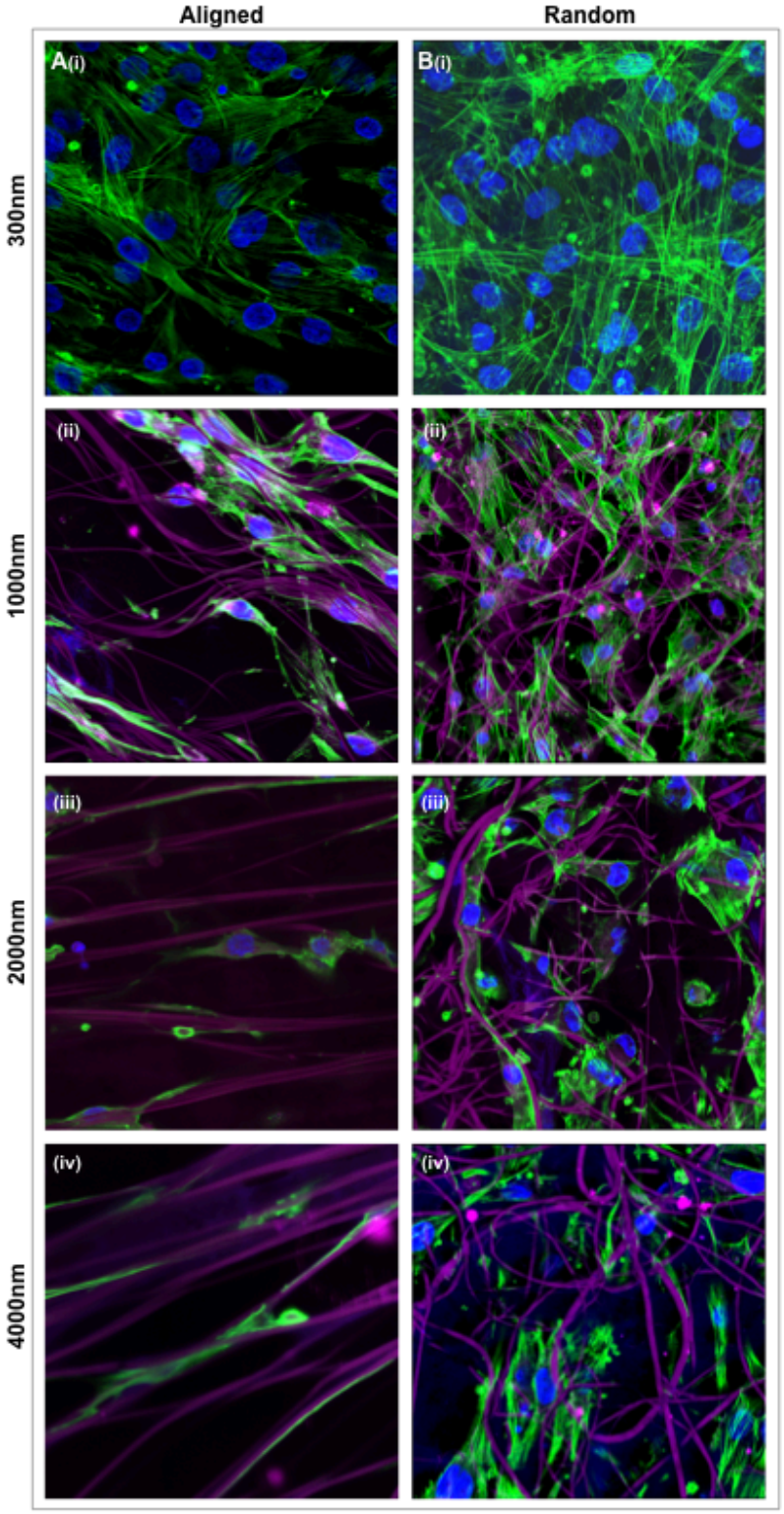

Figure 4-7. Electrospun scaffold architecture modulates the morphology of healthy tenocytes. Representative confocal images of healthy hamstring tendon fibroblasts cultured for 7 days on electrospun scaffolds with an aligned (A) or random (B) orientation of fibres and target fibre diameters of 300nm (i), 1000nm(ii), 2000nm(iii) or 4000nm(iv). Green=phalloidin actin stain, Blue = DAPI nuclear stain, Magenta= scaffold auto-fluorescence.

4.6.6 Transcriptome sequencing of hamstring and rotator cuff derived fibroblasts

The transcriptome of hamstring (n=3) and massive rotator cuff tear (n=3) derived fibroblasts, cultured on the eight distinct electrospun scaffolds for 7 days, was assessed using mRNA sequencing. Due to the risk of contamination during cell culture, sequences were screened against bacterial, yeast and bovine genomes with no alignment detected and a similar GC content across all samples (Appendix C Figures C-1 and C-2). Between 11.8 – 40.1 million paired-end 42nt reads were obtained for hamstring fibroblasts, and 9.7 – 37.7 million for rotator cuff fibroblasts, providing approximately 9.7 to 30.3 times coverage of the protein encoding genome for hamstring derived cells and 8.0 to 30.9 times coverage for rotator cuff derived cells. [310]

4.6.7 Micro-architecture modulates gene expression of healthy tendon fibroblasts

Comparison of the 500 genes showing the most variably expressed genes between all scaffolds is shown in figure 4-8A, with hierarchical clustering analysis performed. The largest Euclidean distance was displayed between the different biological donors, whilst close similarities were observed between scaffolds with either randomly or aligned fibre orientations. A similar pattern is reflected in the principle component analysis (Figure 4-8B-C). The separation of samples according to donor is evident along PC1 accounting for 69% of the variance, whilst PC2 represented 22% and seemed to reflect scaffold anisotropy. This is in agreement with the dendrogram in which clustering around anisotropy was most clearly defined for donors 1 and 2. Comparison of PC2 with PC3 enabled the effect of scaffold microarchitecture on gene expression to be easily visualisation. Separation of 2000nm and 4000nm aligned scaffolds from the remaining architectures was evident.

4.6.8 Effect of fibre diameter on gene expression of healthy tendon fibroblasts

The influence of fibre diameter on the mRNA transcriptome of hamstring tendon fibroblasts was assessed after 7 days in culture. Pairwise comparisons between scaffolds was undertaken and the number of differentially expressed genes (padj <0.05) is summarised in figure 4-9.

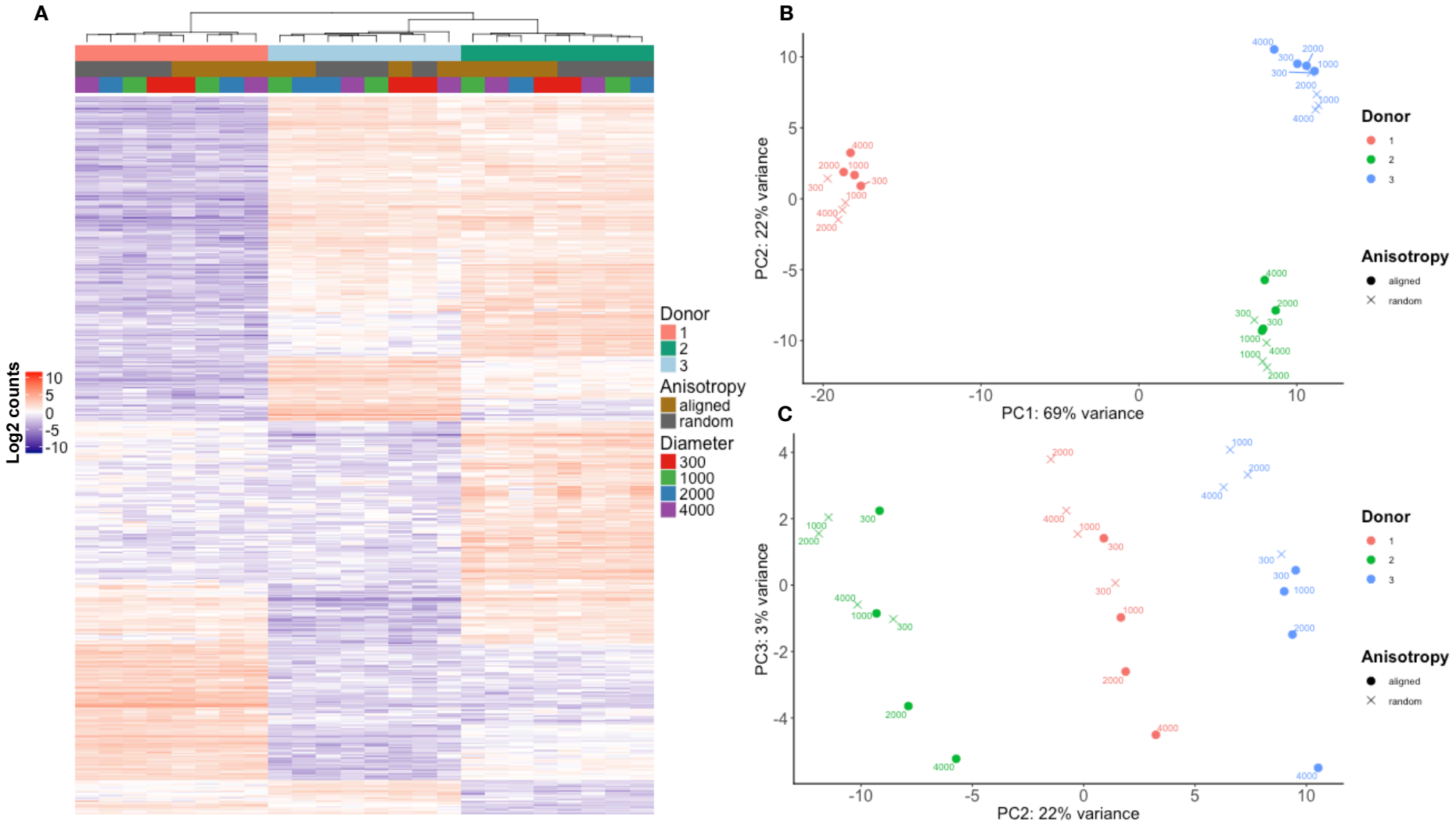

Figure 4-8 Heatmap and Principle component analysis (PCA) of log transformed expression data from all 24 RNA samples sequenced from healthy hamstring fibroblasts seeded on to 8 different electrospun scaffolds. Independent clustering of the samples according to donor, anisotropy and diameter is depicted by the dendrogram (A),1st and 2nd principles component (B) which accounts for 69% and 22% of the variance in gene expression respectively, the effect of scaffold architecture on gene expression is most clearly observed in the 3rd principle component (C). The Heatmap depicts hierarchical clustering of the top 500 PCA genes across all samples.

For randomly orientated scaffolds fibre diameter had a limited effect, with no significant difference in gene expression detected between 1000nm,2000nm and 4000nm scaffolds. However, 300nm scaffolds were clearly different from the remaining random scaffolds, a result that closely mirrors the clustering observed during principle component analysis (Figure 4-8C).

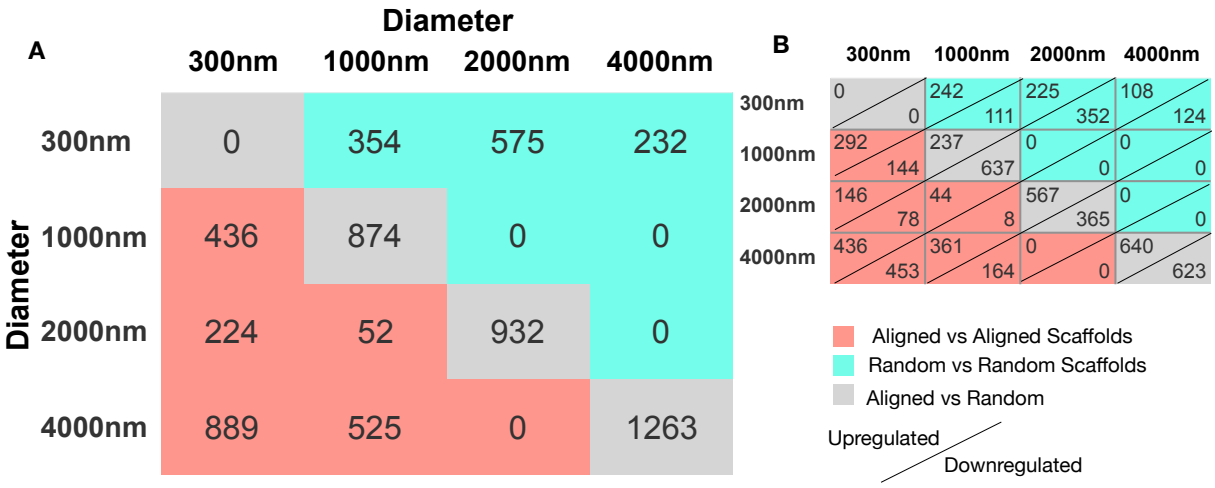

Figure 4-9 Scaffold-by-scaffold comparison of differentially expressed genes between healthy hamstring fibroblasts cultured on scaffolds of different microarchitectures. (A) A pairwise comparison of different fibre diameters is provided for both aligned and random scaffolds. Grey boxes denote a comparison of aligned and random scaffolds for the fibre diameters 300,1000,2000 and 4000 nm. (B) Differential expression has been split into the number of unregulated and downregulated genes. The threshold for differential expression was set at an adjusted p-value (Benjamini-Hochberg correction) of <0.05.

Manipulation of the fibre diameter of scaffolds with aligned fibre orientations had a greater influence on gene expression. Compared to 1000nm aligned scaffolds, 426 and 525 genes were differentially regulated for 300nm aligned and 4000nm aligned scaffolds respectively.

An initial survey of the differentially expressed genes is illustrated by the volcano plots in figures 4-10 and 4-11 for aligned and random scaffolds respectively. Significant genes with greater than a 1.5-fold up or down-regulation are highlighted in red and gene symbols provided. Herein, pairwise comparisons investigating the effect of fibre diameter will be evaluated against 1000nm. The reasoning underpinning selection of 1000nm as the baseline comparison was two-fold (1) an electrospun scaffold for healthcare applications is currently under commercial development with fibre diameters of ~1000nm[311] and (2) a linear numerical scale, placing 300nm as the baseline, would have ignored the greater fibre direction variability observed for 300nm aligned, compared with all other aligned scaffolds (Figure 4-3E).

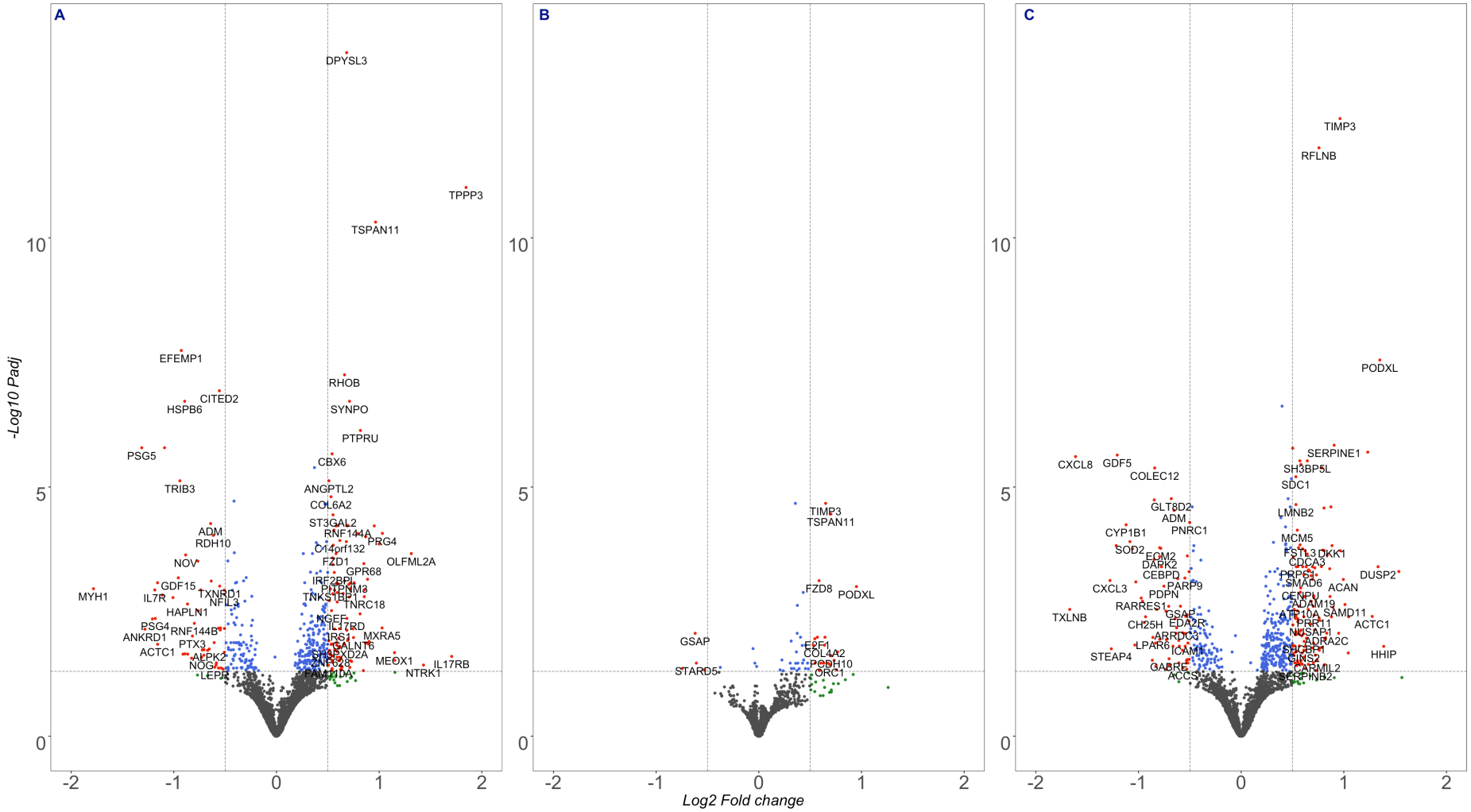

Figure 4-10 Volcano plot of differentially expressed genes for hamstring tendon fibroblasts seeded on aligned scaffolds. Pairwise analysis of aligned scaffolds with fibre diameters of 300nm(A), 2000nm(B) and 4000nm(C) compared with 1000nm aligned scaffolds. Dashed lines denote a false discovery rate (FDR) of 0.05 and a log2 Fold-change ± 0.5. Transcripts coloured red have passed the thresholds for FDR and log2 Fold-change criteria, blue only meet the FDR, green only the log2 Fold-change threshold, whilst for grey neither criteria are met.

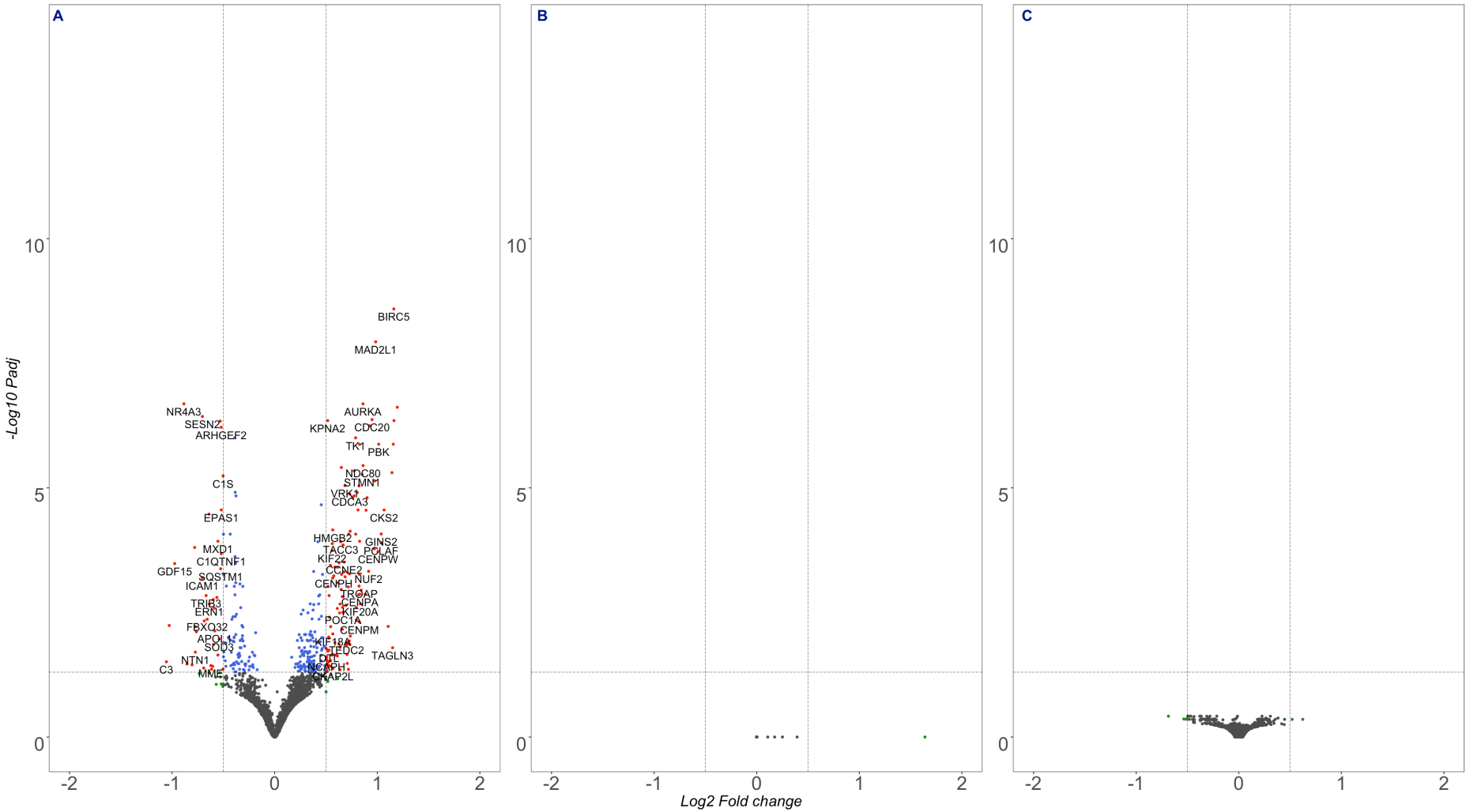

Figure 4-11 Volcano plot of differentially expressed genes for hamstring tendon fibroblasts seeded on random scaffolds. Pairwise analysis of aligned scaffolds with fibre diameters of 300nm(A), 2000nm(B) and 4000nm(C) compared with 1000nm aligned scaffolds. Dashed lines denote a false discovery rate (FDR) of 0.05 and a log2 Fold-change ± 0.5. Transcripts coloured red have passed the thresholds for FDR and log2 Fold-change criteria, blue only meet the FDR, green only the log2 Fold-change threshold, whilst for grey neither criteria are met.

4.6.9 Fibre anisotropy induces differential gene expression

Fibre directionality had the greatest influence on the gene expression of healthy tendon fibroblasts. The effect of fibre alignment was examined across four distinct fibre diameters and pairwise comparisons made between scaffolds with statistically comparable mean fibre diameters, but with aligned or random fibre configurations. A total of 874, 932 and 1263 genes displayed statistically significant differential expression between aligned and randomly orientated scaffolds with fibre diameters of 1000nm, 2000nm and 4000nm respectively (Figure 4-9). As illustrated by pairwise comparisons in figure 4-9 and the volcano plots in figure 4-12A, anisotropy had no significant effect on gene expression for scaffolds with a mean fibre diameter of 300nm.

4.6.10 Functional analysis using gene set enrichment

To profile the biological processes involved in the transcriptional response of healthy tendon fibroblasts to different scaffold microarchitectures, gene set enrichment analysis (GSEA) was performed. Initial GSEA of differentially expressed genes was undertaken using the Broad Institute's hallmark geneset collection[312] and is visualized in figures 4-13, 4-14 and 4-15. To determine which genes have the largest impact on the various biological processes being modulated by scaffold architecture, a leading-edge analysis of the differentially expressed genes was performed. Complete gene lists are available in appendix C-3.

Figure 4-13 shows the results of GSEA and leading-edge analysis for healthy tendon fibroblasts cultured on aligned electrospun scaffolds with variable mean fibre diameters. No enrichment was observed for fibroblasts cultured on 2000nm aligned, compared with 1000nm aligned scaffolds. Conversely, 4000nm aligned scaffolds induced an upregulation of genes involved in DNA and cellular replication (G2M checkpoint, mitotic spindle assembly, p53 pathway and E2F targets) and a downregulation of genes defining inflammatory responses and NFκB mediated TNF-α signalling. A similar pattern of enrichment was also observed for 300nm diameter random scaffolds (figure 4-14A). Comparison of 300nm aligned with 1000nm aligned scaffolds revealed that genes involved with protein synthesis and cellular metabolism

were downregulated, as indicated by the enrichment for mtorc1 signalling and hypoxia hallmark pathways.

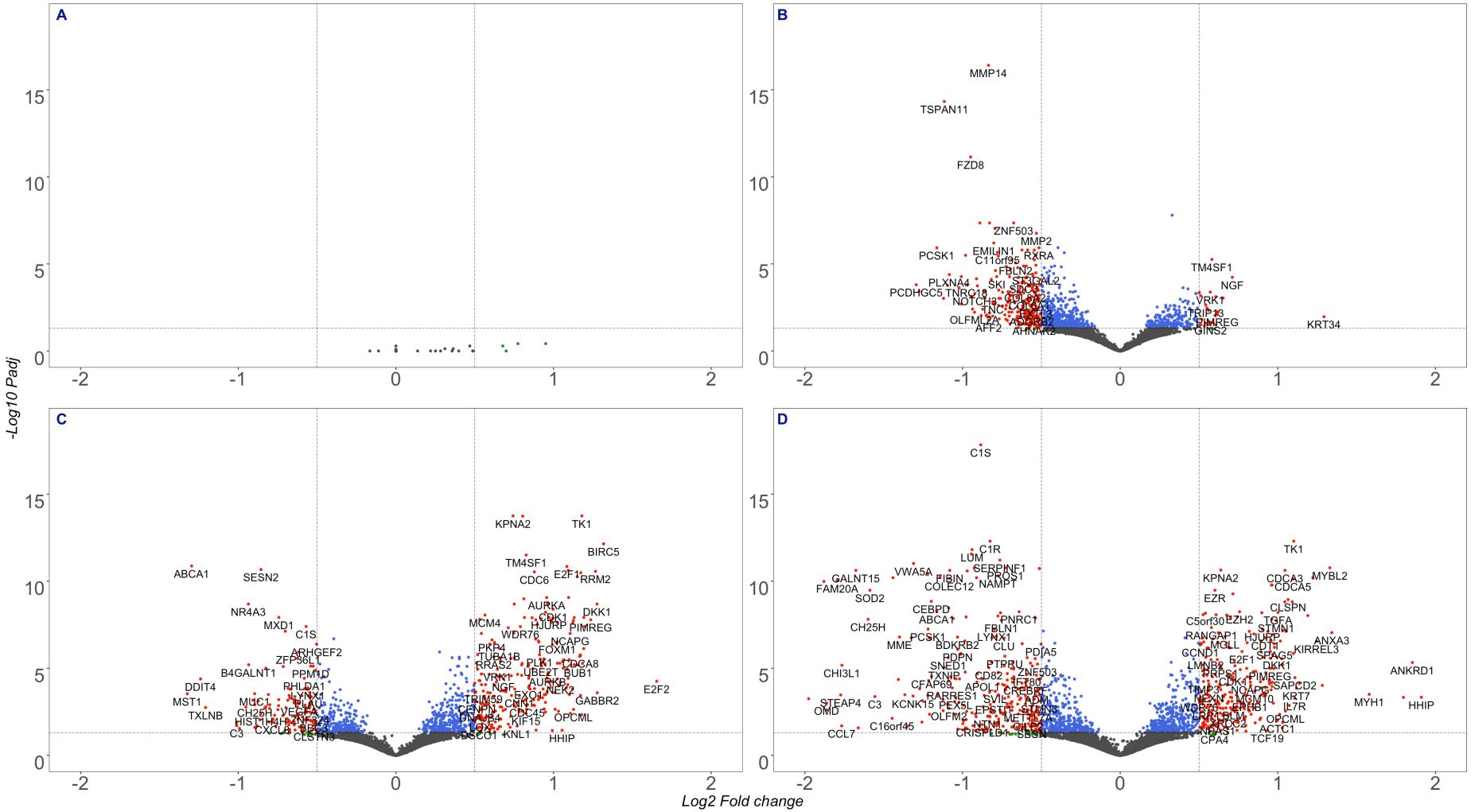

Figure 4-12 Volcano plot highlighting the effect of scaffold anisotropy on healthy tendon fibroblast gene expression. Pairwise analysis of scaffolds with aligned fibre directionality compared with random orientations, but with constant mean fibre diameters of 300nm(A), 1000nm (B), 2000nm(C) and 4000nm(D). Dashed lines denote a false discovery rate (FDR) of 0.05 and a log2 Fold-change ± 0.5. Transcripts coloured red have passed the thresholds for FDR and log2 Fold-change criteria, blue only meet the FDR, green only the log2 Fold-change threshold, whilst for grey neither criteria are met.

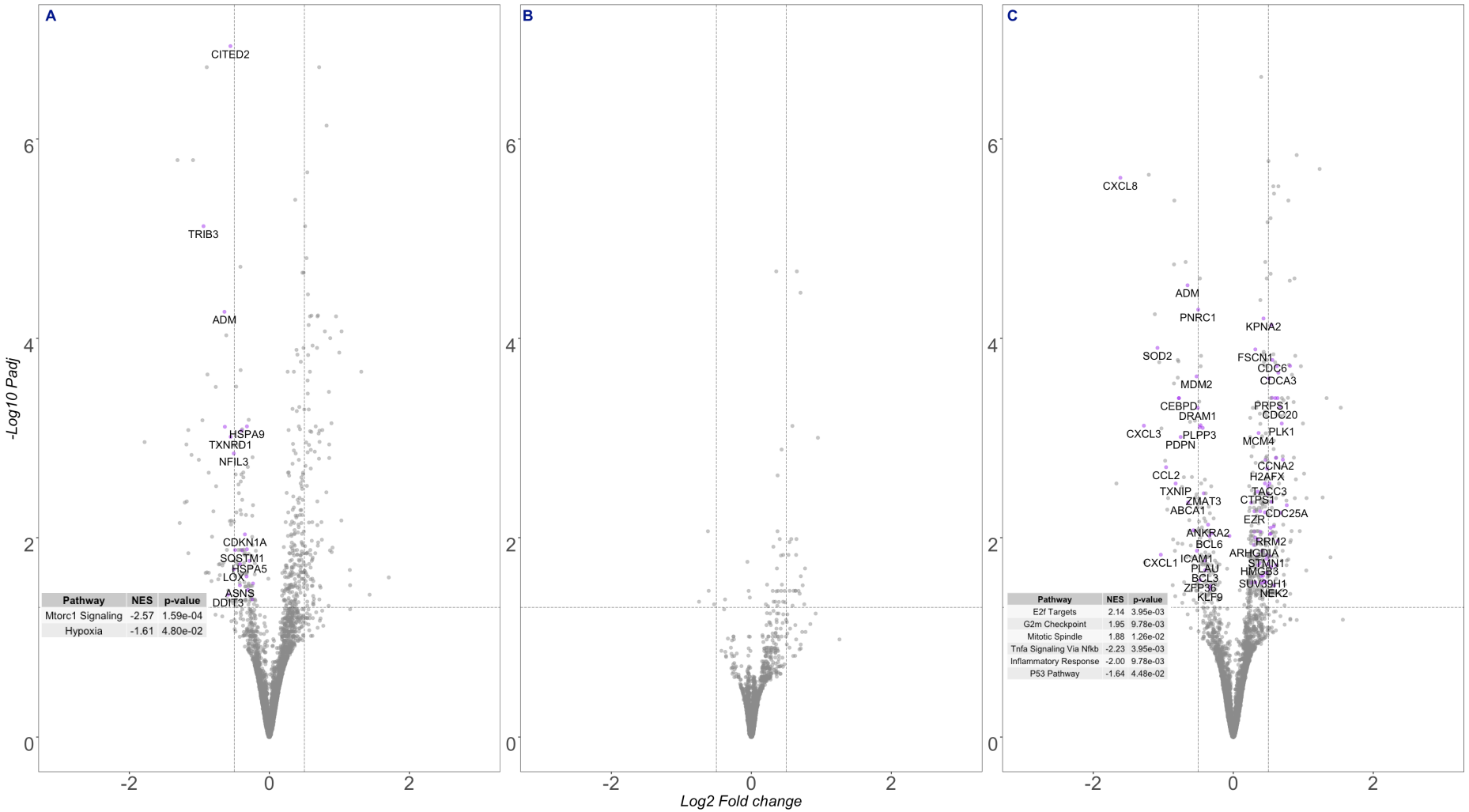

Figure 4-13 Volcano plots showing enriched hallmark pathways and leading-edge analysis for hamstring tendon fibroblasts seeded on aligned scaffolds. Pairwise analysis of aligned scaffolds with fibre diameters of 300nm(A), 2000nm(B) and 4000nm(C) compared with 1000nm aligned scaffolds. Hallmark pathways with significant enrichment are listed in the summary table associated with each plot. Points highlighted in purple with associated gene symbols represent genes with the greatest contribution to the enriched gene sets.

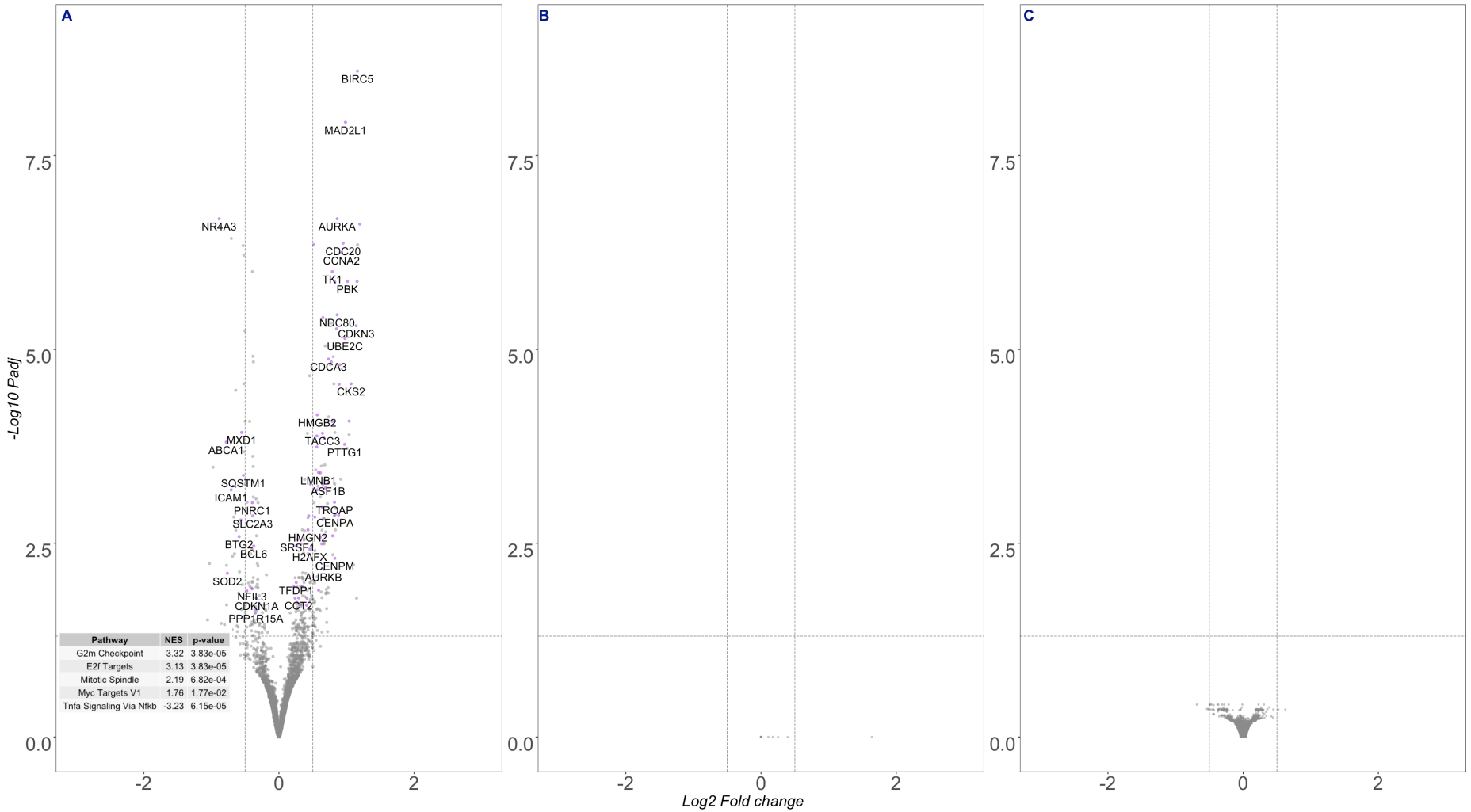

Figure 4-14 Volcano plots showing enriched hallmark pathways and leading-edge analysis for hamstring tendon fibroblasts seeded on random scaffolds. Pairwise analysis of aligned scaffolds with fibre diameters of 300nm(A), 2000nm(B) and 4000nm(C) compared with 1000nm random scaffolds. Hallmark pathways with significant enrichment are listed in the summary table associated with each plot. Points highlighted in purple with associated gene symbols represent genes with the greatest contribution to the enriched gene sets.

The transcriptional response to anisotropy was similar for fibre diameters of 1000nm or larger, but with a more profound effect at 2000 and 4000nm (Figure 4-15B-D). Relative to their randomly orientated counterparts, aligned scaffolds with diameters ≥1000nm downregulated genes involved in inflammation (Inflammatory response, NFκB signalling) and immunomodulation (INF-ɣ response and complement synthesis), whilst upregulating hallmark genesets involved in DNA replications and cell-growth (E2F targets, G2M checkpoint, myc targets).

4.6.11 Micro-architecture influences activation status of healthy tendon fibroblasts

Aligned scaffolds with diameters ≥1000nm were associated with spindle shaped fibroblast morphologies and a downregulation of inflammation associated transcripts. Given the association of spindle morphology and inflammatory phenotype with fibroblast activation this raised the possibility that certain micro-architecture can modify fibroblast activation status. Figures 4-16 and 4-17 show the effect of scaffold diameter and anisotropy on the differential gene expression of these fibroblast activation markers; *PDPN*, *CD248*, *VCAM1*, *CD90/THY1* and *FAP*. Interestingly, aligned scaffolds with diameter ≥1000nm, that induced a downregulation of inflammatory transcripts, also demonstrated a significant reduction in the gene expression of *PDPN* or CD248.

To further explore the influence of scaffold micro-architecture on the activation status of healthy fibroblasts we undertook a more focussed interrogation of the transcriptomic signatures, focusing on angiogenesis as well as other biological processes known to be associated with fibroblast activation, namely; extracellular matrix synthesis, chemokine and cytokine production, immune cell recruitment and modification of tissue architecture though changes to their cytoskeletal apparatus.[313,314] When anisotropy was controlled, fibre diameter did not alter the enrichment of genes involved in the regulation of angiogenesis. Conversely, when anisotropy was varied, only scaffolds with 1000nm aligned fibres demonstrated a weak reduction in genes associated with the GeneOntology angiogenesis geneset (GO:0001525), relative to 1000nm random scaffolds (Appendix C Figure C-5 and Table C-5.1).

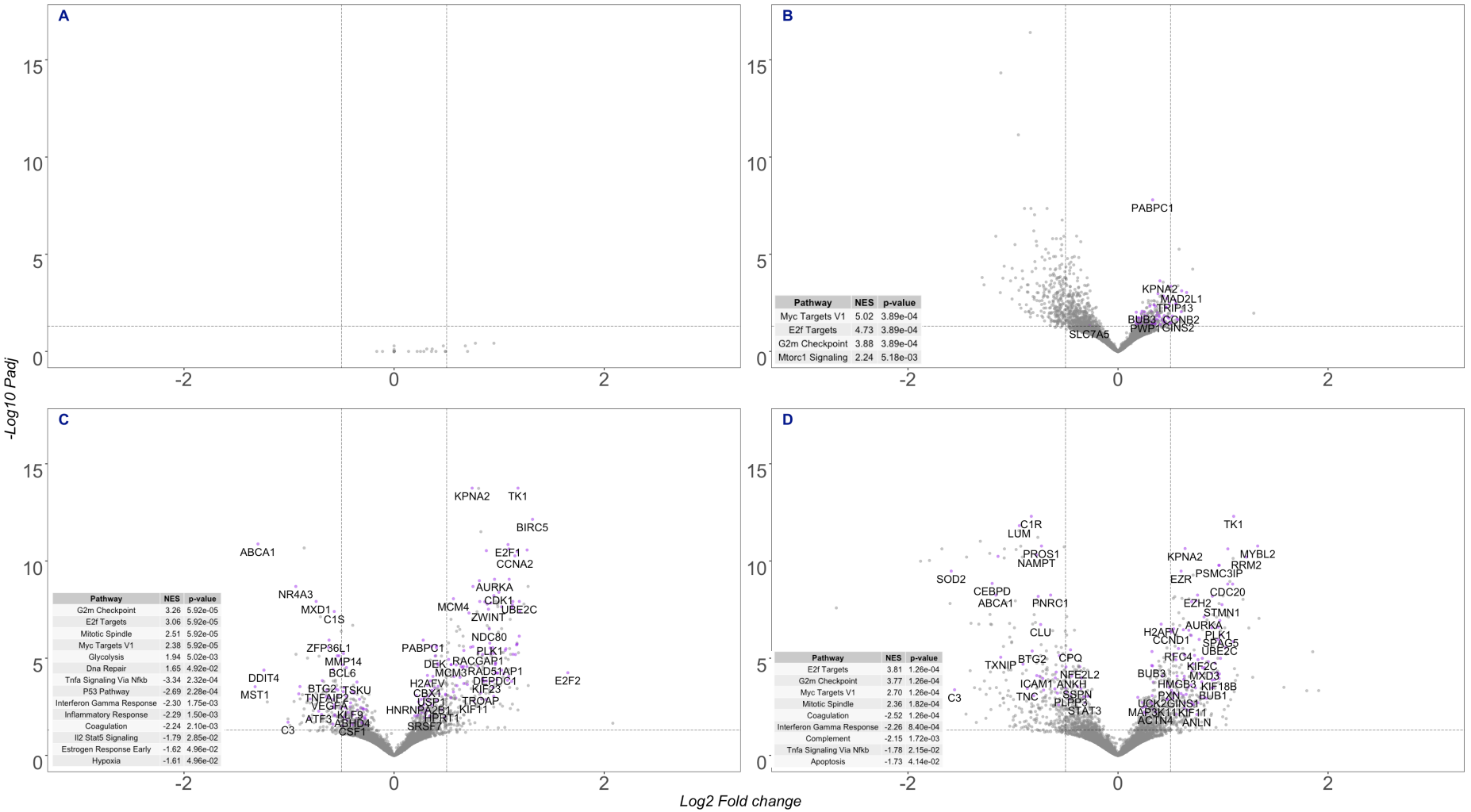

Figure 4-15 Volcano plots showing enriched hallmark pathways and leading-edge analysis for hamstring tendon fibroblasts seeded on anisotropic scaffolds. Pairwise analysis of scaffolds with aligned fibre directionality compared with random orientations but with constant mean fibre diameters of 300nm(A), 1000nm(B), 2000nm(C) and 4000nm(D). Hallmark pathways with significant enrichment are listed in the summary table associated with each plot. Points highlighted in purple with associated gene symbols represent genes with the greatest contribution to the enriched gene sets (Leading-edge analysis).

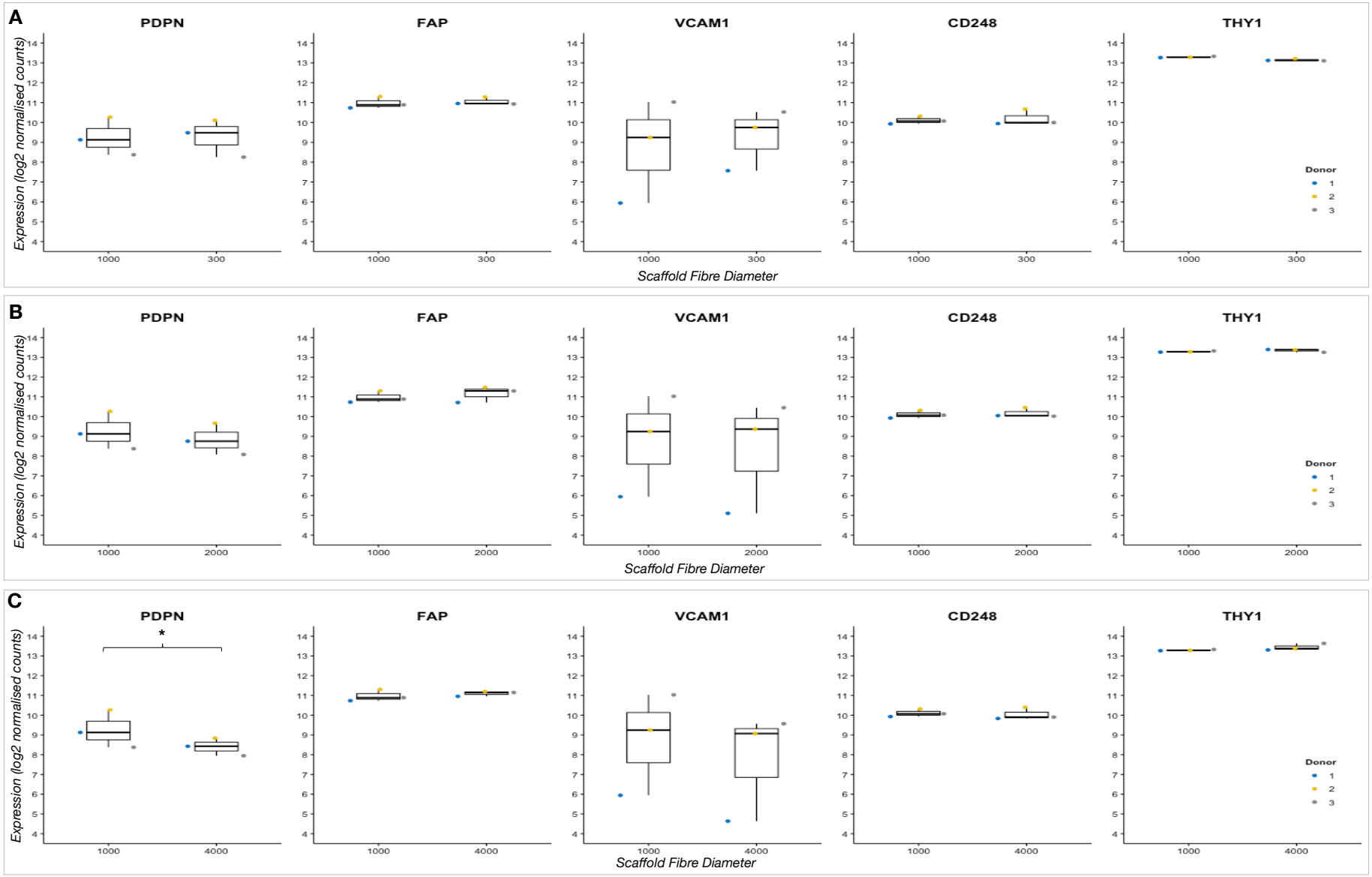

Figure 4-16 Effect of fibre diameter on gene expression of fibroblast activation markers for healthy tendon fibroblasts seeded on aligned PDO scaffolds (A) PDO scaffold with fibres of 300nm diameter in an aligned configuration compared with 1000nm aligned configuration. (B) 2000nm aligned vs 1000nm aligned (C) 4000nm aligned vs 1000nm aligned. *Denotes p-adjusted (Benjamini-Hochberg correction) value of <0.05. Expression values represent normalised count data transformed to a log2 scale.

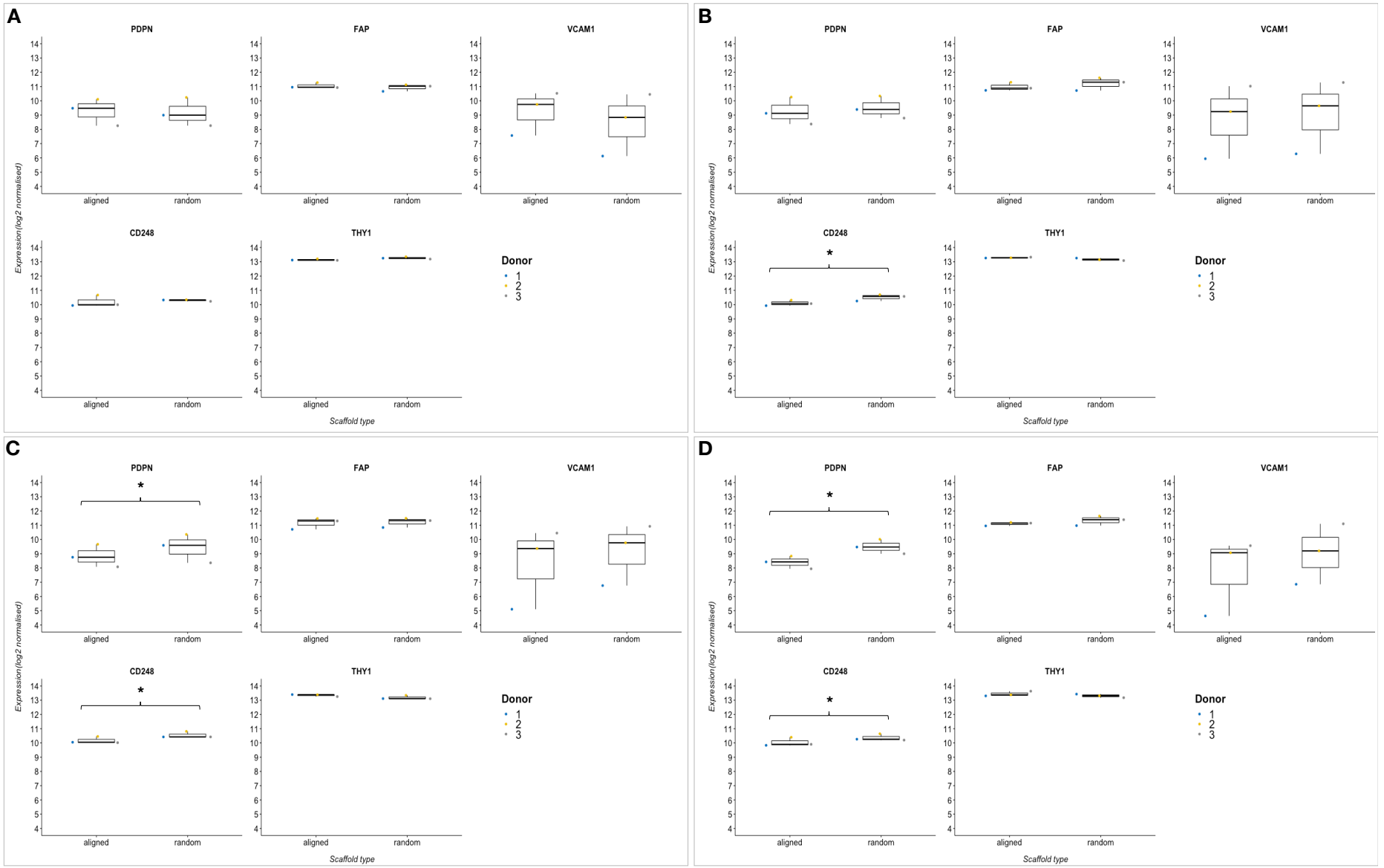

Figure 4-17. Effect of fibre anisotropy on gene expression of fibroblast activation markers for healthy tendon fibroblasts. (A) PDO scaffold with fibres of 300nm diameter in an aligned configuration compared with 300nm random configuration. (B) 1000nm aligned vs 1000nm random (C) 2000nm aligned vs 2000nm random (D) 4000nm aligned vs 4000nm random. *Denotes p-adjusted (Benjamini-Hochberg correction) value of <0.05. Expression values represent normalised count data transformed to a log2 scale.

For aligned fibres with a diameter of 4000nm, relative to 1000nm aligned scaffolds, there was a positive enrichment of genesets for cytoskeletal organisation (GO:0005856, GO:0015629, GO:0030036), a downregulation of genes involved with immune system regulation (GO:0002684, GO:0002682) and no enrichment for any genesets describing the regulation of chemokine or cytokine production and activity (Figure 4-18). Conversely, for randomly orientated scaffolds a similar pattern was seen but in response to smaller fibres diameters. Relative to 1000nm, healthy tendon fibroblasts cultured on 300nm randomly orientated scaffolds, upregulated multiple genes responsible for cytoskeletal assembly (GO:0015630, GO:0000226, GO:0030036**,** GO:0005856, GO:0051493-4) and downregulated those associated with cytokine (GO:0001817) and immune system regulation (GO:0002682, GO:0002684, GO:0050776) (Figure 4-19).

Finally, fibre alignment had a consistent effect on genes controlling extracellular matrix production (GO:0044420, GO:0031012,GO:0005578) (Figure 4-20), with a downregulation of genesets involved in immune regulation (GO:0002682-4, GO:0050776-7,GO:0002697) also observed for the larger diameter, 2000nm and 4000nm, aligned scaffolds (Figure 4-21). However, alignment had a limited effect on genes involved in cytokine production (Appendix Figure C-6).

4.6.12 Diseased tendon fibroblasts display significant transcriptomic differences, are activated and respond to changes in electrospun scaffold micro-architecuture

Compared with healthy fibroblasts isolated from hamstring tendon, fibroblasts isolated from massive rotator cuff tears showed a dramatically different transcriptional profile, with a total of 4913 genes differentially upregulated and 4959 genes downregulated. In keeping with previous work[46], the markers of stromal activation including *PDPN*, *FAP*, *VCAM1* and *CD248* were all significantly upregulated by fibroblasts from diseased tendon, but no differences were detected in the expression of *THY1* (Figure 4-22). In healthy, hamstring derived fibroblasts, the reduced expression of these markers also corresponded to a downregulation of the hallmark pathways describing inflammatory responses including NFκb mediated TNF-α signalling and STAT3 mediated IL-6 signalling.

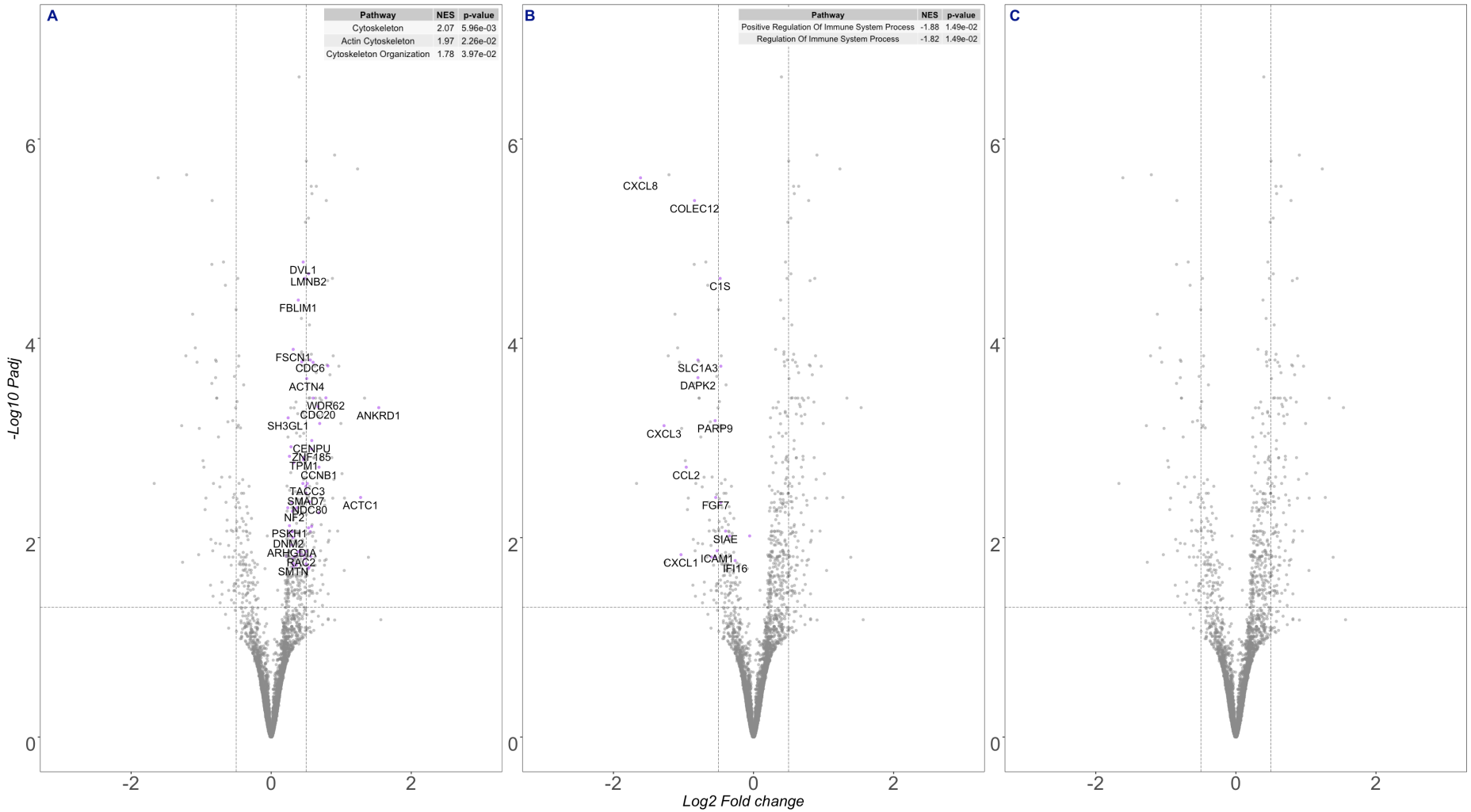

Figure 4-18 Volcano plots showing enriched genesets and leading-edge analysis for hamstring tendon fibroblasts seeded on 4000nm aligned scaffolds. Pairwise analysis of 4000nm aligned scaffolds compared with aligned scaffolds with fibre diameters of 1000nm. Genesets describe extracellular matrix production and/or cytoskeleton apparatus(A), regulation of immune system(B) and cytokine/chemokine production or activity (C). Genesets with significant enrichment are listed in the summary table associated with each plot. Points highlighted in purple with associated gene symbols represent genes with the greatest contribution to the enriched gene sets.

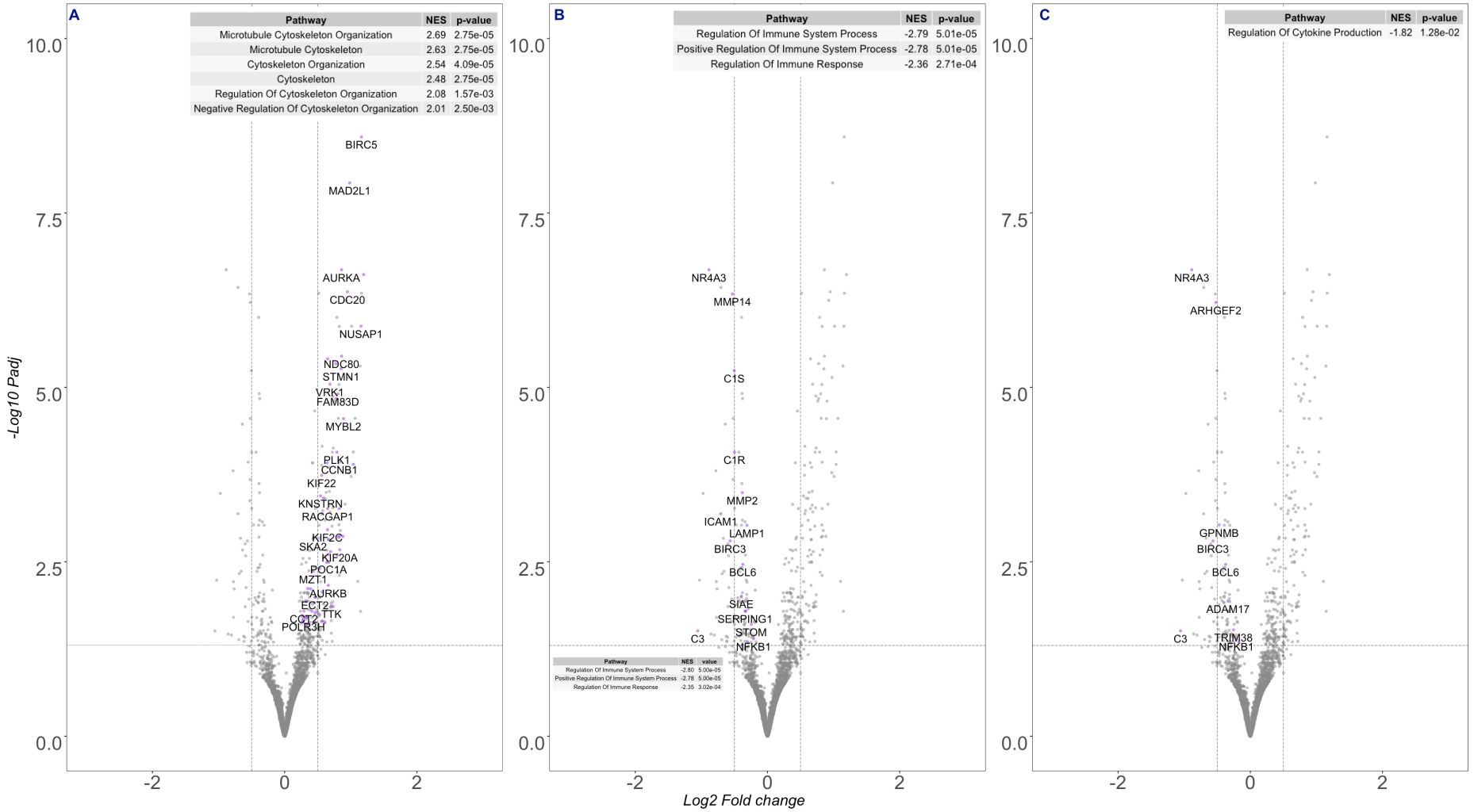

Figure 4-19 Volcano plots showing enriched genesets and leading-edge analysis for hamstring tendon fibroblasts seeded on 300nm random scaffolds. Pairwise analysis of 300nm random scaffolds compared with random scaffolds with fibre diameters of 1000nm. Genesets describe extracellular matrix production and/or cytoskeleton apparatus(A), regulation of immune system(B) and cytokine/chemokine production or activity (C). Genesets with significant enrichment are listed in the summary table associated with each plot. Points highlighted in purple with associated gene symbols represent genes with the greatest contribution to the enriched gene sets.

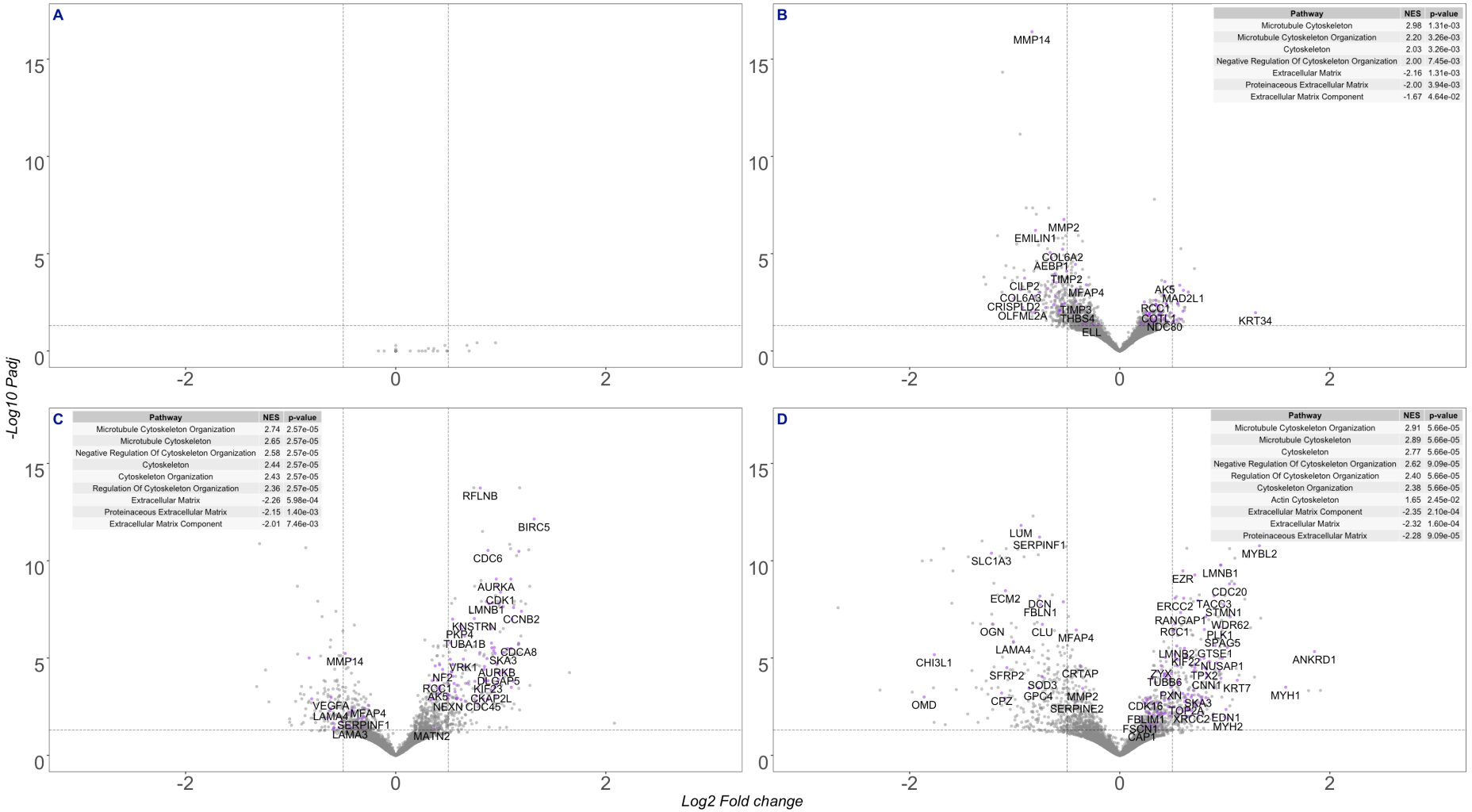

Figure 4-20 Volcano plots showing enriched extracellular matrix/cytoskeleton genesets and leading-edge analysis for hamstring tendon fibroblasts seeded on anisotropic scaffolds. Pairwise analysis of scaffolds with aligned fibre directionality compared with random orientations but with constant mean fibre diameters of 300nm(A), 1000nm(B), 2000nm(C) and 4000nm(D). Significant enrichment of geneset that describe cytokoskejletal organisation or extracellular matrix production are listed in the summary table associated with each plot. Points highlighted in purple with associated gene symbols represent genes with the greatest contribution to the enriched gene sets (Leading-edge analysis).

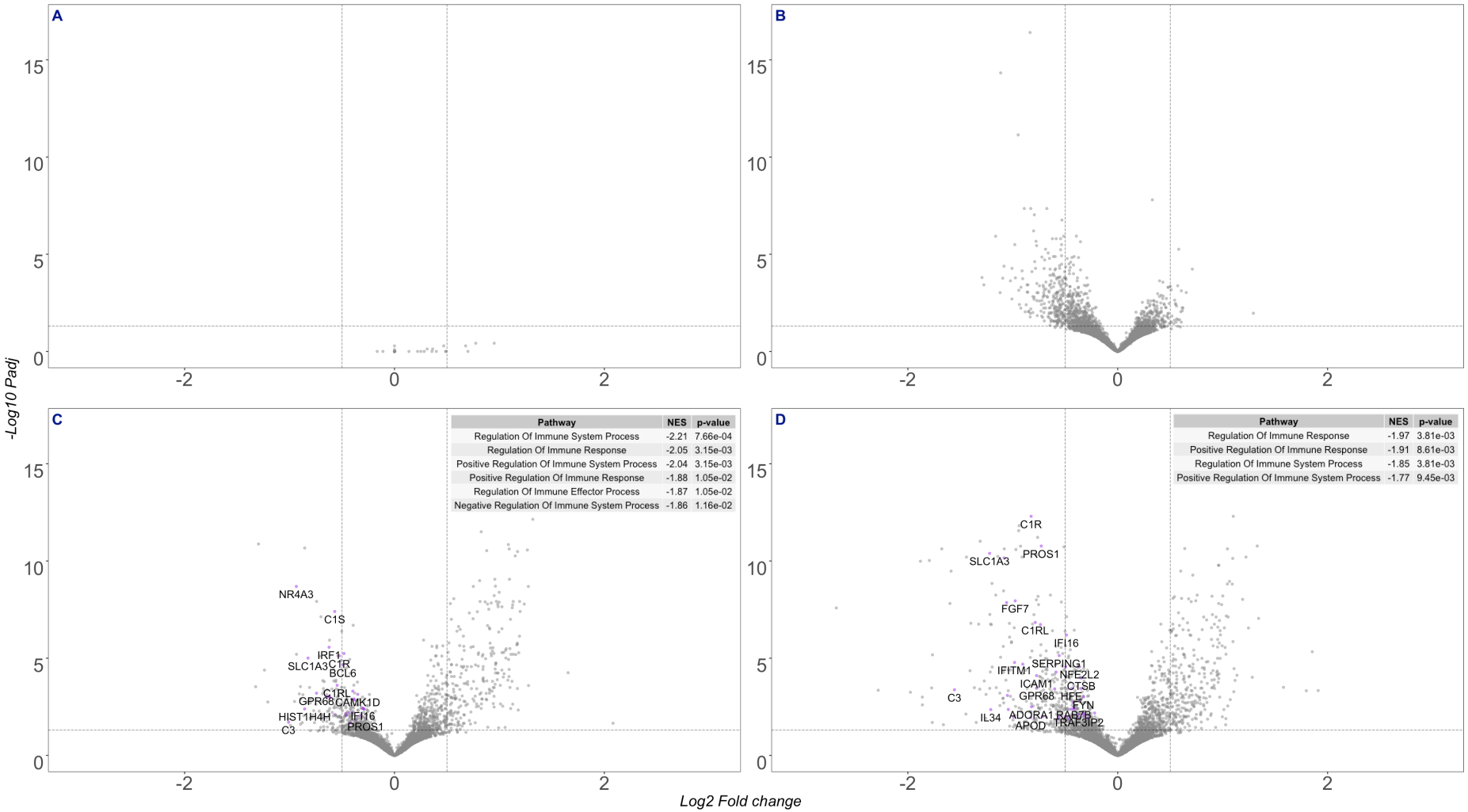

Pathway	NES	p-value
Regulation Of Immune System Process	-2.21	7.66e-04
Regulation Of Immune Response	-2.05	3.15e-03
Positive Regulation Of Immune System Process	-2.04	3.15e-03
Positive Regulation Of Immune Response	-1.88	1.05e-02
Regulation Of Immune Effector Process	-1.87	1.05e-02
Negative Regulation Of Immune System Process	-1.86	1.16e-02

Pathway	NES	p-value
Regulation Of Immune Response	-1.97	3.81e-03
Positive Regulation Of Immune Response	-1.91	8.61e-03
Regulation Of Immune System Process	-1.85	3.81e-03
Positive Regulation Of Immune System Process	-1.77	9.45e-03

Figure 4-21 Volcano plots showing enriched immune genesets and leading-edge analysis for hamstring tendon fibroblasts seeded on anisotropic scaffolds. Pairwise analysis of scaffolds with aligned fibre directionality compared with random orientations but with constant mean fibre diameters of 300nm(A), 1000nm(B), 2000nm(C) and 4000nm(D). Significant enrichment of genesets that describe immune system regulation are listed in the summary table associated with each plot. Points highlighted in purple with associated gene symbols represent genes with the greatest contribution to the enriched gene sets (Leading-edge analysis).

Relative to their diseased counterparts, hamstring derived fibroblasts also demonstrated a downregulation of genes involved in cytokine production (GO:0004896, GO:0036119, GO:0001819, GO:0001817) extracellular matrix assembly (GO:0005578, GO:0031012) and immune system regulation (GO:0045824, GO:0010743, GO:0032675, GO:0045088, GO:0050776) (Figure 4-23).

Differences between healthy and diseased fibroblasts tenocytes is clearly highlighted by the principle component analysis (Figure 4-24) in which PC1, accounting for 60% of the total variance, correlated with tissue type. Mirroring the response observed for hamstring fibroblasts, scaffold micro-architecture influenced the transcriptional profile of tendon fibroblasts from diseased tendons. This was most clearly seen in the fourth principle component with a trend towards separation of aligned scaffolds with diameters 2000nm and 4000nm from the remaining architectures (Figure 4-24B and Appendix C-8).

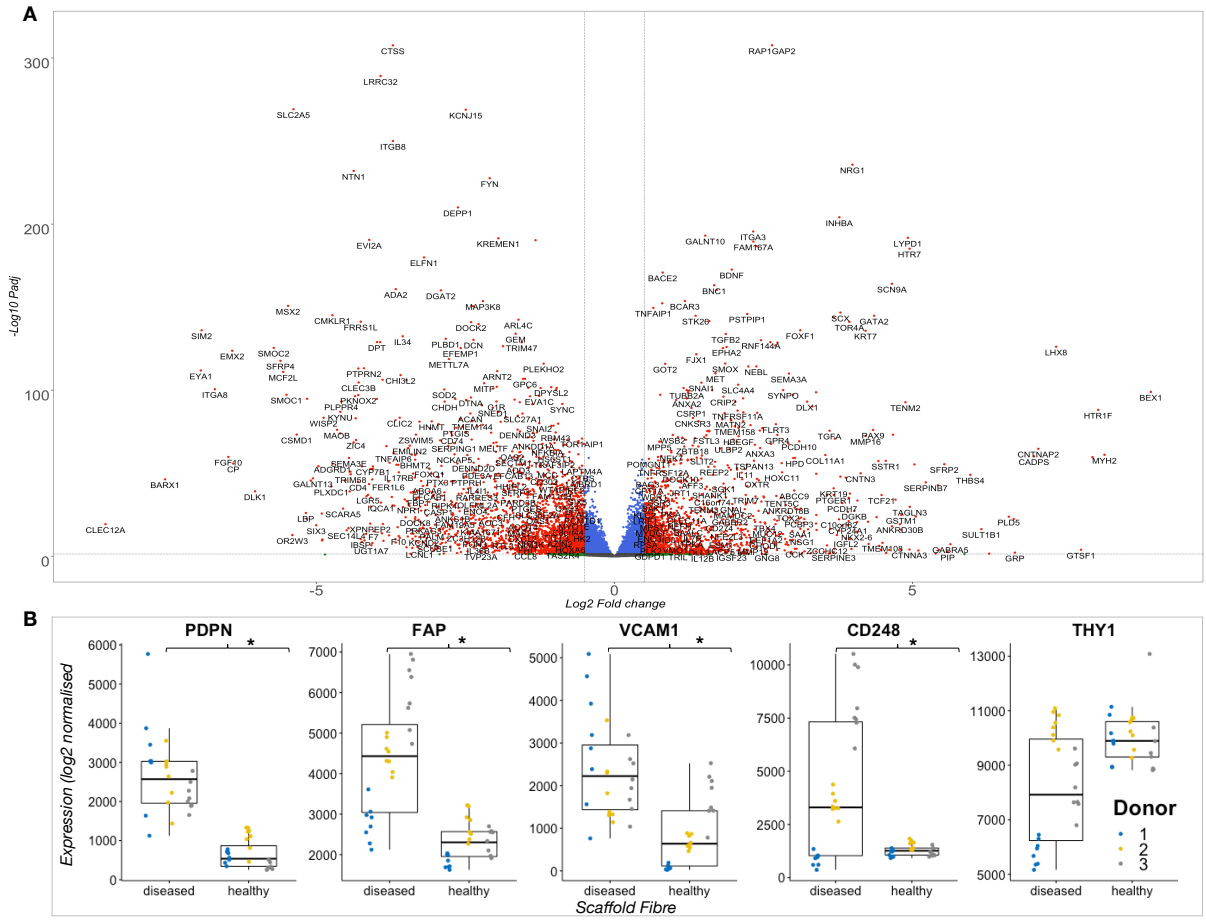

Figure 4-22 Baseline differences in expression between healthy compared with diseased tenocytes (A) Volcano plot, transcripts with logarithmic fold changes greater than 1 and p-adjusted value (Benjamini-Hochberg correction) value of <0.05 are highlighted in red and transcript names provided (B) Boxplots demonstrating the effect of disease status on the expression of fibroblast markers. *Denotes p-adjusted (Benjamini-Hochberg correction) value of <0.05. Expression values represent normalised count data transformed to a log2 scale.

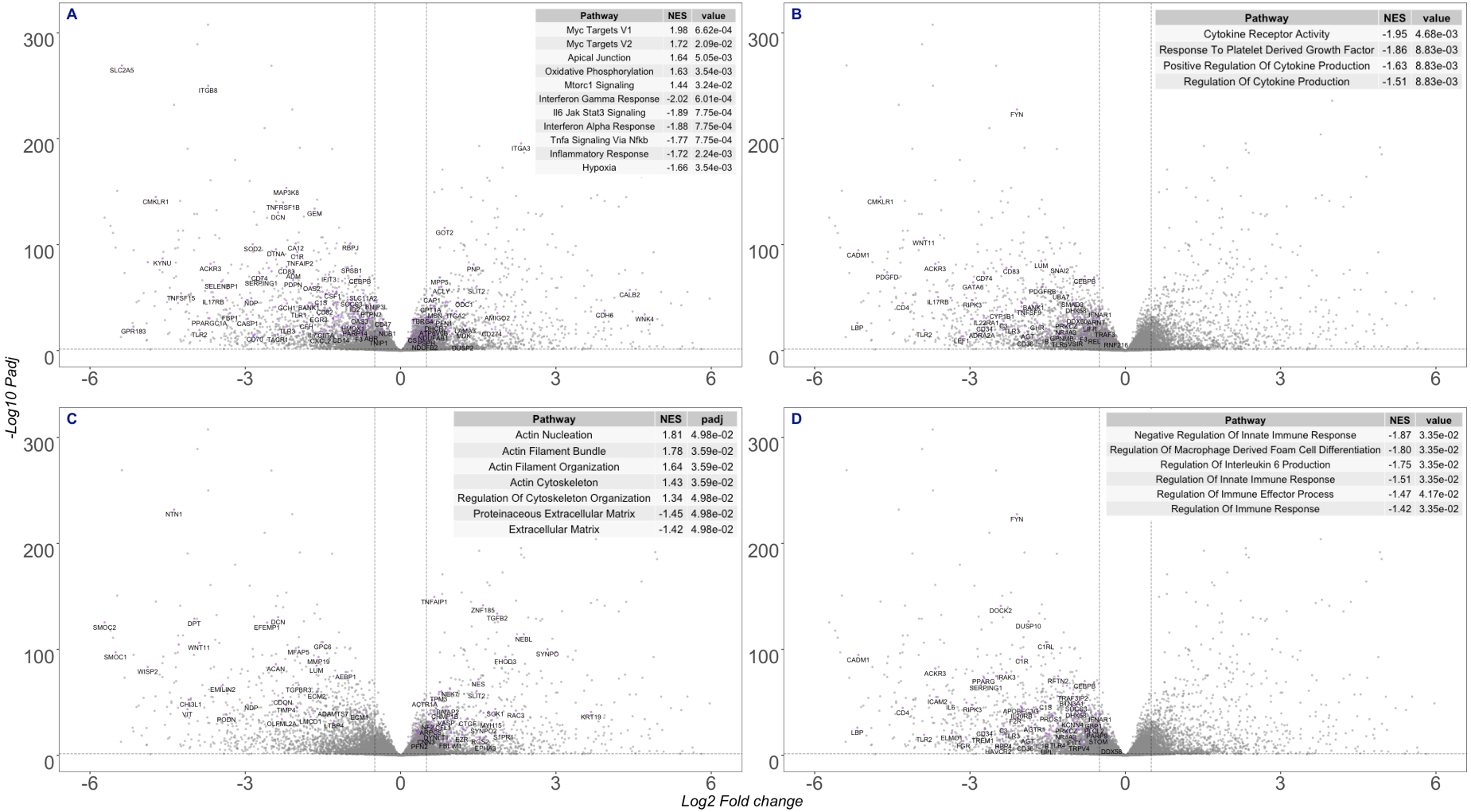

Figure 4-23 Volcano plots showing enriched genesets and leading-edge analysis for healthy compared with diseased fibroblasts. Comparison of transcriptional profile of healthy human hamstring derived tendon fibroblasts with diseased tendon fibroblasts isolated from massive rotator cuff tears. Significant enrichment of genesets that describe hallmark pathways (A), cytokine/chemokine production (B), cytoskeletal and extracellular matrix assembly (C) and immune system regulation (D) are listed in the summary table associated with each plot. Points highlighted in purple with associated gene symbols represent genes with the greatest contribution to the enriched gene sets (Leading-edge analysis).

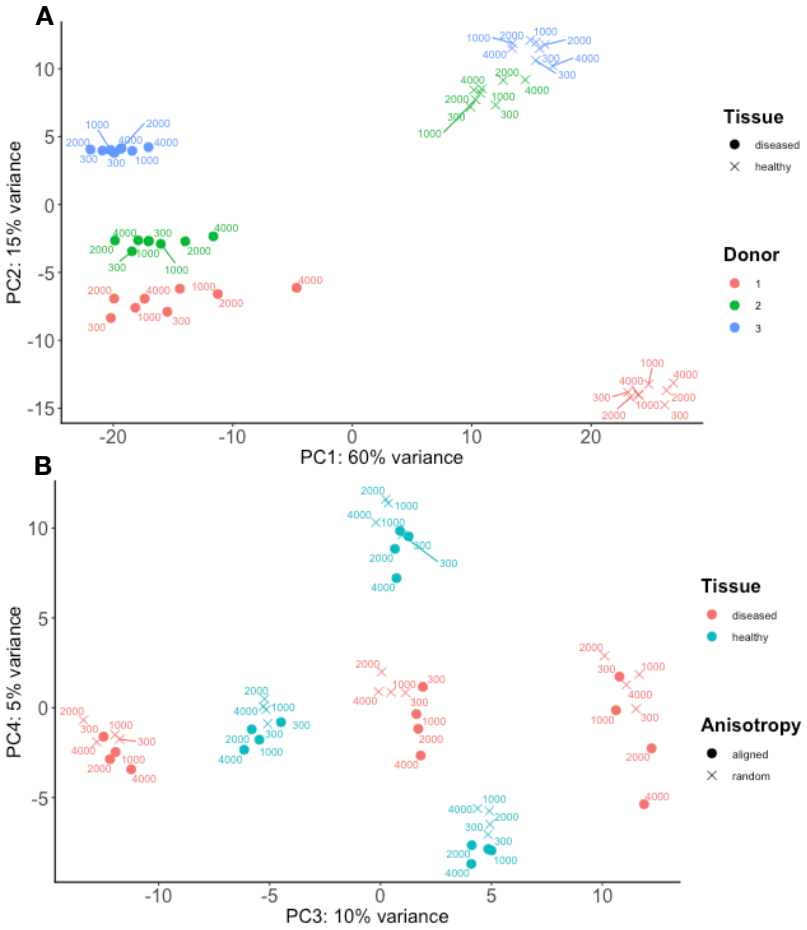

Figure 4-24 Principle component analysis (PCA) of healthy and diseased tendon fibroblasts. Log transformed expression data from all 48 RNA samples sequenced from healthy hamstring fibroblasts and diseased rotator cuff derived fibroblasts seeded onto 8 different electrospun scaffolds. Separation of the samples according to the 1st and 2nd principles components (A), and the 3rd and 4th principle components (B)

4.6.13 The fibre diameter of aligned scaffolds can regulate the activation status of diseased tendon fibroblasts, which are primed to respond

For scaffolds with randomly orientated fibres the manipulation of fibre diameter had a limited effect on the gene expression of fibroblasts from diseased tendons (Appendix C Figure C-9). Conversely, when compared to 1000nm aligned scaffolds a total of 3187 and 352 genes were differentially regulated by 300nm and 4000nm aligned scaffolds respectively (Figures 4-25 and 4-26). At 4000nm, GSEA demonstrated a similar pattern of response as that observed for fibroblasts from healthy tendons (Figure 4-27). This contrasted sharply with the response of fibroblasts from diseased tendons cultured on aligned 300nm scaffolds which, relative to 1000nm aligned scaffolds, demonstrated an opposing response (Figure 4-28). Inflammatory hallmark pathways (Inflammatory response, IL-6 response via stat3, IFN-ɣ response and IFN-α response) were positively enriched, but cell cycle related pathways (DNA repair, mitotic spindle) were negatively enriched. A corresponding enrichment for genesets describing

extracellular matrix production (GO:0005578, GO:0031012, GO:0044420, GO:0022011) and angiogenesis (GO:0001525) was also observed.

The polarising effect of fibre diameter on fibroblast phenotype was also reflected in the expression of fibroblast activation markers (Figure 4-29). Relative to cells cultured on 1000nm aligned scaffolds, there was an upregulation of *VCAM1* and *PDPN* for fibroblasts from diseased tendon cultured on 300nm aligned scaffolds, but a significant downregulation of *VCAM1* when cultured on 4000nm aligned scaffolds. *PDPN* expression also appeared to trend downwards but failed to reach significance.

Compared with healthy tendon fibroblasts, fibroblasts from diseased rotator cuff were primed to respond to 300nm aligned scaffolds, with a far greater transcriptional response observed for all pairwise comparisons of diseased fibroblasts seeded on 300nm aligned scaffolds (Figures 4-9 and 4-25).

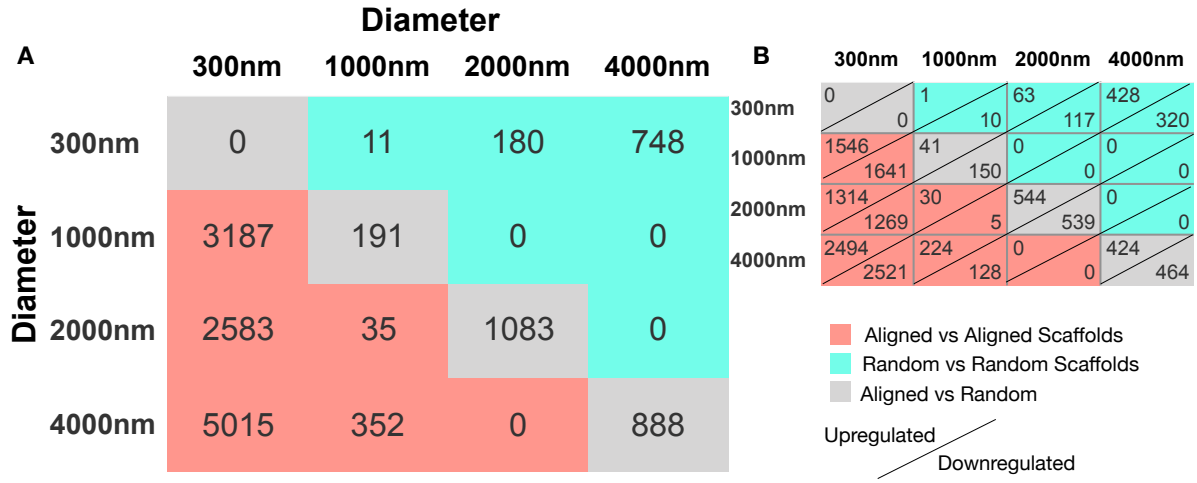

Figure 4-25 Scaffold-by-scaffold comparison of differentially expressed genes between diseased rotator cuff tendon fibroblasts cultured on scaffolds of different microarchitectures. A pairwise comparison of different fibre diameters is provided for both aligned (pink boxes) and random (blue boxes) scaffolds (A). Grey boxes denote a comparison of aligned vs random scaffolds for the fibre diameters 300,1000,2000 and 4000 nm. Differential expression has also been split into the number of unregulated and downregulated genes (B). The threshold for differential expression was set at an adjusted p-value (Benjamini-Hochberg correction) of <0.05.

4.6.14 Scaffold anisotropy regulates the activation status of diseased tendon fibroblasts but not their angiogenic activity

The effect of anisotropy was most clearly seen for scaffolds with 2000nm and 4000nm target fibre diameters (Figure 4-30), closely mirroring the previously observed response for hamstring tendon fibroblasts and echoing the findings of the principle component analysis (Appendix C

figure C-10). Relative to scaffolds with matched diameters but randomly orientated fibres, a total of 191, 1083 and 888 genes were differentially regulated in diseased rotator cuff tendon fibroblast cultured for 7 days on 1000nm, 2000nm and 4000nm aligned scaffolds respectively (Figure 4-25).

At fibre diameters above 1000nm, aligned fibres produced a significant downregulation of the fibroblast activation markers *PDPN* and *VCAM1* in fibroblasts from diseased tendon (Figure 4-31). This was again reflected in the overall transcriptomic response, with GSEA demonstrating a downregulation of inflammatory hallmark pathways (Inflammatory response, IL-6 via STAT3 signalling, TNF-α via NFκB signalling, IFN-ɣ response), extracellular matrix assembly (GO:0005578, GO:0031012, GO:0044420) and immune system regulation (GO:0002682-4). An effect on cytokine production was only observed for 2000nm aligned compared with 2000nm random scaffolds (GO:005125, GO:0019955, GO: 0001817, GO:0001819) and anisotropy had no effect on angiogenic biological pathways (Figures 4-32 and 4-33).

4.6.15 PDPN surface expression on activating and resolving scaffolds

To validate the RNA sequencing findings, the surface expression of PDPN on diseased tendon fibroblasts, cultured on 300nm aligned and 4000nm aligned scaffolds, was assessed (Figure 4-34). When compared with 4000nm aligned scaffolds, diseased tenocytes cultured on 300nm aligned displayed an increased surface expression of PDPN – closely mirroring the effect previously observed for fibre diameter at the mRNA level.

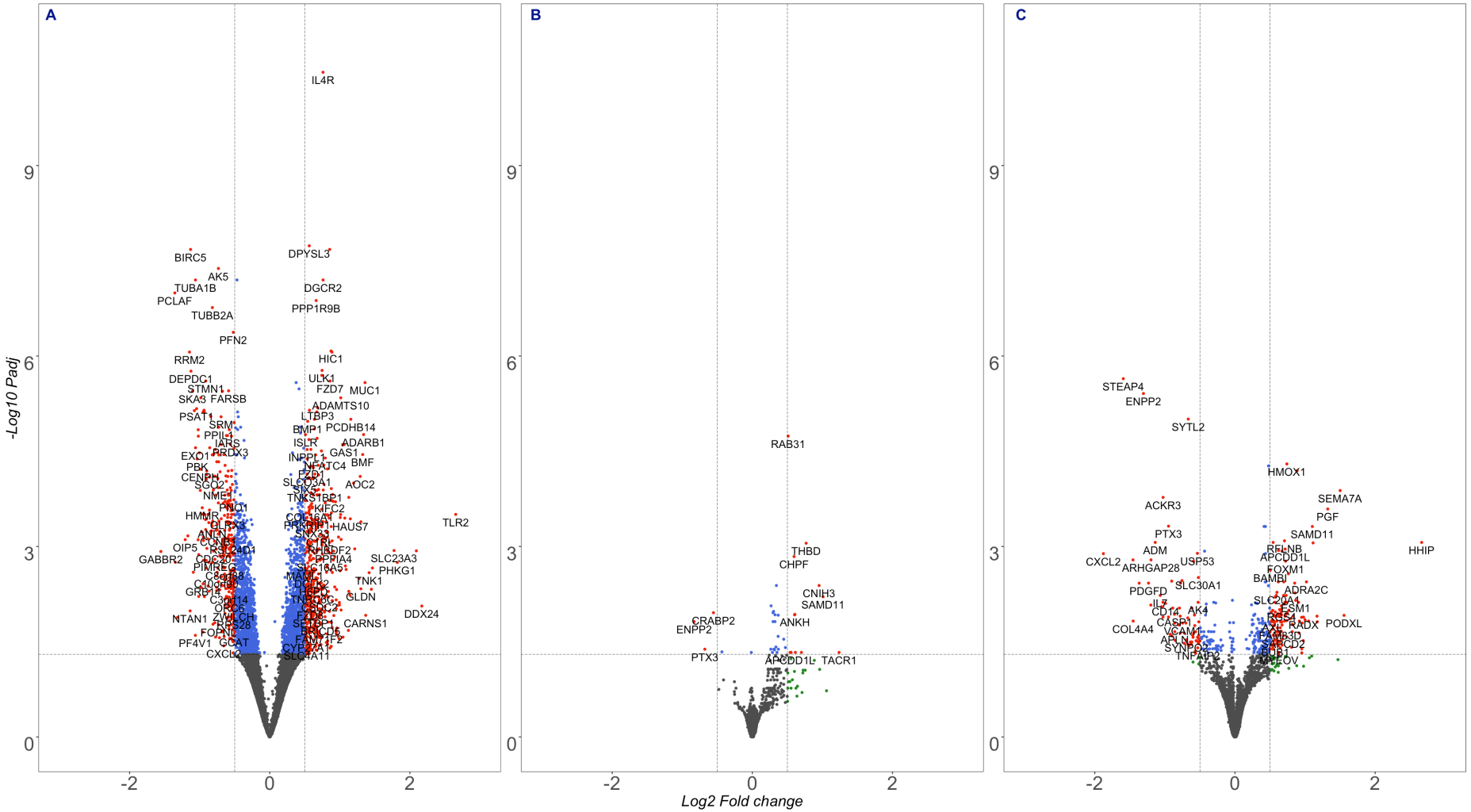

Figure 4-26 Volcano plot of differentially expressed genes for diseased rotator cuff tendon fibroblasts seeded on aligned scaffolds. Pairwise analysis of aligned scaffolds with fibre diameters of 300nm(A), 2000nm(B) and 4000nm(C) compared with 1000nm aligned scaffolds. Dashed lines denote a false discovery rate (FDR) of 0.05 and a log2 Fold-change ± 0.5. Transcripts coloured red have passed the thresholds for FDR and log2 Fold-change criteria, blue only meet the FDR, green only the log2 Fold-change threshold, whilst for grey neither criteria are met.

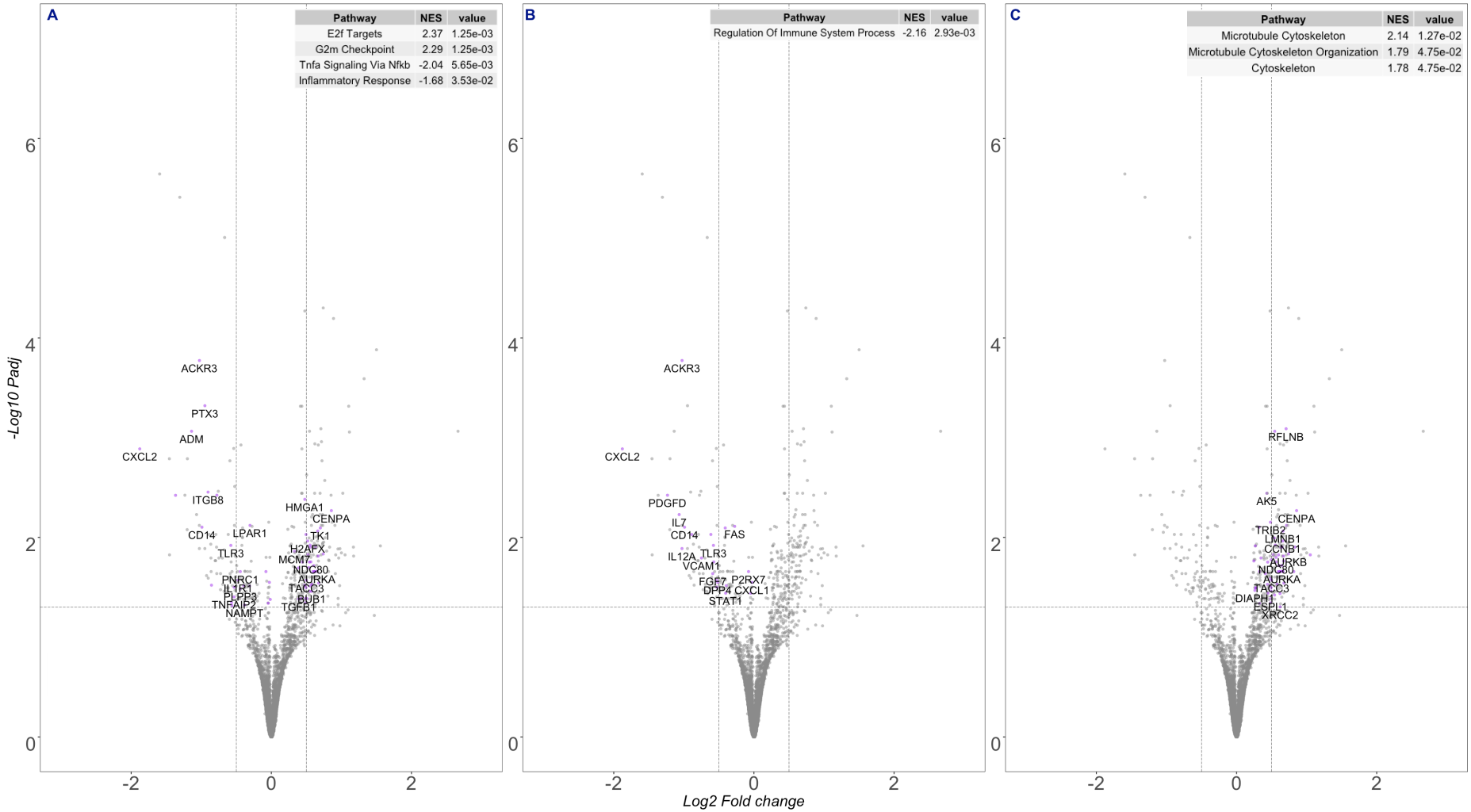

Figure 4-27 Volcano plots showing enriched genesets and leading-edge analysis for diseased rotator cuff tendon fibroblasts seeded on 4000nm aligned scaffolds. Pairwise analysis of 4000nm aligned scaffolds compared with aligned scaffolds with fibre diameters of 1000nm. Significant enrichment of Hallmark pathways (A) genesets describing cytokine/ chemokine production or activity (B) and extracellular matrix production and/or cytoskeleton apparatus(C). Hallmarkpathways or Genesets with significant enrichment are listed in the summary table associated with each plot. Points highlighted in purple with associated gene symbols represent genes with the greatest contribution to the enriched gene sets (leading edge).

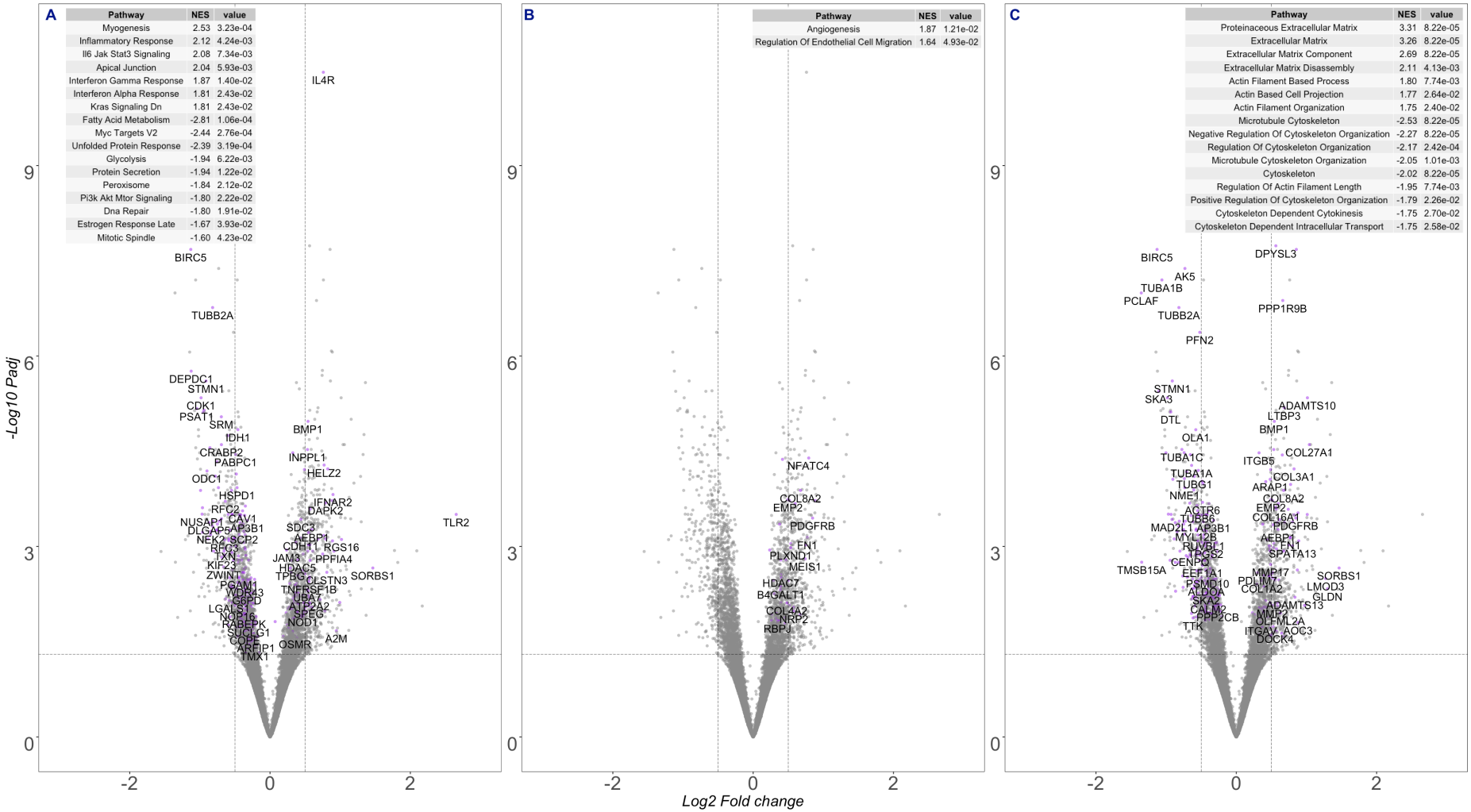

Figure 4-28 Volcano plots showing enriched genesets and leading-edge analysis for diseased rotator cuff tendon fibroblasts seeded on 300nm aligned scaffolds. Pairwise analysis of 300nm aligned scaffolds compared with aligned scaffolds with fibre diameters of 1000nm. Significant enrichment of Hallmark pathways (A) genesets describing angiogenesis (B) and extracellular matrix production and/or cytoskeleton apparatus(C). Genesets or hallmarkpathways with significant enrichment are listed in the summary table associated with each plot. Points highlighted in purple with associated gene symbols represent genes with the greatest contribution to the enriched gene sets (leading edge).

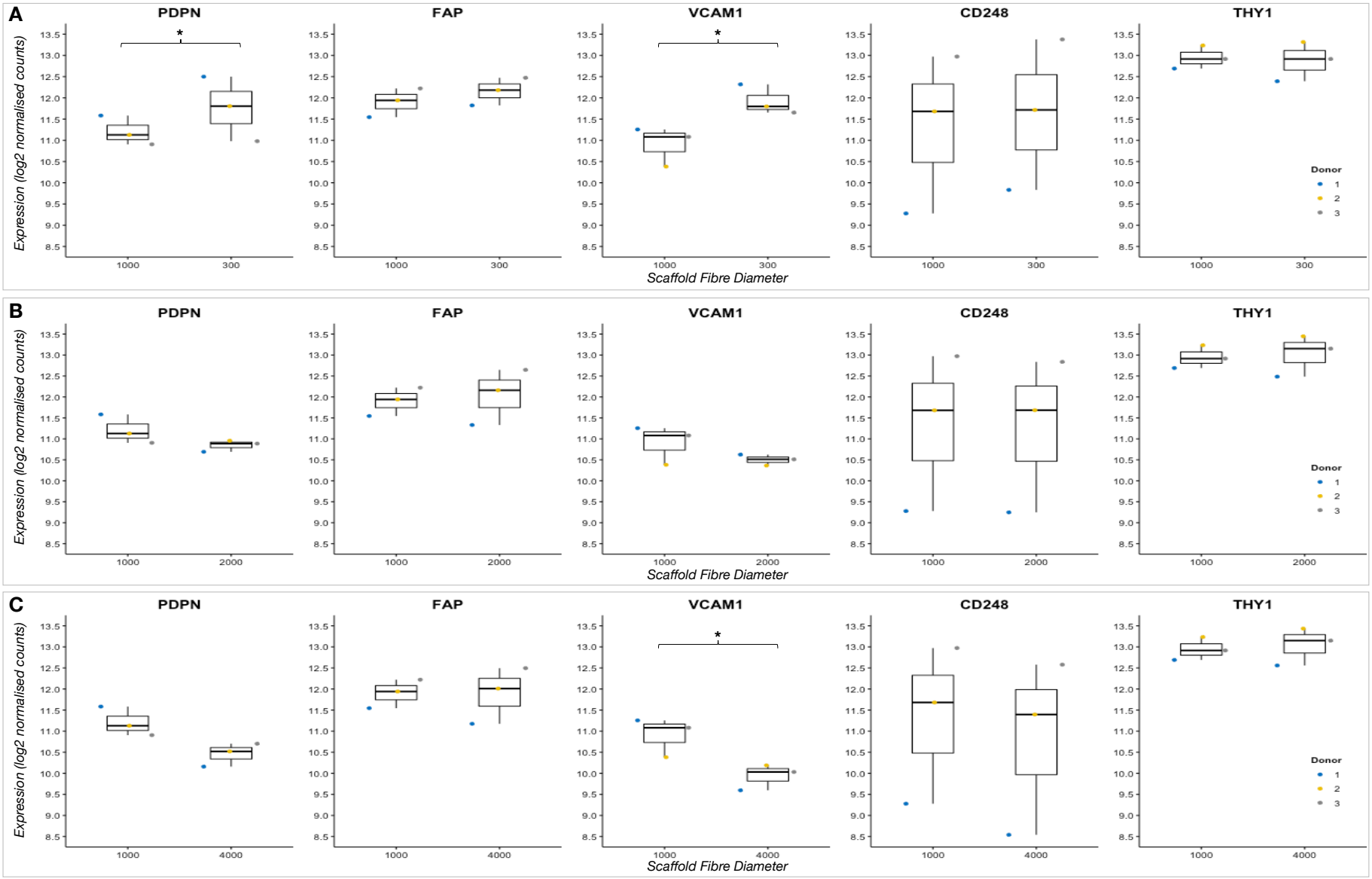

Figure 4-29 Effect of fibre diameter on gene expression of fibroblast activation markers for diseased tendon fibroblasts seeded on aligned PDO scaffolds (A) PDO scaffold with fibres of 300nm diameter in an aligned configuration compared with 1000nm aligned configuration. (B) 2000nm aligned vs 1000nm aligned (C) 4000nm aligned vs 1000nm aligned. *Denotes p-adjusted (Benjamini-Hochberg correction) value of <0.05. Expression values represent normalised count data transformed to a log2 scale.

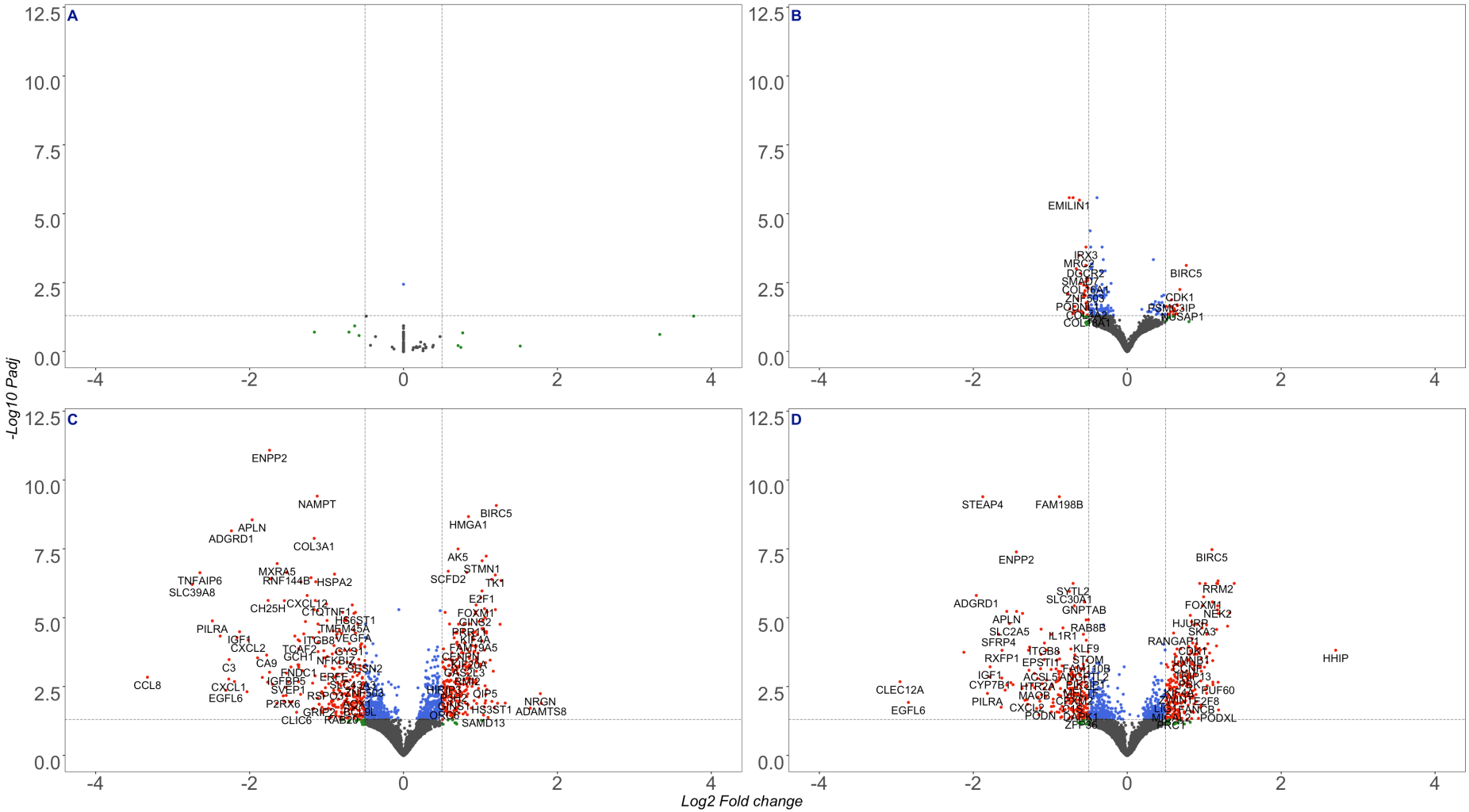

Figure 4-30 Volcano plot highlighting the effect of scaffold anisotropy on diseased rotator cuff tendon fibroblast gene expression. Pairwise analysis of scaffolds with aligned fibre directionality compared with random orientations, but with constant mean fibre diameters of 300nm(A), 1000nm (B), 2000nm(C) and 4000nm(D). Dashed lines denote a false discovery rate (FDR) of 0.05 and a log2 Fold-change ± 0.5. Transcripts coloured red have passed the thresholds for FDR and log2 Fold-change criteria, blue only meet the FDR, green only the log2 Fold-change threshold, whilst for grey neither criteria are met.

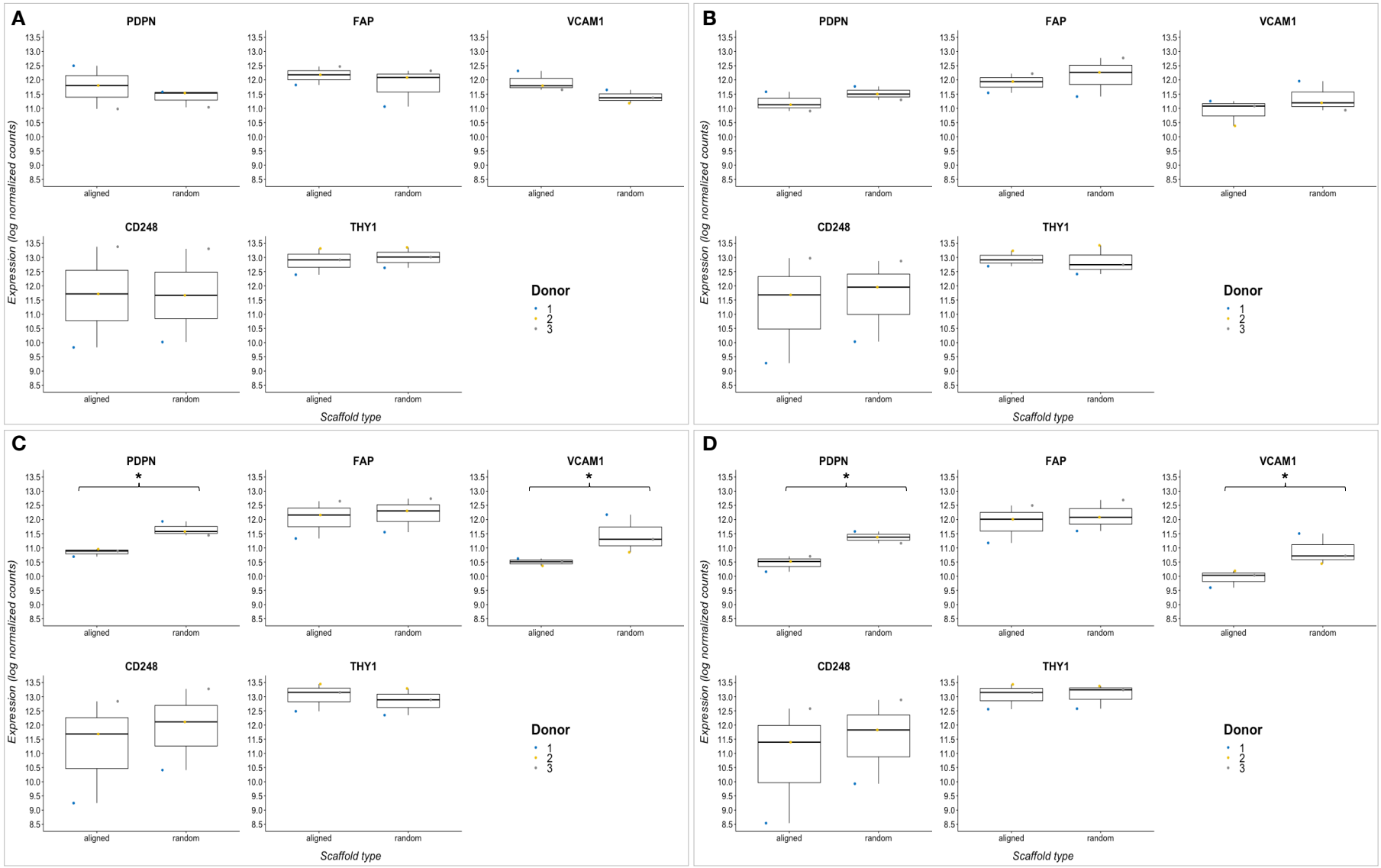

Figure 4-31 Effect of fibre anisotropy on gene expression of fibroblast activation markers for diseased tenocytes. (A) PDO scaffold with fibres of 300nm diameter in an aligned configuration compared with 300nm random configuration. (B) 1000nm aligned vs 1000nm random (C) 2000nm aligned vs 2000nm random (D) 4000nm aligned vs 4000nm random. *Denotes p-adjusted (Benjamini-Hochberg correction) value of <0.05. Expression values represent normalised count data transformed to a log2 scale.

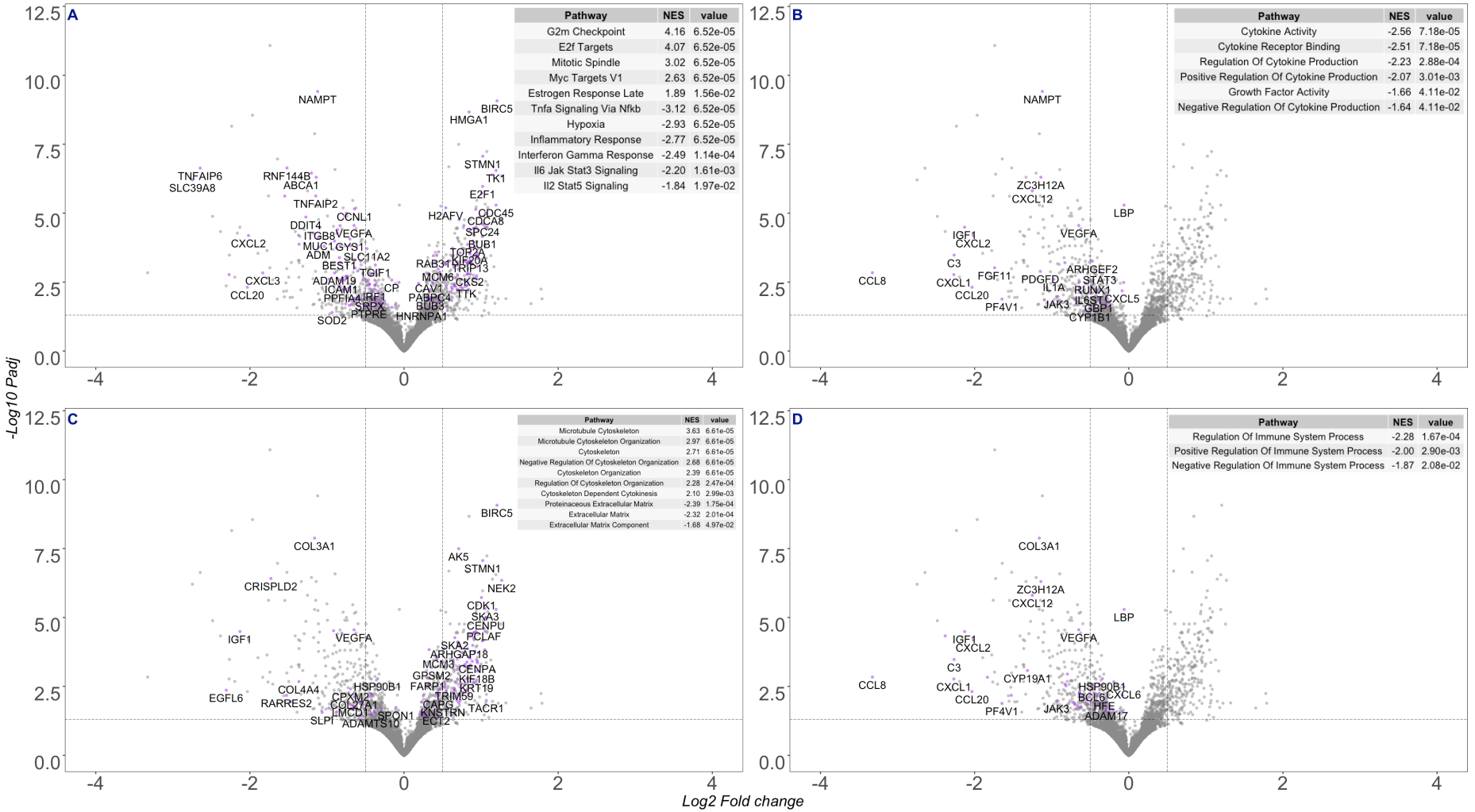

Figure 4-32 Volcano plots comparing the transcriptional profile of diseased rotator cuff tenocytes cultured on 2000nm aligned versus 2000nm random scaffolds. Comparison of transcriptional profile of diseased human rotator cuff derived tendon fibroblasts seeded onto 2000nm aligned or 2000nm randomly orientated electrospun fibres. Significant enrichment of genesets that describe hallmark pathways (A), cytokine/chemokine production (B), cytoskeletal and extracellular matrix assembly (C) and immune system regulation (D) are listed in the summary table associated with each plot. Points highlighted in purple with associated gene symbols represent genes with the greatest contribution to the enriched gene sets (Leading-edge analysis).

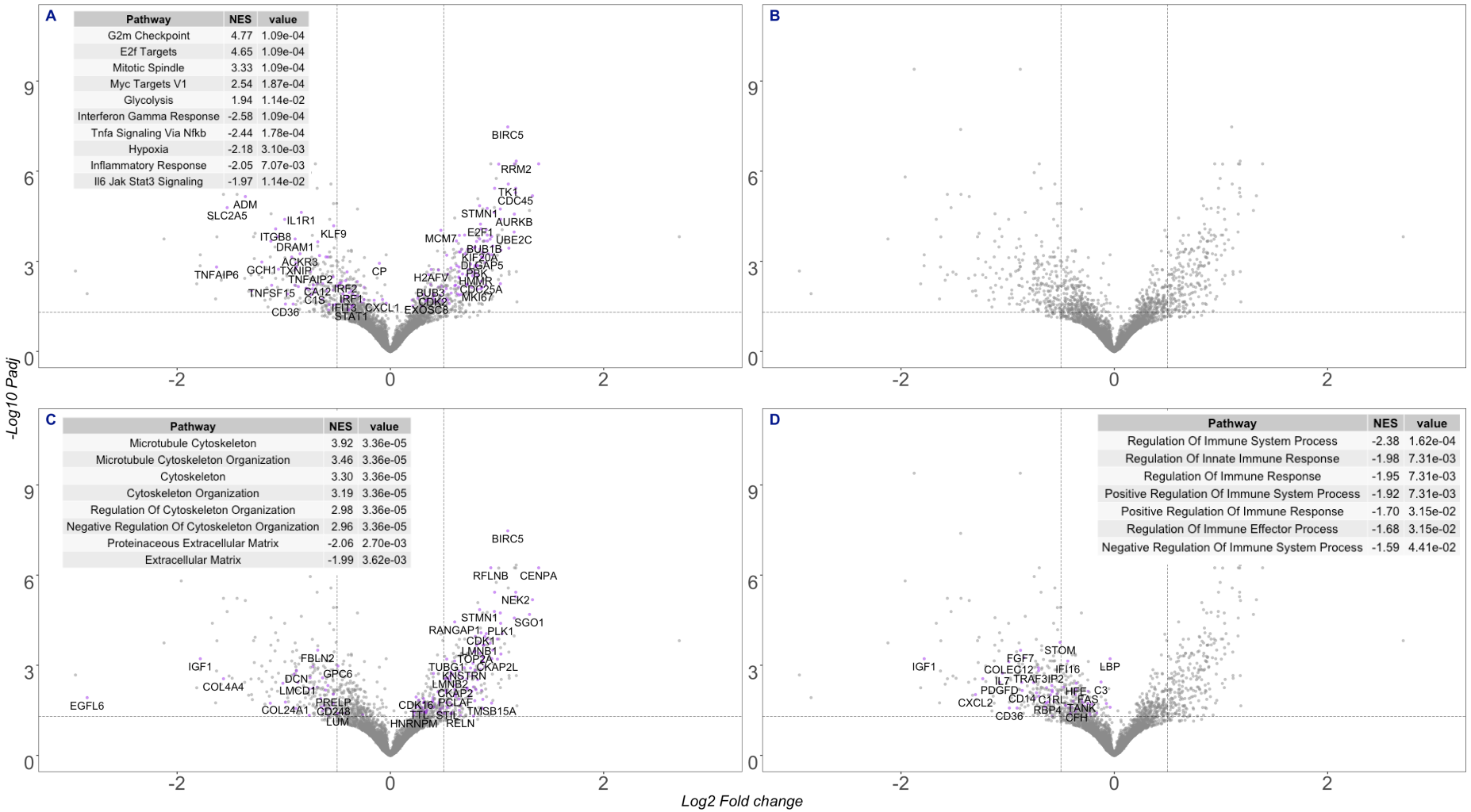

Figure 4-33 Volcano plots comparing the transcriptional profile of diseased rotator cuff tenocytes cultured on 4000nm aligned versus 4000nm random scaffolds. Comparison of transcriptional profile of diseased human rotator cuff derived tendon fibroblasts seeded onto 4000nm aligned or 4000nm randomly orientated electrospun fibres. Significant enrichment of genesets that describe hallmark pathways (A), cytokine/chemokine production (B), cytoskeletal and extracellular matrix assembly (C) and immune system regulation (D) are listed in the summary table associated with each plot. Points highlighted in purple with associated gene symbols represent genes with the greatest contribution to the enriched gene sets (Leading-edge analysis).

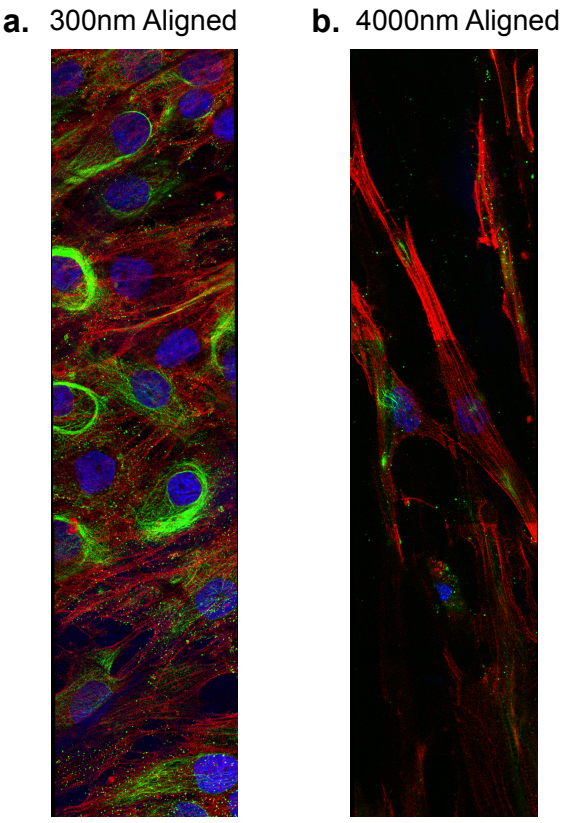

Figure 4-34 - PDPN surface staining for healthy tendon fibroblasts cultured on aligned electrospun scaffolds. Representative tiled confocal images of diseased rotator cuff tendon fibroblasts cultured for 7 days on electrospun scaffolds with aligned orientations and fibre diameters of (A) 300nm or (B) 4000nm. Green = Podoplanin, Blue = DAPI nuclear stain, Red= phalloidin actin stain

4.7 DISCUSSION

This study provides new insights into the effects of microarchitecture on the global transcriptome of tendon derived fibroblasts. We confirm that diseased tenocytes display an activated phenotype and identify that large diameter aligned scaffolds are capable of inducing a reduction in fibroblast activation, with diseased tenocytes primed to respond to architectural cues. To date, the effect of substrate topology on the gene expression of fibroblasts has undergone only a superficial interrogation, with the current literature predominately focused on assays of proliferation or migration. Indeed, a previous study examining 84 cytoskeletal regulators is by far the most comprehensive profiling of gene expression otherwise undertaken.[143]

Fibroblasts from both healthy and diseased tendon underwent a similar transcriptional response to changes in scaffold anisotropy. The upregulation of genes involved with DNA cell cycle regulation is in keeping with previous work demonstrating higher rates of proliferation for fibroblasts cultured on aligned electrospun scaffolds after 7-10days.[144,157,315] Whilst we have not provided functional validation, the enrichment of cell-cycle hallmark pathways has previously been shown to closely correlate with the expression of proteins e.g. BCL2 that are established reporters for cellular proliferation.[312]

Fibre diameter is another commonly manipulated variable, with a general trend in the tissue engineering field towards investigating successively smaller nanofibres. Improvements in NIH3T3 fibroblast adhesions[316], increased dermal fibroblast proliferation[317] and modulation of stem cell differentiation into ligament-like cells[318] have been reported for sub-micron scaffolds and may have spurred this trend. However, the literature is heavily conflicted. Several other groups have instead suggested a critical diameter of 1000-2000nm, with a reduction in proliferation observed for diameters either side of this range.[154,155,319] Appreciable differences in fibre alignment between all of these studies may help to explain the discrepancy. Therefore, to robustly investigate the effect of fibre diameter we produced scaffolds with four different diameters in either random or highly aligned configurations, enabling any diameter-anisotropy interactions to be carefully dissected.

There were almost no significant changes observed in the transcriptional profile of fibroblasts from diseased tendons cultured on random scaffolds when fibre diameters were manipulated in the 300-3500nm range. This suggests that other architectural features, such as fibre alignment, play a more critical function. In contrast, the transcriptional response of tendon fibroblasts showed a marked response to changes in fibre diameter. This response pivoted at 1000-2000nm and was most clearly observed with fibroblasts from diseased tendons. Whilst large diameter fibres (~3500nm) produced an upregulation of proliferative transcriptional pathways, submicron (~300nm) fibres induced the opposite. This transcriptional similarity between submicron aligned and randomly orientated scaffolds was supported by our morphological characterisation. Tendon fibroblasts cultured on ~300nm aligned scaffolds developed a flat, spread, morphology and not the elongation observed on aligned scaffolds of with 1000-3500nm diameters. A similar shape was observed for cells cultured on random scaffolds, regardless of fibre diameter, highlighting a clear correlation between changes in cell shape and phenotype.

The relationship between scaffold architecture and cell shape suggests that certain scaffolds failed to provide tendon fibroblasts with the contact guidance cues required to elongate. Similarly, Liu et al. also demonstrated that below a critical fibre size of 1μm, dermal fibroblasts cultured on randomly orientated electrospun poly(methyl methacrylate) scaffolds exhibited a less elongated morphology.[319] They attributed this loss of contact guidance to a diameter dependent reduction in focal adhesions, with a more chaotic organisation of cell-surface integrins observed for human dermal fibroblasts cultured on submicron fibres.[319] Others have suggested that large inter-fibre distances, or low fibre densities, present an obstacle to the sequential formation of adhesions.[320] This closely echoes the focal adhesion restriction theory, that holds that adhesions grow and mature linearly.[321] While a fibre provides a continuous surface for serial adhesions to form, attempts at perpendicular elongation are restricted by inter-fibre gaps.

For aligned scaffolds, it is likely that the mean pore area is related to inter-fibre distances, with the scaffolds produced in this study demonstrating a linear correlation between pore area and fibre diameter. We observed that the effect of anisotropy on transcriptional response was

blunted or completely lost for scaffolds with micron (~1000nm) and submicron (~300nm) fibres respectively, suggesting a critical pore area of approximately 2μm. This relationship does not hold true for randomly orientated scaffolds, in which the number of fibre intersections is greatly increased. Consequently, mean pore area is no longer a good surrogate measure of inter-fibre distances and would explain why ~3500nm random scaffolds, which despite having a similar pore area to ~1000nm aligned, failed to induce a similar morphological or transcriptomic response. Further work is needed to separate the effect of fibre diameter and inter-fibre distances on fibroblast phenotype. For example, the use of sacrificial fibres would provide a means of manufacturing scaffolds with matched anisotropy and fibre diameter but adjustable inter-fibre distances and porosity.

The terms fibroblast activation, cancer-associated fibroblasts (CAFs) and myofibroblasts all describe an overlapping process by which fibroblasts produce cytokines, chemokines, extracellular matrix proteins and facilitate immunomodulation.[47] Activated fibroblasts are a fundamental feature of acute wound healing but their persistence had also been described in malignancy as well numerous musculoskeletal diseases, including tendinopathies. Fibroblasts isolated from small to medium (1-3cm) rotator cuff tears demonstrated increased expression of the activation markers *PDPN*, *VCAM1* and *CD248*.[46] Similarly, we show here that as tendon disease progresses through to large (3-5cm) and massive (>5cm) tears the expression of these fibroblast activation markers persists, providing further evidence for chronic inflammation in disease progression.

The bilateral relationship between cellular morphology and phenotype is a central tenet of tissue engineering. Indeed, non-functionalised scaffolds are able to manipulate the differentiation of progenitor[147,322] and immune cells[323]. However, despite a long-accepted correlation between fibroblast activation and cell shape[47], this is the first exploration of whether the induction of morphological changes can modulate fibroblast activation. Interestingly, scaffold treated fibroblasts isolated from diseased tendon exhibited a more profound transcriptional response than fibroblasts isolated from healthy hamstring tendons. Our findings are supported by a previously observed priming of tendon cells following exposure to IL-1β[252], resulting in a hyper-responsive state that is likely to be the result of changes in the stromal

epigenome.[324] Whilst we cannot exclude that our observations are a transient phenomenon, it is tempting to speculate that the induction of morphological changes by electropsun scaffolds facilitates fibroblast reprogramming through epigenetic modification. Given the close association between fibroblasts and MSCs[47,325] and successful scaffold-based reprogramming of the latter[129,130], this is perhaps unsurprising. Future work, including epigenetic interrogation of tendon fibroblast response to scaffolds, and *in vivo* implantation of scaffolds into murine tendon injury models, will help to further delineate these observations.

Pro-inflammatory, NF-κB activated CAFS are a major source of angiogenic factors and matrix proteases that are critical to tumour angiogenesis.[326,327] Whilst we observed a polarisation in the inflammatory phenotype and activation status of tenocytes cultured on small, compared with, large diameter aligned scaffolds, we observed only a limited and inconsistent enrichment for angiogenic processes. Several reasons may underpin this discrepancy, firstly many of the genesets describing angiogenic processes have been derived through the genetic profiling of endothelial cells, and may not sufficiently capture transcriptional changes critical to fibroblast-endothelial cell interaction. Secondly, the dominant mechanisms by which activated fibroblasts facilitate vascularisation remains unclear. Pro-inflammatory fibroblasts upregulate several immune chemoattractant, including CXCL2 and CXCL5, that are known to support tumour angiogenesis.[326,328] Scaffold-induced changes in activation status may therefore indirectly modulate angiogenesis through alterations in the recruitment of inflammatory cells, changes to the extracellular matrix or modulation of recruitment of endothelial progenitor cells, hypotheses that the current study has not been able to test.

There are several limitations to this work. Next generation technologies can provide a powerful insight into the global effect of biomaterials on complex cellular systems. Nonetheless, conventional bulk sequencing can only provide an average expression signal, with the assumption of homogeneous cell populations critical to its validity. The phenotype of explanted tendon cells is not currently well characterised, raising the possibility that multiple populations of stromal cells, such as fibroblasts, endothelial cells or pericytes, are present during culture. Subpopulations of fibroblasts, with distinct functions have been described for synovial derived fibroblasts[54], and may also exist in the context of tendon fibroblasts. Distinct roles for epitenon

or paratenon derived and tendon core fibroblasts have already been described in murine and equine models.[34,329] We cannot exclude that a scaffold mediated biasing of stromal cell populations is responsible for the observed transcriptional shifts, an area that single-cell RNA sequencing will be critical to unravelling. Similarly, non-protein coding RNAs, that elicit epigenetic regulation of cell behaviour, were not the focus of this study. However, recent studies implicating small-RNAs in tendinopathy[330] and musculoskeletal stem cell homeostasis[331] opens another exciting avenue, with the cell-material-small-RNA axis largely unexplored.

Secondly, we have presented an analysis of cell-material interactions after 7 days of *in vitro* culture. This transcriptional cross-section may explain why tendon fibroblasts, cultured on ≥1000nm aligned scaffolds, exhibited a downregulation of activation markers and inflammatory pathways, but had not yet also displayed other classical features of cellular quiescence, namely a reduced expression of cell-cycle genes. Alternatively, we cannot exclude that the observed transcriptional changes are a transient phenomenon. Indeed, the matching of material properties to the requirements of each stage of tendon healing will require a temporal understanding of cell-material interactions and remains the focus of future work.

Thirdly, the generalisability of our findings is currently unclear. We present data generated from a single set of manufactured scaffolds, raising the possibility that unintentional variations in material properties, for example stiffness, total polymer mass or surface chemistry, are responsible for the effects this study has attributed to fibre diameter and anisotropy. Similarly, the isolation of stromal cells from the leading edge of rotator cuff tears may not be representative of the global changes effecting torn rotator cuff tendons. Further still, while hamstring derived tendon cells are a well-recognised control, it is possible that observed differences between fibroblasts from healthy and diseased tendons may instead reflect anatomical variability or differences in donor age. Indeed, transcriptional variation underpins the stromal post-code[292] that is responsible for the anatomical compartmentalisation of inflammatory musculoskeletal diseases.[314] However, the consistent identification of fibroblast activation despite use of an alternative control tissues (young post-traumatic supraspinatus tendon)[252] gives validity to our current observations.

Finally, given the well-recognised lack of collinearity between mRNA transcription and protein expression[332], further validation is required. Confirmation of changes in the cytokine and chemokine secretome, immune cell recruitment, as well as functional *in vitro* angiogenesis modelling, will enable detailed interrogation of these preliminary observations.

4.8 CONCLUSIONS

We have shown for the first time that, at a transcriptional level, tendon fibroblasts activation is modulated by the anisotropy of electrospun scaffold fibres, but that fibre diameter also fine tunes this relationship. The response to fibre alignment pivots at fibre diameters of 1000-2000nm, submicron (~300nm) scaffolds elicited a relative activation, whilst larger diameter (~3500nm) aligned scaffolds producing a relative reduction in inflammatory markers and pathways. It appears that scaffolds resembling smaller diameter, disordered, collagen III typically present during the earlier phases of wound healing resulted in tenocyte activation. Conversely, scaffolds mimicking aligned larger diameter collagen I fibrils, present during tissue remodelling, can reverse this phenotype. This has implications for the design of scaffolds used during rotator cuff repair augmentation. These must avoid inducing persistent stromal activation, a characteristic feature of failed tendon healing, and instead provide tissue-resident fibroblasts with temporally appropriate signals to drive successful tendon repair. Fibroblasts have also been implicated in the production of pro-angiogenic cytokines, with appropriate vessel formation increasingly considered to be important in the regeneration of damaged musculoskeletal tissues. However, at a computational level, the activation of tendon fibroblasts did not correspond with any consistent differences in the stromal regulation of angiogenesis and we propose that future investigations of scaffold-mediated angiogenesis consider additional endogenous cellular populations.

Chapter 5 General Discussion

5.1 INTRODUCTION

The prevalence of rotator cuff tears is estimated at 15-20%[198,199], with rates expected to rise as populations age[199] and obesity increases.[19] While many tears are initially asymptomatic, almost half of full-thickness tears demonstrate a progressive increase in size, becoming symptomatic as they enlarge.[333,334] For persistently painful tears surgical repair is often undertaken. Around 9,000 rotator cuff repairs (RCRs) are performed each year by NHS England and this rate has been steadily increasing over the past 20 years.[16] Unfortunately, the UKUFF trial, a large well-conducted randomised controlled trial conducted in 58 centres in the UK, demonstrated that RCRs currently have a failure rate of, on average, 40%.[22] One approach to improve healing rates is the use of biomaterial meshes to reinforce or 'augment' the repair. However, recent controversy surrounding vaginal meshes[335] has highlighted the potential for adverse tissue responses and emphasised the need for robust clinical evaluation of this type of surgical implant or device. In the context of mesh augmented RCR, a large number of commercially available devices has created clinical uncertainty over the role of patch augmentation (unpublished survey, British Society of Shoulder and Elbow Surgeons).

To date, the design of scaffolds for RCR augmentation has primarily focused on improving the mechanical strength of the repair[336]. The role that scaffolds might play in modulating the biological behaviour of diseased tendons has been largely ignored. This failure to consider the biological requirement of the diseased tendon niche may underpin the lack of clear efficacy of current rotator cuff implants. To this end, a new generation of biomaterials, capable of altering cellular phenotypes through the provision of biophysical cues, are now under development.[125,126] However, the design of tailored biomaterials that deliver appropriate biophysical signals, requires a detailed understanding of the pathobiological processes driving tendon disease and the response of these diseased cell to biophysical cues provided by a material implant. While previous work has investigated the contribution of activated tendon derived fibroblasts[252] and infiltrating immune cells[337], the role of another major cell type, endothelial cells, is hitherto unexplored. Further still, there has never been any interrogation of whether different biophysical designs can modulate the biological processes that drive

endothelial cell accumulation in the diseased tendon after repair augmented by a material patch.

This thesis first aimed to establish the state of play in scaffold-augmented RCR and to establish whether there is a clear need for a new generation of bioactive materials for rotator cuff repair. It then moved to explore a novel area of tendon pathobiology – the role of the endothelium. Finally, the ability of topographic signals from electrospun scaffolds to modulate the behavior of tendon derived fibroblasts (tenocytes), the majority population in healthy and diseased tendons, was investigated. In summary, this thesis shows that (1) current commercially available rotator cuff patches are not causing harm but are also not benefitting patients significantly, (2) endothelial-fibroblast crosstalk influences two critical feature of rotator cuff tendon pathobiology; immune cell recruitment and fibroblast activation, and (3) the micro-architectural design of electrospun scaffolds can modulate the activation status of healthy and diseased tenocytes, but that this does not influence fibroblast-derived angiogenic signaling at a computational level.

This body of work has not elucidated the mechanisms that regulate endothelial-fibroblast crosstalk or scaffold driven fibroblast activation, however future studies are proposed herein that detail how this might be accomplished. A summary of thesis findings can be found in box 5-1 and are graphically represented in figure 5-1.

Box 5-1 Summary of thesis findings

What did we already know?

- Surgical repair of RCTs currently has a high failure rate (~40%)
- Biomaterial 'patches' are increasingly used to mechanically reinforce the repair
- Patch design has focused on manipulating biomechanics and not tendon biology
- Persistent immune cell infiltration, fibroblast activation and angiogenesis are characteristic of human rotator cuff tendon pathobiology

What did we want to find out?

- Are the currently available rotator cuff patches safe and effective?
- Does the endothelium play a role in human tendon disease pathogenesis?
- Can electrospun scaffolds with different micro-architectures provide topographical cues that modulate the angiogenic output of resident tendon fibroblasts?

What do we know now?

- Current patches are generally safe but have not delivered a transformational shift in patient outcomes after rotator cuff repair
- Endothelial-fibroblast cross-talk effects leukocyte recruitment + fibroblast activation
- Electrospun scaffold micro-architecture modulates the activation status of tenocytes but this does not influence their angiogenic output

5.2 SUMMARY OF NOVEL FINDINGS

5.2.1 Systematic review of the surgical management of rotator cuff repair with an augmentative patch

An *a priori* registered, systematic review of all available clinical data for patch augmented RCR was undertaken with the aim of robustly assessing efficacy. This is the most comprehensive review to-date that incorporated English and non-English language articles and undertook a duplicate assessment of eligibility, risk of bias and data-extraction, thereby minimising reviewer bias[338].

This study is the first to amalgamate trial data on adverse events following augmented RCR. While a similar complication rate was observed between augmented (2.3%) and standard repairs (2.1%), specific safety concerns were identified for certain patches (Restore®) or techniques (Quadriceps allograft, Humeral Periosteal graft), reinforcing the need for the rigorous clinical evaluation of new medical devices. It is of particular concern that no publicly

available data exists for several commercially available patches in current clinical use (d-cell® and Leeds-Kuff™). However, we should not solely rely on clinical trials for the provision of safety data. The inclusion of all medical devices on a prospective registry permits active, contemporaneous surveillance of medical-device safety, and may identify safety concerns more rapidly than clinical trials - many of which take several years from inception to publication.[339] Indeed, in the cardiovascular arena, automated clinical-data surveillance systems, capable of identifying safety concerns with the first 12 months of monitoring, have already been implemented.[340]

Further, a meta-analysis confirmed an improvement in re-tear rate and a marginal improvement in Patient Reported Outcome Measures (PROMS) following augmented rotator cuff repair. A subsequent subgroup analysis identified a moderate reduction in re-tear rate for synthetic (RR 0.4, 95% CI 0.25-0.64) and decellularised human allograft (RR 0.34, 95% CI 0.18-0.64) patches, but not for xenografts (RR 0.97, 95% CI 0.72-1.30) or human autografts (RR 0.69, 95% CI 0.40-1.18). This corresponded to a small improvement in pain and PROMS for synthetic patches, that was statistically significant but not clinically meaningful. However, it must be remembered that such subgroup analyses are observational in nature. Since individuals are not randomized to one trial or another there is a serious risk of bias through confounding by other study-level characteristics.[208] The conclusion from this work is that there remains a need for well-designed comparative trials that simultaneously assess multiple patch types. Indeed, there is growing support for multi-arm trials, which are more cost-effective, able to accelerate the therapeutic evaluation process[341] and have a greater probability of identifying a superior treatment[342]. In any event, current patch designs have not delivered a paradigm shift in rotator cuff repair and this work has identified a clear need for a new generation of biomaterials that can significantly improve tendon healing.

The assumption that improved rates of rotator cuff healing translate into improved functional outcomes should also be considered. The association between radiologically defined healing and patient reported outcomes, has previously been identified,[22,228] and is again reported in this thesis. However, this is by no means a perfect correlation, perhaps reflecting a failure of our current radiological measures to fully capture the, as yet undefined, aspects of tendon

healing that determine pain and function. That is to say, a mechanically intact repair that is identifiable on USS or MRI, is not necessarily synonymous with biologically normal tendon tissue. Again, this underpins the need for bioactive materials that, not only generate mechanical stronger repair tissue, but also drive diseased tendon tissue towards being phenotypically normal. For now, this remains speculative and further work is needed to assess the concordance between biological, radiological and clinical outcomes.

5.2.2 Endothelial-tenocyte crosstalk alters fibroblast activation and endothelial recruitment of immune cells

Previous work has demonstrated that diseased fibroblasts, isolated from chronically inflamed synovial tissue, increase endothelial attachment of lymphocytes and neutrophils.[282] Fibroblasts derived paracrine signaling has been implicated as a key regulator of the persistent immune cell infiltrates that are observed in chronic inflammation. This is the first study to employ a similar *in vitro* model within the arena of tendon disease. The findings herein show that fibroblasts from healthy hamstring tendons induce a paracrine mediated immunoprotective effect on microvascular endothelial cells (ECs) - reducing the attachment of T-cells and monocytes when compared with fibroblasts isolated from massive rotator cuff tears. Interestingly, previous work reports a similar immunosuppressive phenotype during EC co-cultures with fibroblasts isolated from dermal tissue and the synovial tissue of resolving inflammatory arthritis[73,282] – perhaps suggesting a shared immunoprotective mechanism between healthy fibroblasts isolated from the anatomically diverse locations of skin, synovium or tendon. The ability of fibroblast to maintain the homeostasis of adjacent epithelial cells is well accepted, with a loss fibroblast molecular checkpoints implicated in dysregulated tissue architectures and cellular populations observed within several cancers.[47,343] Similarly, these current results add support to the notion that tendon fibroblasts are not only critical regulators of the ECM, but also possess a more global role in orchestrating the cellular homeostasis of tendon.

Despite the functional difference in immune cell attachment, the expression of EC adhesion receptors were similar during co-cultures with healthy and diseased tendon derived fibroblasts. The mechanisms by which healthy fibroblasts reduce leukocyte attachment

remains unclear. Indeed, extensive investigation of fibroblast-EC crosstalk within other tissue types has begun to reveal a complex set of cellular mechanisms that are dependent on the leucocyte subset[74], is modified by conditions of static or dynamic co-culture[259], and is different between indirect and direct co-culture systems.[71]

However, any cell culture model assessing the mechanisms of leukocyte accumulation observed during tendon disease, must also take account of trans-endothelial migration, leukocyte retention and leukocyte apoptosis. The *in vitro* system described within this thesis has attempted to simultaneously measure attachment, trans-endothelial migration as well the retention of leukocytes. Unexpectedly, an increase in trans-endothelial lymphocyte migration, and similar rates of retention, were observed between co-cultures of healthy and diseased tendon fibroblasts. Similar results have been reported during EC co-cultures of dermal and synovial fibroblasts.[282] The biological relevance of this finding remains unknown and may simply reflect a failure of the current experimental model to recapitulate the pericyte, EC basement membrane and ECM layers leukocytes must navigate during migration into, and subsequent egress out of, diseased tendon tissues.

Previous investigations into fibroblast-EC crosstalk have largely focused on how such signaling effects EC phenotype. However, this thesis has also considered the effects of fibroblast-EC paracrine crosstalk on the phenotype of fibroblasts. This has revealed EC mediated activation of healthy, and to a lesser extent, diseased tendon fibroblasts, resulting in the increased expression of inflammatory cytokines, collagen and matrix proteases - a phenotype typically of both acutely healing wounds and chronic inflammation. Therefore, In the context of acute injury, this crosstalk may represent beneficial angiocrine signalling that facilitates fibroblast-wound healing. Conversely, persistence of vessels in chronically inflamed tendons may perpetuate fibroblast activation and, in part, contribute to a failure of resolution. In any event, the manipulation of angiogenesis should be a key consideration in the design of contemporary rotator cuff scaffolds.

5.2.3 The effect of electrospun scaffold architecture on tendon fibroblast activation

Recapitulation of the topographical signals provided by native ECM is a common goal of three-dimensional culture methods, aimed at controlling the phenotype of tenocytes during *in vitro* culture.[344] A similar strategy has underpinned the design of a new generation of implantable scaffolds for rotator cuff augmentation, by mimicking a healthy biophysical environment we aim to redirect diseased tendon fibroblasts toward a healthy phenotype.[125] While currently available commercial scaffolds fail to match the nano and micro-scale properties of native supraspinatus tendon,[53] electrospinning can provide a means of producing scaffolds with controllable fibre orientations and diameters. Previous reports on the effect of scaffold architecture on the gene expression of tenocytes have focused on the assessment of small number of ECM genes and only a limited number of architectural variants. This thesis presents the first unbiased assessment of how 8 distinct electrospun architectures influence the transcriptome of tenocytes – the major cell population in healthy and diseased tendons. Since fibroblast activation and scaffold architecture are both associate with changes in fibroblast cell shape, it was hypothesised that scaffold induced changes in cell shape would also modulate activation status. Since growing evidence also supports a key role for activated fibroblasts in pathological angiogenesis.[293] , it was further hypothesised that scaffold architecture would alter the expression of angiogenic factors.

In the context of human rotator cuff tendon disease, fibroblasts isolated from small-to-medium tears demonstrate an activated, pro-inflammatory, secretory phenotype.[46] Whilst not novel, an activated phenotype is also identified here for diseased fibroblasts explanted from massive rotator cuff tears. Tendon fibroblasts cultured on ~300nm aligned scaffolds developed a flat, spread, morphology and not the elongation observed on aligned scaffolds with fibres of 1000-3500nm diameters. A similar flat and spread shape was observed for cells cultured on random scaffolds, regardless of fibre diameter. At a transcriptional level, elongated morphologies were associated with pro-inflammatory gene set enrichment pathways and the increased expression of the activation markers *CD248*, *PDPN* and *VCAM1*. Despite a long-accepted correlation between fibroblast activation and cell shape[47], this is the first exploration of whether the induction of morphological changes can, in turn, modulate fibroblast activation. It is shown that scaffolds resembling smaller and [345,346] disordered, collagen III fibres typically present during the earlier phases of wound healing[347,348] resulted in tenocyte activation. Conversely,

scaffolds mimicking aligned larger collagen I fibres, present during tissue remodelling and healthy tendon, may moderate fibroblast activation.

Interestingly, scaffold treated fibroblasts isolated from diseased tendon exhibited a more profound transcriptional response than fibroblasts isolated from healthy hamstring tendons. Our findings are supported by a previously observed priming of tendon cells following exposure to IL-1β[252]. Clearly, when investigating the effects of biomechanical cues on tendon healing, the targeted tissue niche must always frame enquires. Site- and disease-specific changes in a fibroblast phenotype will adjust this niche and significantly influence cell–material interactions.

This thesis builds on recent research demonstrating that the stiffness of fibronectin coated hydrogels differentially regulated murine fibroblast expression of either α-SMA or FAP, that corresponded to an ECM synthetic or contractile phenotype respectively.[53] Given the importance of fibroblast activation during acute wound repair[38], as well as their persistent activation in chronic inflammatory disease[151], future scaffold designs must provide topographical signals that induce temporally appropriate fibroblast activation. However, it is acknowledged that at a computational level the modulation of fibroblast morphology did not significantly influence the angiogenic profile of healthy or diseased tendon fibroblasts. It is proposed that future investigations into scaffold-controlled angiogenesis incorporate additional endogenous immune and endothelial cell populations to better represent the tendon niche.

5.2 Clinical Relevance

Several of the findings presented in this thesis have direct and current clinical implications in management of tendon disease or offer future translational opportunities. Firstly, the most comprehensive systematic review of the clinical literature to-date has not found a clear benefit for any of the current patch designs utilised in rotator cuff augmentation. Overall, a paucity of high-quality clinical trials, and significant clinical heterogenicity between studies, preclude firm conclusions about the efficacy of current patch designs. This places an urgent need for robust, multi-arm, randomised clinical trials, and until such work has been undertaken the routine use

of patch augmentation should not be undertaken, instead we recommend careful patient selection and shared decision making. Further, this work has highlighted complications and adverse events associated with the use of specific patch designs. There is a clear professional responsibility to only utilise devices that have undergone robust clinical evaluation for safety and efficacy. Data provided here on percentage complication risks is the most accurate available but the information available is scant due to the overall lack of investigation and surveillance of these devices. As part of the formed consent process it is critical these data are collated and shared with patients to allow the risks and benefits of standard or augmented rotator cuff repair to be properly understood.

Secondly, this thesis has provided the first evidence of an endothelial-fibroblast axis in human rotator cuff tendon disease. Paracrine crosstalk between endothelial cells and tendon fibroblasts is now implicated in both the accumulation of immune cells and activation of resident fibroblasts. At present these remain associative, with causation yet to be fully proven. Nonetheless, evidence is beginning to accumulate,[349] and the targeting of the endothelium offers a novel avenue for the therapeutic manipulation of tendon disease. Further, the co-culture system described here, provides a simple system for the initial testing of therapeutic compounds and/or medical devices aimed at manipulating the endothelial-tenocyte axis.

Finally, the findings that fibroblast activation can be modulated by the alignment and/or diameter of nanofibre scaffolds has implications for the design of future medical devices. Beyond simply being safe, biomaterials must provide the biological cues required to enhance the repair process and stimulate the formation of healthy tendon tissue. Since fibroblast activation is critical to acute wound healing, but associated with chronic inflammation when persistent, it follows that bioactive rotator cuff scaffolds must deliver temporally appropriate topographical signals. Although the production of biomaterials with diverse topographical architectures (a biomaterial library) is not novel, this work represents the first-time next generation sequencing has been used to assess the effect of a range of topographical architectures on the cellular phenotype of tendon derived fibroblasts. This approach can be expanded to be more akin to drug discovery platforms that combine high-throughput screening and next generation sequencing to accelerate the discovery process.[350,351] Similar work

utilising single cell RNA sequencing to assess the immunomodulatory properties of different biomaterials has recently been undertaken.[349] Together, these represents a step change in the molecular characterisation of cell-material interactions.

5.3 METHODOLOGICAL IMPROVEMENTS

Specific limitations have been extensively discussed within each chapter, and only the most critical methodological improvements are discussed below.

5.3.1 Methodological improvements in the systematic review of current rotator cuff augmentative patches

With regards to undertaking meta-analyses' within different subgroups, less reliance can be placed on such an analysis if it was not first pre-specified in the review protocol. The subgroup analysis undertaken in this thesis was *post-hoc* and not declared *a priori*. To minimize the possibility of finding false positive associations a further subgroup analysis on surgical techniques (on-lay vs bridging) was not undertaken. Nonetheless, this remains an important consideration for clinicians, and should be considered, *a priori*, in future systematic reviews. However, the division of studies by surgical technique risks ignoring trial-level characteristics that may also explain any association between surgical technique and treatment effect. For example, trials of bridging augmentation may include older patients with larger, more chronic, rotator cuff tears than trials comparing on-lay augmentation and standard repair. To this end, the baseline risk of the outcome event (e.g. re-tear rate) for patients under the control condition can be calculated and is likely to reflect differences in patient characteristics.[352] Such an analysis could minimise the future risk of finding spurious associations.

Unfortunately, the very small number of comparative trials that are currently available will hamper the ability to undertake a robust subgroup analysis or meta-regression for some time to come. In fact, for multivariant meta-regression the Cochrane collaboration recommend 10 studies per covariant under investigation.[208] The division of studies based on patch type (xenograft, allograft, autograft or synthetic) and surgical technique (on-lay or bridging) would require a minimum of 60, adequately reported, comparative studies. At present only 15 comparative studies have been published, highlighting that either well designed, large, multi-

arm, randomised controlled trials, or implant registries are better placed to assess the impact of these, or other, co-variants on surgical outcomes.

5.3.2 Methodological improvements concerning EC and fibroblast co-cultures

Within the *in vitro* co-culture study, careful consideration needs to be given to the specificity of the observed EC effect on fibroblast activation, particularly as this observation only became significant after 9-days in culture. This raises the possibility that the increased cellular mass present during co-culture, resulted in the accumulation of generic metabolic products that could have activated tendon derived fibroblasts. Repeating such experiments with different cell lines seeded into the upper chamber, for example a fibroblast and/or osteoblast human cell line, would add weight to the observed effect being EC specific. Further, the use of bulk RNA sequencing to assess the effect of co-culture on fibroblast activation genesets would provide a more sensitive outcome measure, and may permit the detection of any effect of EC co-culture at an earlier timepoint. Alternatively, exogenous cytokines (IL-1β and IL-4) could again be added to increase the effect size. Whilst the current study attempted this, it is possible that extended cytokine stimulation instead induced a state of exhaustion, similar to that observed amongst immune cells following continuous antigenic stimulation.[274,275] Consideration should be given to cytokine stimulation only for the last 24 hours of co-culture.

5.3.3 Methodological improvements concerning cell-material interactions between electrospun scaffolds and tendon derived fibroblasts

Any future assessment of cell-material interactions, particularly when utilising sensitive outcome measures such as RNA sequencing, must consider three major limitations. Firstly, to definitively attribute changes in cellular phenotype to specific biomaterial characteristics, all known co-variants must have been measured and where possible controlled. Thus, in the present study it cannot be excluded that the changes in fibroblast activation status were not the results of confounding factors such as scaffold stiffness or chemical composition. Techniques such as atomic force microscopy and X-ray photoelectron spectroscopy would permit an assessment of micromechanical stiffness, surface topography and chemical composition. It is therefore recommended that prior to cell culture or *in vivo* implantation future

work should undertake exhaustive biomaterial characterisation, enabling a relationship between scaffold parameters and cellular phenotype to be modelled.

Secondly, it is entirely possible that the observed differences between scaffold architectures were the result of unintentional variations between scaffold types, introduced during material production or cell-culture. The routine production of and testing of material repeats would minimise this potential source of bias. Material repeats describe scaffolds that are produced at a later date, ideally from a different batch of polymer solution, but are manufactured to match the stated characteristics of the original materials. Further confounders relate to cell culture itself and includes differences in the time of day that scaffolds were harvested, contaminants introduced during scaffold handling, edge effects during culture, or subtle differences between batches of culture media. This study utilized biological and technical repeats but did not include material repeats. Unfortunately, the need for biological, material and technical repeats must be balanced against increasing costs and cell availability, a concern that is particularly acute when utilising next generation sequencing and primary human cells.

Finally, and in a similar vein, having only assessed the effect of cell-material interactions at a single time point it cannot be excluded that the observed effects on fibroblast phenotype are not simply transitory. To test this hypothesis a minimum of two time points would be needed, but again acting to multiply costs.

5.4 Future Work

We propose here significant programs of future work that build on the findings of this thesis. Further work assessing methodological limitations has been considered in section 5.3.

5.4.1 Determining the clinical efficacy of current and future rotator cuff scaffolds

We have previously highlighted the current paucity of high-quality evidence, and in section 5.3.1 discussed that assessing the superiority of specific patch designs through subgroup meta-analyses is severely limited. Instead, future efforts to identify safe and superior patch augments for RCR must focus on multi-arm superiority RCTs,[342] and/or the establishment of soft-tissue implant registries. More broadly, there is a real need to robustly assess all current

and emerging treatment strategies for RCTs – physiotherapy, corticosteroid injections, nerve ablation, superior capsular reconstruction and subacromial balloon spacers are to name but a few. To this end, establishing a Trials within Cohort (TwiC) multi-centre study would provide a cost effective, efficient and pragmatic means of assessing the efficacy of each treatment.[344]

5.4.2 Determining the mechanism of tenocyte-endothelial cross-talk and establishing a causal link with tendon healing

Future explorations of the tenocyte-endothelial axis should attempt to identify the paracrine factors responsible for the activation of endothelial cells by diseased tendon fibroblasts. Using multiplex analysis for pro-inflammatory cytokines (e.g. MSD platform or mass spectrometry), a broad screen of the co-culture secretome could be undertaken. Subsequent immunoprecipitation of candidate proteins would confirm which cytokines are critical to leukocyte recruitment. A similar methodology could also be employed to investigate which cytokines are responsible for endothelial cell mediated activation of tendon fibroblasts. However, there is also a need to develop our current leukocyte recruitment assay (section 3.5.4). This does not fully recapitulate the physiological recruitment of leukocytes that occurs under conditions of flow. Collaborations with teams already experienced in flow-based adhesion assays (e.g. McGettrick *et al.*[259]) should be explored.

While *in vitro* models enable the mechanisms of EC-fibroblast crosstalk to be dissected, the future clinical relevance of these interactions' rests on how, or even if, this crosstalk influences tendon repair. To this end, transgenic murine models are a powerful tool. In parallel to this thesis we have developed a partial tenotomy model at the murine Achilles. At the earlier timepoints of 72 hours and 2 weeks after partial tenontomy, this model recapitulates acute tendon injury. Ten weeks after partial tenotomy the defect had undergone repair but with persistent tissue calcification and differences in dynamic weight bearing, suggesting a degree of persistent tendinopathy. Combining this tendon injury model with knock–out and knock-in strains allows the role of EC-fibroblast crosstalk during acute repair and/or chronic tendinopathy to be assessed. For example, floxed Delta-like-ligand-4 (Dll4) mice can be generated and crossed with Cdh5-CreERT2 transgenic mice to produce EC-specific Dll4 knockouts. Notch and Dll4 signal in a cell-cell contact dependent fashion between ECs to limit

sprouting, mitosis and angiogenesis.[353] For Notch gain of function, the gene for Fbxw7 can also be target in an inducible and EC-specific manner. Since Fbxw7 mediates polyubiquitination and proteasomal degradation of active Notch[353], tamoxifen activated Fbxw7$^{lox/lox}$ mice overexpress Notch.[79] Indeed, this work is currently underway, with these two strains it should be possible to upregulate or down-regulate musculoskeletal angiogenesis and assess the effect on murine tendon healing at a whole transcriptome level. Furthermore, validation of these findings in the context of human disease may also be possible. The use of microvascular intra-tendinous sclerosis as a treatment for Achilles tendinopathy has been described.[354] Utilising a pioneering tendon biopsy technique[355], it would be possible to obtain tissue samples before and after sclerotherapy and assess the biological effect of vessel ablation in human tendinopathy.

To further examine the hypothesis that NF-κB mediated fibroblast activation is responsible for endothelial activation and leukocyte accumulation *in vivo*, a separate animal model could also be generated. For example, fibroblast-restricted knockout of the NF-κB inhibitor Iκβα could be generated by breeding Iκβα$^{lox/lox}$ with tamoxifen inducible Col1a2-Cre mice.[353] Such a strategy would lead to excision of Iκβα in cells expressing Cre recombinase under the Col1a2 promoter, generating constitutive NF-κB activity in fibroblasts. An assessment of leukocyte infiltration and endothelial phenotype, with or without tendon injury, could then be compared to a murine strain with reduced NF-κB activity. [356,357] For example, floxing IKKβ, which is needed upstream to phosphorylate Iκβα, would prevent NF-κB nuclear translocation.[358] A similar methodology has already been used to assess the role of HIF-1α expression by fibroblasts during dermal wound healing.[359]

5.4.3 Further exploring the effect cell-material interactions on angiogenesis through investigation of immune and endothelial cell populations during mono-culture, co-culture and in vivo

While at a computational level scaffold architecture did not influence the angiogenic output of tendon derived fibroblasts this requires functional validation. This is especially important given that the majority of angiogenesis gene-sets are not cell type specific. Conditioned media, collected during the culture of tenocytes on each distinct scaffold architecture, should be used

to undertake a functional *in vitro* assessment of angiogenesis, such as the endothelial cell tube formation assay.[360] Further, although fibroblasts are the dominant cell population in healing tendons, immune cells and resistant endothelial cells also play critical roles in regulating angiogenesis.[360] If follows that to comprehensively assess the effect of scaffold architecture on angiogenesis, the *in vitro* work described in chapter 4 should be expanded to include immune cells and tissue resident endothelial cells. In the context of immune cells, bulk RNA sequencing will likely obscure biologically relevant differences between cell types, with single cell sequencing methods the more appropriate to assess the effects of electrospun fibre diameter and anisotropy, on the angiogenic phenotype of each immune subset. Building on this, the *in vivo* implantation of scaffolds into dermal or tendon injury murine models could assess the cumulative effect of scaffold topography on wound angiogenesis. Endothelial GFP reporter mice (e.g. Flk1-GFP)[361] would aid in the imaging of vessel ingrowth into scaffolds, whilst also facilitating FACS retrieval of ECs to assess changes in EC phenotype between scaffold variants.

Future electrospun scaffold development must also consider the dynamic nature of the ECM during wound healing. Mimicking the topography of healing ECM will require scaffolds that are able to provide temporally appropriate signaling. The use of polymers with different degradation rates would allow production of scaffolds that provide different topographical cues at distinct points during wound healing.[353] Since the effect of topography is likely to be dependent on cell type, each cellular population involved in tendon repair must be considered, both in isolation and during co-culture. At present, *in vitro* systems, however complex, are unlikely to reconstruct all of the cell-material and cell-cell interactions that contribute towards successful tendon healing. Further, it must be remembered that phenotypic drift currently hampers the reliability of long-term cell culture.[362] Thus, such work would again ultimately require assessment in a relevant animal model, which would also provide an environment of dynamic strain a factor known to influence tenocyte phenotype[363].

Finally, future work must also consider the mechanisms by which scaffold architecture drives the activation status of fibroblasts. Such work must include an assessment of intra-cellular signaling pathways, including NK-κB and STAT, through western blotting, multiplexed

phospho-flow cytometry[364] or multiplexed chemiluminescense (e.g. MSD phosphoproteins). Since the interactions between cells and ECM is largely mediated through integrins[365], it is likely that differential integrin signaling between scaffold variants is responsible for the observed differences in fibroblast phenotype. Exploration of the current dataset will allow candidate integrins to be identified and their role elucidated through antibody blockade or siRNA knockdown. Interestingly, podoplanin has previously been demonstrated to regulate cell shape, localise to cellular filopodia and control invasion of cancer associated fibroblasts into collagen matrices. Since *PDPN* expression was correlated with scaffold induced fibroblast activation, it is important to assess whether PDPN is simply a surrogate marker or an active participant in scaffold induced fibroblast activation.[366] PDPN signals through Rho GTPases[367], therefore treatment with RhoA, Cdc42 or Rac-1 inhibitors[368] may alter the cell spreading and transcriptional phenotype that this thesis observed for tenocytes cultured on randomly orientated electrospun scaffolds.

5.5 CONCLUSIONS

This thesis has utilised a number of different scientific methodologies to establish that (1) currently available rotator cuff patches are not fit for purpose, some cause adverse tissue responses and have been abandoned, and overall there is no evidence of meaningful benefit to patients, (2) the endothelial-fibroblast axis influences immune cell recruitment and tendon fibroblast activation – characteristic features of rotator cuff pathobiology and (3) the micro-architectural design of electrospun scaffolds can modulate the activation status of tenocytes but, at the computational level, this does not influence their angiogenic output.

Together, the findings of this thesis support the hypothesis that angiogenesis plays an important role in the pathobiology of human tendon disease. However, at present we have not identified a means of regulating angiogenesis through alterations to the topographical cues provided by implantable electrospun scaffolds.

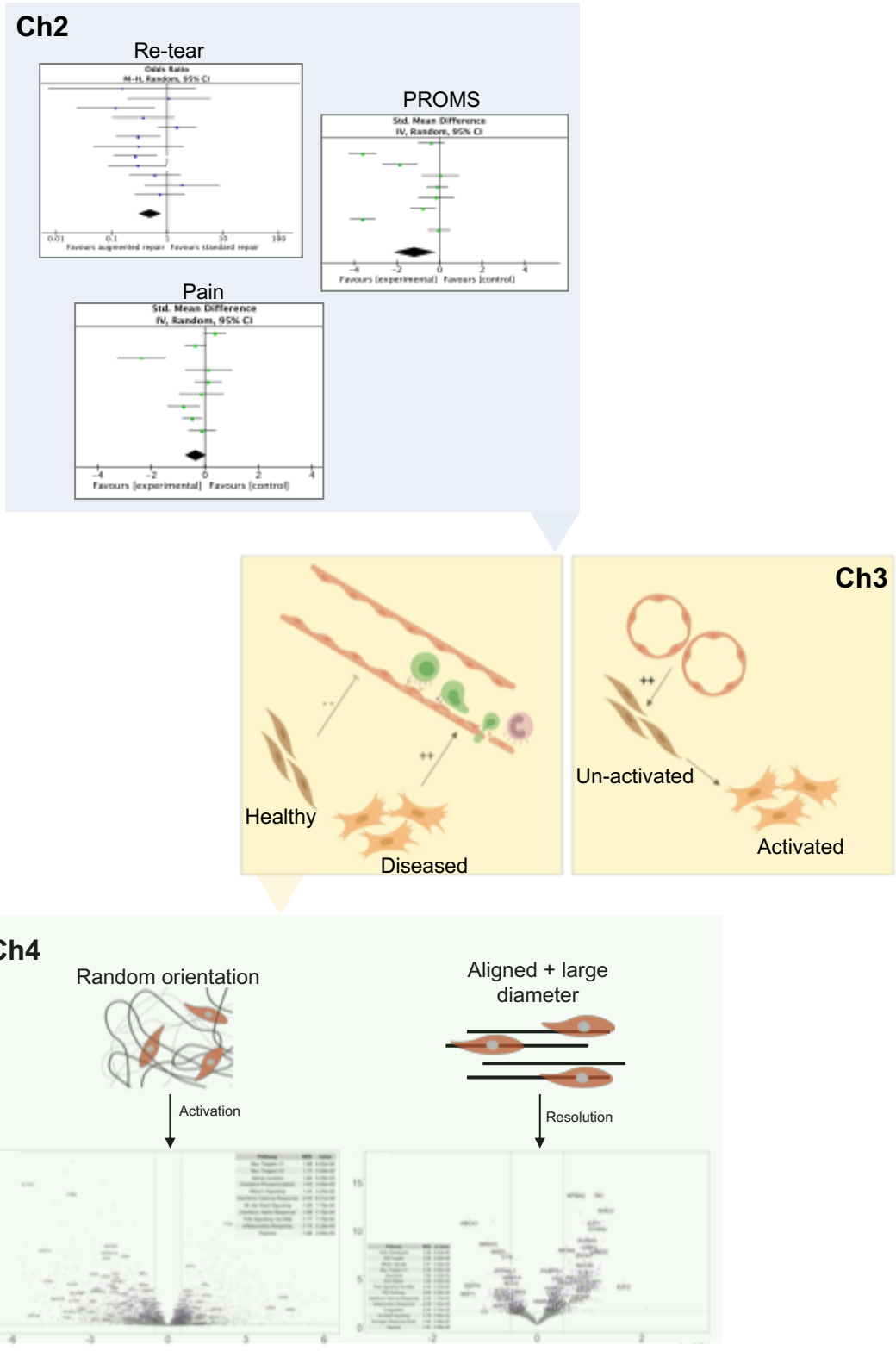

Figure 5-1. Graphical summary of key findings. Chapter 2 (top left): Evidence synthesis of current patches used in rotator cuff augmentation found a statistically significant, but not a clinically meaningful, improvement following patch augmentation with current designs. Chapter 3 (middle): A endothelial-fibroblast axis is demonstrated. Cross-talk from diseased tenocytes increases leukocyte attachment to the endothelium, while endothelial cell co-culture causes fibroblast activation. Chapter 4(bottom left): Bulk RNA sequencing of healthy or diseased tenocytes cultured on 8 scaffolds with distinct architectures. Fibres with random alignment caused fibroblast activation, whilst large diameter aligned scaffolds decreased activation

Chapter 6 References

1. McPherson EJ, Friedman RJ, An YH, et al. Anthropometric study of normal glenohumeral relationships. J Shoulder Elb Surg. 1997 Mar 1;6(2):105–12.

2. Chan LK. The range of passive arm circumduction in primates: Do hominoids really have more mobile shoulders? Am J Phys Anthropol. 2008 Jul;136(3):265–77.

3. Lee S, Kim K, O'Driscoll S, et al. Dynamic Glenohumeral Stability Provided by the Rotator Cuff Muscles in the Mid-Range and End-Range of Motion. J Bone Jt Surg. 2000;82(6):849–57.

4. Burkhart SS, Esch JC, Jolson RS. The Rotator Crescent and Rotator Cable: An Anatomic Description of the Shoulder's "Suspension Bridge." Arthrosc J Arthrosc Relat Surg. 1993;9(6):611–6.

5. Wang JH-CC. Mechanobiology of tendon. J Biomech. 2006 Jan 1;39(9):1563–82.

6. Benjamin M, Kaiser E, Milz S. Structure-function relationships in tendons: A review. J Anat. 2008;212(3):211–28.

7. Dyer RF, Enna CD. Ultrastructural Features of Adult Human Tendon. Cell Tiss Res. 1976;259:247–59.

8. Riley GP, Harrall RL, Constant CR, et al. Tendon degeneration and chronic shoulder pain: changes in the collagen composition of the human rotator cuff tendons in rotator cuff tendinitis. Ann Rheum Dis. 1994;53(6):359–66.

9. Kadler KE, Holmes DF, Trotter JA, et al. Collagen fibril formation. J Biochem. 1996;316:1–11.

10. Fratzl P, Misof K, Zizak I, et al. Fibrillar structure and mechanical properties of collagen. J Struct Biol. 1998;122:119–22.

11. Svensson RB, Hansen P, Hassenkam T, et al. Mechanical properties of human patellar tendon at the hierarchical levels of tendon and fibril. J Appl Physiol. 2012;112(3):419–26.

12. Reese SP, Underwood CJ, Weiss JA. Effects of decorin proteoglycan on fibrillogenesis, ultrastructure, and mechanics of type I collagen gels. Matrix Biol. 2013;32(7–8):414–23.

13. Shute J. Glycosaminoglycan and Chemokine/Growth Factor Interactions. In: Lever R, editor. Heparin - A Century of Progress. 2012. p. 307–24.

14. Urwin M, Symmons D, Allison T, et al. Estimating the burden of musculoskeletal disorders in the community: the comparative prevalence of symptoms at diVerent anatomical sites, and the relation to social deprivation. Ann Rheum Dis. 1998;57:649–55.

15. Piitulainen K, Ylinen J, Kautiainen H, et al. The relationship between functional disability and health-related quality of life in patients with a rotator cuff tear. Disabil Rehabil. 2012;34(24):2071–5.

16. Judge A, Murphy RJ, Maxwell R, et al. Temporal trends and geographical variation in the use of subacromial decompression and rotator cuff repair of the shoulder in England. Bone Jt J. 2014;96 B(1):70–4.

17. Mitchell C, Adebajo A, Hay E, et al. Shoulder pain: Diagnosis and management in primary care. BMJ. 2005;8:331–1124.

18. Yamaguchi K, Ditsios K, Middleton WD, et al. The Demographic and Morphological Features of Rotator Cuff Disease. A Comparison of Asymptomatic and Symptomatic Shoulders. J Bone Jt Surg Am. 2006;88(8):1699–704.

19. Franceschi F, Papalia R, Paciotti M, et al. Obesity as a risk factor for tendinopathy: A systematic review. Int J Endocrinol. 2014;2014.

20. Bruns J, Kampen J, Kahrs J, et al. Achilles tendon rupture: experimental results on spontaneous repair in a sheep-model. Knee Surgery, Sport Traumatol Arthrosc. 2000;8(6):364–9.

21. Maffulli N, Barrass V, Ewen SW. Light microscopic histology of achilles tendon ruptures. A comparison with unruptured tendons. Am J Sports Med. 2000;28(6):857–63.

22. Carr A, Cooper C, Campbell MK, et al. Effectiveness of open and arthroscopic rotator cuff repair (UKUFF). Bone Joint J. 2017 Jan 4;99–B(1):107–15.

23. Ng C, Ballantyne J, Brenkel I. Quality of life and functional outcome after primary total hip replacement. A five-year follow-up. J Bone Joint Surg Br. 2007;89(7):868–73.

24. Laupacis A, Bourne R, Rorabeck C, et al. The Effect of Elective Total Hip Replacement on Health-Related Quality of Life. J Bone Jt Surg. 1993;75(11):1619–26.

25. Flynn JE, Graham JH. Healing of tendon wounds. Am J Surg. 1965;109(3):315–24.

26. Peacock E. Physiology of tendon repair. Am J Surg. 1965;109(3):283–6.

27. Gelberman RH, Vandeberg JS, Manske PR, et al. The early stages of flexor tendon healing: A morphologic study of the first fourteen days. J Hand Surg Am. 1985;10(6):776–84.

28. Gelberman RH, Manske PR, Akeson WH, et al. Flexor Tendon Repair. J Orthop Res. 1986;4(1):119–28.

29. Fenwick S, Hazleman B, Riley G. The Vasculature and its role in the damaged and healing tendon. Arthritis Res. 2002;4(4):252–60.

30. Gelberman RH, Vandeberg JS, Lundborg GN, et al. Flexor tendon healing and restoration of the gliding surface. An ultrastructural study in dogs. J bone Jt Surg Am Vol. 1983;65(1):70–80.

31. Williams IF, Craig AS, Parry DAD, et al. Development of collagen fibril organization and collagen crimp patterns during tendon healing. Int J Biol Macromol. 1985;7(5):275–82.

32. Voleti PB, Buckley MR, Soslowsky LJ. Tendon Healing: Repair and Regeneration. Annu Rev Biomed Eng. 2012;14(1):47–71.

33. Postacchini F, De Martino C. Regeneration of rabbit calcaneal tendon maturation of collagen and elastic fibers following partial tenotomy. Connect Tissue Res. 1980;8(1):41–7.

34. Dyment NA, Liu CF, Kazemi N, et al. The Paratenon Contributes to Scleraxis-Expressing Cells during Patellar Tendon Healing. PLoS One. 2013;8(3):e59944.

35. Gumucio JP, Phan AC, Ruehlmann DG, et al. Synergist ablation induces rapid tendon growth through the synthesis of a neotendon matrix. J Appl Physiol. 2014;117(11):1287–91.

36. Dyment NA, Hagiwara Y, Matthews BG, et al. Lineage tracing of resident tendon progenitor cells during growth and natural healing. PLoS One. 2014;9(4):e96113.

37. Howell K, Chien C, Bell R, et al. Novel Model of Tendon Regeneration Reveals Distinct Cell Mechanisms Underlying Regenerative and Fibrotic Tendon Healing. Sci Rep. 2017;7:1–14.

38. Darby IA, Laverdet B, Bonté F, et al. Fibroblasts and myofibroblasts in wound healing. Clin Cosmet Investig Dermatol. 2014;7:301–11.

39. Rees JD, Wilson AM, Wolman RL. Current concepts in the management of tendon disorders. Rheumatology. 2006 May 1;45(5):508–21.

40. Millar NL, Murrell GAC, McInnes IB. Inflammatory mechanisms in tendinopathy – towards translation. Nat Rev Rheumatol. 2017;13(2):110–22.

41. Marsolais D, Coté CH, Frenette J. Neutrophils and macrophages accumulate sequentially following Achilles tendon injury. J Orthop Res. 2001 Nov;19(6):1203–9.

42. Dean BJF, Gettings P, Dakin SG, et al. Are inflammatory cells increased in painful human tendinopathy? A systematic review. Br J Sports Med. 2016;50(4):216–20.

43. Kragsnaes MS, Fredberg U, Stribolt K, et al. Stereological Quantification of Immune-Competent Cells in Baseline Biopsy Specimens From Achilles Tendons. Am J Sports Med. 2014 Oct 31;42(10):2435–45.

44. Matthews TJW, Hand G., Rees J, et al. Pathology of the torn rotator cuff tendon: REDUCTION IN POTENTIAL FOR REPAIR AS TEAR SIZE INCREASES. J Bone Jt Surg - Br Vol. 2006;88–B(4):489–95.

45. Dakin SG, Martinez FO, Yapp C, et al. Inflammation activation and resolution in human tendon disease. Sci Transl Med. 2015;7(311):311ra173.

46. Dakin SG, Buckley CD, Al-Mossawi MH, et al. Persistent stromal fibroblast activation is present in chronic tendinopathy. Knee Surg Sport Traumatol Arthrosc. 2017;19(1):16.

47. Kalluri R. The biology and function of fibroblasts in cancer. Nat Rev Cancer. 2016;16(9):582–98.

48. Darby I, Skalli O, Gabbiani G. Alpha-Smooth Muscle Actin is Transiently expressed by Myofibroblasts during experimental Wound healing. Lab Investig. 1990;63(1):21–9.

49. Choi IY, Karpus ON, Turner JD, et al. Stromal cell markers are differentially expressed in the synovial tissue of patients with early arthritis. PLoS One. 2017;12(8):e0182751.

50. Bauer S, Jendro MC, Wadle A, et al. Fibroblast activation protein is expressed by rheumatoid myofibroblast-like synoviocytes. Arthritis Res Ther. 2006;8(6):R171.

51. Zeisberg M, Strutz F, Müller GA. Role of fibroblast activation in inducing interstitial fibrosis. J Nephrol. 2000;13 Suppl 3:S111-20.

52. Öhlund D, Handly-Santana A, Biffi G, et al. Distinct populations of inflammatory fibroblasts and myofibroblasts in pancreatic cancer. J Exp Med. 2017 Mar 6;214(3):579–96.

53. Avery D, Govindaraju P, Jacob M, et al. Extracellular matrix directs phenotypic heterogeneity of activated fibroblasts. Matrix Biol. 2018 Apr;67:90–106.

54. Croft AP, Campos J, Jansen K, et al. Distinct fibroblast subsets drive inflammation and damage in arthritis. Nature. 2019 Jun 29;570(7760):246–51.

55. Dakin SG, Ly L, Colas RA, et al. Increased 15-PGDH expression leads to dysregulated resolution responses in stromal cells from patients with chronic tendinopathy. Sci Rep. 2017 Dec 8;7(1):11009.

56. Codman EA, Akerson IB. The Pathology Associated with Rupture of the Supraspinatus Tendon. Ann Surg. 1931 Jan;93(1):348–59.

57. Hegedus E, Cook C, Brennan M, et al. Vascularity and tendon pathology in the rotator cuff: a review of literature and implications for rehabilitation and surgery. Br J Sports Med. 2010;44(12):838–47.

58. Fearon A, Dahlstrom JE, Twin J, et al. The Bonar score revisited: Region of evaluation significantly influences the standardized assessment of tendon degeneration. J Sci Med Sport. 2014;17(4):346–50.

59. Silvestri E, Biggi E, Molfetta L, et al. Power Doppler analysis of tendon vascularization. Int J Tissue React. 2003;25(4):149–58.

60. Snyder SJ, Arnoczky SP, Bond JL, et al. Histologic Evaluation of a Biopsy Specimen Obtained 3 Months After Rotator Cuff Augmentation With GraftJacket Matrix. Arthrosc J Arthrosc Relat Surg. 2009;25(3):329–33.

61. Jackson JR, Seed MP, Kircher CH, et al. The codependence of angiogenesis and chronic inflammation. FASEB J. 1997;11(6):457–65.

62. Carmeliet P, Jain RK. Angiogenesis in cancer and other diseases. Nature. 2000 Sep 14;407(6801):249–57.

63. Kiriakidis S, Andreakos E, Monaco C, et al. VEGF expression in human macrophages is NF-kappaB-dependent: studies using adenoviruses expressing the endogenous NF-kappaB inhibitor IkappaBalpha and a kinase-defective form of the IkappaB kinase 2. J Cell Sci. 2003 Feb 15;116(Pt 4):665–74.

64. Distler JHW, Hagen C, Hirth A, et al. Bucillamine induces the synthesis of vascular endothelial growth factor dose-dependently in systemic sclerosis fibroblasts via nuclear factor-kappaB and simian virus 40 promoter factor 1 pathways. Mol Pharmacol. 2004 Feb 1;65(2):389–99.

65. Costa C, Soares R, Reis-Filho JS, et al. Cyclo-oxygenase 2 expression is associated with angiogenesis and lymph node metastasis in human breast cancer. J Clin Pathol. 2002 Jun 1;55(6):429–34.

66. Dean BJF, Franklin SL, Carr AJ. A systematic review of the histological and molecular changes in rotator cuff disease. Bone Joint Res. 2012;1(7):158–66.

67. Costa C, Incio J, Soares R. Angiogenesis and chronic inflammation: Cause or consequence? Angiogenesis. 2007;10(3):149–66.

68. Fiedler U, Reiss Y, Scharpfenecker M, et al. Angiopoietin-2 sensitizes endothelial cells to TNF-α and has a crucial role in the induction of inflammation. Nat Med. 2006 Feb 5;12(2):235–9.

69. Vestweber D. How leukocytes cross the vascular endothelium. Nat Rev Immunol. 2015;15(11):692–704.

70. McEver RP. Selectins: initiators of leucocyte adhesion and signalling at the vascular wall. Cardiovasc Res. 2015 Aug 1;107(3):331–9.

71. McGettrick HM, Smith E, Filer A, et al. Fibroblasts from different sites may promote or inhibit recruitment of flowing lymphocytes by endothelial cells. Eur J Immunol. 2009;39(1):113–25.

72. McGettrick HM, Butler LM, Buckley CD, et al. Tissue stroma as a regulator of leukocyte recruitment in inflammation. J Leukoc Biol. 2012 Mar 1;91(3):385–400.

73. Filer A, Ward LSC, Kemble S, et al. Identification of a transitional fibroblast function in very early rheumatoid arthritis. Ann Rheum Dis. 2017;annrheumdis-2017-211286.

74. Smith E, McGettrick HM, Stone MA, et al. Duffy antigen receptor for chemokines and CXCL5 are essential for the recruitment of neutrophils in a multicellular model of rheumatoid arthritis synovium. Arthritis Rheum. 2008 Jul;58(7):1968–73.

75. Rafii S, Butler J, Ding B-S. Angiocrine functions of organ-specific endothelial cells. Nature. 2016;529(7586):316–25.

76. Kusumbe A, Ramasamy S, Adams R. Coupling of angiogenesis and osteogenesis by a specific vessel subtype in bone. Nature. 2014;507(7492):323–8.

77. Licht T, Goshen I, Avital A, et al. Reversible modulations of neuronal plasticity by VEGF. Proc Natl Acad Sci. 2011;108(12):5081–6.

78. Poulos MG, Crowley MJP, Gutkin MC, et al. Vascular Platform to Define Hematopoietic Stem Cell Factors and Enhance Regenerative Hematopoiesis. Stem cell reports. 2015 Nov 10;5(5):881–94.

79. Ramasamy SK, Kusumbe AP, Wang L, et al. Endothelial Notch activity promotes angiogenesis and osteogenesis in bone. Nature. 2014 Mar 20;507(7492):376–80.

80. Christov C, Chrétien F, Abou-Khalil R, et al. Muscle Satellite Cells and Endothelial Cells: Close Neighbors and Privileged Partners. Mol Biol Cell. 2007;18:1397–409.

81. Tei K, Matsumoto T, Mifune Y, et al. Administrations of peripheral blood CD34-positive cells contribute to medial collateral ligament healing via vasculogenesis. Stem Cells. 2008;26(3):819–30.

82. Takayama K, Kawakami Y, Mifune Y, et al. The effect of blocking angiogenesis on anterior cruciate ligament healing following stem cell transplantation. Biomaterials. 2015;60:9–19.

83. Dondossola E, Holzapfel B, Alexander S, et al. Examination of the foreign body response to biomaterials by nonlinear intravital microscopy. Nat Biomed Eng. 2016;1:0007.

84. Lorbach O, Bachelier F, Vees J, et al. Cyclic Loading of Rotator Cuff Reconstructions. Am J Sports Med. 2008 Aug 30;36(8):1504–10.

85. Green S, Buchbinder R, Glazier R, et al. Systematic review of randomised controlled trials of interventions for painful shoulder: selection criteria, outcome assessment, and efficacy. BMJ. 1998 Jan 31;316(7128):354–60.

86. Dean BJF, Lostis E, Oakley T, et al. The risks and benefits of glucocorticoid treatment for tendinopathy: A systematic review of the effects of local glucocorticoid on tendon. Semin Arthritis Rheum. 2014 Feb;43(4):570–6.

87. Gilroy DW, Colville-Nash PR, Willis D, et al. Inducible cyclooxygenase may have anti-inflammatory properties. Nat Med. 1999 Jun;5(6):698–701.

88. van der Windt DA, Koes BW, Boeke AJ, et al. Shoulder disorders in general practice: prognostic indicators of outcome. Br J Gen Pract. 1996 Sep;46(410):519–23.

89. Coghlan J, Buchbinder R, Green S, et al. Surgery for rotator cuff disease (Review). Cochrane Database Syst Rev. 2008;(1).

90. Coghlan J, Buchbinder R, Green S, et al. Surgery for rotator cuff disease. Cochrane Database Syst Rev. 2008;(1):CD005619.

91. Carr AJ, Murphy R, Dakin SG, et al. Platelet-Rich Plasma Injection With Arthroscopic Acromioplasty for Chronic Rotator Cuff Tendinopathy. Am J Sports Med. 2015 Dec 23;43(12):2891–7.

92. Jeong JY, Park KM, Sundar S, et al. Clinical and radiologic outcome of arthroscopic rotator cuff repair: single-row versus transosseous equivalent repair. J Shoulder Elb Surg. 2018 Jun 1;27(6):1021–9.

93. Badylak SF, Freytes DO, Gilbert TW. Extracellular matrix as a biological scaffold material: Structure and function. Acta Biomater. 2009;5:1–13.

94. Peterson B, Whang PG, Iglesias R, et al. Osteoinductivity of commercially available demineralized bone matrix. Preparations in a spine fusion model. J Bone Joint Surg Am. 2004;86–A(10):2243–50.

95. Urist M. Bone: Formation by Autoinduction. Science (80-). 1965;150(3698):893–9.

96. van der Stok J, Hartholt KA, Schoenmakers DAL, et al. The available evidence on demineralised bone matrix in trauma and orthopaedic surgery: A systematic review. Bone Joint Res. 2017;6(7):423–32.

97. Derwin K, Badylak S, Steinmann S, et al. Extracellular matrix scaffold devices for rotator cuff repair. J Shoulder Elb Surg. 2010;19(3):467–76.

98. Ono Y, Davalos Herrera D, Woodmass J, et al. Graft Augmentation Versus Bridging for Large to Massive Rotator Cuff Tears: A Systematic Review. Arthrosc J Arthrosc Relat Surg. 2017;33(3):673–80.

99. Güngörmüş C, Kolankaya D, Aydin E. Histopathological and biomechanical evaluation of tenocyte seeded allografts on rat Achilles tendon regeneration. Biomaterials. 2015;51:108–18.

100. Walton JR. Restore Orthobiologic Implant: Not Recommended for Augmentation of Rotator Cuff Repairs. J Bone Jt Surg. 2007;89(4):786–91.

101. Zhu J, Marchant RE. Design properties of hydrogel tissue-engineering scaffolds. Expert Rev Med Devices. 2011;8(5):607–26.

102. Dai W, Wold LE, Dow JS, et al. Thickening of the Infarcted Wall by Collagen Injection Improves Left Ventricular Function in Rats A Novel Approach to Preserve Cardiac Function After Myocardial Infarction. J Am Coll Cardiol. 2005;46:714–9.

103. Liu Y, Gan L, Carlsson DJ, et al. A Simple, Cross-linked Collagen Tissue Substitute for Corneal Implantation. Investig Opthalmology Vis Sci. 2006;47(5):1869.

104. Liu M, Zeng X, Ma C, et al. Injectable hydrogels for cartilage and bone tissue engineering. Bone Res. 2017;5:17014.

105. Awad HA, Butler DL, Boivin GP, et al. Autologous Mesenchymal Stem Cell-Mediated Repair of Tendon. Tissue Eng. 1999;5(3):267–77.

106. Young RG, Butler DL, Weber W, et al. Use of mesenchymal stem cells in a collagen matrix for achilles tendon repair. J Orthop Res. 1998;16(4):406–13.

107. Yang G, Rothrauff BB, Lin H, et al. Enhancement of tenogenic differentiation of human adipose stem cells by tendon-derived extracellular matrix. Biomaterials. 2013;34(37):9295–306.

108. Moshiri A, Oryan A, Meimandi-Parizi A. Role of tissue-engineered artificial tendon in healing of a large achilles tendon defect model in rabbits. J Am Coll Surg. 2013;217(3):421–441.e8.

109. He M, Gan AWT, Lim AYT, et al. The effect of fibrin glue on tendon healing and adhesion formation in a rabbit model of flexor tendon injury and repair. J Plast Surg Hand Surg. 2013;47(6):509–12.

110. Sung H-W, Huang R-N, Huang LLH, et al. In vitro evaluation of cytotoxicity of a naturally occurring cross-linking reagent for biological tissue fixation. J Biomater Sci Polym Ed. 1999;10(1):63–78.

111. Wood R. Development of a Reconstituted Collagen Tendon Prosthesis. J Bone Jt Surg. 1989;71–A(8):1183–91.

112. Yunoki S, Hatayama H, Ebisawa M, et al. A novel fabrication method to create a thick collagen bundle composed of uniaxially aligned fibrils: An essential technology for the development of artificial tendon/ligament matrices. J Biomed Mater Res - Part A. 2015;103(9):3054–65.

113. Stuart K, Panitch A. Characterization of gels composed of blends of collagen I, collagen III, and chondroitin sulfate. Biomacromolecules. 2009;10(1):25–31.

114. Encalada-Diaz I, Cole BJ, MacGillivray JD, et al. Rotator cuff repair augmentation using a novel polycarbonate polyurethane patch: Preliminary results at 12 months' follow-up. J Shoulder Elb Surg. 2011;20(5):788–94.

115. Nada A, Debnath U, Robinson D, et al. Treatment of massive rotator-cuff tears with a polyester ligament (Dacron) augmentation: clinical outcome. J Bone Joint Surg Br. 2010;92(10):1397–402.

116. Daghighi S, Sjollema J, van der Mei HC, et al. Infection resistance of degradable versus non-degradable biomaterials: An assessment of the potential mechanisms. Biomaterials. 2013;34(33):8013–7.

117. Visuri T, Kiviluoto O, Eskelin M. Carbon fiber for repair of the rotator cuff. A 4-year follow-up of 14 cases. Acta Orthop Scand. 1991;62(4):356–9.

118. King J, Bulstrode C. Polylactate-coated Carbon Fiber in Extra-articular Reconstruction of the Unstable Knee. Clin Orthop Relat Res. 1985;196:139–42.

119. Szabó G, Barabás J, Bogdán S, et al. Long-term clinical and experimental/surface analytical studies of carbon/carbon maxillofacial implants. Maxillofac Plast Reconstr Surg. 2015;37(1):34.

120. Amis A, Kempson S, Campbell J, et al. Anterior cruciate ligament replacement. Biocompatibility and biomechanics of polyester and carbon fibre in rabbits. J Bone Jt Surgery, Br Vol. 1988;70(4):628–34.

121. Inui A, Kokubu T, Makino T, et al. Potency of double-layered poly L-lactic acid scaffold in tissue engineering of tendon tissue. Int Orthop. 2010;34(8):1327–32.

122. Cooper J, Lu H, Ko F, et al. Fiber-based tissue-engineered scaffold for ligament replacement: design considerations and in vitro evaluation. Biomaterials. 2005;26(13):1523–32.

123. Orr S, Chainani A, Hippensteel K, et al. Aligned multilayered electrospun scaffolds for rotator cuff tendon tissue engineering. Acta Biomater. 2015;24:117–26.

124. Beason D, Connizzo B, Dourte L, et al. Fiber-aligned polymer scaffolds for rotator cuff repair in a rat model. J Shoulder Elb Surg. 2012;21:245–50.

125. Hakimi O, Mouthuy P-A, Zargar N, et al. A layered electrospun and woven surgical scaffold to enhance endogenous tendon repair. Acta Biomater. 2015;26:124–35.

126. Mouthuy P-A, Zargar N, Hakimi O, et al. Polydioxanone Electrospun Filaments To Mimic Tendon Hierarchical Architecture. Br J Sports Med. 2014;48(Suppl 2):A48–A48.

127. Lu H, Cooper J, Manuel S, et al. Anterior cruciate ligament regeneration using braided biodegradable scaffolds: in vitro optimization studies. Biomaterials. 2005;26:4805–16.

128. Baldwin M, Snelling S, Dakin S, et al. Augmenting endogenous repair of soft tissues with nanofibre scaffolds. J R Soc Interface. 2018;15(141).

129. Crowder S, Leonardo V, Whittaker T, et al. Material Cues as Potent Regulators of Epigenetics and Stem Cell Function. Cell Stem Cell. 2016;18(1):39–52.

130. Downing T, Soto J, Morez C, et al. Biophysical regulation of epigenetic state and cell reprogramming. Nat Mater. 2013;12(12):1154–62.

131. Mabry K, Payne S, Anseth K. Microarray analyses to quantify advantages of 2D and 3D hydrogel culture systems in maintaining the native valvular interstitial cell phenotype. Biomaterials. 2016;74:31–41.

132. Engler A, Sen S, Sweeney H, et al. Matrix Elasticity Directs Stem Cell Lineage Specification. Cell. 2006;126(4):677–89.

133. Dalby M, Gadegaard N, Wilkinson C. The response of fibroblasts to hexagonal nanotopography fabricated by electron beam lithography. J Biomed Mater Res - Part A. 2008;84(4):973–9.

134. Dalby MJ, Gadegaard N, Tare R, et al. The control of human mesenchymal cell differentiation using nanoscale symmetry and disorder. Nat Mater. 2007;6(12):997–1003.

135. Magnusson SP, Qvortrup K, Larsen JO, et al. Collagen fibril size and crimp morphology in ruptured and intact Achilles tendons. Matrix Biol. 2002;21(4):369–77.

136. Wang V, Wang F, McNickle A, et al. Medial Versus Lateral Supraspinatus Tendon Properties: Implications for Double-Row Rotator Cuff Repair. Am J Sports Med. 2010;38(12):2456–63.

137. Franchi M, Trirè A, Quaranta M, et al. Collagen Structure of Tendon Relates to Function. Sci World J. 2007;7:404–20.

138. Fang M, Holl M. Variation in type I collagen fibril nanomorphology: the significance and origin. Bonekey Rep. 2013;2(April):1–7.

139. Chaudhury S, Xia Z, Thakkar D, et al. Gene expression profiles of changes underlying different-sized human rotator cuff tendon tears. J Shoulder Elb Surg. 2016;25(10):1561–70.

140. Lynch H. Effect of Fiber Orientation and Strain Rate on the Nonlinear Uniaxial Tensile Material Properties of Tendon. J Biomech Eng. 2003;125(5):726.

141. Sankar S, Sharma CS, Rath SN, et al. Electrospun nanofibres to mimic natural hierarchical structure of tissues: Application in musculoskeletal regeneration. J Tissue Eng Regen Med. 2018;12:e604-19.

142. Pan H, Li L, Hu L, et al. Continuous aligned polymer fibers produced by a modified electrospinning method. Polymer (Guildf). 2006;47(14):4901–4.

143. Fee T, Surianarayanan S, Downs C, et al. Nanofiber alignment regulates NIH3T3 cell orientation and cytoskeletal gene expression on electrospun PCL+gelatin nanofibers. PLoS One. 2016;11(5):e0154806.

144. Full SM, Delman C, Gluck JM, et al. Effect of fiber orientation of collagen-based electrospun meshes on human fibroblasts for ligament tissue engineering applications. J Biomed Mater Res - Part B Appl Biomater. 2015;103(1):39–46.

145. Mi HY, Salick MR, Jing X, et al. Electrospinning of unidirectionally and orthogonally aligned thermoplastic polyurethane nanofibers: Fiber orientation and cell migration. J Biomed Mater Res - Part A. 2015;103(2):593–603.

146. Kendal A, Snelling S, Dakin S, et al. Resorbable electrospun polydioxanone fibres modify the behaviour of cells from both healthy and diseased human tendons. Eur Cells Mater. 2017;33:169–82.

147. Rowland DCL, Aquilina T, Klein A, et al. A comparative evaluation of the effect of polymer chemistry and fiber orientation on mesenchymal stem cell differentiation. J Biomed Mater Res - Part A. 2016;104(11):2843–53.

148. Yin Z, Chen X, Chen J, et al. The regulation of tendon stem cell differentiation by the alignment of nanofibers. Biomaterials. 2010;31(8):2163–75.

149. Delaine-Smith R, Green N, Matcher S, et al. Monitoring fibrous scaffold guidance of three-dimensional collagen organisation using minimally-invasive second harmonic generation. PLoS One. 2014;9(2):e89761.

150. Moffat K, Kwei AS-P, Spalazzi J, et al. Novel nanofiber-based scaffold for rotator cuff repair and augmentation. Tissue Eng Part A. 2009;15(1):115–26.

151. Naylor A, Filer A, Buckley C. The role of stromal cells in the persistence of chronic inflammation. Clin Exp Immunol. 2013;171(1):30–5.

152. Chaurey V, Block F, Su Y-H, et al. Nanofiber size-dependent sensitivity of fibroblast directionality to the methodology for scaffold alignment. Acta Biomater. 2012 Nov 1;8(11):3982–90.

153. Bashur C, Dahlgren L, Goldstein A. Effect of fiber diameter and orientation on fibroblast morphology and proliferation on electrospun poly(d,l-lactic-co-glycolic acid) meshes. Biomaterials. 2006;27(33):5681–8.

154. Kumbar S, Nukavarapu S, James R, et al. Electrospun poly(lactic acid-co-glycolic acid) scaffolds for skin tissue engineering. Biomaterials. 2008;29(30):4100–7.

155. Hsia H, Nair M, Mintz R, et al. The fiber diameter of synthetic bioresorbable extracellular matrix influences human fibroblast morphology and fibronectin matrix assembly. Plast Reconstr Surg. 2011;127(6):2312–20.

156. Cardwell RD, Dahlgren LA, Goldstein AS. Electrospun fibre diameter, not alignment, affects mesenchymal stem cell differentiation into the tendon/ligament lineage. J Tissue Eng Regen Med. 2014 Dec;8(12):937–45.

157. Erisken C, Zhang X, Moffat K, et al. Scaffold Fiber Diameter Regulates Human Tendon Fibroblast Growth and Differentiation. Tissue Eng Part A. 2013;19(3–4):519–28.

158. Grier W, Iyoha E, Harley B. The influence of pore size and stiffness on tenocyte bioactivity and transcriptomic stability in collagen-GAG scaffolds. J Mech Behav Biomed Mater. 2017;65:295–305.

159. Yang J, Shi G, Bei J, et al. Fabrication and surface modification of macroporous poly(L-lactic acid) and poly(L-lactic-co-glycolic acid) (70/30) cell scaffolds for human skin fibroblast cell culture. J Biomed Mater Res. 2002;62(3):438–46.

160. Tang Y, Wong C, Wang H, et al. Three-Dimensional Tissue Scaffolds from Interbonded

Poly(ε-Caprolactone) Fibrous Matrices with Controlled Porosity. Tissue Eng Part C Methods. 2011;17(2):209–18.

161. Butler S, Kohles S, Thielke R, et al. Interstitial fluid flow in tendons or ligaments: a porous medium finite element simulation. Med Biol Eng Comput. 1997;35(6):742–6.

162. Rnjak-Kovacina J, Wise S, Li Z, et al. Tailoring the porosity and pore size of electrospun synthetic human elastin scaffolds for dermal tissue engineering. Biomaterials. 2011;32(28):6729–36.

163. Mandal B, Kundu S. Cell proliferation and migration in silk fibroin 3D scaffolds. Biomaterials. 2009;30(15):2956–65.

164. Gu B, Park S, Kim M, et al. Fabrication of sonicated chitosan nanofiber mat with enlarged porosity for use as hemostatic materials. Carbohydr Polym. 2013;97(1):65–73.

165. Murphy CM, O'Brien FJ. Understanding the effect of mean pore size on cell activity in collagen-glycosaminoglycan scaffolds. Cell Adhes Migr. 2010;4(3):377–81.

166. Zhang Q, Luo H, Zhang Y, et al. Fabrication of three-dimensional poly(ε-caprolactone) scaffolds with hierarchical pore structures for tissue engineering. Mater Sci Eng C. 2013;33(4):2094–103.

167. Branco da Cunha C, Klumpers D, Li W, et al. Influence of the stiffness of three-dimensional alginate/collagen-I interpenetrating networks on fibroblast biology. Biomaterials. 2014;35(32):8927–36.

168. Mabry KM, Lawrence R, Anseth K. Dynamic stiffening of poly(ethylene glycol)-based hydrogels to direct valvular interstitial cell phenotype in a three-dimensional environment. Biomaterials. 2015;49:47–56.

169. Jeong J, Liang Y, Jang M, et al. Stiffness-modulated water retention and neovascularization of dermal fibroblast-encapsulating collagen gel. Tissue Eng Part A. 2013;19(11–12):1275–84.

170. Kessler D, Dethlefsen S, Haase I, et al. Fibroblasts in Mechanically Stressed Collagen Lattices Assume a "Synthetic" Phenotype. J Biol Chem. 2001;276(39):36575–85.

171. Maeda E, Sugimoto M, Ohashi T. Cytoskeletal tension modulates MMP-1 gene expression from tenocytes on micropillar substrates. J Biomech. 2013;46(5):991–7.

172. Park SH, Choi Y-J, Moon SW, et al. Three-Dimensional Bio-Printed Scaffold Sleeves With Mesenchymal Stem Cells for Enhancement of Tendon-to-Bone Healing in Anterior Cruciate Ligament Reconstruction Using Soft-Tissue Tendon Graft. Arthrosc J Arthrosc Relat Surg. 2018 Jan;34(1):166–79.

173. Hamzeh S, Miraftab M, Yoosefinejad A. Study of electrospun nanofibre formation process and their electrostatic analysis. J Ind Text. 2014;44(1):147–58.

174. Taylor G. Disintegration of water drops in an electric field. Proc R Soc London Ser A Math Phys Sci. 1964 Jul 28;280(1382):383–97.

175. Reneker DH, Yarin AL, Fong H, et al. Bending Instability of Electrically Charged Liquid Jets of Polymer Solutions in Electrospinning Bending instability of electrically charged liquid jets of polymer solutions in electrospinning. J Appl Phys. 2000;87(9):4531–47.

176. Deitzel J., Kleinmeyer J, Harris D, et al. The effect of processing variables on the morphology of electrospun nanofibers and textiles. Polymer (Guildf). 2001 Jan 1;42(1):261–72.

177. Eda G, Shivkumar S. Bead-to-fiber transition in electrospun polystyrene. J Appl Polym Sci. 2007 Oct 5;106(1):475–87.

178. Tarus B, Fadel N, Al-Oufy A, et al. Effect of polymer concentration on the morphology and mechanical characteristics of electrospun cellulose acetate and poly (vinyl chloride) nanofiber mats. Alexandria Eng J. 2016 Sep 1;55(3):2975–84.

179. Beachley V, Wen X. Effect of electrospinning parameters on the nanofiber diameter and length. Mater Sci Eng C Mater Biol Appl. 2009 Apr 30;29(3):663–8.

180. Yuan XY, Zhang YY, Dong C, et al. Morphology of ultrafine polysulfone fibers prepared by electrospinning. Polym Int. 2004;53(11):1704–10.

181. Zhang C, Yuan X, Wu L, et al. Study on morphology of electrospun poly(vinyl alcohol) mats. Eur Polym J. 2005;41:423–32.

182. Reneker DH, Chun I. Nanometre diameter fibres of polymer, produced by electrospinning. Vol. 7, Nanotechnology. 1996.

183. Zargham S, Bazgir S, Tavakoli A, et al. The Effect of Flow Rate on Morphology and Deposition Area of Electrospun Nylon 6 Nanofiber. J Eng Fiber Fabr. 2012 Dec 15;7(4):155892501200700.

184. Katta P, Alessandro M, Ramsier RD, et al. Continuous Electrospinning of Aligned Polymer Nanofibers onto a Wire Drum Collector. 2004;

185. Li W-J, Mauck RL, Cooper JA, et al. Engineering controllable anisotropy in electrospun biodegradable nanofibrous scaffolds for musculoskeletal tissue engineering. J Biomech. 2007 Jan 1;40(8):1686–93.

186. Mohan SD, Mitchell Abc GR, Davis FJ. Chain extension in electrospun polystyrene fibres: a SANS study.

187. Brooks H, Tucker N. Electrospinning predictions using artificial neural networks. Polymer (Guildf). 2015 Feb 10;58:22–9.

188. Khanlou HM, Sadollah A, Ang BC, et al. Prediction and optimization of electrospinning parameters for polymethyl methacrylate nanofiber fabrication using response surface methodology and artificial neural networks. Neural Comput Appl. 2014 Sep 30;25(3–4):767–77.

189. Buchko CJ, Chen LC, Shen Y, et al. Processing and microstructural characterization of porous biocompatible protein polymer thin films. Polymer (Guildf). 1999 Dec 1;40(26):7397–407.

190. Mit-uppatham C, Nithitanakul M, Supaphol P. Ultrafine Electrospun Polyamide-6 Fibers: Effect of Solution Conditions on Morphology and Average Fiber Diameter. Macromol Chem Phys. 2004 Nov 26;205(17):2327–38.

191. Zhao YY, Yang QB, Lu XF, et al. Study on correlation of morphology of electrospun products of polyacrylamide with ultrahigh molecular weight. J Polym Sci Part B Polym Phys. 2005 Aug 15;43(16):2190–5.

192. Koski A, Yim K, Shivkumar S. Effect of molecular weight on fibrous PVA produced by electrospinning. Mater Lett. 2004 Jan 1;58(3–4):493–7.

193. Huang C, Chen S, Lai C, et al. Electrospun polymer nanofibres with small diameters. Nanotechnology. 2006 Mar 28;17(6):1558–63.

194. Lach AA, Morris HL, Martins JA, et al. Pyridine as an additive to improve the deposition of continuous electrospun filaments. H Ribeiro M, editor. PLoS One. 2019 Apr

25;14(4):e0214419.

195. Cheryl L. Casper †, Jean S. Stephens †, Nancy G. Tassi †, et al. Controlling Surface Morphology of Electrospun Polystyrene Fibers: Effect of Humidity and Molecular Weight in the Electrospinning Process. 2003;

196. Linsell L, Dawson J, Zondervan K, et al. Prevalence and incidence of adults consulting for shoulder conditions in UK primary care; patterns of diagnosis and referral. Rheumatology. 2006 Feb 1;45(2):215–21.

197. Virta L, Joranger P, Brox JI, et al. Costs of shoulder pain and resource use in primary health care: a cost-of-illness study in Sweden. BMC Musculoskelet Disord. 2012 Dec 10;13(1):17.

198. Sher JS, Uribe JW, Posada A, et al. Abnormal findings on magnetic resonance images of asymptomatic shoulders. J Bone Jt Surg Am. 1995;77(1):10–5.

199. Yamamoto A, Takagishi K, Osawa T, et al. Prevalence and risk factors of a rotator cuff tear in the general population. J Shoulder Elb Surg. 2010;19(1):116–20.

200. Rashid MS, Cooper C, Cook J, et al. Increasing age and tear size reduce rotator cuff repair healing rate at 1 year. Acta Orthop. 2017;88(6):606–11.

201. Ozaki J, Fujimoto S, Masuhara K, et al. Reconstruction of chronic massive rotator cuff tears with synthetic materials. Clin Orthop Relat Res. 1986;(202):173–83.

202. Shea KP, Obopilwe E, Sperling JW, et al. A biomechanical analysis of gap formation and failure mechanics of a xenograft-reinforced rotator cuff repair in a cadaveric model. J Shoulder Elb Surg. 2012;21(8):1072–9.

203. Shea KP, McCarthy MB, Ledgard F, et al. Human Tendon Cell Response to 7 Commercially Available Extracellular Matrix Materials: An In Vitro Study. Arthrosc J Arthrosc Relat Surg. 2010 Sep 1;26(9):1181–8.

204. Mori D, Funakoshi N, Yamashita F. Arthroscopic surgery of irreparable large or massive rotator cuff tears with low-grade fatty degeneration of the infraspinatus: Patch autograft procedure versus partial repair procedure. Arthrosc - J Arthrosc Relat Surg. 2013;29(12):1911–21.

205. Smith RDJ, Zargar N, Brown CP, et al. Characterizing the macro and micro mechanical properties of scaffolds for rotator cuff repair. J Shoulder Elb Surg. 2017;26(11):2038–46.

206. Sedrakyan A, Campbell B, Merino JG, et al. IDEAL-D: A rational framework for evaluating and regulating the use of medical devices. BMJ. 2016;353:1–7.

207. Malcarney HL, Bonar F, Murrell GAC. Early Inflammatory Reaction after Rotator Cuff Repair with a Porcine Small Intestine Submucosal Implant. Am J Sports Med. 2005;33(6):907–11.

208. The Cochrane Collaboration. Cochrane Handbook for Systematic Reviews of Interventions. Version 5.1.0. Higgins JPT GS (editors), editor. 2011.

209. Dissemination C for R and. Systematic Reviews: CRDs guidance for undertaking reviews in health care. 2009.

210. Shamseer L, Moher D, Clarke M, et al. Preferred reporting items for systematic review and meta-analysis protocols (prisma-p) 2015: Elaboration and explanation. BMJ. 2015;349(January):1–25.

211. Greenall G, Carr A, Beard D, et al. Systematic review of the surgical management of

rotator cuff repair with an augmentative patch: a feasibility study protocol. Syst Rev. 2018 Dec 13;7(1):187.

212. DeOrio JK, Cofield RH. Results of a second attempt at surgical repair of a failed initial rotator-cuff repair. J Bone Joint Surg Am. 1984 Apr;66(4):563–7.

213. Gerber C, Fuchs B, Hodler J. The Results of Repair of Massive Tears of the Rotator Cuff. J Bone Jt Surg Am. 2000;82(4):505–15.

214. Ferguson DP, Lewington MR, Duncan Smith T, et al. Graft Utilization in the Augmentation of Large-to-Massive Rotator Cuff Repairs A Systematic Review.

215. Thangarajah T, Pendegrass CJ, Shahbazi S, et al. Augmentation of Rotator Cuff Repair With Soft Tissue Scaffolds. Orthop J Sport Med. 2015 Jun;3(6):2325967115587495.

216. Bailey JR, Kim C, Alentorn-Geli E, et al. Rotator Cuff Matrix Augmentation and Interposition: A Systematic Review and Meta-analysis. Am J Sports Med. 2018 Jun 15;036354651877476.

217. Steinhaus ME, Makhni EC, Cole BJ, et al. Outcomes After Patch Use in Rotator Cuff Repair. Arthrosc J Arthrosc Relat Surg. 2016 Aug 1;32(8):1676–90.

218. Papalia R, Franceschi F, Zampogna B, et al. Augmentation techniques for rotator cuff repair. Br Med Bull. 2013 Mar 1;105(1):107–38.

219. Higgins JPT, Altman DG, Gøtzsche PC, et al. The Cochrane Collaboration's tool for assessing risk of bias in randomised trials. BMJ. 2011 Oct 18;343:d5928.

220. Sterne JA, Hernán MA, Reeves BC, et al. ROBINS-I: a tool for assessing risk of bias in non-randomised studies of interventions. BMJ. 2016 Oct 12;355:i4919.

221. Leuzinger J, Sternberg C, Smolen D, et al. [Patch Augmentation in Rotator Cuff Repair Surgery with Elder Patients]. Z Orthop Unfall. 2016;154(5):504–12.

222. Ciampi P, Scotti C, Nonis A, et al. The benefit of synthetic versus biological patch augmentation in the repair of posterosuperior massive rotator cuff tears: A 3-year follow-up study. Am J Sports Med. 2014;42(5):1169–75.

223. Maillot C, Harly E, Demezon H, et al. Surgical repair of large-to-massive rotator cuff tears seems to be a better option than patch augmentation or débridement and biceps tenotomy: a prospective comparative study. J Shoulder Elb Surg. 2018;27(9):1545–52.

224. Petriccioli D, Bertone C, Marchi G, et al. Open repair of isolated traumatic subscapularis tendon tears with a synthetic soft tissue reinforcement. Musculoskelet Surg. 2013;97(1 SUPPL).

225. Schlegel TF, Abrams JS, Bushnell BD, et al. Radiologic and clinical evaluation of a bioabsorbable collagen implant to treat partial-thickness tears: a prospective multicenter study. J Shoulder Elb Surg. 2018;27(2):242–51.

226. Barber FA, Burns JP, Deutsch A, et al. A prospective, randomized evaluation of acellular human dermal matrix augmentation for arthroscopic rotator cuff repair. Arthrosc - J Arthrosc Relat Surg. 2012;28(1):8–15.

227. Bryant D, Holtby R, Willits K, et al. A randomized clinical trial to compare the effectiveness of rotator cuff repair with or without augmentation using porcine small intestine submucosa for patients with moderate to large rotator cuff tears: a pilot study. J Shoulder Elb Surg. 2016;25(10):1623–33.

228. Iannotti JP, Codsi MJ, Kwon YW, et al. Porcine small intestine submucosa augmentation of surgical repair of chronic two-tendon rotator cuff tears. J Bone Jt Surg

Am. 2006;88(6):1238–44.

229. Gilot GJ, Alvarez-Pinzon AM, Barcksdale L, et al. Outcome of Large to Massive Rotator Cuff Tears Repaired With and Without Extracellular Matrix Augmentation: A Prospective Comparative Study. Arthroscopy. 2015;31(8):1459–65.

230. Mori D, Funakoshi N, Yamashita F. Arthroscopic Surgery of Irreparable Large or Massive Rotator Cuff Tears With Low-Grade Fatty Degeneration of the Infraspinatus: Patch Autograft Procedure Versus Partial Repair Procedure. Arthrosc J Arthrosc Relat Surg. 2013 Dec 1;29(12):1911–21.

231. Ito J, Morioka T. Surgical treatment for large and massive tears of the rotator cuff. Int Orthop. 2003;27(4):228–31.

232. Vitali M, Cusumano A, Pedretti A, et al. Employment of Synthetic Patch with Augmentation of the Long Head of the Biceps Tendon in Irreparable Lesions of the Rotator Cuff: Our Technique Applied to 60 Patients. Tech Hand Up Extrem Surg. 2015;19(1):32–9.

233. Yoon JP, Chung SW, Kim JY, et al. Outcomes of Combined Bone Marrow Stimulation and Patch Augmentation for Massive Rotator Cuff Tears. Am J Sports Med. 2016;44(4):963–71.

234. Jeon YS, Lee J, Kim RG, et al. Does Additional Biceps Augmentation Improve Rotator Cuff Healing and Clinical Outcomes in Anterior L-Shaped Rotator Cuff Tears? Clinical Comparisons With Arthroscopic Partial Repair. Am J Sports Med. 2017;45(13):2982–8.

235. Gupta AK, Hug K, Berkoff DJ, et al. Dermal tissue allograft for the repair of massive irreparable rotator cuff tears. Am J Sports Med. 2012;40(1):141–7.

236. Gupta AK, Hug K, Boggess B, et al. Massive or 2-tendon rotator cuff tears in active patients with minimal glenohumeral arthritis: Clinical and radiographic outcomes of reconstruction using dermal tissue matrix xenograft. Am J Sports Med. 2013;41(4):872–9.

237. Petri M, Warth RJ, Horan MP, et al. Outcomes After Open Revision Repair of Massive Rotator Cuff Tears With Biologic Patch Augmentation. Arthrosc - J Arthrosc Relat Surg. 2016;32(9):1752–60.

238. Tempelaere C, Desmoineaux P, Lespagnol F, et al. Surgical repair of massive rotator cuff tendon tears: Autologous quadriceps tendon graft versus arthroscopic repair. Orthop Traumatol Surg Res. 2017;103(3):435–40.

239. Scheibel M, Brown A, Woertler K, et al. Preliminary results after rotator cuff reconstruction augmented with an autologous periosteal flap. Knee Surgery, Sport Traumatol Arthrosc. 2007;15(3):305–14.

240. Moore DR, Cain EL, Schwartz ML, et al. Allograft reconstruction for massive, irreparable rotator cuff tears. Am J Sports Med. 2006;34(3):392–6.

241. Tashjian RZ, Deloach J, Porucznik CA, et al. Minimal clinically important differences (MCID) and patient acceptable symptomatic state (PASS) for visual analog scales (VAS) measuring pain in patients treated for rotator cuff disease. J Shoulder Elb Surg. 2009 Nov;18(6):927–32.

242. Mori D, Funakoshi N, Yamashita F, et al. Effect of fatty degeneration of the infraspinatus on the efficacy of arthroscopic patch autograft procedure for large to massive rotator cuff tears. Am J Sports Med. 2015;43(5):1108–17.

243. Ferguson DP, Lewington MR, Smith TD, et al. Graft Utilization in the Augmentation of Large-to-Massive Rotator Cuff Repairs. Am J Sports Med. 2016 Nov 20;44(11):2984–92.

244. Berry M, Stanek JJ. The PIP mammary prosthesis: A product recall study. J Plast Reconstr Aesthetic Surg. 2012 Jun 1;65(6):697–704.

245. Hirst A, Philippou Y, Blazeby J, et al. No Surgical Innovation Without Evaluation. Ann Surg. 2018;269(2):1.

246. Millar N, Hueber A, Reilly J, et al. Inflammation Is Present in Early Human Tendinopathy. Am J Sports Med. 2010;38(10):2085–91.

247. Phipps Ying Zhang RP, James Cao H, Graf B, et al. Production in Human Lung Fibroblasts 2 E Cyclooxygenase-2 Expression and Prostaglandin Cutting Edge: CD40 Engagement Up-Regulates. J Immunol. 1998;160:1053–7.

248. Rg J, Distler HW, Jü A, et al. The induction of matrix metalloproteinase and cytokine expression in synovial fibroblasts stimulated with immune cell microparticles. Proc Natl Acad Sci. 2005;102(8):2892–7.

249. Mosca MJ, Carr AJ, Snelling SJB, et al. Differential expression of alarmins-S100A9, IL-33, HMGB1 and HIF-1α in supraspinatus tendinopathy before and after treatment. BMJ open Sport Exerc Med. 2017;3(1):e000225.

250. Smith RS, Smith TJ, Blieden TM, et al. Commentary Fibroblasts as Sentinel Cells Synthesis of Chemokines and Regulation of Inflammation. Am J Pathol. 1997;151(2):317–22.

251. Douglas MR, Morrison KE, Salmon M, et al. Why does inflammation persist: a dominant role for the stromal microenvironment? Expert Rev Mol Med. 2002 Dec 9;4(25):1–18.

252. Dakin SG, Buckley CD, Al-Mossawi MH, et al. Persistent stromal fibroblast activation is present in chronic tendinopathy. Arthritis Res Ther. 2017;19(1):16.

253. Springer TA. Traffic signals for lymphocyte recirculation and leukocyte emigration: The multistep paradigm. Cell. 1994 Jan 28;76(2):301–14.

254. Ley K, Laudanna C, Cybulsky MI, et al. Getting to the site of inflammation: the leukocyte adhesion cascade updated. Nat Rev Immunol. 2007 Sep 1;7(9):678–89.

255. Nash GB, Buckley CD, Ed Rainger G. The local physicochemical environment conditions the proinflammatory response of endothelial cells and thus modulates leukocyte recruitment. FEBS Lett. 2004 Jul 2;569(1–3):13–7.

256. Buckley CD, Barone F, Nayar S, et al. Stromal Cells in Chronic Inflammation and Tertiary Lymphoid Organ Formation. Annu Rev Immunol. 2015;33(1):715–45.

257. Dean BJF, Franklin SL, Murphy RJ, et al. Glucocorticoids induce specific ion-channel-mediated toxicity in human rotator cuff tendon: a mechanism underpinning the ultimately deleterious effect of steroid injection in tendinopathy? Br J Sports Med. 2014;48(22):1620–6.

258. Schmittgen TD, Livak KJ. Analyzing real-time PCR data by the comparative C(T) method. Nat Protoc. 2008;3(6):1101–8.

259. Jeffery HC, Buckley CD, Moss P, et al. Analysis of the effects of stromal cells on the migration of lymphocytes into and through inflamed tissue using 3-D culture models. J Immunol Methods. 2013;400–401(1):45–57.

260. Park A-M, Tsunoda I, Yoshie O. Heat shock protein 27 promotes cell cycle progression

by down-regulating E2F transcription factor 4 and retinoblastoma family protein p130. J Biol Chem. 2018 Oct 12;293(41):15815–26.

261. Broermann A, Winderlich M, Block H, et al. Dissociation of VE-PTP from VE-cadherin is required for leukocyte extravasation and for VEGF-induced vascular permeability in vivo. J Exp Med. 2011 Nov 21;208(12):2393–401.

262. Akbar M, McLean M, Garcia-Melchor E, et al. Fibroblast activation and inflammation in frozen shoulder. PLoS One. 2019;14(4):1–16.

263. Kuzet S-E, Gaggioli C. Fibroblast activation in cancer: when seed fertilizes soil. Cell Tissue Res. 2016 Sep 29;365(3):607–19.

264. Li Y, Bao J, Bian Y, et al. S100A4+ Macrophages Are Necessary for Pulmonary Fibrosis by Activating Lung Fibroblasts. Front Immunol. 2018 Aug 6;9:1776.

265. Doucet C, Brouty-Boyé D, Pottin-Clemenceau C, et al. IL-4 and IL-13 specifically increase adhesion molecule and inflammatory cytokine expression in human lung fibroblasts. Int Immunol. 1998 Oct 1;10(10):1421–33.

266. Pierce GF, Vande Berg J, Rudolph R, et al. Platelet-derived growth factor-BB and transforming growth factor beta 1 selectively modulate glycosaminoglycans, collagen, and myofibroblasts in excisional wounds. Am J Pathol. 1991 Mar;138(3):629–46.

267. Elias JA, Lentz V, Cummings PJ. Transforming growth factor-beta regulation of IL-6 production by unstimulated and IL-1-stimulated human fibroblasts. J Immunol. 1991 May 15;146(10):3437–43.

268. Nilsen EM, Johansen FE, Jahnsen FL, et al. Cytokine profiles of cultured microvascular endothelial cells from the human intestine. Gut. 1998 May;42(5):635–42.

269. Rahim M, El Khoury LY, Raleigh SM, et al. Human Genetic Variation, Sport and Exercise Medicine, and Achilles Tendinopathy: Role for Angiogenesis-Associated Genes. Omi A J Integr Biol. 2016 Sep;20(9):520–7.

270. Salles JI, Duarte MEL, Guimarães JM, et al. Vascular Endothelial Growth Factor Receptor-2 Polymorphisms Have Protective Effect against the Development of Tendinopathy in Volleyball Athletes. Lucía A, editor. PLoS One. 2016 Dec 8;11(12):e0167717.

271. Rahim M, Hobbs H, van der Merwe W, et al. Investigation of angiogenesis genes with anterior cruciate ligament rupture risk in a South African population. J Sports Sci. 2018 Mar 4;36(5):551–7.

272. Sanchez B, Li L, Dulong J, et al. Impact of Human Dermal Microvascular Endothelial Cells on Primary Dermal Fibroblasts in Response to Inflammatory Stress. Front Cell Dev Biol. 2019 Apr 3;7:44.

273. Pang G, Couch L, Batey R, et al. IL-10, ICAM-1 and VCAM-1 gene expression and cytokine production in human duodenal fibroblasts stimulated with lipopolysaccharide, IL-la and TNF-a. Vol. 96, Clin Exp Immunol. 1994.

274. Yi JS, Cox MA, Zajac AJ. T-cell exhaustion: characteristics, causes and conversion. Immunology. 2010 Apr;129(4):474–81.

275. Bi J, Tian Z. NK Cell Exhaustion. Front Immunol. 2017 Jun 28;8:760.

276. Wherry EJ. T cell exhaustion. Nat Immunol. 2011 Jun 18;12(6):492–9.

277. Klingberg F, Hinz B, White ES. The myofibroblast matrix: implications for tissue repair and fibrosis. J Pathol. 2013 Jan;229(2):298–309.

278. Shi-Wen X, Chen Y, Denton CP, et al. Endothelin-1 promotes myofibroblast induction through the ETA receptor via a rac/phosphoinositide 3-kinase/Akt-dependent pathway and is essential for the enhanced contractile phenotype of fibrotic fibroblasts. Mol Biol Cell. 2004 Jun;15(6):2707–19.

279. Villaschi S, Nicosia RF. Paracrine interactions between fibroblasts and endothelial cells in a serum-free coculture model. Modulation of angiogenesis and collagen gel contraction. Lab Invest. 1994 Aug;71(2):291–9.

280. Korff T, Kimmina S, Martiny-Baron G, et al. Blood vessel maturation in a 3-dimensional spheroidal coculture model: direct contact with smooth muscle cells regulates endothelial cell quiescence and abrogates VEGF responsiveness. FASEB J. 2001 Feb;15(2):447–57.

281. Hackett L, Millar NL, Lam P, et al. Are the Symptoms of Calcific Tendinitis Due to Neoinnervation and/or Neovascularization? J Bone Jt Surg. 2016 Feb 3;98(3):186–92.

282. McGettrick HM, Buckley CD, Filer A, et al. Stromal cells differentially regulate neutrophil and lymphocyte recruitment through the endothelium. Immunology. 2010;131(3):357–70.

283. Aird WC. Phenotypic heterogeneity of the endothelium: I. Structure, function, and mechanisms. Circ Res. 2007 Feb 2;100(2):158–73.

284. Denton CP, Shi-Wen X, Sutton A, et al. Scleroderma fibroblasts promote migration of mononuclear leucocytes across endothelial cell monolayers. Clin Exp Immunol. 1998 Nov;114(2):293–300.

285. McGettrick HM, Buckley CD, Ed Rainger G, et al. Influence of stromal cells on lymphocyte adhesion and migration on endothelial cells. Methods Mol Biol. 2010;616:49–68.

286. Patel BKR, Wang L-M, Lee C-C, et al. Stat6 and Jak1 Are Common Elements in Platelet-derived Growth Factor and Interleukin-4 Signal Transduction Pathways in NIH 3T3 Fibroblasts*.

287. Curbishley SM, Eksteen B, Gladue RP, et al. CXCR 3 activation promotes lymphocyte transendothelial migration across human hepatic endothelium under fluid flow. Am J Pathol. 2005 Sep;167(3):887–99.

288. Srinivasan B, Kolli AR, Esch MB, et al. TEER measurement techniques for in vitro barrier model systems. J Lab Autom. 2015;20(2):107.

289. Marcu R, Choi YJ, Xue J, et al. Human Organ-Specific Endothelial Cell Heterogeneity. iScience. 2018 Jun 29;4:20–35.

290. Magnusson S, Qvortrup K, Larsen J, et al. Collagen fibril size and crimp morphology in ruptured and intact Achilles tendons. Matrix Biol. 2002;21(4):369–77.

291. Kendal A, Snelling S, Dakin S, et al. Resorbable electrospun polydioxanone fibres modify the behaviour of cells from both healthy and diseased human tendons. Eur Cells Mater. 2017;33(March):169–82.

292. Filer A, Antczak P, Parsonage GN, et al. Stromal transcriptional profiles reveal hierarchies of anatomical site, serum response and disease and identify disease specific pathways. PLoS One. 2015;10(3):1–17.

293. Newman AC, Nakatsu MN, Chou W, et al. The requirement for fibroblasts in angiogenesis: fibroblast-derived matrix proteins are essential for endothelial cell lumen formation. Mol Biol Cell. 2011 Oct;22(20):3791–800.

294. Matthijs Blankesteijn W. Has the search for a marker of activated fibroblasts finally come to an end? J Mol Cell Cardiol. 2015;88:120–3.

295. Li X, Cho B, Martin R, et al. Nanofiber-hydrogel composite-mediated angiogenesis for soft tissue reconstruction. Sci Transl Med. 2019 May 1;11(490):eaau6210.

296. Engler AJ, Sen S, Sweeney HL, et al. Matrix Elasticity Directs Stem Cell Lineage Specification. Cell. 2006;126(4):677–89.

297. Dalby M, Gadegaard N, Tare R, et al. The control of human mesenchymal cell differentiation using nanoscale symmetry and disorder. Nat Mater. 2007;6(12):997–1003.

298. Zhang C, Wang X, Zhang E, et al. An epigenetic bioactive composite scaffold with well-aligned nanofibers for functional tendon tissue engineering. Acta Biomater. 2018;66:141–56.

299. Klein K, Ospelt C, Gay S. Epigenetic contributions in the development of rheumatoid arthritis. Arthritis Res Ther. 2012;14(6).

300. Liu H, Li X, Zhou G, et al. Electrospun sulfated silk fibroin nanofibrous scaffolds for vascular tissue engineering. Biomaterials. 2011;32(15):3784–93.

301. Ziabari M, Mottaghitalab V, Haghi AK. Evaluation of electrospun nanofiber pore structure parameters. Korean J Chem Eng. 2008;25(4):923–32.

302. Chen L, Fei C, Zhu L, et al. RNA-seq approach to analysis of gene expression profiles in dark green island and light green tissue of cucumber mosaic virus-infected nicotiana tabacum. PLoS One. 2017;12(5):1–19.

303. Kim D, Langmead B, Slazberg S. HISAT: a fast spliced aligner with low memory requirements. Nat Methods. 2015;12(4):357–60.

304. Broad Institute. Picard Tools [Internet]. [cited 2019 Jun 2].

305. Liao Y, Smyth GK, Shi W. FeatureCounts: An efficient general purpose program for assigning sequence reads to genomic features. Bioinformatics. 2014;30(7):923–30.

306. Love MI, Huber W, Anders S. Moderated estimation of fold change and dispersion for RNA-seq data with DESeq2. Genome Biol. 2014;15(12):550.

307. Zhu A, Ibrahim JG, Love MI. Heavy-tailed prior distributions for sequence count data: removing the noise and preserving large differences. Bioinformatics. 2018;(November):1–9.

308. Cremers J, Klugkist I. One direction? A tutorial for circular data analysis using R with examples in cognitive psychology. Front Psychol. 2018;9(OCT):1–13.

309. Pollen AA, Nowakowski TJ, Shuga J, et al. Low-coverage single-cell mRNA sequencing reveals cellular heterogeneity and activated signaling pathways in developing cerebral cortex. Nat Biotechnol. 2014;32(10):1053–8.

310. Korpelainen E, Tuimala J, Somervuo P, et al. RNA-seq Data Analysis. A practical approach. 2015. 1-27 p.

311. Hakimi O, Mouthuy PA, Zargar N, et al. A layered electrospun and woven surgical scaffold to enhance endogenous tendon repair. Acta Biomater. 2015;26:124–35.

312. Liberzon A, Birger C, Thorvaldsdóttir H, et al. The Molecular Signatures Database Hallmark Gene Set Collection. Cell Syst. 2015;1(6):417–25.

313. Tomasek JJ, Gabbiani G, Hinz B, et al. Myofibroblasts and mechano-regulation of connective tissue remodelling. Nat Rev Mol Cell Biol. 2002 May;3(5):349–63.

314. Parsonage G, Filer AD, Haworth O, et al. A stromal address code defined by fibroblasts. Trends Immunol. 2005 Mar;26(3):150–6.

315. Chen C-H, Chen S-H, Kuo C-Y, et al. Response of Dermal Fibroblasts to Biochemical and Physical Cues in Aligned Polycaprolactone/Silk Fibroin Nanofiber Scaffolds for Application in Tendon Tissue Engineering. Nanomaterials. 2017;7(8):219.

316. Chen M, Patra PK, Warner SB, et al. Role of Fiber Diameter in Adhesion and Proliferation of NIH 3T3 Fibroblast on Electrospun Polycaprolactone Scaffolds. Tissue Eng. 2007;13(3):579–87.

317. Hodgkinson T, Yuan X-F, Bayat A. Electrospun silk fibroin fiber diameter influences in vitro dermal fibroblast behavior and promotes healing of ex vivo wound models. J Tissue Eng. 2014;5:204173141455166.

318. Bashur C a, Shaffer RD, Dahlgren L a, et al. Effect of fiber diameter and alignment of electrospun polyurethane meshes on mesenchymal progenitor cells. Tissue Eng Part A. 2009;15(9):2435–45.

319. Liu Y, Ji Y, Ghosh K, et al. Effects of fiber orientation and diameter on the behavior of human dermal fibroblasts on electrospun PMMA scaffolds. J Biomed Mater Res - Part A. 2009 Sep 15;90A(4):1092–106.

320. Kubow KE, Shuklis VD, Sales DJ, et al. Contact guidance persists under myosin inhibition due to the local alignment of adhesions and individual protrusions. Sci Rep. 2017 Dec 30;7(1):14380.

321. Ohara PT, Buck RC. Contact guidance in vitro. Exp Cell Res. 1979 Jul;121(2):235–49.

322. Zhang C, Yuan H, Liu H, et al. Well-aligned chitosan-based ultrafine fibers committed teno-lineage differentiation of human induced pluripotent stem cells for Achilles tendon regeneration. Biomaterials. 2015 Jun 1;53:716–30.

323. Garg K, Pullen NA, Oskeritzian CA, et al. Macrophage functional polarization (M1/M2) in response to varying fiber and pore dimensions of electrospun scaffolds. Biomaterials. 2013 Jun;34(18):4439–51.

324. Ospelt C, Reedquist KA, Gay S, et al. Inflammatory memories: Is epigenetics the missing link to persistent stromal cell activation in rheumatoid arthritis? Autoimmun Rev. 2011;10(9):519–24.

325. Hilkens MU, Catharien MPC, Rae M, et al. Equivalent to Mesenchymal Stem Cells Immunoregulatory Cells and Functionally Adult Human Fibroblasts Are Potent. J Immunol. 2007;179:1595–604.

326. Erez N, Truitt M, Olson P, et al. Cancer-Associated Fibroblasts Are Activated in Incipient Neoplasia to Orchestrate Tumor-Promoting Inflammation in an NF-κB-Dependent Manner. Cancer Cell. 2010 Feb 17;17(2):135–47.

327. Özdemir BC, Pentcheva-Hoang T, Carstens JL, et al. Depletion of Carcinoma-Associated Fibroblasts and Fibrosis Induces Immunosuppression and Accelerates Pancreas Cancer with Reduced Survival. Cancer Cell. 2014 Jun 16;25(6):719–34.

328. Condeelis J, Pollard JW. Macrophages: Obligate Partners for Tumor Cell Migration, Invasion, and Metastasis. Cell. 2006 Jan;124(2):263–6.

329. Cadby JA, Buehler E, Godbout C, et al. Differences between the cell populations from

the peritenon and the tendon core with regard to their potential implication in tendon repair. PLoS One. 2014;9(3):e92474.

330. Millar NL, Gilchrist DS, Akbar M, et al. MicroRNA29a regulates IL-33-mediated tissue remodelling in tendon disease. Nat Commun. 2015 Nov 10;6(1):6774.

331. Castel D, Baghdadi MB, Mella S, et al. Small-RNA sequencing identifies dynamic microRNA deregulation during skeletal muscle lineage progression. Sci Rep. 2018 Dec 9;8(1):4208.

332. Carninci P, Kasukawa T, Katayama S, et al. The transcriptional landscape of the mammalian genome. Science. 2005 Sep 2;309(5740):1559–63.

333. Maman E, Harris C, White L, et al. Outcome of Nonoperative Treatment of Symptomatic Rotator Cuff Tears Monitored by Magnetic Resonance Imaging. J Bone Jt Surgery-American Vol. 2009 Aug;91(8):1898–906.

334. Keener JD, Galatz LM, Teefey SA, et al. A Prospective Evaluation of Survivorship of Asymptomatic Degenerative Rotator Cuff Tears. J Bone Jt Surg. 2015 Jan;97(2):89–98.

335. Wise J. NICE to ban mesh for vaginal wall prolapse. BMJ. 2017 Nov 28;359:j5523.

336. Aurora A, McCarron J, van den Bogert A, et al. The biomechanical role of scaffolds in augmented rotator cuff tendon repairs. J Shoulder Elb Surg. 2012;21(8):1064–71.

337. Stolk M, Klatte-Schulz F, Schmock A, et al. New insights into tenocyte-immune cell interplay in an in vitro model of inflammation. Sci Rep. 2017 Dec 29;7(1):9801.

338. Buscemi N, Hartling L, Vandermeer B, et al. Single data extraction generated more errors than double data extraction in systematic reviews. J Clin Epidemiol. 2006 Jul 1;59(7):697–703.

339. Mehran R, Leon MB, Feigal DA, et al. Post-Market Approval Surveillance. Circulation. 2004 Jun 29;109(25):3073–7.

340. Resnic FS, Majithia A, Marinac-Dabic D, et al. Registry-Based Prospective, Active Surveillance of Medical-Device Safety. N Engl J Med. 2017 Feb 9;376(6):526–35.

341. Barthel F-S, Parmar M, Royston P. How do multi-stage, multi-arm trials compare to the traditional two-arm parallel group design – a reanalysis of 4 trials. Trials. 2009 Dec 17;10(1):21.

342. Parmar MKB, Carpenter J, Sydes MR. More multiarm randomised trials of superiority are needed. Lancet (London, England). 2014 Jul 26;384(9940):283–4.

343. Wiseman BS, Werb Z. Stromal effects on mammary gland development and breast cancer. Science. 2002 May 10;296(5570):1046–9.

344. Bibby AC, Torgerson DJ, Leach S, et al. Commentary: considerations for using the 'Trials within Cohorts' design in a clinical trial of an investigational medicinal product. Trials. 2018 Dec 8;19(1):18.

345. Asgari M, Latifi N, Heris HK, et al. In vitro fibrillogenesis of tropocollagen type III in collagen type I affects its relative fibrillar topology and mechanics. Sci Rep. 2017;7(1):1392.

346. Lovell CR, Smolenski KA, Duance VC, et al. Type I and III collagen content and fibre distribution in normal human skin during ageing. Vol. 117, British Journal of Dermatology. 1987.

347. Gay S, Vijanto J, Raekallio J, et al. Collagen types in early phases of wound healing in children. Acta Chir Scand. 1978;144(4):205–11.

348. Haukipuro K, Melkko J, Risteli L, et al. Synthesis of type I collagen in healing wounds in humans. Ann Surg. 1991 Jan;213(1):75–80.

349. Noah AC, Li TM, Martinez LM, et al. Adaptive and Innate Immune Cell Responses in Tendons and Lymph Nodes After Tendon Injury and Repair. bioRxiv. 2019 Jun 4;658310.

350. Ye C, Ho DJ, Neri M, et al. DRUG-seq for miniaturized high-throughput transcriptome profiling in drug discovery. Nat Commun. 2018 Dec 17;9(1):4307.

351. Woollard PM, Mehta NAL, Vamathevan JJ, et al. The application of next-generation sequencing technologies to drug discovery and development. Drug Discov Today. 2011 Jun 1;16(11–12):512–9.

352. Arends LR, Hoes AW, Lubsen J, et al. Baseline risk as predictor of treatment benefit: three clinical meta-re-analyses. Stat Med. 2000 Dec 30;19(24):3497–518.

353. Qu F, Holloway JL, Esterhai JL, et al. Programmed biomolecule delivery to enable and direct cell migration for connective tissue repair. Nat Commun. 2017 Dec 24;8(1):1780.

354. Ohberg L, Alfredson H. Ultrasound guided sclerosis of neovessels in painful chronic Achilles tendinosis: pilot study of a new treatment. Br J Sports Med. 2002 Jun 1;36(3):173-5; discussion 176-7.

355. Murphy RJ, Floyd Dean BJ, Wheway K, et al. A Novel Minimally Invasive Ultrasound-Guided Technique to Biopsy Supraspinatus Tendon. Oper Tech Orthop. 2013 Jun;23(2):56–62.

356. Weih F, Carrasco D, Durham SK, et al. Multiorgan inflammation and hematopoietic abnormalities in mice with a targeted disruption of RelB, a member of the NF-κB/Rel family. Cell. 1995 Jan 27;80(2):331–40.

357. Ijaz T, Wakamiya M, Sun H, et al. Generation and characterization of a novel transgenic mouse harboring conditional nuclear factor-kappa B/RelA knockout alleles. BMC Dev Biol. 2016 Dec 23;16(1):32.

358. Li Q, Estepa G, Memet S, et al. Complete lack of NF-kappaB activity in IKK1 and IKK2 double-deficient mice: additional defect in neurulation. Genes Dev. 2000 Jul 15;14(14):1729–33.

359. Duscher D, Maan ZN, Whittam AJ, et al. Fibroblast-Specific Deletion of Hypoxia Inducible Factor-1 Critically Impairs Murine Cutaneous Neovascularization and Wound Healing. Plast Reconstr Surg. 2015 Nov;136(5):1004–13.

360. DeCicco-Skinner KL, Henry GH, Cataisson C, et al. Endothelial cell tube formation assay for the in vitro study of angiogenesis. J Vis Exp. 2014 Sep 1;(91):e51312.

361. Xu Y, Yuan L, Mak J, et al. Neuropilin-2 mediates VEGF-C-induced lymphatic sprouting together with VEGFR3. J Cell Biol. 2010 Jan 11;188(1):115–30.

362. Walia B, Huang AH. Tendon stem progenitor cells: Understanding the biology to inform therapeutic strategies for tendon repair. J Orthop Res. 2019 Jun 18;37(6):1270–80.

363. Scott A, Danielson P, Abraham T, et al. Mechanical force modulates scleraxis expression in bioartificial tendons. J Musculoskelet Neuronal Interact. 2011;11(2):124–32.

364. Davies R, Vogelsang P, Jonsson R, et al. An optimized multiplex flow cytometry

protocol for the analysis of intracellular signaling in peripheral blood mononuclear cells. J Immunol Methods. 2016 Sep 1;436:58–63.

365. van der Flier A, Arnoud S. Function and interactions of integrins. Cell Tissue Res. 2001;305:285–98.

366. Neri S, Ishii G, Hashimoto H, et al. Podoplanin-expressing cancer-associated fibroblasts lead and enhance the local invasion of cancer cells in lung adenocarcinoma. Int J Cancer. 2015 Aug 15;137(4):784–96.

367. Quintanilla M, Montero-Montero L, Renart J, et al. Podoplanin in Inflammation and Cancer. Int J Mol Sci. 2019 Feb 6;20(3):707.

368. Ward LSC, Sheriff L, Marshall JL, et al. Podoplanin regulates the migration of mesenchymal stromal cells and their interaction with platelets. J Cell Sci. 2019;132:jcs222067.

Appendices

APPENDIX A - ADDITIONAL INFORMATION FOR CHAPTER 2

Table A-1 Embase search Strategy

	Searches	Results
1	exp rotator cuff rupture/	5732
2	exp rotator cuff injury/	8726
3	exp tendon injury/	20086
4	(rotator cuff tear or rotator cuff rupture or rotator cuff injur* or supraspinatus tear or supraspinatus rupture or supraspinatus injur* or infraspinatus tear or infraspinatus rupture or infraspinatus injur* or subscapularis tear or subscapularis rupture or subscapularis injur* or tendon tear or tendon rupture or tendon injur* or shoulder pain or shoulder injur*).mp.	38603
5	or/1-4	39799
6	exp tissue repair/	17952
7	exp shoulder surgery/	4863
8	(tissue repair or shoulder surgery or augment*).mp.	212917
9	exp tissue scaffold/	11559
10	exp extracellular matrix/	99144
11	exp bioprosthesis/	7140
12	exp allograft/	40591
13	exp autograft/	13831
14	exp surgical mesh/	12582
15	exp acellular dermal matrix/	1282
16	(tissue scaffold or extracellular matrix or bioprosthesis or allograft or autograft or surgical	321825
17	or/6-16	533208
18	5 and 17	3914
19	Clinical trial/	1042043
20	Randomized controlled trial/	481803

21	Randomization/	84993
22	Single blind procedure/	29844
23	Double blind procedure/	141452
24	Crossover procedure/	55396
25	Placebo/	333461
26	Randomi?ed controlled trial$.tw.	155939
27	Rct.tw.	23487
28	Random allocation.tw.	1668
29	Randomly allocated.tw.	27352
30	Allocated randomly.tw.	2233
31	(allocated adj2 random).tw.	860
32	Single blind$.tw.	19262
33	Double blind$.tw.	178171
34	((treble or triple) adj blind$).tw.	698
35	Placebo$.tw.	254195
36	Prospective study/	401796
37	Retrospective study/	538437
38	Longitudinal study/	109396
39	(Case control adj (study or studies)).tw.	103770
40	(Cohort adj (study or studies)).tw.	187964
41	or/19-40	2619904
42	18 and 41	794
43	limit 42 to dd=20060401-20170228	370

APPENDIX B ADDITIONAL INFORMATION FOR CHAPTER 3

Figure B-1 Schematic diagram depicting co-culture method and mRNA extraction for cultures of tendon-derived fibroblasts and HMEC-1 endothelial cells.

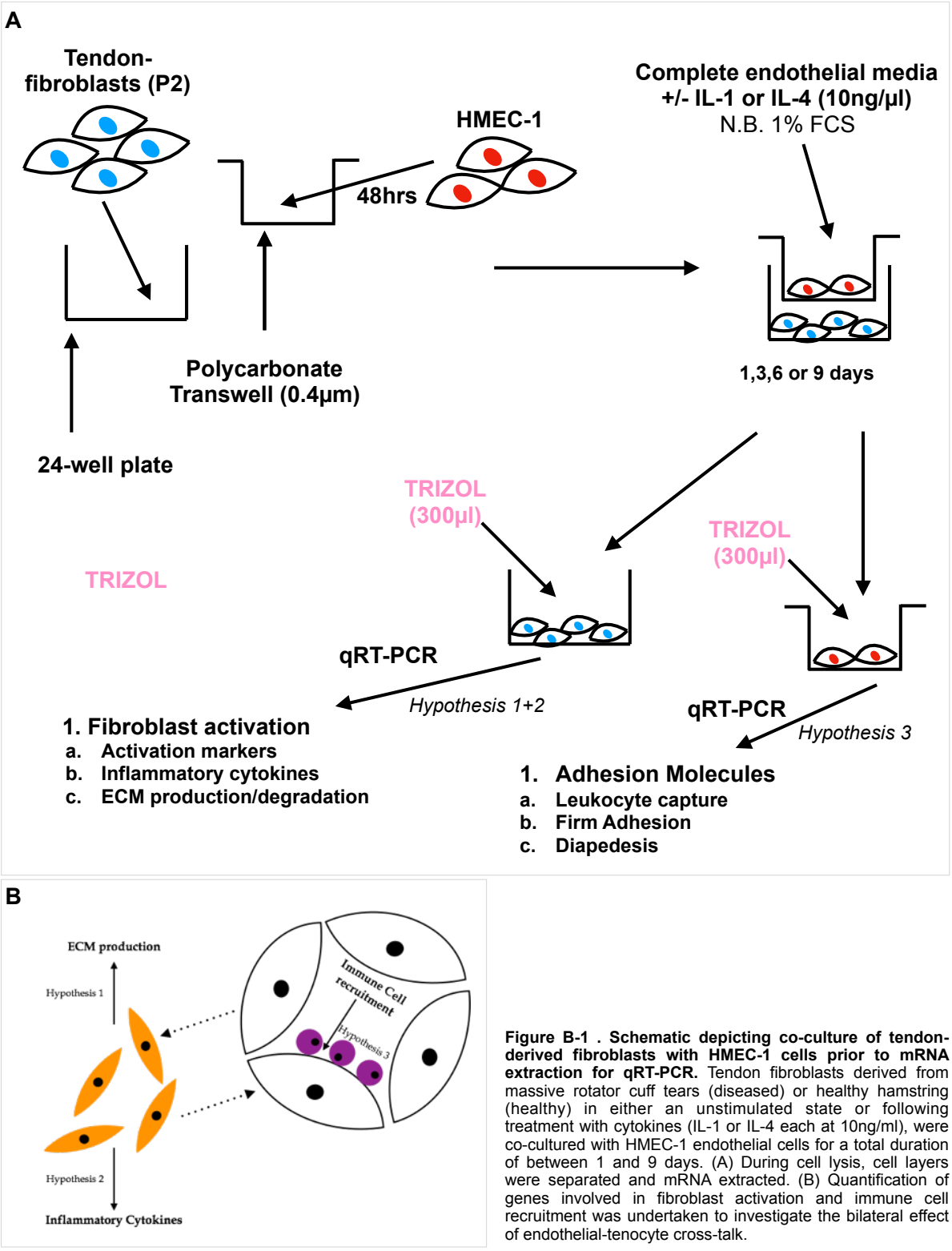

Figure B-1 . Schematic depicting co-culture of tendon-derived fibroblasts with HMEC-1 cells prior to mRNA extraction for qRT-PCR. Tendon fibroblasts derived from massive rotator cuff tears (diseased) or healthy hamstring (healthy) in either an unstimulated state or following treatment with cytokines (IL-1 or IL-4 each at 10ng/ml), were co-cultured with HMEC-1 endothelial cells for a total duration of between 1 and 9 days. (A) During cell lysis, cell layers were separated and mRNA extracted. (B) Quantification of genes involved in fibroblast activation and immune cell recruitment was undertaken to investigate the bilateral effect of endothelial-tenocyte cross-talk.

Figure B-2 Effect of exogenous IL-1β and IL-4 on inflammatory cytokine expression by EC co-cultured tendon fibroblasts

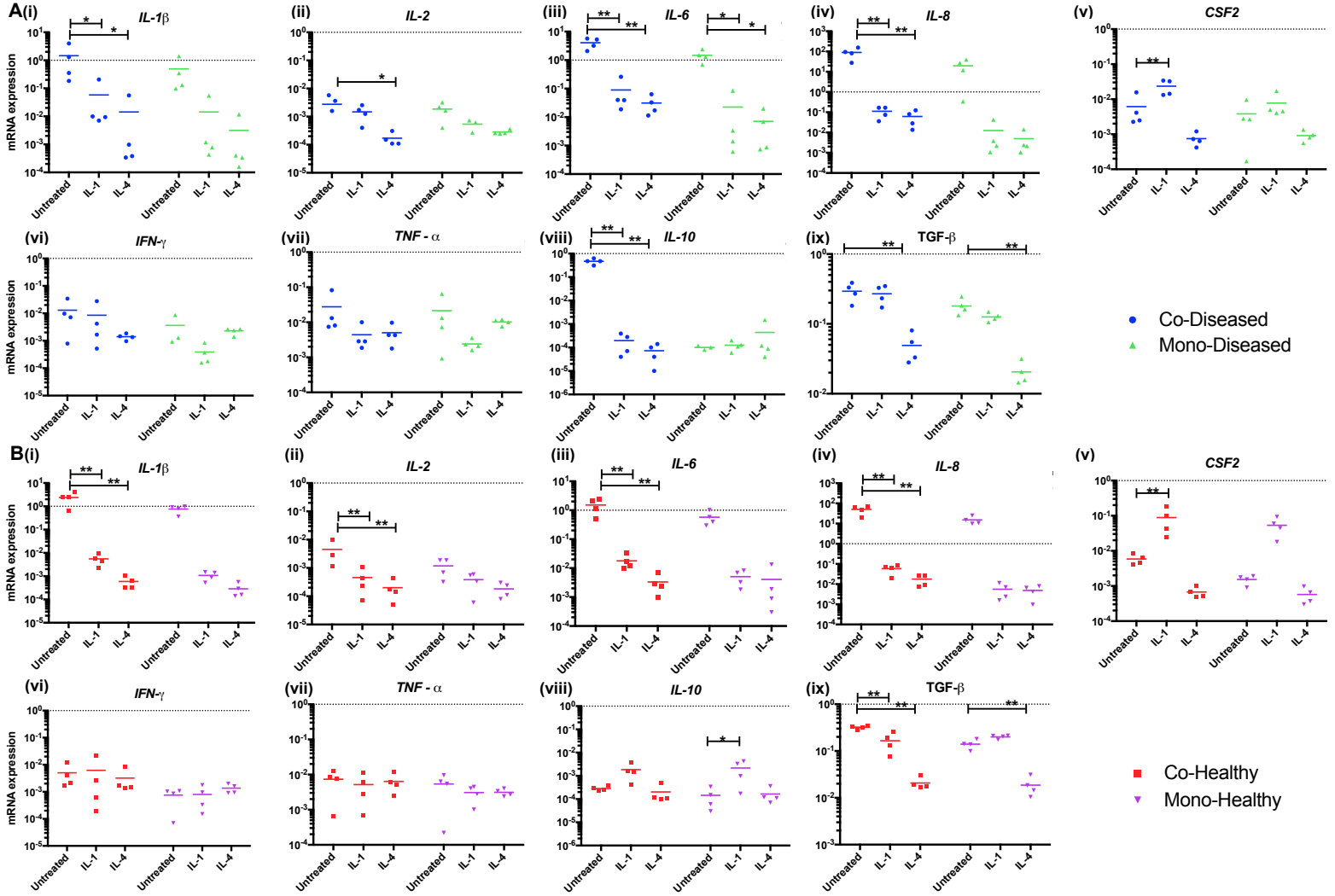

Figure B-2. Effect of exogenous IL-1β or IL-4 on the mRNA expression of inflammatory cytokines by tendon fibroblasts during co-culture with HMEC-1. Fibroblast mRNA was isolated from massive rotator cuff tears (diseased) or healthy hamstring (healthy) that had been cultured with HMEC-1 cells in either an unstimulated state or following treatment with cytokines (IL-1 or IL-4 each at 10ng/ml). *p<0.05, **p<0.005 compared to unstimulated co-culture by 2-way ANOVA with Sidak's correction for multiple testing.

Figure B-3 Effect of endothelial cell co-culture on tendon fibroblasts collagen III:I ratio

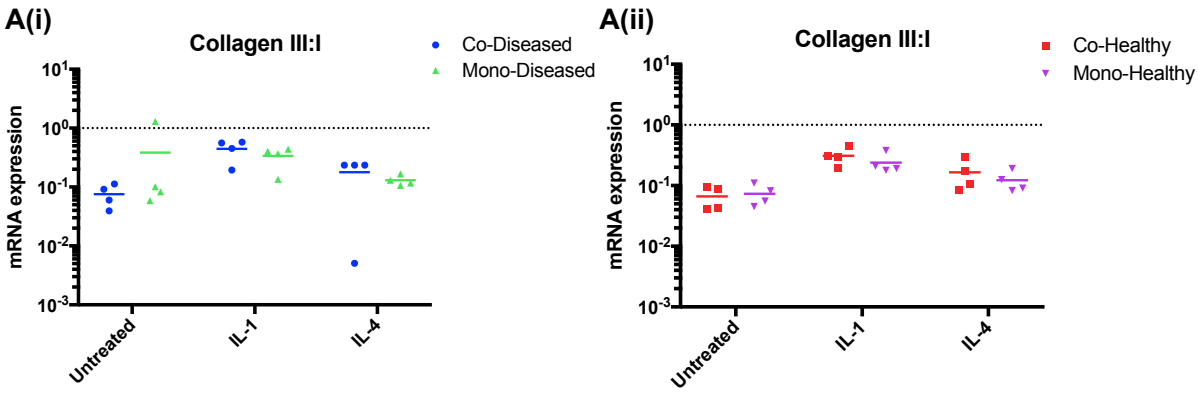

Figure B-3. Effect of HMEC-1 endothelial cell co-culture on the mRNA collagen III:I ratio by tendon fibroblasts. mRNA was isolated from tendon fibroblasts derived from massive rotator cuff tears (diseased) or healthy hamstring (healthy) that had been co-cultured with HMEC-1 cells in either an unstimulated state or following treatment with cytokines (IL-1 or IL-4 each at 10ng/ml). Gene expression was assessed by qRT-PCR and values were expressed as relative expression units (REU) compared with housekeepers (GAPDH and TOP1) according to the $2^{-\Delta CT}$ method. Data are mean of three technical replicated for explant derived fibroblasts from 4 healthy and 4 diseased tendons. *p<0.05, **p<0.005 compared to tendon fibroblast mono-culture by 2-way ANOVA with Sidak's correction for multiple testing.

Figure B-4 Effect of exogenous IL-1β and IL-4 on collagen expression by EC co-cultured tendon fibroblasts

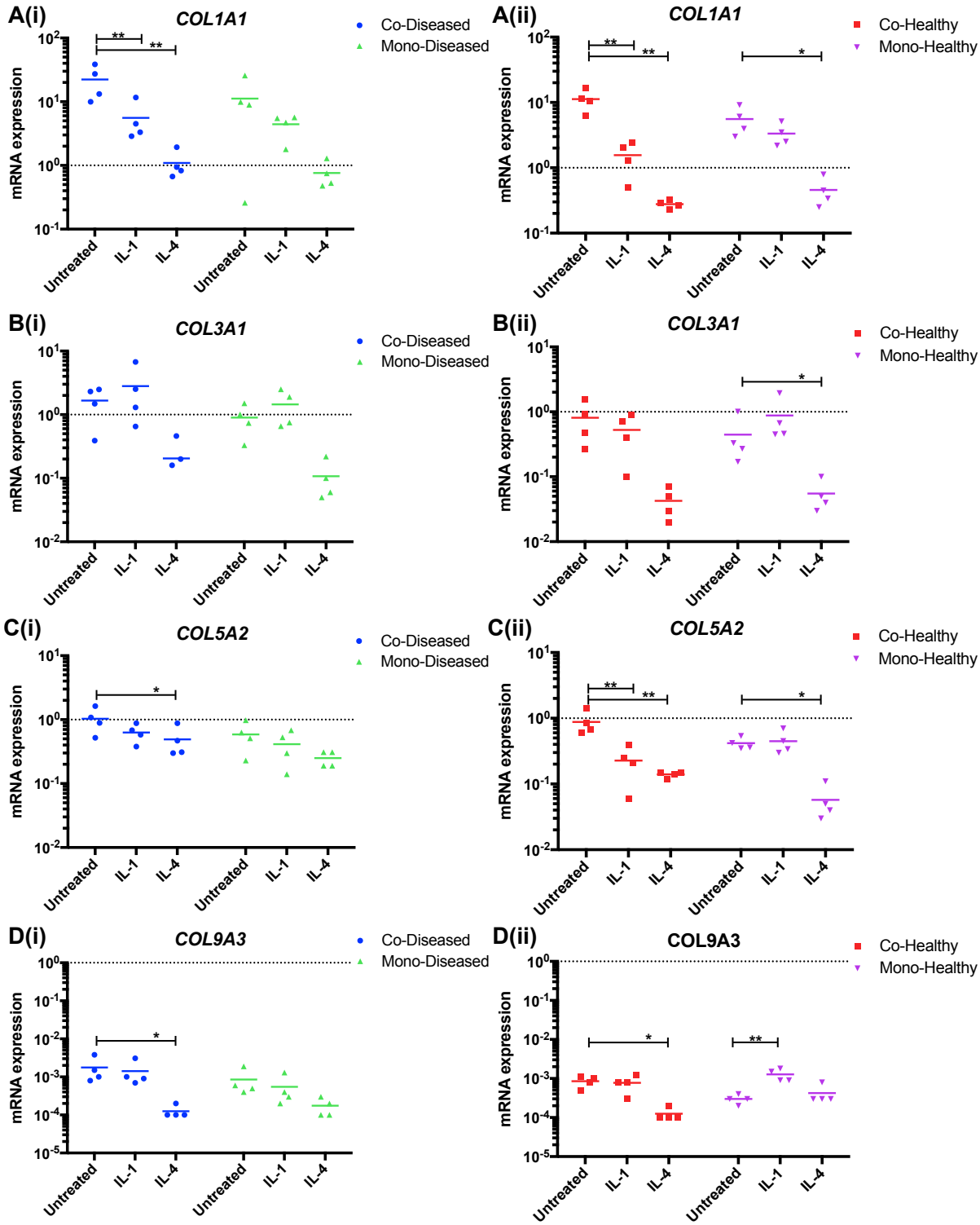

Figure B-4. Effect of exogenous IL-1β or IL-4 on the mRNA expression of collagens I,III,VI and IX by tendon fibroblasts during co-culture with HMEC-1. mRNA was isolated from tendon fibroblasts derived from massive rotator cuff tears (diseased) or healthy hamstring (healthy) that had been co-cultured with HMEC-1 cells in either an unstimulated state or following treatment with cytokines (IL-1 or IL-4 each at 10ng/ml). Gene expression was assessed by qRT-PCR and values were expressed as relative expression units (REU) compared with housekeepers (GAPDH and TOP1) according to the $2^{-\Delta CT}$ method. Data are mean of three technical replicated for explant derived fibroblasts from 4 healthy and 4 diseased tendons. *p<0.05, **p<0.005 compared to unstimulated cultures by 2-way ANOVA with Sidak's correction for multiple testing.

Figure B-5 Effect of exogenous IL-1β and IL-4 on tendon matrix protein expression by EC co-cultured tendon fibroblasts

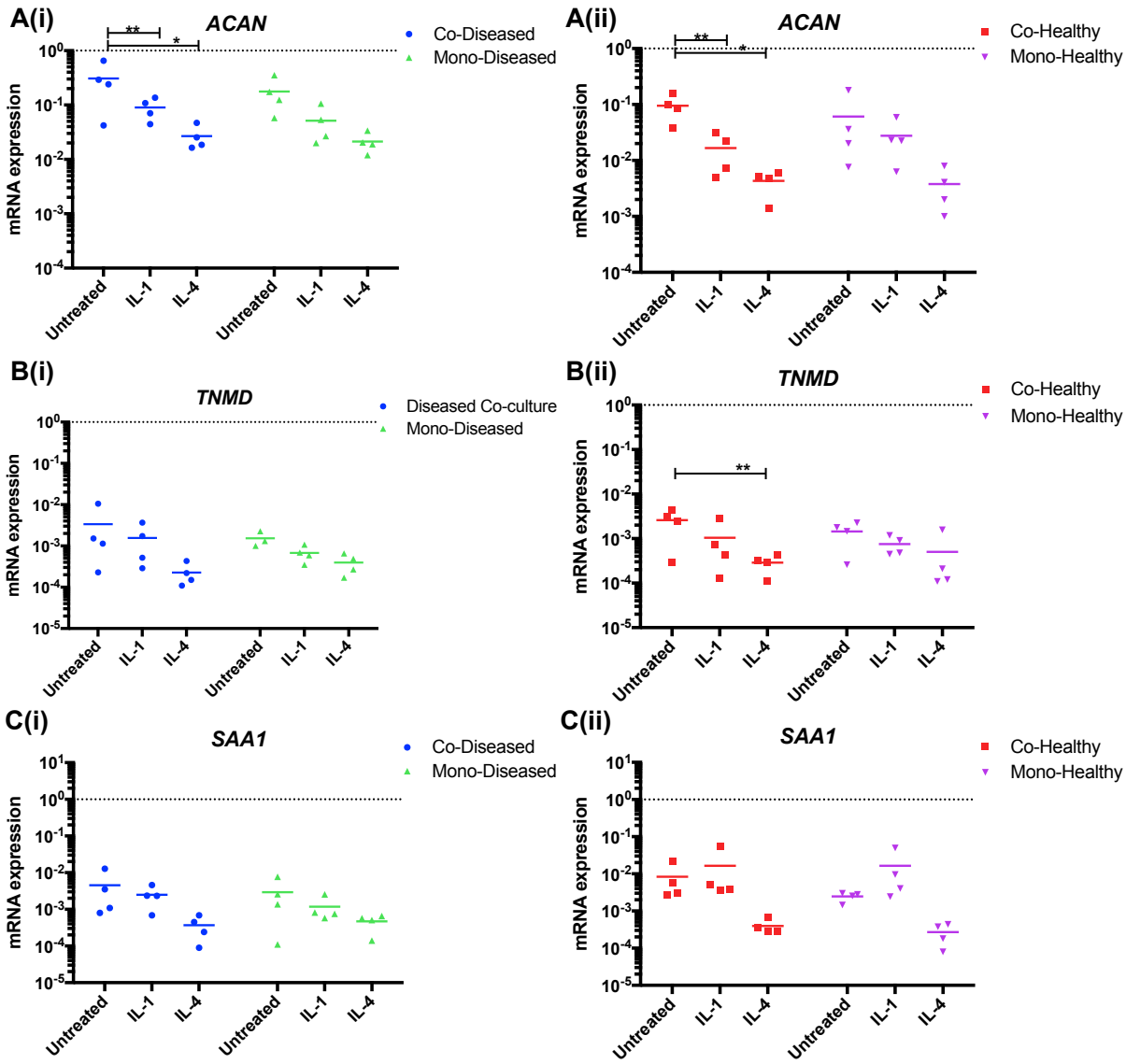

Figure B-5. Effect of exogenous IL-1β or IL-4 on the mRNA expression of tendon matrix proteins by tendon fibroblasts during co-culture with HMEC-1. mRNA was isolated from tendon fibroblasts derived from massive rotator cuff tears (diseased) or healthy hamstring (healthy) that had been co-cultured with HMEC-1 cells in either an unstimulated state or following treatment with cytokines (IL-1 or IL-4 each at 10ng/ml). Gene expression was assessed by qRT-PCR and values were expressed as relative expression units (REU) compared with housekeepers (GAPDH and TOP1) according to the $2^{-\Delta CT}$ method. Data are mean of three technical replicated for explant derived fibroblasts from 4 healthy and 4 diseased tendons. *p<0.05, **p<0.005 compared to unstimulated cultures by 2-way ANOVA with Sidak's correction for multiple testing.

Figure B-6 Effect of exogenous IL-1β and IL-4 on ECM protease expression by EC co-cultured tendon fibroblasts

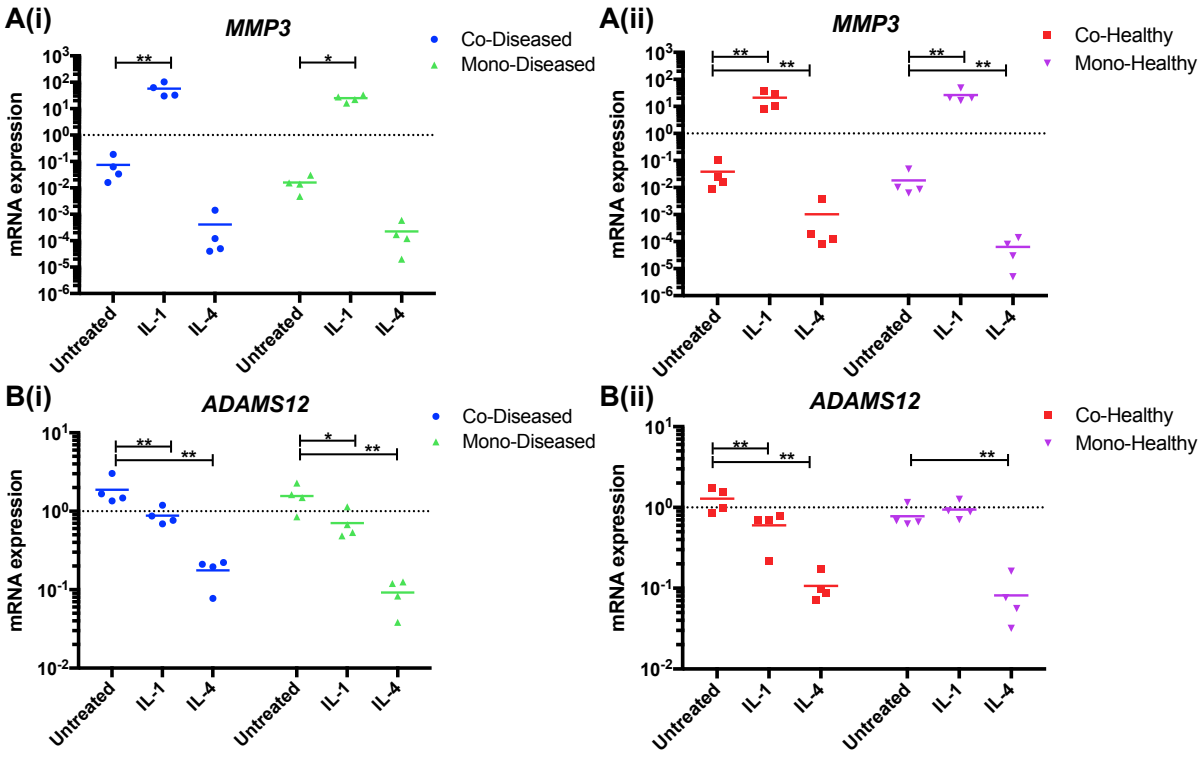

Figure B-6 . Effect of exogenous IL-1β or IL-4 on the mRNA expression of ECM proteases by tendon fibroblasts during co-culture with HMEC-1. mRNA was isolated from tendon fibroblasts derived from massive rotator cuff tears (diseased) or healthy hamstring (healthy) that had been co-cultured with HMEC-1 cells in either an unstimulated state or following treatment with cytokines (IL-1 or IL-4 each at 10ng/ml). Gene expression was assessed by qRT-PCR and values were expressed as relative expression units (REU) compared with housekeepers (GAPDH and TOP1) according to the $2^{-\Delta CT}$ method. Data are mean of three technical replicated for explant derived fibroblasts from 4 healthy and 4 diseased tendons. *p<0.05, **p<0.005 compared to tendon unstimulated cultures by 2-way ANOVA with Sidak's correction for multiple testing.

Figure B-7 Effect of exogenous IL-1β and IL-4 on NF-κB, IFN and STAT6 pathway genes by EC co-cultured tendon fibroblasts

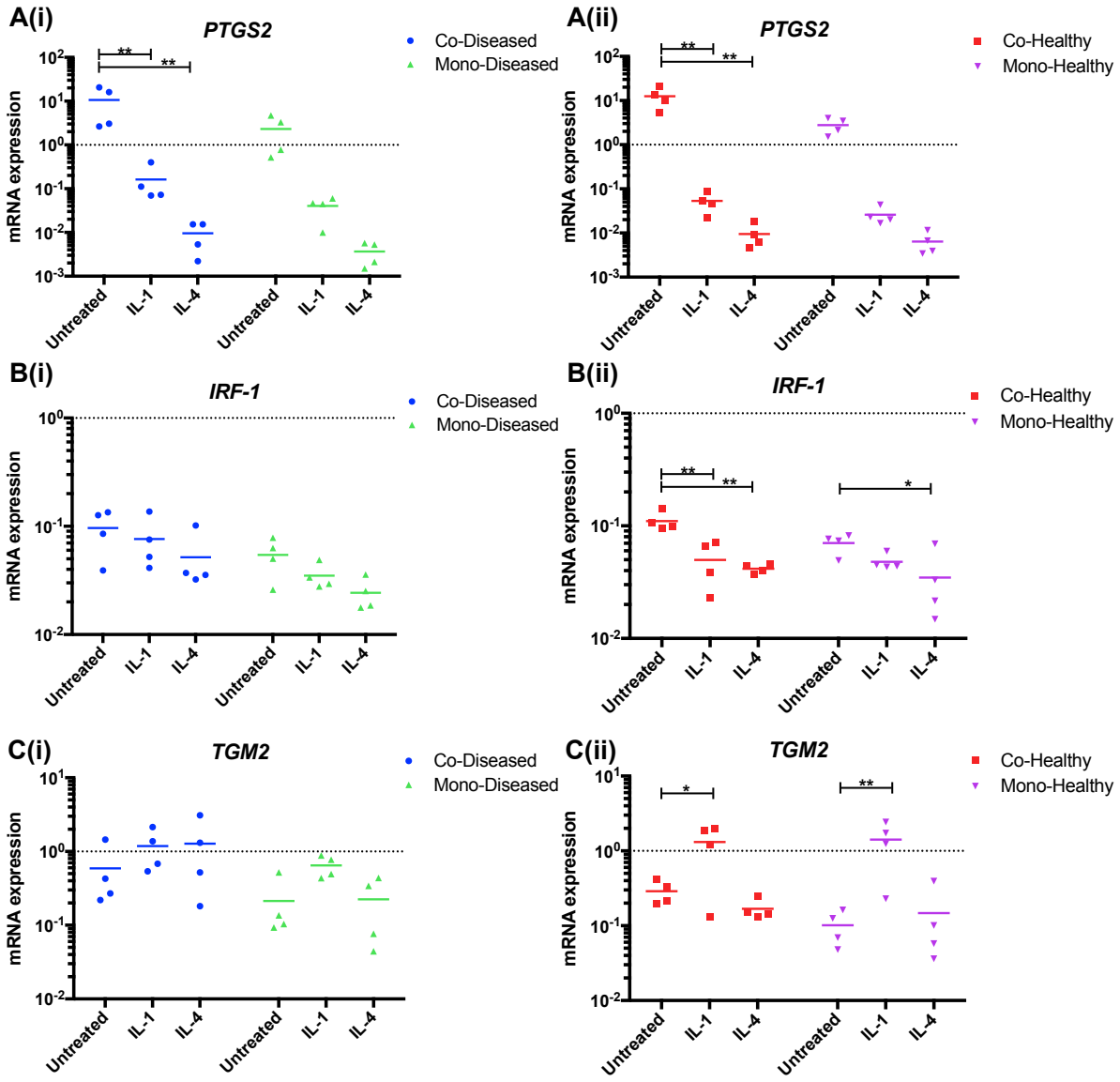

Figure B-7. Effect of exogenous IL-1β or IL-4 on the mRNA expression of NK-κB, IFN and STAT6 pathway genes by tendon fibroblasts during co-culture with HMEC-1. mRNA was isolated from tendon fibroblasts derived from massive rotator cuff tears (diseased) or healthy hamstring (healthy) that had been co-cultured with HMEC-1 cells in either an unstimulated state or following treatment with cytokines (IL-1 or IL-4 each at 10ng/ml). Gene expression was assessed by qRT-PCR and values were expressed as relative expression units (REU) compared with housekeepers (GAPDH and TOP1) according to the $2^{-\Delta CT}$ method. Data are mean of three technical replicated for explant derived fibroblasts from 4 healthy and 4 diseased tendons. *p<0.05, **p<0.005 compared to tendon unstimulated cultures by 2-way ANOVA with Sidak's correction for multiple testing.

Figure B-8 Effect of exogenous IL-1β and IL-4 on FOXF2 and HSPB1 by EC co-cultured tendon fibroblasts

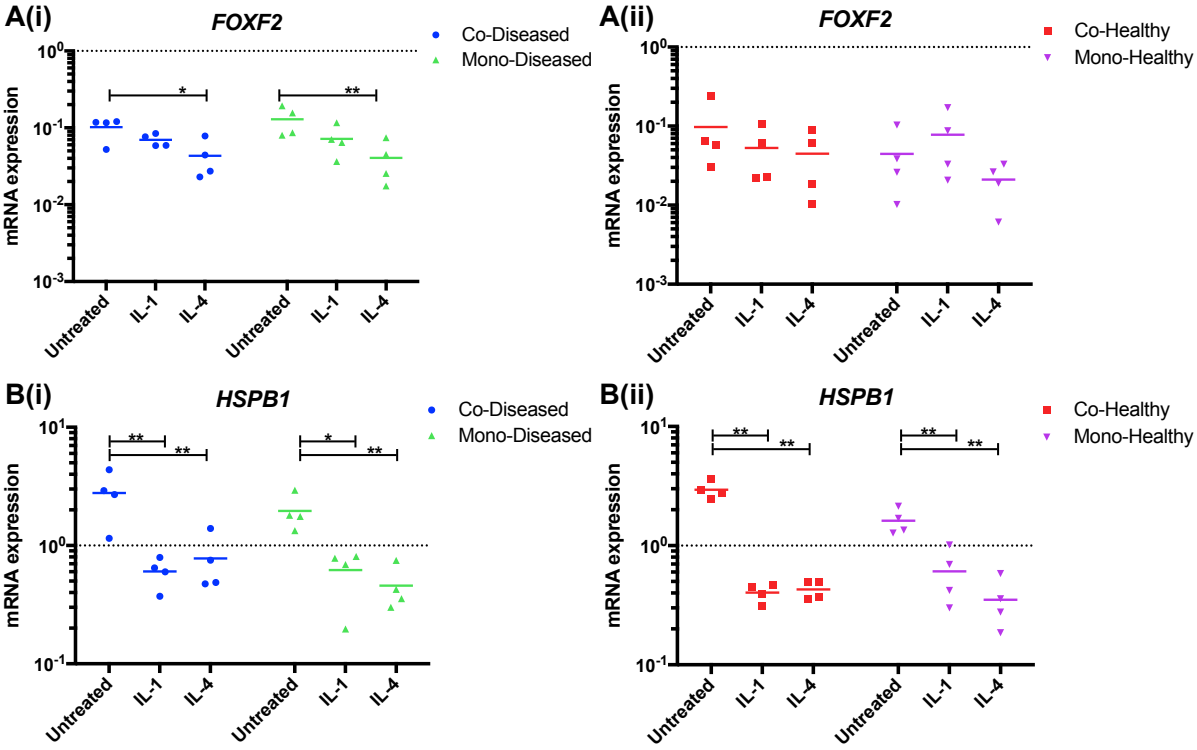

Figure B-8. Effect of exogenous IL-1β or IL-4 on the mRNA expression of the cell-cycle regulators FOXF2 and HSPB1 by tendon fibroblasts. mRNA was isolated from tendon fibroblasts derived from massive rotator cuff tears (diseased) or healthy hamstring (healthy) that had been co-cultured with HMEC-1 cells in either an unstimulated state or following treatment with cytokines (IL-1 or IL-4 each at 10ng/ml). Gene expression was assessed by qRT-PCR and values were expressed as relative expression units (REU) compared with housekeepers (GAPDH and TOP1) according to the $2^{-\Delta CT}$ method. Data are mean of three technical replicated for explant derived fibroblasts from 4 healthy and 4 diseased tendons. *p<0.05, **p<0.005 compared to unstimulated culture by 2-way ANOVA with Sidak's correction for multiple testing.

Figure B-9 Effect of exogenous IL-1β and IL-4 on peripheral blood leukocytes to HMEC-1 endothelial cells during co-culture with tendon-derived fibroblasts

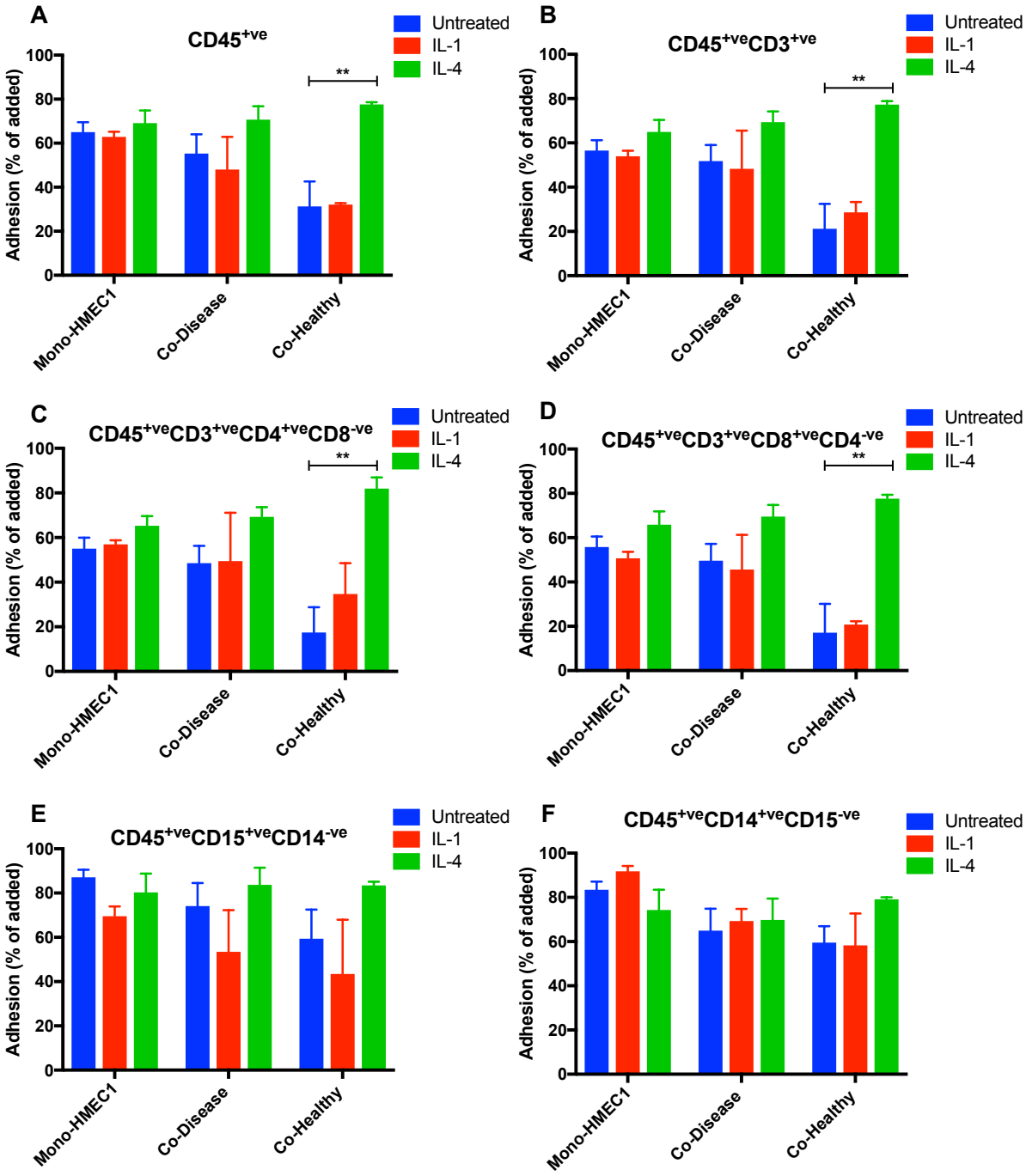

Figure B-9 . Effect of exogenous IL-1β and IL-4 on the adhesion of peripheral blood leukocytes to HMEC-1 endothelial cells during co-culture. Co-cultures were established by inserting a confluent monolayer of HMEC-1 cells cultured on a 24-well filter, into a fibroblast coated 12-well filter and allowed to equilibrate for 24-hours in the presence or absence of IL-1 (10ng/ml) or IL-4 (10ng/ml). Fibroblasts were derived from hamstrings (Healthy) or massive rotator cuff tears (Diseased). Leukocytes were allowed to settle for 30-minutes after which non-adherent cells were washed off and analysed using flow cytometry for (A) $CD45^{+ve}$ Peripheral blood leukocytes, (B) $CD3^{+ve}$ T-cells, (C) $CD4^{+ve}$ T-cells, (D) $CD8^{+ve}$ T-cells, (E) $CD15^{+ve}$ Neutrophils and (F) $CD14^{+ve}$ Monocytes. Total adherent cells were calculated by subtracting each fraction of non-adherent from the total added. For each population data were expressed as a percentage of the cells added. Data are mean +/- SEM for explant derived fibroblasts from 3 healthy and 3 diseased tendons. *p<0.05, **p<0.005 compared to untreated cultures by 2-way ANOVA with Dunnett's correction for multiple testing.

Figure B-10 Effect of co-culture with tendon-derived fibroblasts on the expression of inhibitors of leukocyte adhesion by HMEC-1 endothelial cells

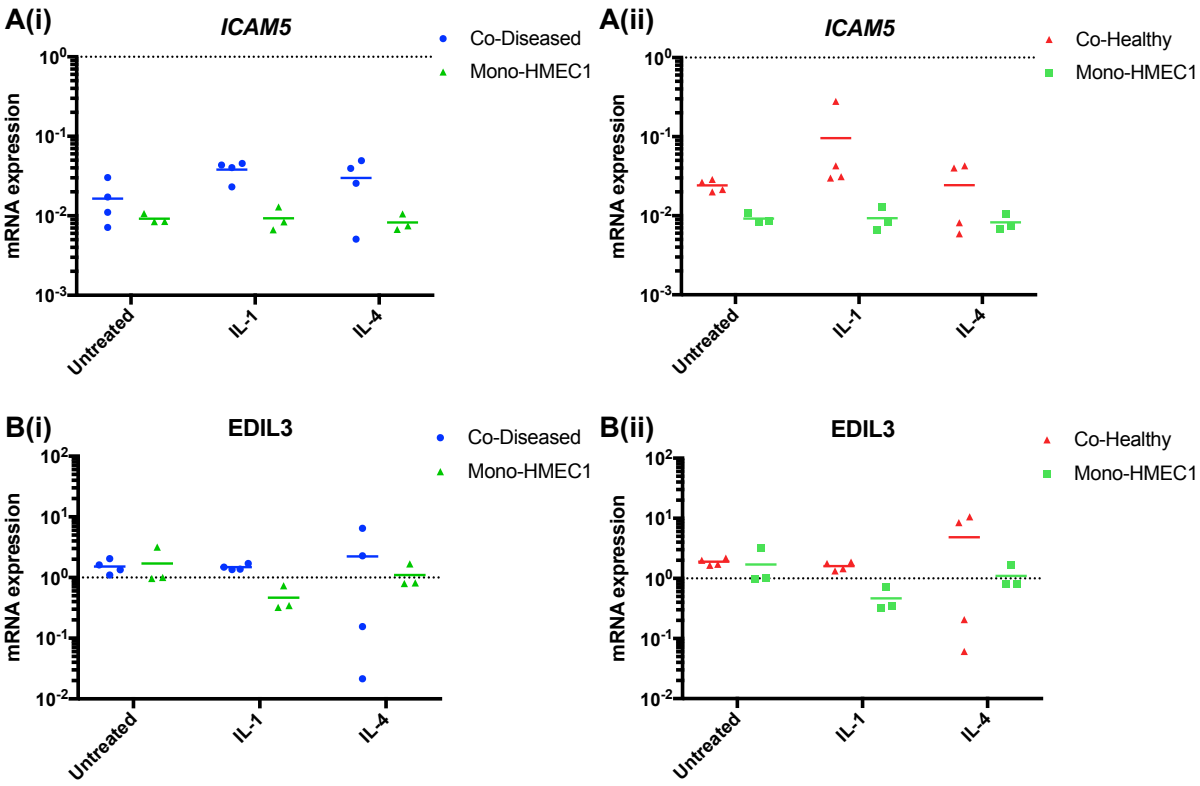

Figure B-10 . Effect of tendon fibroblast co-culture on the mRNA expression of endogenous inhibitors of leucocyte adhesion by HMEC-1 endothelial cells. Endothelial mRNA was isolated from HMEC-1 endothelial cells cultured indirectly with tendon fibroblasts derived from massive rotator cuff tears (diseased) or healthy hamstring (healthy) in either an unstimulated state or following treatment with cytokines (IL-1 or IL-4 each at 10ng/ml). Gene expression was assessed by qRT-PCR and values were expressed as relative expression units (REU) compared with housekeepers (TOP1, TBP and SDHA) according to the $2^{-\Delta CT}$ method. Data are mean of three technical replicated for explant derived fibroblasts from 4 healthy and 4 diseased tendons. *p<0.05, **p<0.005 compared to HMEC-1 mono-culture by 2-way ANOVA with Sidak's correction for multiple testing.

APPENDIX C ADDITIONAL INFORMATION FOR CHAPTER 4

C-1 RNA-sequencing analysis pipeline

```
"""

from ruffus import *
import sys
import argparse
import gzip
from cgatcore import pipeline as P
import cgatcore.experiment as E
import statistics
P.get_parameters("pipeline.yml")

PARAMS = P.PARAMS

#this lists the input files, the format of thise input files, and the
format of the output files. The (.*) is assigned a character 1 that we
then call at the end of regex
@transform('*.fastq.gz', regex(r'(.*).fastq.gz'), r'\1_fastqc.zip')
def fastqc(infiles, outfiles):
    statement = ''' fastqc %(fastq_inputs)s %(infiles)s'''
    P.run(statement, job_threads=8)

@merge(fastqc,'multiqc.html')
def multiqc(infiles, outfiles):
    statement = '''multiqc -n %(outfiles)s . '''
    P.run(statement, job_threads=8)

@collate('*.fastq.gz', regex(r"(.)_[12]\.fastq.gz"), r'\1.sam')
#@transform('*_1.fastq.gz', suffix ('_1.fastq.gz'),'.sam')
def mapping(infiles,outfile):
    infile1 = infiles[0]
    infile2 = infiles[1]
# infile2 = infile.replace('_1.fastq.gz','_2.fastq.gz')
    statement = '''hisat2 %(mapping_options)s -x %(mapping_ref_genome)s -
1 %(infile1)s -2 %(infile2)s -S %(outfile)s 2>%(outfile)s.log '''
    P.run(statement, job_threads=8)

@transform(mapping, suffix ('.sam'),'.bam' )
def sam2bam(infile, outfile):
    statement = '''samtools sort -@ %(samtools_threads)s -o %(outfile)s
%(infile)s '''
    P.run(statement, job_threads= PARAMS['samtools_threads'])

@transform(sam2bam, suffix('.bam'), 'bam.bai')
def indexbam(infile,outfile):
    statement= '''samtools index %(infile)s'''
    P.run(statement)

@follows(indexbam)
@transform(sam2bam, suffix('.bam'), '_metrics.txt')
def pic_metrics(infile,outfile):
    statement= '''picard CollectAlignmentSummaryMetrics R=
%(picard_ref_genome)s I=%(infile)s O=%(outfile)s 2> %(outfile)s.log'''
    P.run(statement, job_memory= '16G')


@merge(pic_metrics, "mapping_multiqc.html")
def mapping_multiqc(infiles, outfile):
   statement = '''multiqc -n %(outfile)s . '''
```

Figure C-1 RNA-sequencing quality control metrics for tendon fibroblasts isolated from human hamstring

A

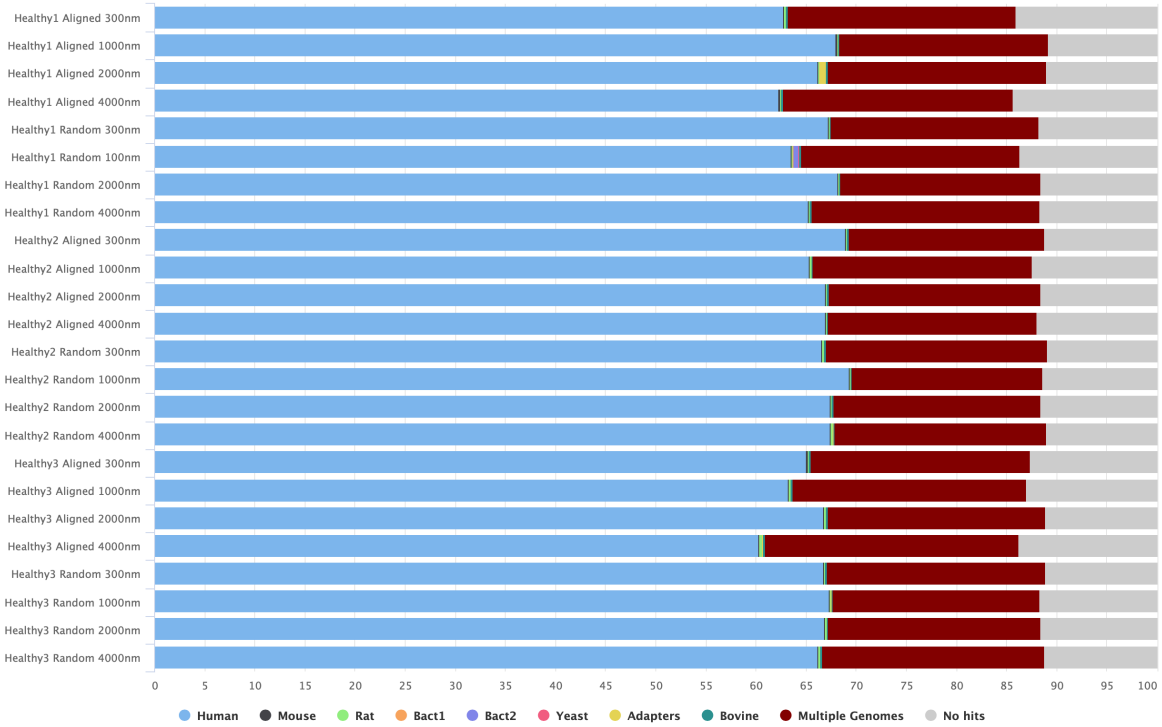

B

Sample Name	Aligned Reads (%)	Duplicated Reads (%)	GC Content (%)	Total Sequences (Millions)
Healthy1 Aligned 300nm	95%	48.8%	49%	16.4
Healthy1 Aligned 1000nm	96%	51.6%	49%	18.0
Healthy1 Aligned 2000nm	96%	54.0%	49%	21.7
Healthy1 Aligned 4000nm	95%	54.1%	50%	18.2
Healthy1 Random 300nm	96%	55.4%	49%	31.1
Healthy1 Random 1000nm	89%	53.4%	49%	17.4
Healthy1 Random 2000nm	95%	49.5%	49%	17.9
Healthy1 Random 4000nm	96%	53.7%	49%	21.8
Healthy2 Aligned 300nm	96%	52.9%	49%	29.8
Healthy2 Aligned 1000nm	95%	44.5%	48%	9.7
Healthy2 Aligned 2000nm	96%	54.0%	49%	23.4
Healthy2 Aligned 4000nm	95%	50.8%	49%	19.1
Healthy2 Random 300nm	94%	54.4%	49%	22.6
Healthy2 Random 1000nm	96%	56.2%	49%	37.7
Healthy2 Random 2000nm	96%	53.9%	49%	24.7
Healthy2 Random 4000nm	96%	52.1%	49%	19.1
Healthy3 Aligned 300nm	96%	47.3%	49%	11.9
Healthy3 Aligned 1000nm	96%	51.3%	49%	17.5
Healthy3 Aligned 2000nm	96%	52.3%	49%	16.5
Healthy3 Aligned 4000nm	94%	54.2%	50%	14.6
Healthy3 Random 300nm	96%	47.9%	49%	14.2
Healthy3 Random 1000nm	96%	47.0%	49%	15.9
Healthy3 Random 2000nm	96%	52.0%	49%	21.5
Healthy3 Random 4000nm	96%	35.8%	49%	5.3

Figure C-1. Quality control metrics of RNA-sequencing data for healthy human tendon fibroblasts derived from hamstring and cultured on scaffolds. (A) Sequencing data was screened (FastQ screen, Babraham Institute, Cambridge UK) against a range of non-human genomes to assess for contamination during *in vitro* culture , (B) Summary statistics of important quality control metrics, an average of the paired-end reads is reported for; duplicated reads, GC content and total sequences.

Figure C-2 RNA-sequencing quality control metrics for tendon fibroblasts isolated from human massive rotator cuff tears

A

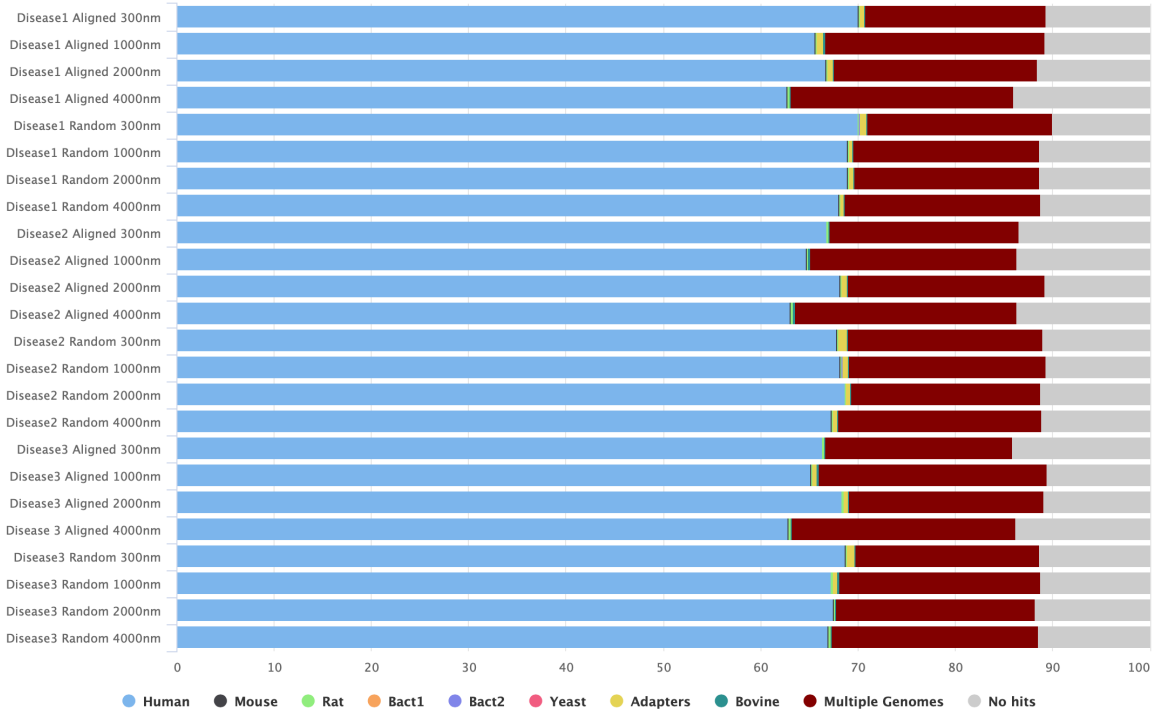

B

Sample Name	Aligned Reads (%)	Duplicated Reads (%)	GC Content (%)	Total Sequences (Millions)
Disease1 Aligned 300nm	95%	52.0%	49%	23.2
Disease1 Aligned 1000nm	95%	49.7%	48%	15.3
Disease1 Aligned 2000nm	95%	47.8%	48%	19.0
Disease1 Aligned 4000nm	94%	50.1%	49%	19.0
Disease1 Random 300nm	95%	47.7%	49%	17.9
Disease1 Random 1000nm	95%	47.7%	49%	20.8
Disease1 Random 2000nm	95%	47.8%	49%	17.3
Disease1 Random 4000nm	95%	51.1%	49%	20.1
Disease2 Aligned 300nm	95%	52.6%	49%	23.8
Disease2 Aligned 1000nm	95%	50.7%	49%	18.0
Disease2 Aligned 2000nm	93%	48.8%	48%	15.3
Disease2 Aligned 4000nm	95%	54.0%	48%	20.2
Disease2 Random 300nm	95%	49.2%	49%	14.3
Disease2 Random 1000nm	95%	50.0%	49%	14.0
Disease2 Random 2000nm	95%	53.3%	49%	21.9
Disease2 Random 4000nm	95%	51.7%	49%	16.1
Disease3 Aligned 300nm	95%	57.1%	49%	40.1
Disease3 Aligned 1000nm	95%	47.4%	49%	11.8
Disease3 Aligned 2000nm	95%	56.9%	49%	33.7
Disease3 Aligned 4000nm	95%	54.5%	49%	25.7
Disease3 Random 300nm	95%	52.4%	50%	24.9
Disease3 Random 1000nm	95%	58.1%	49%	29.8
Disease3 Random 2000nm	95%	55.9%	49%	24.5
Disease3 Random 4000nm	95%	50.9%	50%	15.5

Figure C-2. Quality control metrics of RNA-sequencing data for diseased human rotator cuff tear derived fibroblasts cultured on scaffolds. (A) Sequencing data was screened (FastQ screen, Babraham Institute, Cambridge UK) against a range of non-human genomes to assess for contamination during *in vitro* culture , (B) Summary statistics of important quality control metrics, an average of the paired-end reads is reported for; duplicated reads, GC content and total sequences.

C-3 Hallmark pathway leading edge analysis for healthy fibroblasts

Table C-3.1 Leading edge genes contributing to enriched hallmark pathways for healthy fibroblasts cultured on 300nm aligned scaffolds compared with 1000nm aligned

Hallmark Pathways – 300A vs 1000A	
mTORC1 signalling	Hypoxia
TRIB3	CITED2
HSPA9	ADM
PSAT1	NFIL3
WARS	CDKN1A
TXNRD1	PNRC1
NFIL3	HMOX1
CDKN1A	HSPA5
SQSTM1	LOX
HSPA5	
ME1	
GCLC	
UFM1	
ASNS	
MAP2K3	
DDIT3	
HSP90B1	

Table C-3.2 Leading edge genes contributing to enriched hallmark pathways for healthy fibroblasts cultured on 4000nm aligned scaffolds compared with 1000nm aligned

Hallmark Pathways – 4000A vs 1000A					
E2F Targets	G2M checkpoint	Mitotic spindle	NFκb signalling	Inflammatory Response	p53 Pathway
KPNA2	KPNA2	FSCN1	PNRC1	CXCL8	MDM2
MCM5	MCM5	ACTN4	SOD2	ADM	VWA5A
MYBL2	CDC6	AURKA	CEBPD	NAMPT	DRAM1
TK1	MYBL2	PLK1	DRAM1	PDPN	ZFP36L1
CDCA3	E2F1	PXN	CXCL3	CCL2	TXNIP
PRPS1	AURKA	SUN2	PLPP3	ABCA1	ZMAT3
AURKA	CDC20	NDC80	NAMPT	LPAR1	ANKRA2
CDC20	PLK1	EZR	CCL2	CXCL6	BMP2
PLK1	CCNA2	NUSAP1	ABCA1	ICAM1	
MCM4	UBE2C	BIRC5	BMP2		
H2AFX	H2AFX	BCAR1	CXCL6		
TACC3	TACC3	MAP3K11	BCL6		
MCM2	MCM2	ARHGDIA	ICAM1		
CTPS1	NDC80	LMNB1	CXCL1		
PSMC3IP	H2AFV	KIF2C	PLAU		
CDC25A	CDC25A	KIF22	BCL3		
MCM7	NUSAP1	CCNB2	ZFP36		
POLD1	BIRC5	TPX2	PHLDA1		
SPAG5	EZH2		KLF9		
BIRC5	UBE2S				
EZH2	TGFB1				
RRM2	TROAP				
UBE2S	LMNB1				
LMNB1	STMN1				
STMN1	MCM3				
UBE2T	KIF2C				
MCM3	HMGB3				
KIF2C	CCNF				
HMGB3	GINS2				
KIF22	KIF22				
CCNB2	CCNB2				

Table C-3.3 Leading edge genes contributing to enriched hallmark pathways for healthy fibroblasts cultured on 300nm random scaffolds compared with 1000nm random

Hallmark Pathways – 300R vs 1000R				
G2M checkpoint	E2F Targets	Mitotic spindle	myc Targets	NFκb signalling
BIRC5	BIRC5	BIRC5	MAD2L1	NR4A3
MAD2L1	MAD2L1	AURKA	CDC20	MXD1
AURKA	AURKA	CCNB2	KPNA2	ABCA1
CCNB2	CCNB2	NUSAP1	CCNA2	SQSTM1
CDC20	CDC20	NDC80	RFC4	ICAM1
KPNA2	KPNA2	CDK1	MCM5	PNRC1
CCNA2	TK1	PLK1	H2AFZ	SLC2A3
PBK	TRIP13	KIF22	SRSF1	BIRC3
NUSAP1	CDKN3	LMNB1	MCM4	BTG2
NDC80	STMN1	RACGAP1	TFDP1	BCL6
CDC6	CDCA3	FBXO5	LDHA	SOD2
CDKN3	CDK1	KIF2C	BUB3	NFIL3
STMN1	UBE2T	NEK2	SNRPG	MSC
UBE2C	CKS2	DLGAP5	CCT2	CDKN1A
CDK1	MYBL2	TPX2	RRM1	PPP1R15A
CKS2	HMGB2		MCM2	
MYBL2	PLK1		GLO1	
GINS2	TACC3		CDK2	
PLK1	CDKN2C		TYMS	
TACC3	MELK			
CDKN2C	PTTG1			
PTTG1	KIF22			
KIF22	LMNB1			
LMNB1	ASF1B			
E2F1	RACGAP1			
RACGAP1	UBE2S			
UBE2S	KIF2C			
FBXO5	MCM5			
TROAP	PSMC3IP			
KIF2C	RRM2			
CENPA	SPAG5			

Table C-3.4 Leading edge genes contributing to enriched hallmark pathways for healthy fibroblasts cultured on 1000nm aligned scaffolds compared with 1000nm random

Hallmark Pathways – 1000A vs 1000R			
E2F Targets	G2M checkpoint	mTORC1 signalling	myc Targets
KPNA2	KPNA2	TMEM97	PABPC1
HMGB2	MAD2L1	TUBG1	KPNA2
MAD2L1	BIRC5	HPRT1	MAD2L1
BIRC5	HMGN2	HSPD1	GLO1
TRIP13	STMN1	CCT6A	CDC20
TK1	CDC20	RRM2	KARS
STMN1	BUB3	PPA1	HNRNPA1
CDC20	CCNB2	AURKA	TYMS
TUBG1	NCL	TXNRD1	HPRT1
CCNB2	ODC1	MAP2K3	BUB3
TIPIN	CDK1	PSAT1	CCT5
CDK1	MYBL2	ME1	DDX18
MYBL2	LMNB1	SLC7A5	ODC1
LMNB1	PBK		HSPD1
RRM2	CDKN3		C1QBP
DEK	NDC80		CCT2
CDKN3	GINS2		HNRNPA2B1
AURKA	AURKA		SET
RAD51C	DKC1		DEK
PRIM2	PRIM2		PABPC4
UBE2T	CDC6		PWP1
PTTG1	UBE2C		NCBP2
RAN	NUSAP1		SERBP1
CDCA3	PTTG1		HDAC2
CSE1L	RAD23B		HNRNPA3
ASF1B			SNRPA
TP53			SRM
			RAD23B
			RAN
			GOT2
			NPM1

Hallmark Pathways – 2000A vs 2000R

G2M checkpoint	E2F Targets	Mitotic Spindle	myc targets	Glycolysis	DNA repair	NFκb signalling	p53 pathway	INFγ response	Inflammatory response	Coagulation	STAT5 signalling	Estrogen Response	Hypoxia
KPNA2	TK1	BIRC5	KPNA2	STMN1	RFC5	ABCA1	MXD1	C1S	ABCA1	C1S	MXD1	BHLHE40	BHLHE4
BIRC5	KPNA2	AURKA	CCNA2	AURKA	ZWINT	NR4A3	ZFP36L1	IRF1	MXD1	MMP14	BHLHE40	TSKU	DDIT4
E2F1	BIRC5	CDK1	CDC20	CDK1	FEN1	MXD1	PPM1D	C1R	IRF1	C1R	PHLDA1	MUC1	SRPX
CDC6	CDCA3	LMNB1	MCM5	PGM2	TYMS	IRF1	DDIT4	NAMPT	MMP14	MST1	MUC1	FAM102A	PNRC1
STMN1	RRM2	KIF2C	MCM4	KIF20A	ERCC2	NAMPT	BTG2	TNFAIP2	NAMPT	PLAU	BMP2	RARA	VEGFA
CCNA2	STMN1	CCNB2	MAD2L1	DEPDC1	RFC3	BCL6	MKNK2	ICAM1	BTG2	MMP2	NDRG1	CYP26B1	GAA
AURKA	AURKA	NDC80	PABPC1	CENPA	ARL6IP	BHLHE4	RRAD	SECTM1	ICAM1	FYN	POU2F1	SVIL	NDRG1
CDC20	CDC20	PLK1	RRM1	PRPS1		PHLDA1	MDM2	SOD2	CD82	KLF7	GABARAPL	TOB1	KLF7
MCM5	HMGB2	TPX2	BUB3	HMMR		BTG2	BMP2			CLU	RGS16	HSPB8	ATF3
CDK1	MCM5	NUSAP1	TFDP1	TGFA		PLAU	CD82			PROS1	CSF1	HR	TGFB3
UBE2C	CDK1	RACGAP	DEK	CITED2		TNFAIP2	TRIB3			C3	COL6A1	KDM4B	
LMNB1	TRIP13	TOP2A	CDK2			PNRC1	CDKN2			ACOX2			
MAD2L1	MCM4	BUB1	MCM2			BCL3	NDRG1						
TACC3	ASF1B	EZR	TYMS			ICAM1	ATF3						
PBK	LMNB1	FBXO5	H2AFZ			VEGFA	ABHD4						
KIF2C	MAD2L1	DLGAP5	USP1			TNC	XPC						
MYBL2	TACC3	NEK2	MCM7			DUSP4	SLC7A1						
CCNB2	KIF2C	KIF20B	MCM6			BMP2	RGS16						
EZH2	MYBL2	MAPRE1	SRSF1			SPSB1	TSC22D						
NDC80	CCNB2	KIF23	CDC45			KLF9	TOB1						
CDKN3	EZH2	ANLN	SET			ATF3	TSPYL2						
PLK1	CDKN3	KIF4A	EIF4E			SOD2	PLK3						
PTTG1	PLK1	TTK	HNRNPA1			MSC	DDIT3						
BUB3	CDCA8	ECT2	HNRNPA2B			SESN1	SESN1						
TFDP1	PTTG1	KIF22	HDAC2				VWA5A						
TPX2	PSMC3IP		CCT5										
NUSAP1	SPAG5		HNRNPR										
DBF4	SPC24		HNRNPD										
RACGAP1	RACGAP1		HPRT1										
TOP2A	UBE2T		PRPS2										
GINS2	TOP2A		CCT2										
UBE2S	UBE2S		TCP1										
BUB1	DEK		CTPS1										
AURKB	RAD51AP		HSPD1										
HMGN2	AURKB		SERBP1										
MCM3	MCM3		RFC4										
CDKN2C	CDKN2C		HNRNPA3										
FBXO5	GINS1		ODC1										
MCM2	MCM2		RANBP1										
E2F2	MELK		SRSF7										
CENPA	DEPDC1												
NEK2	DLGAP5												
H2AFV	PRPS1												
EXO1	CENPM												
HMMR	RFC3												
KIF20B	DIAPH3												
KIF23	HMMR												
CKS2	CKS2												
KIF4A	KIF4A												
H2AFZ	H2AFZ												
CBX1	TMPO												
TMPO	TUBG1												
TTK	USP1												
TROAP	MCM7												
KIF22	KIF22												
H2AFX	H2AFX												
NCL	PLK4												
PLK4	MCM6												
MCM6	SRSF1												
SRSF1	ORC6												
CHAF1A													
ORC6													
CDC45													
PRC1													
KIF11													

Table C-3.5 Leading edge genes contributing to enriched hallmark pathways for healthy fibroblasts cultured on 2000nm aligned scaffolds compared with 2000nm random

Table C-3.6 Leading edge genes contributing to enriched hallmark pathways for healthy fibroblasts cultured on 4000nm aligned scaffolds compared with 4000nm random

Hallmark Pathways – 4000A vs 4000R

E2F Targets	G2M checkpoint	myc Targets	Mitotic spindle	Coagulation	INFγ Response	Complement	NFκb signalling	Apoptosis
TK1	MYBL2	KPNA2	LMNB1	C1S	C1S	C1S	NAMPT	LUM
MYBL2	KPNA2	CDC20	EZR	C1R	C1R	C1R	SOD2	SOD2
KPNA2	LMNB1	MCM5	BIRC5	PROS1	NAMPT	CLU	CEBPD	DCN
CDCA3	CDC20	CCNA2	AURKA	CLU	SECTM1	CPQ	ABCA1	CLU
RRM2	BIRC5	CTPS1	PLK1	CPQ	SOD2	SERPING1	PNRC1	BTG2
PSMC3IP	EZH2	MCM7	KIF22	SERPING1	SERPING1	DPP4	BTG2	TXNIP
LMNB1	TACC3	MCM4	KIF2C	DPP4	TXNIP	CTSB	NFE2L2	ANKH
CDC20	CDC6	RFC4	NUSAP1	CTSK	ICAM1	CPM	BCL6	BMP2
BIRC5	MCM5	HNRNPA2B1	RACGAP1	CTSB	SSPN	C3	ICAM1	MMP2
EZH2	STMN1	CDK2	CCNB2	PLAU	EPSTI1	F8	BMP2	PDGFRB
TACC3	AURKA	BUB3	CDK1	MMP2	IRF2	LAMP2	PLAU	
MCM5	UBE2S	MAD2L1	TPX2	C3	STAT3	FYN	PHLDA1	
STMN1	H2AFV	HNRNPA3	NDC80	F8	PLA2G4A	IRF2	TNC	
AURKA	PLK1	HNRNPD	ARHGDIA	LAMP2		PLA2G4A	NR4A3	
UBE2S	CCNA2	MCM2	PXN	FYN			KLF9	
PLK1	CCND1	H2AFZ	BUB1				PLPP3	
CTPS1	H2AFX	TYMS	NEK2					
MCM7	E2F1	PABPC1	KIF23					
MCM4	TROAP	HNRNPA1	ARF6					
HMGB2	UBE2C	CDC45	TOP2A					
SPAG5	AURKB	RRM1	MAP3K11					
H2AFX	KIF22	TFDP1	KIF11					
UBE2T	KIF2C	SET	KIF4A					
AURKB	NUSAP1	CCT5	DLGAP5					
KIF22	RACGAP1	DEK	ACTN4					
PRPS1	MCM3	MCM6	ANLN					
TRIP13	PBK		ESPL1					
KIF2C	CCNB2							
RACGAP1	CDK1							
MCM3	BUB3							
CCNB2	MAD2L1							
CDK1	TPX2							
MAD2L1	NDC80							
MXD3	RAD54L							
SPC24	GINS2							
ASF1B	PTTG1							
PTTG1	HMGB3							
HMGB3	CHAF1A							
KIF18B	CDC25A							
MELK	CDKN3							
CDC25A	EXO1							
CDKN3	HNRNPD							
HNRNPD	MCM2							
MCM2	HMGN2							
HELLS	BUB1							
H2AFZ	H2AFZ							
DIAPH3	ORC6							
GINS3	CCNF							
POLD1	SUV39H1							
TIMELESS	UCK2							
ORC6	NEK2							
SUV39H1	TMPO							
GINS1	DBF4							
CDCA8	CHEK1							
TMPO	KIF23							
CENPM	TOP2A							
CHEK1	CDC45							
	KIF11							
	CKS2							

C-4 Leading edge analysis of Immune regulation Genesets for healthy fibroblasts

Table C-4.1 Leading edge genes contributing to enriched genesets describing immune system regulation for healthy fibroblasts cultured on 4000nm aligned scaffolds compared with 1000nm aligned

Immune Genesets – 4000A vs 1000A	
Positive Regulation of Immune System Process	Regulation of Immune System Process
CXCL8	CXCL8
COLEC12	COLEC12
C1S	C1S
C1R	SLC1A3
DAPK2	C1R
CXCL3	DAPK2
CCL2	PARP9
C1RL	CXCL3
CXCL6	CCL2
BCL6	FGF7
ICAM1	C1RL
CXCL1	SIAE
DPP4	CXCL6
IFI16	BCL6
	ICAM1
	CXCL1
	PDK4
	DPP4
	IFI16

Table C-4.2 Leading edge genes contributing to enriched genesets describing immune system regulation for healthy fibroblasts cultured on 2000nm aligned scaffolds compared with 2000nm random

Immune Genesets – 2000A vs 2000A					
Negative Regulation of Immune System Process	Positive Regulation of Immune Response	Positive Regulation of Immune System Process	Regulation of Immune Effector Process	Regulation of Immune Response	Regulation of Immune System Process
IRF1	NR4A3	NR4A3	NR4A3	NR4A3	NR4A3
BCL6	C1S	C1S	SLC1A3	C1S	C1S
RARA	C1R	MMP14	BCL6	IRF1	IRF1
GPR68	C1RL	C1R	RARA	C1R	MMP14
NR1D1	RARA	BCL6	ICAM1	BCL6	C1R
TOB2	IFI16	C1RL	FYN	C1RL	SLC1A3
IFI16	MMP2	RARA	TGFB3	RARA	BCL6
HIST1H4H	FYN	GPR68	ITPKC	NR1D1	C1RL
TGFB3	CLU	CAMK1D	PROS1	ICAM1	RARA
	COLEC12	ICAM1	STAT2	IFI16	GPR68
		VEGFA	C3	MMP2	CAMK1D
		ADAM17	MAP1A	FYN	NR1D1
		IFI16		TGFB3	ICAM1
		MMP2		CLU	VEGFA
		FYN		COLEC12	TOB2
		CLU			ADAM17
		COLEC12			IFI16
					MMP2
					HIST1H4H
					FYN
					TGFB3
					CLU
					COLEC12
					CYP26B1
					IL6R
					ITPKC

Table C-4.3 Leading edge genes contributing to enriched genesets describing immune system regulation for healthy fibroblasts cultured on 4000nm aligned scaffolds compared with 4000nm random

Immune Genesets – 4000A vs 4000R			
Regulation of Immune Response	Positive Regulation of Immune Response	Regulation of Immune System Process	Positive Regulation of Immune System Process
C1S	C1S	C1S	C1S
C1R	C1R	C1R	C1R
PROS1	COLEC12	PROS1	COLEC12
COLEC12	C1RL	SLC1A3	DAPK2
C1RL	CLU	COLEC12	C1RL
CLU	IFI16	FGF7	CLU
IFI16	SERPING1	DAPK2	IFI16
SERPING1	CTSK	C1RL	SERPING1
IFITM1	CTSB	CLU	DPP4
BCL6	MMP2	IFI16	BCL6
CTSK	NR4A3	SERPING1	CTSK
ICAM1	C3	IFITM1	ICAM1
CTSB		DPP4	CTSB
HFE		NFE2L2	GPR68
MMP2		BCL6	MMP2
NR4A3		CTSK	NR4A3
C3		ICAM1	C3
		CTSB	CXCL8
		GPR68	FYN
		HFE	WIPF1
		MMP2	RAB7B
		NR4A3	CTSL
		C3	EFNB1
		CXCL8	IL7
		FYN	IL34
		WIPF1	PTEN
		SIAE	ADAM17
		ADORA1	UBE2D1
		RAB7B	TGFBR2
		CTSL	CCL2
		FCGRT	PDE4D
		EFNB1	TNFSF13B
		IL7	ARNT
		IL34	SOCS5
		PTEN	MASP1
		ADAM17	IL13RA2
		TRAF3IP2	
		UBE2D1	
		PARP9	
		IFNGR1	
		TGFBR2	
		TOB2	
		CCL2	
		MITF	
		PDE4D	
		TNFSF13B	
		CYP26B1	
		APOD	
		ARNT	
		SOCS5	

Table C-4.4 Leading edge genes contributing to enriched genesets describing regulation of immune response for healthy fibroblasts cultured on 300nm random scaffolds compared with 1000nm random

Immune Genesets – 300R vs 1000R		
Positive Regulation of Immune System Process	Regulation of Immune Response	Regulation of Immune System Process
NR4A3	NR4A3	NR4A3
MMP14	C1S	MMP14
C1S	C1R	C1S
C1R	MMP2	C1R
MMP2	ICAM1	MMP2
ICAM1	LAMP1	ICAM1
LAMP1	BIRC3	LAMP1
BIRC3	BCL6	BIRC3
BCL6		BCL6
ADAM17		SIAE
SERPING1		ADAM17
CDKN1A		SERPING1
		CDKN1A
		STOM
		TRIM38
		C3
		NFKB1
		ITGB2
		CEBPB

C-5 Leading edge analysis of Angiogenesis Genesets for healthy fibroblasts.

Figure C-5 Scaffold anisotropy displays a limited ability to modulate healthy tendon fibroblast expression of genes involved in the regulation of angiogenesis

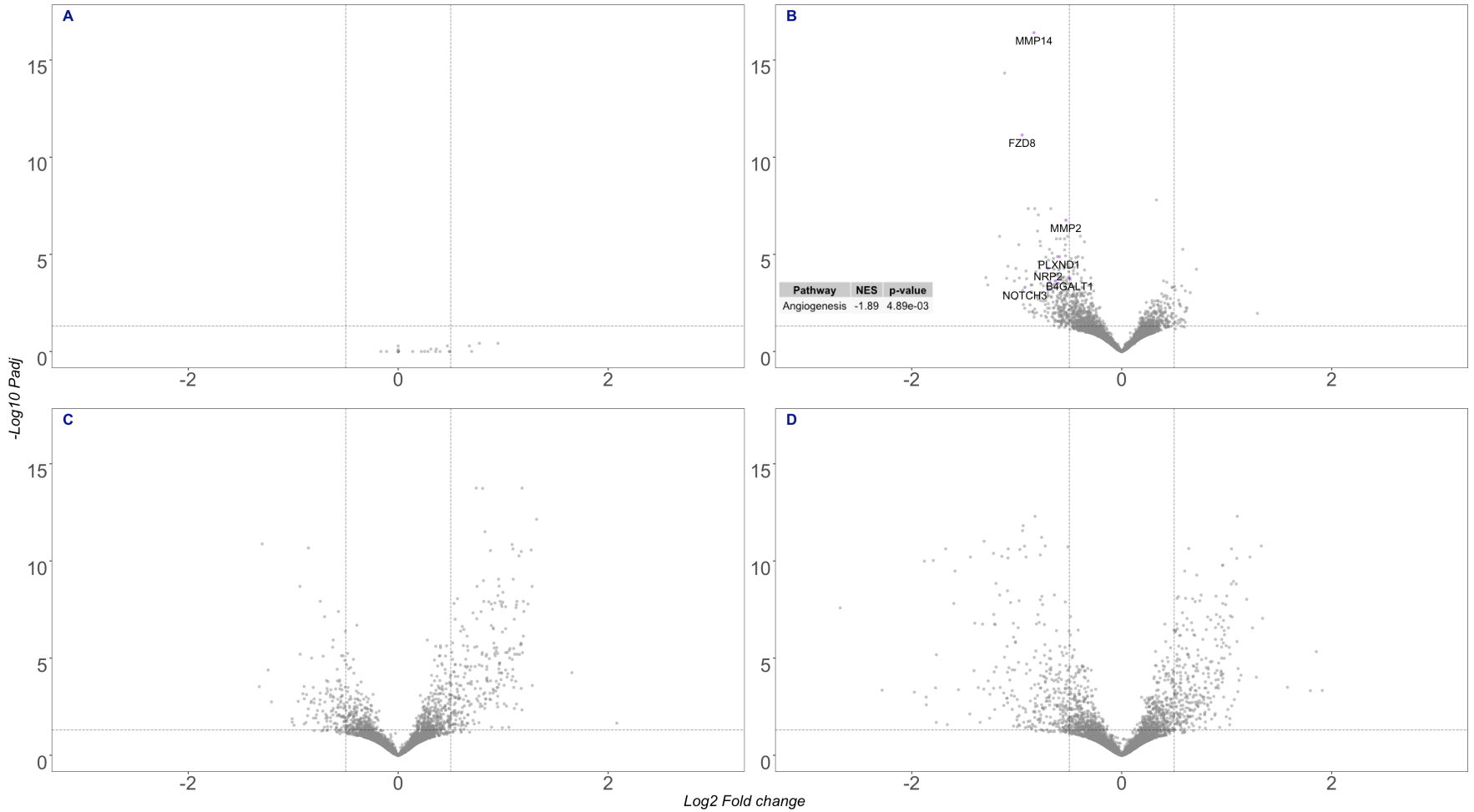

Figure C-5 Volcano plots showing enriched angiogenesis gene sets and leading-edge analysis for hamstring tendon fibroblasts seeded on random scaffolds. Pairwise analysis of scaffolds with aligned fiber directionality compared with random orientations but with constant mean fiber diameters of 300nm(A), 1000nm(B), 2000nm(C) and 4000nm(D). Angiogenesis gene sets with significant enrichment are listed in the summary table associated with each plot. Points highlighted in purple with associated gene symbols represent genes with the greatest contribution to the enriched gene sets (Leading-edge analysis).

Table C-5.1 Leading edge genes contributing to enriched genesets describing regulation of angiogenesis for healthy fibroblasts cultured on 1000nm aligned scaffolds compared with 1000nm random

Angiogenesis Genesets – 1000A vs 1000R
Angiogenesis
MMP14
FZD8
MMP2
PLXND1
NRP2
B4GALT1
COL18A1
UNC5B
COL8A2
NOTCH3
COL4A2

C-6 Leading edge analysis of cytokine or chemokine Genesets for healthy fibroblasts

Figure C-6 Scaffold anisotropy displays a limited ability to modulate healthy tendon fibroblast expression of genes involved in the regulation of cytokine or chemokine production and activity

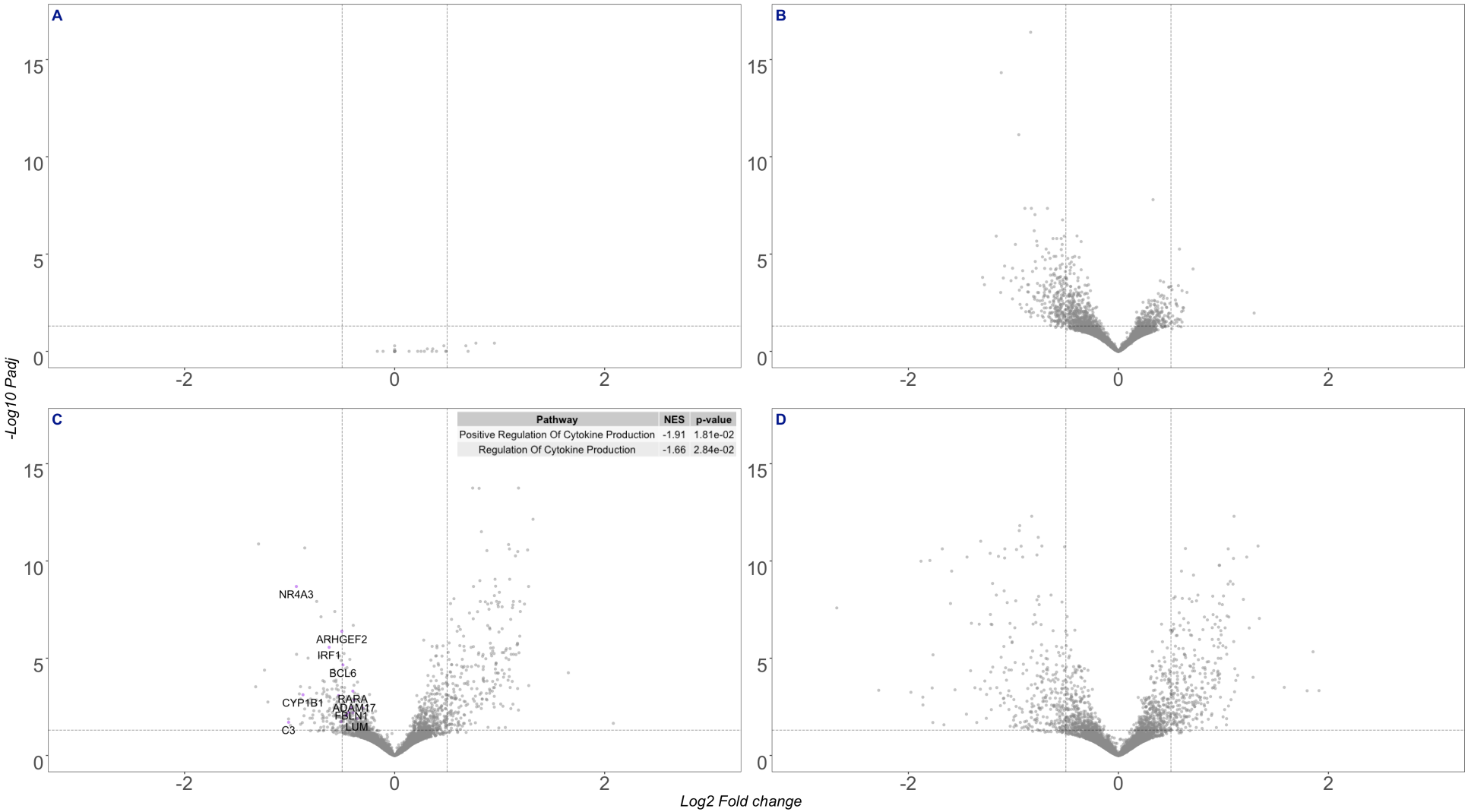

Figure C-6 Volcano plots showing enriched cytokine and chemokine genesets and leading-edge analysis for hamstring tendon fibroblasts seeded on anisotropic scaffolds. Pairwise analysis of scaffolds with aligned fiber directionality compared with random orientations but with constant mean fiber diameters of 300nm(A), 1000nm(B), 2000nm(C) and 4000nm(D). Significant enrichment of genesets that describe immune system regulation are listed in the summary table associated with each plot. Points highlighted in purple with associated gene symbols represent genes with the greatest contribution to the enriched gene sets (Leading-edge analysis).

Table C-6.1 Leading edge genes contributing to enriched genesets describing regulation of cytokine or chemokine production by healthy fibroblasts cultured on 2000nm random scaffolds compared with 2000nm random

Cytokine/Chemokine Genesets – 2000A vs 2000R	
Positive Regulation of Cytokine Production	Regulation of cytokine production
NR4A3	NR4A3
ARHGEF2	ARHGEF2
IRF1	IRF1
RARA	BCL6
CYP1B1	RARA
BCL3	CYP1B1
ADAM17	BCL3
IFI16	ADAM17
CLU	FBLN1
NFATC4	IFI16
IL6R	TGFB3
LUM	CLU
ZBTB20	NFATC4
C3	IL6R

Table C-6.2 Leading edge genes contributing to enriched genesets describing regulation of cytokine or chemokine production by healthy fibroblasts cultured on 300nm random scaffolds compared with 1000nm random

Cytokine/Chemokine Genesets – 300R vs 1000R
Regulation of Cytokine Production
NR4A3
ARHGEF2
GPNMB
BIRC3
BCL6
ADAM17
TRIM38
C3
NFKB1
CEBPB
ATP6AP2

C-7 Leading edge analysis of ECM and cytoskeletal Genesets for healthy fibroblasts

Table C-7.1 Leading edge genes contributing to enriched genesets describing regulation of ECM production and cytoskeletal apparatus for healthy fibroblasts cultured on 1000nm aligned scaffolds compared with 1000nm random

ECM and cytoskeletal Genesets – 1000A vs 1000R

Microtubule Cytoskeleton Organisation	Microtubule Cytoskeleton	Cytoskeleton	Negative Regulation of Cytoskeleton Organisation	Extracellular Matrix	Proteinaceous Extracellular Matrix	Extracellular Matrix Component
TUBA1B	AK5	AK5	BIRC5	MMP14	MMP2	COL18A1
BIRC5	VRK1	VRK1	RCC1	MMP2	EMILIN1	COL8A2
RCC1	TUBA1B	TUBA1B	STMN1	EMILIN1	COL6A2	MFAP4
STMN1	MAD2L1	MAD2L1	KNSTRN	COL6A2	FBLN2	COL4A2
KNSTRN	BIRC5	BIRC5	TUBG1	FBLN2	TIMP2	COL6A3
TUBG1	PKP4	PKP4	MAPRE1	AEBP1	CILP2	COL6A1
CDK1	ANXA11	ANXA11	MYBL2	CPXM2	COL18A1	TNC
CAV1	STMN1	STMN1	PLK2	TIMP2	COL8A2	TIMP3
MYBL2	CDC20	CFL2	NDC80	LTBP3	MFAP4	AGRN
PLK2	KNSTRN	CDC20	HAUS4	CILP2	COL4A2	COL5A3
NDC80	KARS	KNSTRN	AURKA	COL18A1	BGN	COL4A1
HAUS4	TUBB4B	KARS		COL8A2	COL6A3	THBS4
PCLAF	TUBG1	TUBB4B		MFAP4	COL6A1	LAMA3
AURKA	CCNB2	TUBG1		COL4A2	TNC	HMCN1
	CCT5	COTL1		BGN	LTBP4	NTN1
	FAM83D	CCNB2		COL6A3	CRISPLD2	COL5A1
	TUBA1C	ACTB		COL6A1	TIMP3	LAMB2
	RUVBL1	CCT5		SSC5D	AGRN	
	MAPRE1	KRT34		TNC	VEGFA	
	CCT6A	FAM83D		LTBP4	LTBP2	
	CDK1	TUBA1C		CRISPLD2	COL5A3	
	CCT2	RUVBL1		TIMP3	OLFML2A	
	TUBB6	MAPRE1		AGRN	COL4A1	
	PLK2	CORO1C		VEGFA	THBS4	
	HAUS4	CCT6A		LTBP2	LAMA3	
	SKA2	CDK1		COL5A3	HMCN1	
	TUBB2A	CCT2		OLFML2A	CD248	
	AURKA	TUBB6		COL4A1	NTN1	
	RGS20	LMNB1		THBS4	COL5A1	
	RASSF3	PLK2		LAMA3	LAMB2	
	TPGS2	HAUS4		HMCN1		
	NCAPG	TPM1		CD248		
	CDC6	SKA2				
	CALM2	TUBB2A				
	NUSAP1	AURKA				
	OLA1	RGS20				
	MZT1	RASSF3				
	RAN	KRT19				
	CDC16	TPGS2				
		NCAPG				
		TRPC4				
		CDC6				
		CALM2				
		NEXN				
		NUSAP1				
		FHL2				
		WDR1				
		OLA1				
		MZT1				
		AFAP1L1				
		RAN				
		CDC16				
		LIMA1				
		NPM1				
		DCAF13				
		ZYX				
		BICD2				
		TMEM63B				
		PTPN14				
		DIDO1				
		LZTS3				
		TCTN2				
		SEPT9				
		DGKQ				
		CCDC102A				
		ELL				
		DIDO1				

Table C-7.2 Leading edge genes contributing to enriched genesets describing regulation of ECM production and cytoskeletal apparatus for healthy fibroblasts cultured on 2000nm aligned scaffolds compared with 2000nm random

ECM and cytoskeletal Genesets – 2000A vs 2000R

Microtubule Cyotoskeleton Organisation	Microtuble Cytoskeleton	Negative Regulation of Cytoskeleton Organisation	Cytoskeleton	Cytoskeleton Organisation	Regulation of Cytoskelton Organisation	Extracellular Matrix	Proteinaceous Extracellular Matrix	Extracellular Matrix Component
BIRC5	BIRC5	BIRC5	RFLNB	RFLNB	BIRC5	MMP14	SLC1A3	MMP14
STMN1	STMN1	STMN1	BIRC5	BIRC5	STMN1	SLC1A3	VEGFA	SLC1A3
AURKA	AURKA	AURKA	CDC6	STMN1	AURKA	CPXM2	TNC	CPXM2
CDK1	CDK1	MYBL2	STMN1	AURKA	MYBL2	VEGFA	MFAP4	VEGFA
TACC3	TACC3	KNSTRN	AURKA	CDK1	KNSTRN	TNC	FBLN1	TNC
KIF2C	KIF2C	NDC80	CDC20	TACC3	NDC80	MFAP4	LAMA4	MFAP4
MYBL2	MYBL2	SPAG5	CENPU	KIF2C	SKA2	FBLN1	MMP2	FBLN1
KNSTRN	KNSTRN	TPX2	CDK1	MYBL2	PLK1	LAMA4	ADAMTS10	LAMA4
NDC80	NDC80	CCNB1	LMNB1	KNSTRN	SPAG5	MMP2	SERPINF1	MMP2
TUBA1B	TUBA1B	RACGAP1	MAD2L1	CORO1C	TPX2	ADAMTS10	LUM	ADAMTS10
PLK1	PLK1	AURKB	TACC3	NDC80	CCNB1	TGFB3	CD248	TGFB3
SPAG5	SPAG5	EZR	FAM83D	TUBA1B	SKA3	CLU	CILP2	CLU
TPX2	TPX2	FBXO5	KIF2C	PLK1	RACGAP1	SERPINF1	COL6A3	SERPINF1
NUSAP1	NUSAP1	WDR62	CCNB2	SPAG5	AURKB	SFRP2	COL6A1	SFRP2
CCNB1	CCNB1	NEK2	KNSTRN	TPX2	EZR	LUM	COL6A2	LUM
RACGAP1	RACGAP1	RCC1	CORO1C	NUSAP1	WDR1	CD248	LAMA3	CD248
CDK2	CDK2	MAPRE1	NCAPG	CCNB1	FBXO5	CILP2	ADAMTS14	CILP2
AURKB	AURKB	KIF23	PKP4	RACGAP1	WDR62	COL6A3	NTN1	COL6A3
EZR	EZR	KIF4A	SKA2	CDK2	NF2	COL6A1	LGALS3BP	COL6A1
FBXO5	FBXO5	CKAP2	TUBA1B	AURKB	NEK2	COL6A2	GPC4	COL6A2
SGO1	SGO1	NEK7	TUBB6	EZR	RCC1	SSC5D	COL7A1	SSC5D
WDR62	WDR62	TUBG1	PLK1	WDR1	MAPRE1	LAMA3	ADAMTSL4	LAMA3
KIF20A	KIF20A	TTK	CDCA8	FBXO5	KIF23	ADAMTS14	CCBE1	ADAMTS14
CENPA	CENPA		SPAG5	SGO1	CTGF	NTN1	CYR61	NTN1
NEK2	NEK2		TPX2	WDR62	KIF4A	SOD3	MATN2	SOD3
RCC1	RCC1		CEP55	NF2	CKAP2	LGALS3BP		LGALS3BP
KIF23	KIF23		NUSAP1	KIF20A	TPM1	GPC4		GPC4
KIF4A	KIF4A		CCNB1	CENPA	NEK7	COL7A1		COL7A1
PCLAF	PCLAF		SKA3	NEK2	TUBG1	ADAMTSL4		ADAMTSL4
NEK7	NEK7		RACGAP1	DIAPH3	TTK	CCBE1		CCBE1
TUBG1	TUBG1		TOP2A	RCC1	ECT2	CYR61		CYR61
TTK	TTK		GTSE1	KIF23	PLK4	MATN2		MATN2
PLK4	PLK4		VRK1	ANLN	NEXN			
KIF18A	KIF18A		CDK2	KIF4A	KIF18A			
PRC1	PRC1		AURKB	PCLAF	PRC1			
KIF11	KIF11		MCM3	TPM1	KIF11			
PSRC1	PSRC1		EZR	NEK7	PSRC1			
KIF18B	KIF18B		WDR1	TUBG1				
			FBXO5	TTK				

MCM2	CNN1
DTL	
SGO1	
WDR62	
NF2	
KIF20A	
CTNNAL1	
DLGAP5	
NEK2	
TUBB4B	
ERCC2	
MZT1	
KIF20B	
MAPRE1	
KIF23	
ANLN	
KIF4A	
CKAP2	
TRIM59	
TPM1	
NEK7	
CBX1	
TUBG1	
ERCC6L	
TTK	
AK5	
CNN1	
ACTB	
CKAP2L	
ECT2	
LMNB2	
KIF22	
TUBA1C	
TRPC4	
PLK4	
ORC6	
NEXN	
KRT19	
CDC45	
RANGAP1	
BUB1B	
KIF18A	
TPM3	
PRC1	
KIF11	
PSRC1	

Table C-7.3 Leading edge genes contributing to enriched genesets describing regulation of ECM production and cytoskeletal apparatus for healthy fibroblasts cultured on 4000nm aligned scaffolds compared with 4000nm random

ECM and cytoskeletal Genesets – 4000A vs 4000R

Microtubule Cytoskeleton Organisation	Microtuble cytoskeleton	Cytoskeleton	Negative Regulation of Cytoskeleton Organisation	Regulation of Cytoskeleton Organisation	Cytoskeleton Organisation	Actin Cytoskeleton	Extracellular matrix Component	Extracellular Matrix	Proteinaceous Extracellular Matric
MYBL2	MYBL2	RFLNB	MYBL2	MYBL2	RFLNB	RFLNB	LUM	LUM	LUM
EZR	EZR	LMNB1	EZR	EZR	MYBL2	EZR	SERPINF1	SERPINF1	SERPINF1
BIRC5	BIRC5	EZR	BIRC5	BIRC5	EZR	NF2	SLC1A3	SLC1A3	SLC1A3
TACC3	TACC3	PKP4	STMN1	NF2	BIRC5	CORO1C	ECM2	DCN	ECM2
STMN1	STMN1	CDC20	WDR62	STMN1	TACC3	TPM1	DCN	FBLN1	DCN
WDR62	WDR62	BIRC5	AURKA	WDR62	NF2	SMTN	CPXM2	MFAP4	FBLN1
AURKA	AURKA	TACC3	RCC1	AURKA	STMN1	ZYX	FBLN1	LAMA4	OGN
RCC1	RCC1	ERCC2	SPAG5	RCC1	WDR62	WDR1	OGN		MFAP4
PLK1	PLK1	NF2	AURKB	PLK1	AURKA	NCAPG	CLU		LAMA4
SPAG5	SPAG5	CDC6	KNSTRN	SPAG5	RCC1	MYH1	MFAP4		CHI3L1
AURKB	AURKB	STMN1	RACGAP1	AURKB	PLK1	PXN	LAMA4		CRTAP
CDK2	CDK2	RANGAP1	TPX2	TPM1	CORO1C	ORC6	CHI3L1		GPC4
KNSTRN	KNSTRN	WDR62	CCNB1	KNSTRN	SPAG5	CDH2	CRTAP		TNC
DVL1	DVL1	AURKA	NDC80	RACGAP1	AURKB	DBN1	SFRP2		MMP2
KIF2C	KIF2C	PLK1	CCNF	CTGF	TPM1	ZNF185	SOD3		CPZ
NUSAP1	NUSAP1	CENPU	NEK2	TPX2	ANKRD1	KRT19	GPC4		OMD
RACGAP1	RACGAP1	CORO1C	BIRC2	CCNB1	CDK2	FBLIM1	TNC		COL14A1
CDK1	CDK1	SPAG5	KIF23	NDC80	KNSTRN	ACTN4	MMP2		
TUBA1B	TUBA1B	GTSE1	TUBG1	WDR1	DVL1	VASP	CPZ		
TPX2	TPX2	LMNB2	KIF11	SKA2	KIF2C	MYL9	OMD		
CCNB1	CCNB1	AURKB	NEK7	ARHGDIA	NUSAP1	ANLN	COL14A1		
NDC80	NDC80	TPM1	KIF4A	NEXN	RACGAP1	ACTG1	SERPINE2		
KIF18B	KIF18B	KIF22	HAUS8	PSRC1	CDK1	ARPC5L			
PSRC1	PSRC1	CDK2		CCNF	ZYX	CRYAB			
NEK2	NEK2	KNSTRN		SKA3	TUBA1B	ACTC1			
BIRC2	BIRC2	DHCR24		XRCC3	TPX2	MYH2			
KIF20A	KIF20A	DVL1		NEK2	CCNB1	FSCN1			
KIF23	KIF23	KIF2C		BIRC2	NDC80	PDLIM7			
TUBG1	TUBG1	NUSAP1		CHEK1	WDR1	BAIAP2L1			
SGO1	SGO1	SMTN		SORBS3	CNN1	TPM3			
KIF11	KIF11	RACGAP1		KIF23	KIF18B	CDC42EP1			
PCLAF	PCLAF	MCM3		ARF6	DIAPH3	FMN2			
NEK7	NEK7	CCNB2		TUBG1	PSRC1	BCAR1			
KIF4A	KIF4A	CDK1		KIF11	NEK2	DAPK3			
HAUS8	HAUS8	MAD2L1		NEK7	BIRC2	ACTA2			
XRCC2	XRCC2	ZYX		KIF4A	KIF20A	CFL1			
		TUBA1B		EDN1	SORBS3	AFAP1L1			
		TPX2		HAUS8	KIF23	GAS2L1			
		FAM83D			ARF6	CAP1			
		CCNB1			TUBG1				
		CEP55			DBN1				

WDR1
NCAPG
SKA2
TUBB6
ARHGDIA
ACTB
CNN1
KIF18B
AKT1
TRIM59
TUBB4B
KRT7
NEXN
MCM2
MYH1
PXN
PSRC1
TIMELESS
ORC6
TUBA1C
CEP78
CCNF
SKA3
POC1A
CDCA8
NEK2
CDH2
CDK16
BIRC2
CHEK1
KIF20A
NSUN2
COTL1
DTL
SORBS3
KIF23
TUBG1
TOP2A
CDC45
DBN1
SGO1
MAP3K11
KIF11
ZNF185
NEK7
KRT19
KIF4A
CCT5
TRPC4
HAUS8
DLGAP5
XRCC2
FBLIM1

SGO1
KIF11
PCLAF
NEK7
KRT19
KIF4A
HAUS8
XRCC2
ACTN4
VASP
PAK4
ANLN
ESPL1
ACTG1
ARPC5L
KRT14

CCNE1
ACTN4
REEP4
RASSF3
ELL2
VASP
MYL9
PDLIM1
ANLN
ESPL1
ACTG1
ARPC5L
KRT14
BUB1B
CRYAB
LRRFIP1
CKAP2L
ACTC1

Figure C-8 Heatmap and dendrogram of healthy and diseased tendon fibroblasts cultured on 8 scaffolds with different microarchitectures

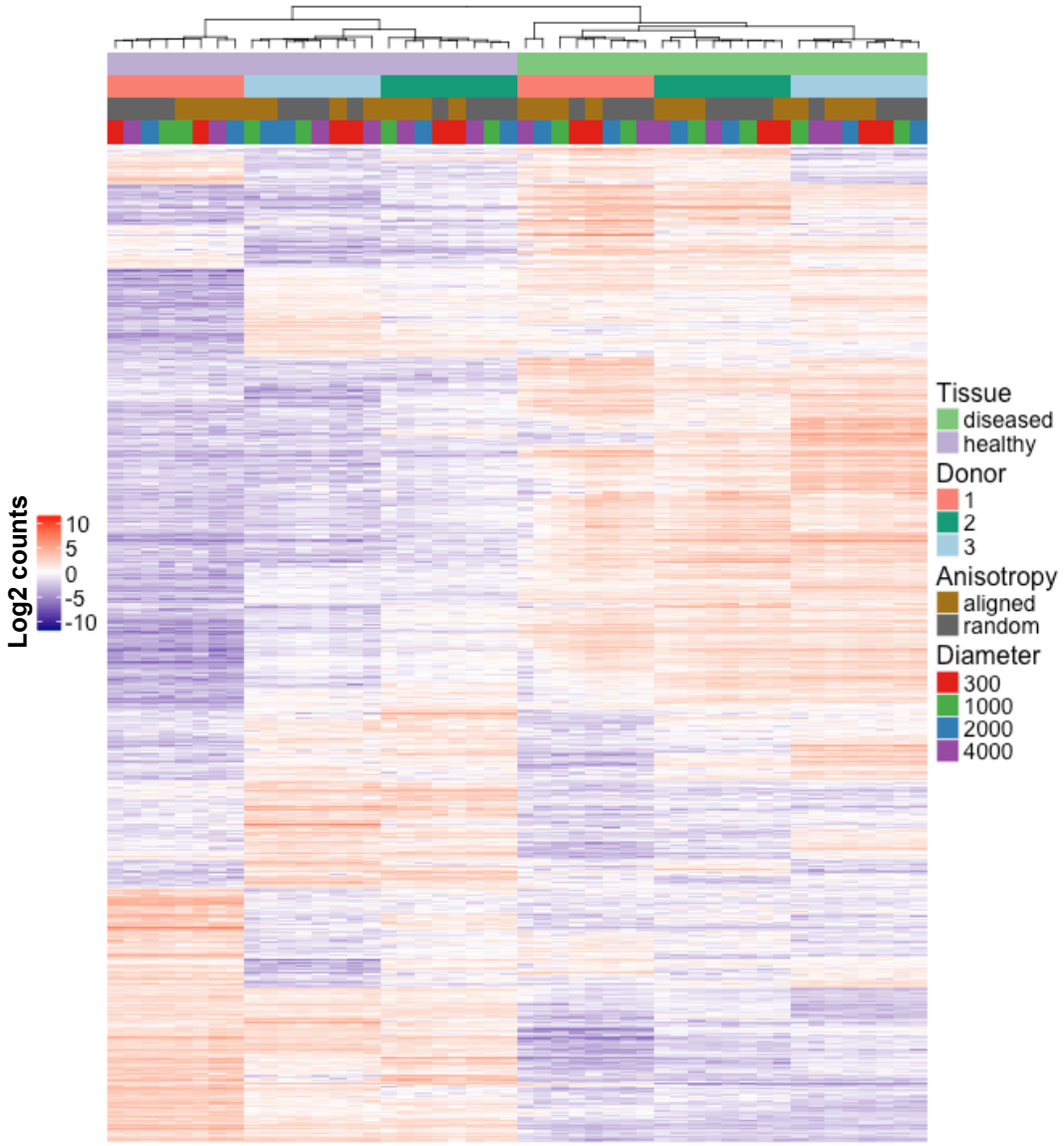

Figure C-8 Heatmap of healthy and diseased tendon fibroblasts cultured on 8 distinct scaffold microarchitectures. Log transformed expression data from 48 RNA samples sequenced from healthy hamstring and diseased rotator cuff tendon fibroblasts seeded onto 8 different electrospun scaffolds. Independent hierarchical clustering was undertaken on the top 500 most variably expressed genes and mapped to the variables of tissue type, donor, anisotropy and fiber diameter.

Figure C-9 In response to the variation of fibre diameter for randomly orientated scaffolds, the gene expression of diseased tendon fibroblast is largely unchanged

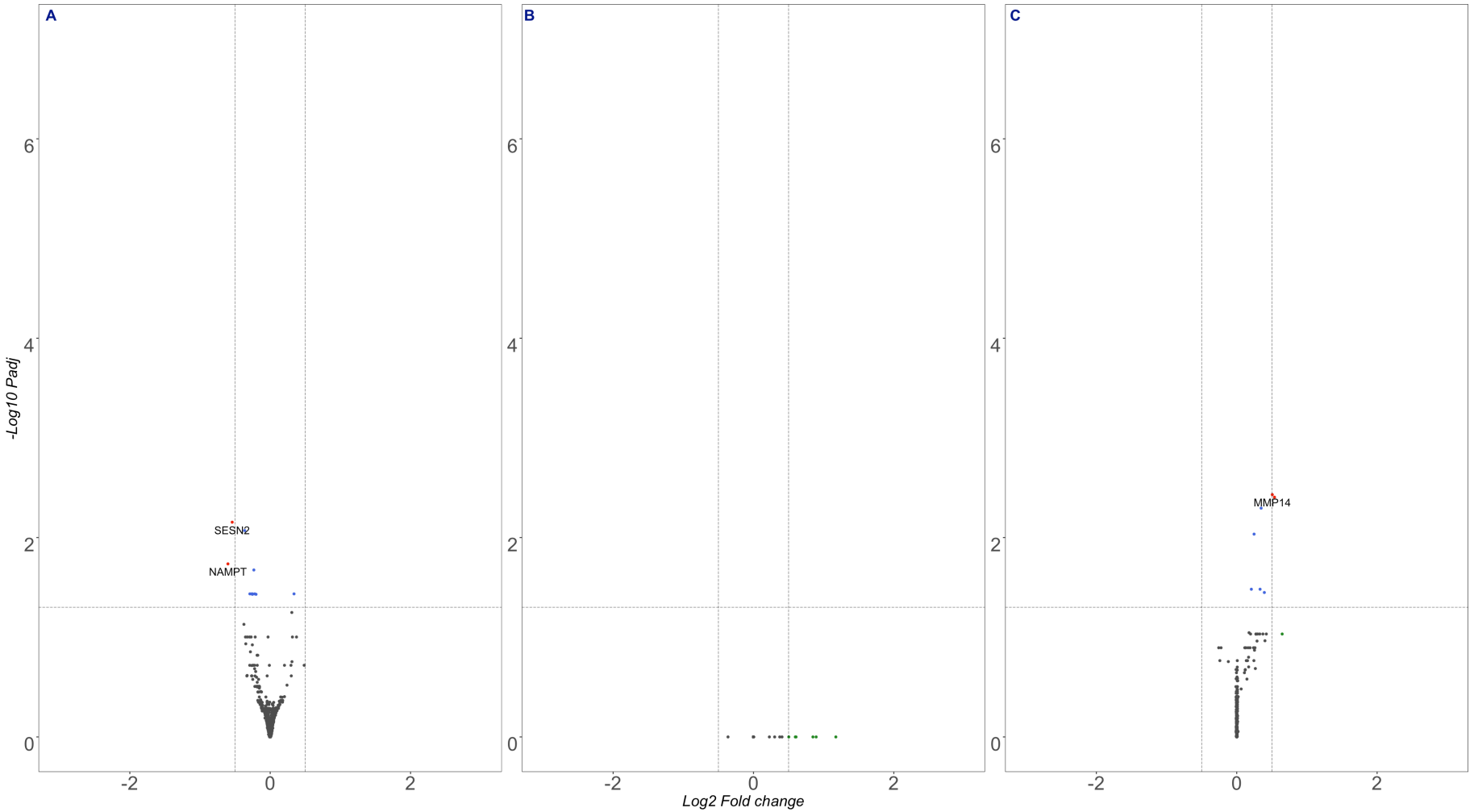

Figure C-9 Volcano plot of differentially expressed genes for diseased rotator cuff tendon fibroblasts seeded on scaffolds with randomly orientated fibers. Pairwise analysis of random scaffolds with fibre diameters of 300nm(A), 2000nm(B) and 4000nm(C) compared with 1000nm random scaffolds. Dashed lines denote a false discovery rate (FDR) of 0.05 and a log2 Fold-change ± 0.5. Transcripts coloured red have passed the thresholds for FDR and log2 Fold-change criteria, blue only meet the FDR, green only the log2 Fold-change threshold, whilst for grey neither criteria are met.

Figure C-10 Heatmap and PCA of diseased tendon fibroblasts cultured on scaffolds with different microarchitectures

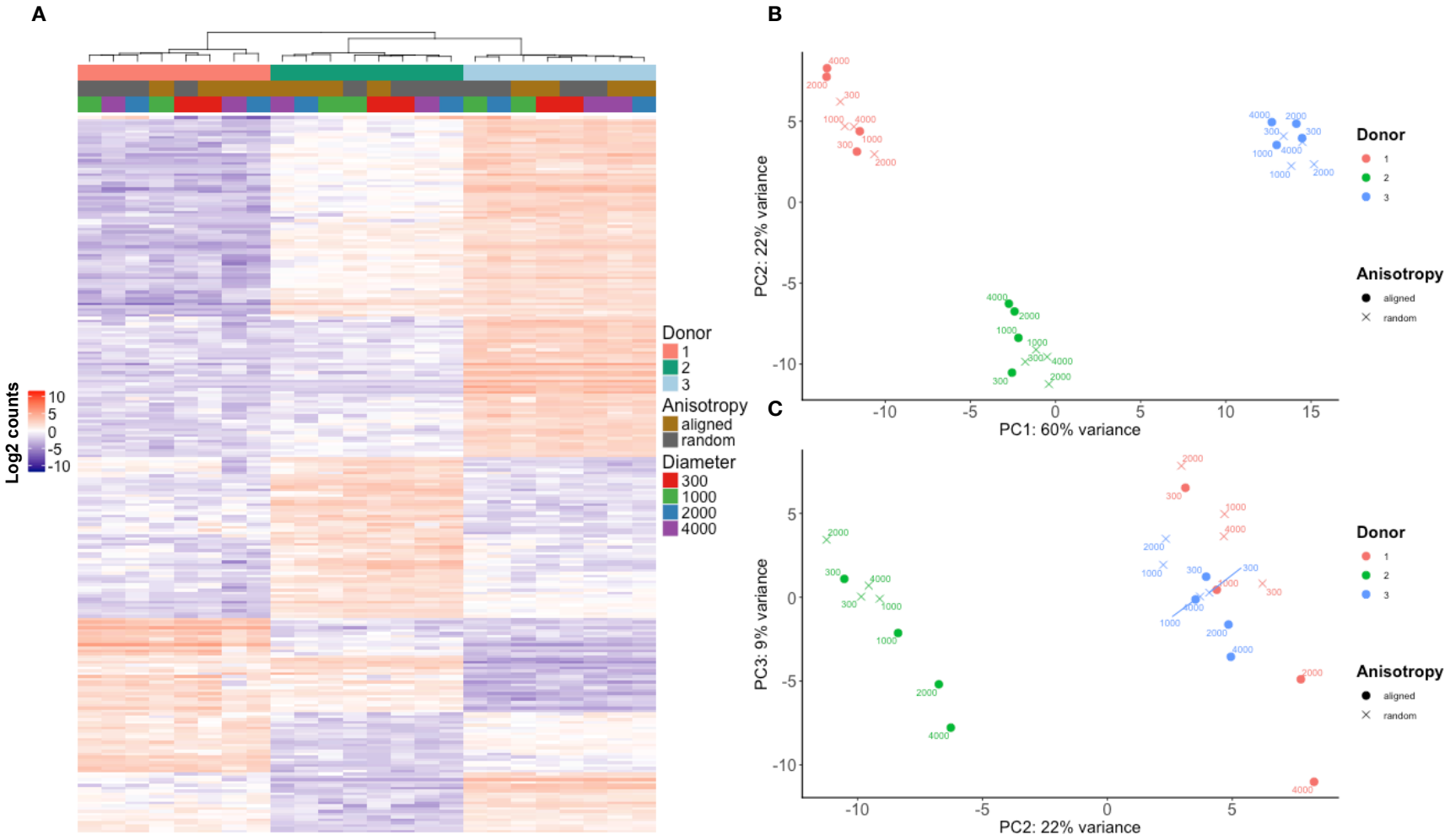

Figure C-10 Heatmap and Principle component analysis (PCA) of diseased tendon fibroblasts cultured on electrospun scaffolds. Log transformed expression data from all 24 RNA samples sequenced from healthy hamstring fibroblasts seeded on to 8 different electrospun scaffolds. Independent clustering of the samples according to donor, anisotropy and diameter is depicted by the dendrogram (A) and 1st and 2nd principles component (B) which accounts for 69% and 22% of the variance in gene expression respectively. The effect of scaffold architecture on gene expression is most clearly observed in the 3rd principle component (C). The Heatmap depicts hierarchical clustering of the top 500 PCA genes across all samples.